UNIVERSITÀ
DEGLI STUDI
DI PADOVA

UNIVERSITÀ DEGLI STUDI DI PADOVA

Sede Amministrativa: Università degli Studi di Padova

Dipartimento di Ingegneria Industriale - DII

SCUOLA DI DOTTORATO DI RICERCA IN IINGEGNERIA INDUSTRIALE

INDIRIZZO: INGEGNERIA CHIMICA, DEI MATERIALI E MECCANICA

CICLO XXVIII

MACHINABILITY OF TI6AL4V ALLOY PRODUCED BY ELECTRON BEAM MELTING UNDER DIFFERENT LUBRICATING CONDITIONS

Direttore della Scuola: Ch.mo Prof. Paolo Colombo

Coordinatore d'indirizzo: Ch.mo Prof. Enrico Savio

Supervisore: Ch.ma Prof. ssa Stefania Bruschi

Dottorando: Alberto Bordin

To Piera

ABSTRACT

In the last decade, the growing diffusion of metal additive manufacturing technologies is revolutionising the manufacturing processes of the most advanced industrial fields. Nowadays, more and more companies operating in the aeronautic and in the biomedical field are employing the additive manufacturing technology of Electron Beam Melting (EBM) to produce prosthesis and aero engine parts made of the titanium alloy Ti6Al4V, traditionally produced by hot forging and machining. Thanks to this technology, it is possible to realise a complex shape component with tailored mechanical and geometrical properties, passing from the 3D CAD model directly to the near net shape geometry without any intermediate manufacturing steps, thus cutting the production costs. However, finishing machining operations are still necessary to remove the surface porosity that is a direct and inevitable consequence of additive manufacturing technologies, and to achieve higher surface quality and geometrical accuracy. Aiming to optimize the machining operation and to avoid detrimental surface damages left on the final product, the material machinability has to be taken into account. At the moment, many efforts coming from both the academic and industrial research have been spent to enhance the poor machinability of wrought Ti6Al4V alloy due to the increasing demand from the aeronautic field; however no published works and technical data are available regarding the machinability of EBM Ti6Al4V that presents different mechanical properties. Within the biomedical field, the surgical replacements made of Ti6Al4V are traditionally machined under flood coolants, made of synthetic or vegetable oil and water emulsions. As a consequence, costly sterilizing and cleaning operations are performed to remove the toxic and pollutant chemical residuals left on the finished products at the end of the manufacturing process. Thus, there is a need to revise the traditional lubricating strategies applied in machining operations of surgical implants, proposing an innovative solution that might satisfy technological, environmental and economic issues.

In this PhD thesis, an innovative cryogenic cooling line has been developed and implemented to turn EBM Ti6Al4V alloy, as a promising alternative to standard cooling methods applied in machining surgical implants. The alloy machinability has been firstly investigated trough an experimental approach, evaluating the effects of three different cooling methods namely: dry, wet and cryogenic and of different cutting parameters, on the tool wear, on the surface integrity and

on the chip morphology. Subsequently, a FE numerical model has been developed to simulate the turning operation of EBM Ti6Al4V alloy, capable to predict the effects of different process conditions.

Due to the beneficial effects induced by the cryogenic cooling on the surface integrity of turned Ti6AL4V EBM test pieces, the feasibility of such technology for biomedical applications has been validated by means of wear tests: the wear resistance of cryogenically machined specimens clearly increased with a strong reduction of metallic particles loss. Finally, cryogenic turning has been employed to machine real acetabular cups, in comparison with standard cooling methods applied in machining surgical implants. The beneficial effects imparted by cryogenic cooling in terms of improved material machinability, improved wear resistance and satisfying achievable geometrical accuracy, foresee a potential applicability of this technology in the biomedical field for years to come.

SOMMARIO

Nell'ultimo decennio la crescente diffusione delle moderne tecnologie di formatura additiva da polvere metallica sta rivoluzionando i processi produttivi dei più avanzati settori manifatturieri. Oggigiorno, sempre più aziende operanti nel settore aeronautico e biomedicale stanno impiegando la tecnologia additiva denominata "Electron Beam Melting" per realizzare protesi ortopediche e componenti di motori aeronautici in lega di Ti6Al4V, tradizionalmente ottenuti per forgiatura e lavorazioni alle macchine utensili. Grazie a tale tecnologia, è possibile realizzare un componente di forma complessa, con proprietà geometriche e meccaniche taylorizzate, passando direttamente dal disegno al prodotto semi finito senza passaggi intermedi, abbattendo i costi di produzione. Tuttavia, lavorazioni alle macchine utensili di finitura sono tutt'ora necessarie per eliminare la porosità superficiale intrinseca a tale tecnologia e per ottenere una qualità superficiale e una precisione dimensionale non raggiungibili altrimenti. Al fine di ottimizzare la lavorazione meccanica e non indurre danneggiamenti superficiali al prodotto finito che ne inficiano la vita di servizio, è fondamentale conoscere la lavorabilità del materiale. Allo stato attuale, molti lavori di carattere scientifico e industriale sono stati condotti per migliorare la bassa lavorabilità della lega Ti6Al4V lavorata a caldo, grazie a una forte domanda dal settore aeronautico, ma non sono reperibili documenti e informazioni tecniche fruibili sul comportamento della lega prodotta per Electron Beam Melting, che manifesta differenti proprietà microstrutturali e meccaniche. Nel campo biomedicale, le protesi ortopediche in lega di Ti6Al4V sono lavorate alle macchine utensili applicando abbondante lubrificazione, realizzata con emulsioni di olio sintetico o vegetale e acqua. Al fine di rimuovere le sostanze tossico-inquinanti lasciate dalla lavorazione sui prodotti finiti, costose operazioni di lavaggio e sterilizzazione sono eseguite a fine processo. Nasce quindi l'esigenza di rivisitare le tradizionali strategie di lubrificazione impiegate nei processi di asportazione di truciolo in campo biomedicale, proponendo una soluzione che soddisfi dei requisiti tecnologici (bassa lavorabilità della lega), ambientali (fluido lubrificante non inquinante e tossico per l'uomo) ed economici (che riduca i costi di lavaggio e sterilizzazione).

In questa tesi di dottorato, un sistema di lubrificazione criogenico è stato implementato per realizzare la tornitura della lega Ti6Al4V EBM, come alternativa da applicarsi in campo biomedicale. La lavorabilità della lega è stata investigata mediante un approccio sperimentale,

valutando gli effetti di tre regimi di lubrificazione: a secco, lubrificante standard e mediante azoto liquido; e dei parametri di taglio, valutando l'usura dell'utensile, l'integrità superficiale e la morfologia del truciolo. In seguito un modello numerico agli elementi finiti è stato sviluppato per simulare il processo di tornitura su tale lega, capace di predire gli effetti di diversi parametri di processo. Visti i benefici apportati dalla lubrificazione criogenica sull'integrità superficiale di componenti torniti di Ti6AL4V EBM, l'applicabilità di tale tecnologia in campo biomedicale è stata validata mediante delle prove di usura: la resistenza all'usura del materiale è risultata notevolmente incrementata con minor rilascio di particelle metalliche. In fine, la tornitura criogenica è stata applicata nella lavorazione di reali coppe acetabolari, comparandone gli effetti con le più tradizionali strategie di lubrificazione. I positivi risultati in termini di miglioramento della lavorabilità, di resistenza all'usura accompagnati da soddisfacente precisione dimensionale, fanno intravvedere un'efficiente applicazione della tornitura criogenica in campo biomedicale negli anni futuri.

Index

Chapter 1

Introduction

1.1. Industrial and scientific background

Since the year 2007, Eurocoating S.p.a, an Italian company operating in the biomedical field, has invested important capitals to revolutionise the production of biomedical surgical implants by using innovative Additive Manufacturing (AM) technologies such as Electron Beam Melting and Direct Melting Laser Sintering. The continuous investment in research and development and the co-operation with the main "3D-printer" manufacturers, led Eurocoating S.p.a to become an international reference for the production of metal surgical replacements, in particular of acetabular cups. During the first years of this adventure, the company conducted important researches devoted to characterize the biomedical alloys generated through AM technologies, mainly the titanium alloy Ti6Al4V. These researches highlighted the formation of peculiar microstructures by using these innovative forming techniques instead of more traditional processes. In fact, historically most of the common surgical replacements are manufactured by hot forging, or else they are machined from hot worked wrought products, subsequently parts of the surfaces are grinded and polished. Even if the chemical properties of the manufactured alloys are equivalent, the severe cooling rates reached locally during AM forming processes determine refined microstructures or even metastable microstructures in comparison with forged ones, and subsequent heat treatments are needed to respect the biomedical standards. Nowadays, AM technologies are more diffused than ten years ago, and relevant published researches have clarified most of the metallurgical mechanisms and the consequential mechanical, electro-chemical and physical properties of the most common biomedical alloys, such as Ti6AL4V and CoCrMo. Being these alloys widely used in the aeronautic industry for the production of aero engine parts, the largest aero engine manufacturers have become the main users and investors of such technologies, demanding bigger and more and more performing AM printing machines to satisfy high production volumes. What persuades them to progressively shifting towards this new concept of manufacturing is the possibility to design complex product shapes and direct

print their near net shape geometry in just one manufacturing step, avoiding high tooling costs. At the same time, no more assemblies are needed to create internal cavities and complex forms; as a consequence stiffer and lighter products are achievable: an ideal condition for aeronautic applications. In the case of biomedical applications, the advantages are even more. In fact, complex trabecular structures needed to favourite the integration of the prosthesis with human tissues and at the same time having closer mechanical properties to the bones, can be designed on dedicated 3D CAD software's and directly print them, avoiding costly post process plasma spray coatings. Even if AM technologies offer the chance to drastically reduce the amount of machining operations needed to reach the final product shape, they are still required. In fact, additive manufactured goods, when extracted from the metal 3D printer, present a globally distributed surface porosity whether they are produced by Electron Beam Melting (EBM) or by Direct Melting Laser Sintering (DMLS), an example is reported in the Figure 1.1. This surface porosity can be left in its as built condition if the geometrical feature does not require a particular functionality; otherwise it has to be removed by means of standard machining operations as milling and turning. Moreover, if a strict geometrical accuracy has to be achieved because the printed part is joined with another component, the mating surface or geometrical feature needs to be machined to reach the desired surface quality and the dimensional specifications. At the moment, AM forming technologies cannot accomplish the geometrical accuracy obtainable by machining operations. On the basis of these last technical issues regarding AM technologies, a novel branch of research focused in machining of Additive Manufactured materials and products emerges among the latest manufacturing technologies. In 2012, Eurocoating S.p.a, launched the ambitious research project titled: Natural and Efficient Machining Operation "NEMO", aimed to investigate the machinability of AM alloys, mainly Ti6L4V, and to propose efficient, sustainable and innovative machining processes to be applied in the manufacturing chain of surgical implants.

Figure 1.1 Surface porosity generated on a Ti6Al4V dental pin produced by Direct Melting Laser Sintering.

The works developed in this thesis follows the goals of the project, being the Industrial Engineering Department of the University of Padova the main scientific partner. The

research in the field of machining operations dates back to the eighteen century; however after the Second World War with the advancing of the aeronautic field, with the introduction of exotic difficult to cut superalloys and the progressive development of modern high productive machine tools, the scientific research became relevant to afford the problems encountered in industry. Several steps ahead have been made to enhance the machinability of aeronautic alloys, mainly titanium, nickel and cobalt base alloys, thanks to the introduction of innovative materials to produce high performance cutting tools. Furthermore, innovative lubricating strategies have been proposed and some of them are now adopted in industry such as Minimum Quantity Lubrication and High Pressure cooling. The efforts of the academic community have been mainly concentrated to improve the productivity of machining processes of aeronautic parts, reducing the tool wear when high cutting parameters are set and at the same time guaranteeing the quality of the final workpieces. With the introduction of Additive Manufacturing technologies, many of these challenges are overtaken due to the reduction of machining operation needed, however these processes have still to be monitored and optimized to improve the service life of the components, to limit the costs and to implement green and sustainable solutions. The first technical issue to assess regarding the research on machining operations deals with the machinability of materials used in a specific industrial application. At the moment, no published works can be found in literature dealing with the machinability of alloys produced by Additive Manufacturing such as Ti6Al4V, whether milling, turning or drilling operations are considered. As above mentioned, Additive Manufactured Ti6Al4V alloys manifest different microstructures and mechanical properties than standard wrought Ti6Al4V, hence they will behave differently during cutting processes, in other words they are characterized by a different machinability that needs to be investigated to set the correct process conditions. With regard to the production of AM surgical implants made of Ti6Al4V alloys, the machinability of these innovative materials should be known to improve their service life, which is quite a crucial task in biomedical applications, by limiting the surface defects and microstructural alterations that are left by the machining operation. This task corresponds to the first objective of the NEMO project. Traditionally, cutting operations are realised by adopting a lubricoolant flood to reduce the heat and the friction forces arisen in the cutting zone, to improve the tool service life and the surface quality of the final workpiece. Metal cutting fluids used as lubricoolant are generally prepared on the shop floor as water emulsions, mixing synthetic ore vegetable oils with water in a little volume percentage. The latest researches have proved their toxicity on the human body due to long exposure of machine tools operators with such fluids, risking serious breathe and skin health problems. Furthermore, they are expensive to dispose and dangerous for the ambient. Within the biomedical industries that produce surgical implants, they are still the first choice among other alternatives proposed by the academy, especially because Ti6Al4V alloy is renowned of being a difficult to cut material due to its low thermal conductivity and chemical composition. For this particular case, the extensive usage of traditional metal working fluids adds an additional and not negligible cost due to the cleaning and sterilizing operations that have to be carried out at the end of the manufacturing process to remove the chemical pollutants and the residuals released by the cutting fluid when the water portion evaporates. A cleaner, efficient and feasible metal working fluid or cooling strategy dedicated for machining AM Ti6Al4V surgical implants is the second main goal of the project NEMO. More in detail, the delivered cooling alternative should efficiently preserve the tool wear, improve the product surface

integrity, offer the possibility to enhance the mechanical properties of biomedical material with regard to fatigue, corrosion and fretting resistance and finally that guarantee the respect of the geometrical tolerances.

The latest researches in the field of machining, are now pointing towards the development of numerical models to simulate cutting processes, in order to reduce costly and time consuming experimental tests. In the last ten years relevant improvements have been done, with the development of numerical models based on the Finite Element Method that are not only capable of predicting the main cutting variables, such as the cutting forces and the cutting temperatures, but also some complex material phenomena that alter the surface integrity of machined components. Thanks to the availability of more powerful but at the same time more user friendly FE software's, the main difficulty encountered shifted from the mathematical implementation of the model to the right setting of the boundary conditions and the physical equations that govern the cutting process. However, the availability of reliable and solid material constitutive models that are able to describe the material behaviour under cutting process condition is still the Achilles' heel of numerical modelling of cutting processes. Many works have been published on FE models to simulate cutting processes of wrought Ti6Al4V alloy, but none of them regards the alloy produced by AM technologies. Being this material characterized by a different microstructure, these models need to be revised in order to take into account a different material behaviour. The last main objective of the research project is the development of a Finite Element numerical model capable to simulate the cutting operations on AM materials, offering the possibility to predict both the cutting variables and microstructural alterations.

The work presented in this thesis is concentrated on just one of the investigated AM biomedical alloys throughout the PhD, namely the Ti6Al4V alloy produced by Electron Beam Melting (EBM). All the research activities have been conducted in collaboration with Eurocoating S.p.a that has provided the materials, other than having made its facilities available for research duties.

The aim of the present work is to investigate the machinability of the alloy Ti6AL4V made by the Electron Beam Melting technique in turning operations through experimental and numerical approaches, proposing an innovative cooling strategy devoted to fulfil the biomedical requirements. In order to achieve this main purpose, the following main goals ca be distinguished:

- Design, implement and validate an innovative sustainable and clean cooling method, applicable for the turning operation of AM surgical implants.
- Qualify and quantify the machinability of EBM Ti6AL4V in semi-finishing turning, under different process conditions, such as different cutting parameters and lubricating condition.
- Validate the effects of this innovative cooling method on machined workpieces made of EBM Ti6Al4V, by performing sliding wear tests under physiological process conditions, and by qualifying the geometrical accuracy achievable in machining real surgical implants.
- Develop, implement and validate a FE code to simulate the cylindrical turning operation on EBM Ti6Al4V under different process conditions.

1.2. Overview of the dissertation

The work is organised in seven chapters:

The second chapter reports a literature review of the main topics afforded in this work. An overview on the latest scientific methodologies to investigate the machinability of materials trough experimental and numerical approaches is presented, reporting the main findings regarding wrought Ti6Al4V alloy. A particular emphasis is given to the alternative lubricating strategies to standard cooling methods.

The third chapter defines the experimental approaches, the methodologies and the instrumentations used to qualify and to quantify the machinability of EBM Ti6Al4V alloy in terms of surface integrity, tool wear and chip morphology. Furthermore, the cryogenic cooling apparatus developed and implemented in the CNC lathe as an innovative cooling approach is described.

The fourth chapter consists of the main experimental findings achieved by the turning tests to characterize the material machinability. The tool wear is quantified by means of SEM, EDS analyses and optical profilometery. The quality of the machined surfaces under different process conditions is defined through the measurement of surface roughness parameters, by analysing the surface defects through SEM scanning and optical profilometry. Finally the material microstructural alterations are examined by XRD analyses and micro-hardness measurements. This chapter evidences the main effects carried by the application of a cryogenic fluid to turn the EBM Ti6Al4V alloy.

The fifth chapter validates the applicability of the cryogenic cooling as a method to improve the machined surface integrity of biomedical components subjected to turning operations. Sliding wear tests of cylindrical pins turned under dry and cryogenic cooling on CoCrMo flat plates are performed with a tribometer reproducing the loads and the environmental conditions found in real hip replacements. The wear mechanism and the wear rate are defined by weight measurements, SEM analysis and surface roughness measurements.

The sixth chapter reports the numerical model developed (based on Finite Element Method) to simulate the turning process of EBM Ti6AL4V under different process conditions, the model is implemented in the commercial FE code STFC DEFORM 3D®. A simplified model is initially implemented and calibrated to predict the cutting forces and the cutting temperatures arising in the turning process, than this model is further sophisticated to predict microstructural alterations such as the grain deformations within the severe plastic deformed layer.

The seventh chapter finally introduce one of the first experimental works aimed at qualifying the geometrical accuracy achievable when cryogenic cooling is applied in turning a real industrial workpiece: the acetabular cup produced. The work individuates the main causes of thermal induced geometrical deviations by performing a preliminary testing on discretized test

specimens made with EBM Ti6AL4V alloy, the effect of cryogenic cooling is compared with dry and wet turning. In the end, a suitable machining strategy is proposed to make cryogenic cooling a feasible alternative for machining acetabular cups.

Chapter 2

Literature Review

2.1. Introduction

The analysis of the industrial and scientific problem starts with the literature review of the latest works that have afforded the ambitious challenge to machine difficult to cut materials. Before immerging into the recent advantages of machining wrought Ti6Al4V and the important attempts that have been done in the last twenty years to enhance its poor machinability proposing innovative tools materials and lubricating strategies, an overview on modern experimental approaches developed to investigate the machinability is presented. Beside more and more sophisticated experimental approaches being used in the most advanced research centres, numerical modelling of cutting processes is another important branch of the research to consider; hence it is examined in the last paragraph of this chapter giving emphasis of titanium alloys. Last but not the least, the current researches on innovative additive manufactured alloys and the understanding of their machinability is discussed.

2.2. Electron Beam Melting, the technology and its applications

In the recent years more and more companies are attracted by the innovative Metal Additive Manufacturing techniques to produce components that traditionally are made by casting or forging and machining. It is not surprisingly that nowadays big industrial companies operating in advanced industrial fields are investing millions of Euros on these technologies; in some cases they cooperate with the machine producers to develop and to improve their own customized machines. Among the power bed AM technologies available in the market, Electron Beam Melting (EBM) and Direct Melting Laser Sintering (DMLS) are those most employed and diffused. In the first case the core of the technology is based on an Electron Beam as a focused source of energy to melt the metal powder, while on the second one a Laser Beam is employed. In brief, the metallic part is printed layer by layer on a build table on

which the metal powder is spread. Each section of the part is accurately covered by a controlled high energy Electron Beam that scans and melts the powder locally. A schematic illustration of the EBM process is presented in Figure 2.2, meanwhile a detailed image of the internal structure of an EBM printer is showed in Figure 2.1.

The focusing system is an electron optical one substantially similar to a scanning electron microscope: an electron gun, operating in vacuum, generates a focused beam. The electrons are emitted by a tungsten filament heated at a temperature above 2500 °C, and accelerated through an anode. A first system of coils (magnetic field lens) brings the beam into focus, while a second system of deflection coils steers the beam. The beam deflection occurs in absence of moving parts: the electron beam gun is stationary. This delivers very high scanning speeds. Related to the involved energies, one of the most considerable difference between EBM and DMLS consists in the pre-heating of the powder. In Electron Beam Melting, in fact, before melting the gun preheats the powder layer using a relatively low beam current and a relatively high scan speed. This results in two effects. The most important is the reduction of the thermal gradient between the just-melted layer and the already built up body of the part [1]; as a consequence, the substantial high temperature maintenance allows the reduction of residual stresses. Preheating also allows the partial sintering of the powder, which holds it in place during the subsequent melting. Pre-heating has another eminent effect: it assists, in terms of energy, the re - melting of the just consolidated underlying substrate, allowing the incomplete homologous wetting due to oxide films to be avoided [2].

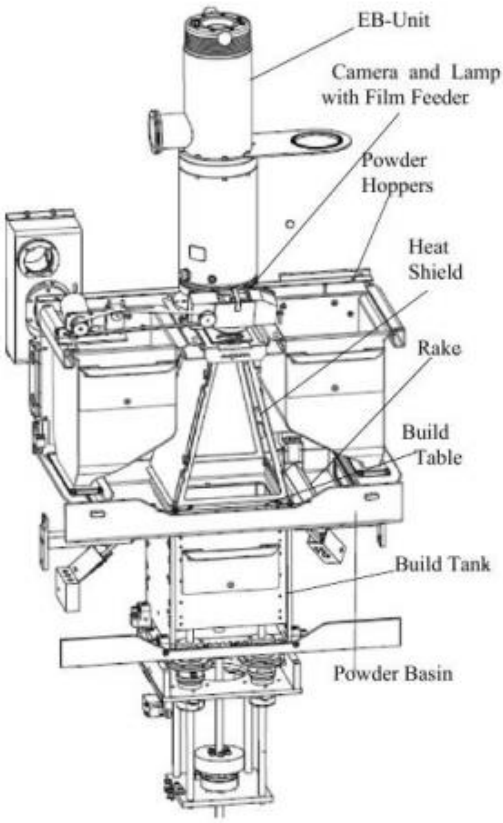

Figure 2.1 Internal layout of an EBM printer.

Moreover, Electron Beam Melting process takes place under high vacuum. This prevents a loss of energy that would be caused by the collision between the fast moving electrons and the

gas molecules (making the process 95% energy efficient). As an immediate result, vacuum prevents the absorption of atmospheric impurities.
Because of the dimension of the melting pool and the accuracy of the beam, the surface finishing of the part produced by EBM is less refined than the one obtained by DMLS [3]. A finishing operation is practiced through a sand blasting after the process; this removes from the partially sintered particles from the surface. The blasting is carried out using the same powder involved in the EBM process, in order to avoid contamination and recover the removed powder, which is sieved and recycled (up to 95%) in the process. Parts are built up on supports, for facilitating the removal of the parts themselves after the building. Because they are constituted by partially sintered powder, the supports are easy to remove (also by hand).The powder employed in EBM, as well as that used in DMLS, is pre-alloyed and does not contain additives or binders (as a consequence, no heat treatment is required for removing them; after building, the part has full density). The powder has a retained chemical composition due to the vacuum level in the chamber, the very small melted volume and the rapid cooling from melted metal to solid state. The layer thickness in EBM technologies is usually larger than in SLM.

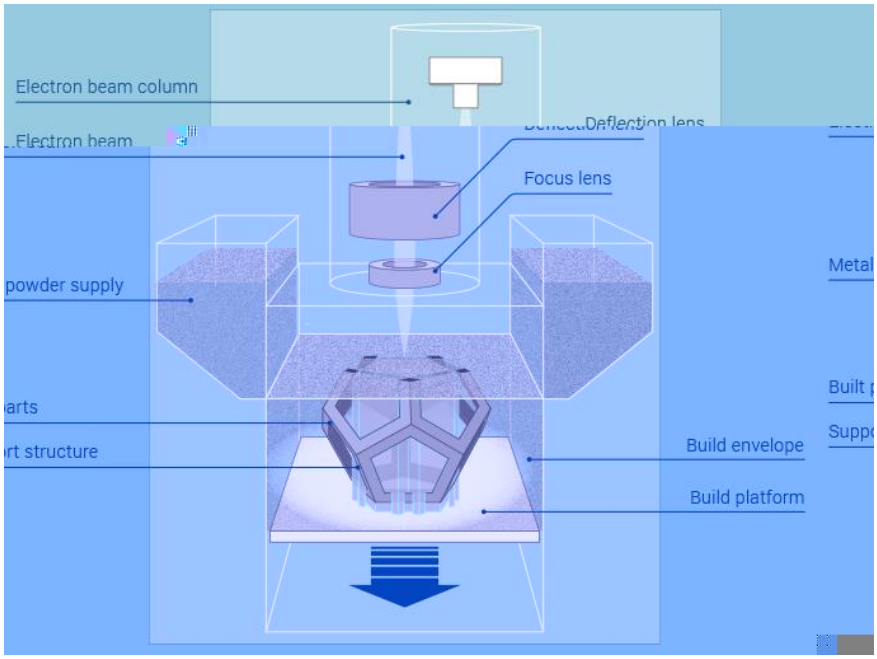

Figure 2.2 Schematic illustration of the Electron Beam Melting process.

Advantages:

- Ability to achieve a high energy level in a narrow beam.
- Vacuum melt quality can yield high strength properties of the material.
- Vacuum environment eliminates impurities such as oxides and nitrides.
- Permits welding in refractory metals and combinations of dissimilar metals.
- No tooling required – unlike castings.
- Performed in a hot powder bed – allows for complex shapes, ages as part of process, and no induced residual stresses.
- Melting takes places in seconds – extremely fine grain size.

- Powder utilization nearly >90%.
- If compared with DMLS a higher efficiency in generating the beam of energy resulting in lower power consumption as well as lower maintenance and installation costs.
- High actual overall power resulting in high building speeds.
- Deflection of the beam can achieved without moving parts resulting in high scanning speed and low maintenance.

Disadvantages:

- Requires vacuum which adds another system on the machine which rises the costs and must be maintained
- Electron beam technology produces X-rays during operation (Solution: The vacuum tank shields the rays perfectly if properly designed).

This technology has been firstly developed by surgical replacements producers that during the first years of the 2000's, they experimented and implemented these technologies in their production sites[4,5]. Later on, some aeronautic industries started to develop new concepts for aero engine parts such as the fuel nozzles and the turbine and compressor blades, or structural components designed to be built by AM technologies, such as EBM. In the very recent years, some important companies operating in the automotive field are also investing in these technologies to create innovative complex components (mainly destined for super cars or racing cars). Up to now, because of the applications where this technology has been applied and investigated, the following metal alloys have been developed to be 3D printed by EBM technology:

- Ti6Al4V
- Ti6AL4V ELI
- ASTM F75CoCrMo
- Titanium Grade 2
- Nickel alloys (Inconel 718, Inconel 625)
- 17-4PH SS and 316L SS
- Tool Steel (H13)
- Invar
- Titanium aluminide
- 7075 Aluminium alloy

The latest advantages in the field of material development for Electron Beam Melting process present exotic applications with high purity copper, high purity niobium and other specifically designed materials for aerospace applications such as GRCop-84.

2.3. Ti6Al4V alloy produced by Electron Beam Melting, a comparison with wrought Ti6Al4V

Wrought products account for 70% of the titanium and titanium alloy market [6]and among those the Ti6Al4V (martensitic α+β alloy) is the most widespread titanium alloy (major than 60 % of all titanium alloys produced in USA and EU), thanks to an high biocompatibility, high corrosion resistance, high mechanical properties up to 600°C and a very low density. At room temperature, the microstructure of pure titanium consists of 100 % alpha. For α + β alloys, when α and β stabilizers (such as aluminium and vanadium) are added as alloy constituents, the beta phase begins to appear at grain boundaries [6].Other alloying elements can be added, and each alters the α → β transition temperature. When α stabilizers are added (such as aluminium), the α → β transition temperature is increased, and when β stabilizers are added (such as vanadium), the α → β transition temperature is decreased. For instance, for pure titanium, the transition temperature is 885 ◦C, and for the Ti6Al4V alloy the transition temperature increases up to 995 ◦C. In the case of the Ti6Al4V alloy, thermomechanical processing also has an effect on the amount of β phase in the final microstructure (an example is appreciable in Figure 2.3), where the percent of the β phase increases with increasing process temperature in the α + β phase, with 100% β formation when processed in the β phase, with or without deformation.

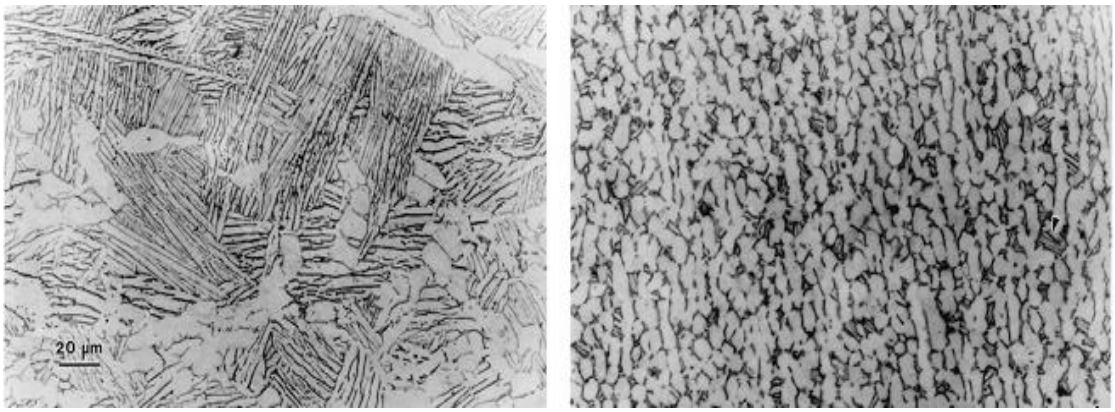

Figure 2.3 Effect of the thermomechanical process on the microstructure of wrought Ti6Al4V alloy: on the left a bimodal α+β microstructure, on the right a globular α+β microstructure.

In order to understand the peculiar microstructure that characterizes the Ti6Al4V alloy made by Electron Beam Melting, it is fundamental to clarify the effects of cooling rate from β phase on the material microstructure at room temperature.
Depending on the desired mechanical properties, the following heat treatments can be applied to Ti6Al4V alloy: partial annealing (600 ÷ 650 °C / 1h), full annealing (700 ÷ 850°C / furnace cooling to 600 °C / air cooling) or solutioning (880 ÷ 950 °C / water quenching) and ageing (400 ÷ 600 °C) [7]. Phase composition of titanium alloys after cooling from β phase range is controlled by the cooling rate. Kinetics of phase transformations is related to the value of β-phase stability coefficient Kβ resulting from the chemical composition of the alloy [8].One important characteristic of the alloy is a range of α+β→ β phase transformation temperature that determines conditions of thermomechanical processing intended for development of

suitable microstructure (Figure 2.4). Start and finish temperatures of α+β→ β phase transformation, vary depending on the contents of β stabilizing elements (Table 2.1).

Table 2.1 Start and finish temperature of the α+β → β phase transformation for selected titanium alloys (vh = vc = 0.08°C s-1) [8].

Phase transformation	**Alloy**	
Temperature [°C]	**Ti-6Al-4V**	**Ti-6Al-2Mo-2Cr**
$T^{ns}_{\alpha+\beta\rightarrow\beta}$ $T^{f}_{\beta\rightarrow\alpha+\beta}$	890	840
$T^{ps}_{\alpha+\beta\rightarrow\beta}$	930	920
$T^{f}_{\alpha+\beta\rightarrow\beta}$	985	980
$T^{s}_{\beta\rightarrow\alpha+\beta}$	950	940
$T^{f}_{\beta\rightarrow\alpha+\beta}$	870	850
ns – nucleation start	s – start	
ps – precipitation start	f – finish	

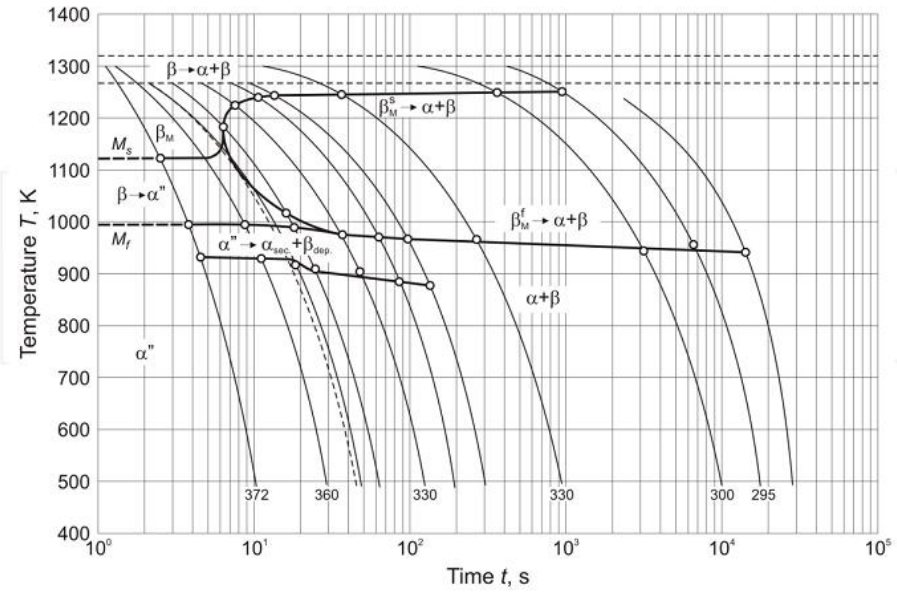

Figure 2.4 CCT diagram for Ti6Al4V alloy [8].

Cooling Ti-6Al-4V alloys from above β transus temperature at the rate higher than 18°C s-1 leads to development of martensitic microstructure consisting of α'(α") phases. Start and finish temperatures of the martensitic transformation β→ α'(α") or β→ α" do not depend on cooling rate but on β-stabilizing elements content and decrease with increasing Kβ value. For the intermediate cooling rates, down to 3.5°C s-1, martensitic transformation is accompanied by diffusional transformation β→ α + β and the volume fraction of martensitic phases decreases to the benefit of stable α and β phases. Cooling rates below 2°C s-1 lead to a diffusion controlled nucleation and growth of stable α and β phases in the shape of colonies of parallel α-phase lamellae in primary β-phase grains. The important parameters for a lamellar

microstructure with respect to mechanical properties of the alloy are the β-grain size, size of the colonies of α-phase lamellae, thickness of the α-lamellae and the morphology of the interlamellar interface (β-phase). Increases in cooling rate leads to refinement of the microstructure – both α colony size and α-lamellae thickness are reduced. Additionally new colonies tend to nucleate not only on β-phase boundaries but also on boundaries of other colonies, growing perpendicularly to the existing lamellae. This leads to formation of characteristic microstructure called "basket weave" or Widmanstätten microstructure, an example is reported in Figure2.5 [9].

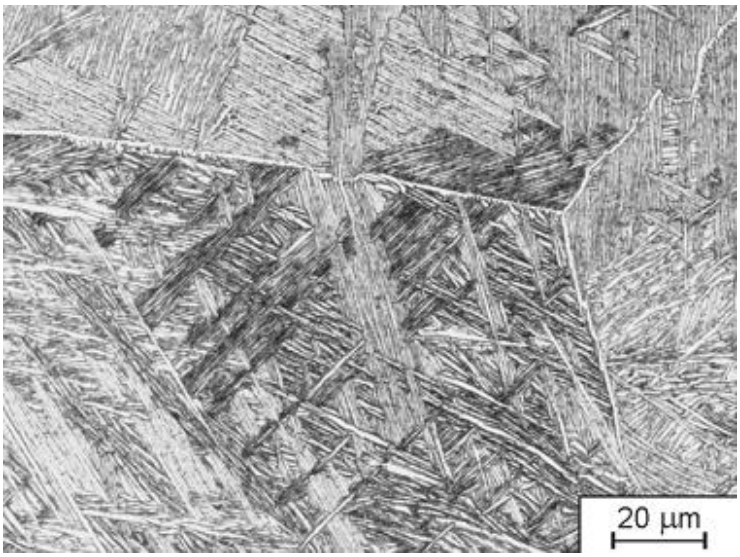

Figure 2.5 "Basket-weave" or Widmanstätten microstructure of wrought Ti6Al4V alloy after cooling from β-phase range at the rate of 9°Cs^-1 [8].

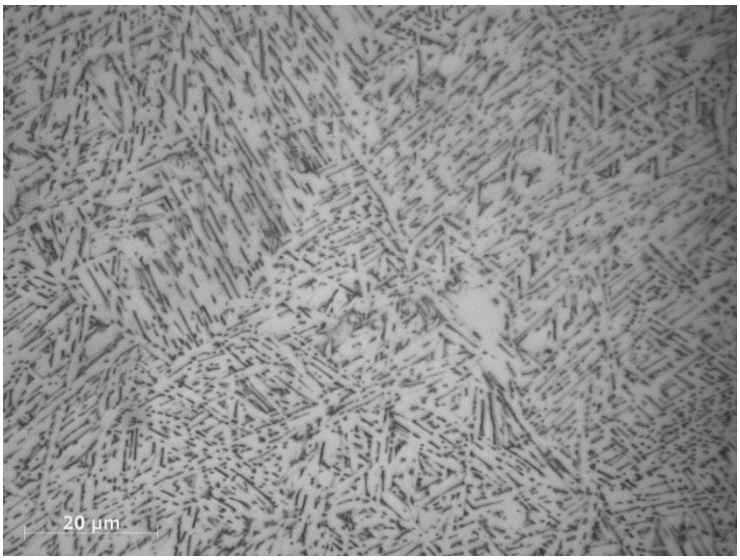

Figure 2.6 Microstructure of the as built Ti6Al4V EBM normal to the building direction.

Bearing these metallurgical considerations in mind and by considering the process characteristics of the Electron Beam Melting forming technology, the microstructure of the as built alloy presented in Figure 2.6 can be more easily understood. During wrought products processing, the microstructure is globular-lamellar, since the cooling rate is slow and

combined with the presence of mechanical deformation, on the contrary during Electron Beam Melting process the cooling rate is high and no mechanical deformation is over imposed on the workpiece, as a consequence it is not surprisingly that fine microstructures are achieved. By observing the Figure 2.6 that shows the Electron Beam Melted Ti6Al4V alloy microstructure, it consists of α-phase fine lamellae, organized in a basketweave morphology. This microstructure is the result of the rapid solidification and the subsequent annealing due to the temperature of the working zone. It is reasonable to hypothesize that, at first, a martensitic hcp phase forms, since the large undercooling promotes the formation of a metastable phase through a non-diffusive mechanism. Then, the permanency at a temperature above 600 °C makes the stabilization of the microstructure possible. As an evidence of this interpretation, Facchini et al.[10] found the sporadic presence within microstructure, of areas showing pre-existing martensitic packages, but coarse needles. He carried out an XRD analysis on the as built alloy, finding a pattern that showed the presence of a of 7% of bcc β phase in an hcp matrix. He concluded that , because of the pre-heating at an average temperature between 600 °C and 700 °C, the formerly produced martensite (the solidification rate of the melting pool is very high) is then transformed in an α+β mixture by the soaking at the process temperature [11].
As a consequence of the peculiar microstructure originated by hot working and Electron Beam Melting forming processes, different mechanical properties are originated as listed in the Table2.2, therefore a different machinability can be expected between Wrought and EBM Ti6Al4V alloys.

Table 2.2 Comparison between the mechanical properties of wrought and EBM Ti6Al4V alloys.

Material	**E [Gpa]**	**UTS [Mpa]**	**YS [Mpa]**	**Elongation (%)**	**HRC**
EBM Ti6Al4V	120	965	910	13.1	35
Wrought Ti6Al4V	118	872	790	16	31

2.4. Recent approaches in evaluating the machinability of metallic alloys

Within the development of modern high productive CNC machines, and the growing demand for high productions of mechanical components that requires more and more complex geometrical features to be machined, the study of the materials machinability has become of crucial importance in the last 40 years. There are industrial sectors, such as the aeronautical one, in which machining operations are often the bottle neck of the entire manufacturing process chain, mainly because exotic alloys are employed as main materials to realise aero engine components, such as nickel, titanium and cobalt base alloys. In the last decades, it has been proved by many researchers that these alloy families present quite a poor machinability and many efforts are currently being made to enhance it. Two main important targets can be identified: the improvement of production rates in parallel with the improvement of the final product quality that can be more technically translated as the necessity to guarantee a certain surface integrity for the final products. The university research, in collaborations with the

main tool's manufacturers brands and in some cases with alloys producers, have made giant steps in defining the modern methods and approaches to investigate the machinability of the materials. The development of more and more powerful computers and numerical software packages based on the Finite Element Method, has provided researchers the possibility to investigate the materials machinability performing numerical simulations of cutting processes. A dedicated paragraph is discussed later in this chapter. Before analysing the recent advantages in the field, it is necessary to give a general definition of the machinability. According to its classical definition, the machinability is a general term used to rate the ease of machining a material relatively to the tool life, the surface finish produced and the power consumed. Although this definition might appear quite simple, it depends on the material properties, its interaction with the tools materials and its chemistry. According to that, the main methods applied to investigate the material machinability can be classified into three main families, the first regards the study of the tool wear mechanisms and the tool life, the second regards the analysis of the machined surface integrity and the third one the on line measurements of machining parameters such as the cutting forces, the cutting temperature and the acoustic emission. Being the cutting process a complex phenomenon with several variables playing their own effect, all the analysis and the variables observed have to be correlated together. It is noteworthy that a comprehensive analysis of the machinability should integrate them to provide a complete picture of the phenomenon. In the following paths, a literature review regarding the state of the art in terms of the experimental approaches conducted to investigate the titanium alloys machinability is presented.

2.4.1. Experimental methods used to investigate the surface integrity

The Surface integrity can be defined as the surface condition of a workpiece after being altered by a manufacturing process. There are experimental methods to evaluate the surface integrity; some can be applied directly at the shop floor, during the production process while others need complex laboratory facilities and instrumentations. The first indication of the product surface integrity can be gained by measuring the Mean Surface Roughness Ra or other metrological parameters such as Rz or Rt according to the standard ISO4287 [12]. Its measurement is carried out with a portable or fixed Roughness Tester. The Mean Surface Roughness Ra is principally influenced by the cutting parameters in both milling and turning operations, namely the cutting speed, the feed rate and the depth of cut. Although a better surface integrity (lower surface roughness) might generally correspond to lower cutting parameters, it is not surprisingly that in some cases the surface roughness trends present fluctuations and unexpected increments or decrements linked to the tool wear condition and the other variables such as the chip flow evacuation.

Che Haron et al. [13] investigated the machinability of the Ti-6Al-2Sn-4Zr-6Mo alloy in dry turning, adopting uncoated cemented carbide tools and maintaining a constant depth of cut equal to 2 mm, testing four values of cutting speed: 45 m/min, 60 m/min, 75 m/min, 100 m/min and two values of feed rate: 0.35 and 0.25 mm/rev. With regard to the cutting speed effect, the lower surface roughness of 3.2 μm was achieved by adopting a cutting speed equal to 60 m/min in the first stages of the machining operation for a feed rate adopted equal to 0.25 mm/rev, reaching the minimum value after one minute of machining under such cutting condition. When the lowest cutting speed equal to 45 m/min was set, higher values of Ra

concentrated around 4 μm were measured in the first stages of machining. When the feed rate was lowered, the surface roughness values condensed around a value of 2.3 microns. In machining operations that produce periodic surface textures, as for the case of turning, the surface roughness in mainly influenced by the feed rate and by the tool nose radius, because the latter directly alters the pitch of the helical profile that forms the surface texture, nevertheless the cutting speed can exert an influential effect in high speed turning of difficult to cut materials, an example is reported in Figure 2.7.

Ibrahim et al. [14] found an increment of more than 100 % in the surface roughness values when setting a cutting speed equal to 55 m/min and an adopted depth of cut equal to 0.2 mm in turning Ti6Al4V ELI under dry cutting conditions and maintaining a fixed tool nose radius equal to 0.4 mm. According to his main findings, the increment of the cutting speed provoked a contraction of the trends with a general lowering of the Ra values for the cutting speeds of 75 and 95 m/min within the advancing of the turning process. He ascribed this trend to the increasing tool wear provoked by the increment of the cutting speed and of the cutting length that amplified the tool nose radius, lowering the average values of Ra.

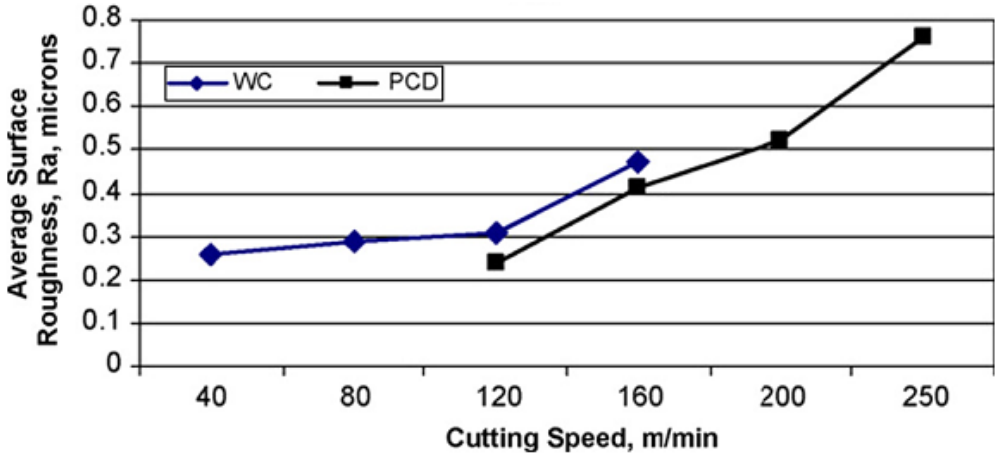

Figure 2.7 Effect of the cutting speed on the surface roughness in rough turning wrought Ti6Al4V alloy with two different cutting tool materials (Vc = 40 – 160 m/min, f = 0.1 mm/tooth, DoC = 1mm [15].

The tool wear influences the surface roughness of the machined components, thus as it is often performed at shop floor level, measuring the surface roughness can give a direct indication on the tool wear state. According to several experimental investigations [15], when the tool is fresh, the surface roughness values are found to be higher than with slightly used tools, and the tool wear close to its half-life generates slightly lower surface roughness values than its fresher times. This effect can be considered as the 'warming up' of the tool material, because when the tool is first used, there can be micron-level sharp edges or peaks at its surface that can be trimmed out to create a smoother, or at least a better fit contact surface with the workpiece. When approaching its half-life, the tool is more fit to the workpiece; hence the surface roughness values decrease. However, after the half-life, the tool starts wearing even more, and this causes anomalies in the tool-workpiece contact surface, which increases the surface roughness values significantly.

Among the cutting parameters, the depth of cut affects the surface integrity less than the others. There are no congruent experimental findings on its behaviour, and contrasting results have been found. Some researchers found that for some materials and cutting conditions when the depth of cut was increased, surface quality lowered [16], whereas other researchers disagreed by showing that for other materials and cutting conditions, depth of cut does not have a significant effect on surface roughness [17].
As previously stated, the metrological parameters are quite simple to define and measure, but at the same time they provide scarce information's on surface integrity. Modern laboratories and research centres are now provided by optical profilometers to digital scan the surface topography of components. These measuring instruments were initially based on contact techniques, but with the advancement of electronic and optical technologies, non-contact instruments became more and more popular thanks to their higher sensibility and the offered possibility to avoid direct contact with the features to be measured. The most advanced profilometers available in the market are now based on white light interferometry with confocal and focus variation techniques. The power of such technique, a part of providing the 3D digital image of the surface, is to provide the possibility to perform measurements on the acquired points coordinates. The use of digital profilometry to investigate the surface integrity of machined surfaces, found its first applications during late nineties and in the first years of the 2000s decade.

Ibrahim et al.[14] acquired the surface topography generated by fresh and worn tools, when turning Ti6Al4V ELI with multi-layered coated carbide inserts in dry cutting conditions, testing the effect of the cutting parameters: three values of cutting speed (55, 75, 95 m/min), three values of feed rate (0.15, 0.25, 0.35 mm/rev) and three values of depth of cut (0.1, 0.15, 0.25 mm). In this work, he found some peaks and deeper grooves due to the feed rate effect as showed in Figure 2.8, more in detail smoother surfaces were acquired for the lowest feed rate tested equal to 0.15 mm/rev, while rougher surfaces corresponded to the highest feed rate equal to 0.35 mm/rev. For the same tested cutting conditions, the lowest and the highest values of surface roughness were measured respectively, stating that there is a strong correlation between the machined surface topography and the surface roughness parameters.

Ginting et al.[17], deeply characterized the surface integrity of Ti6242S alloy in dry milling, comparing the performances of coated (TiC+TiN+TiCN) and uncoated carbide mills, adopting the following cutting parameters: cutting speed Vc of 100 – 125 m/min, feed rate f of 0.15 – 0.20 mm/ tooth, axial depth of cut a_z of 1.5 – 2.5 mm, and radial depth of cut a_r of 8.8 mm. The surface quality was measured and observed using a profilometer and a confocal optical microscope equipped with laser tracer for providing a 3-D image of surface topography. Samples of the machined surface with an area of 2x1.5 mm were acquired. From the main observations, it could be seen that the average values of Ra (0.50 microns for the uncoated tool and 0.59 microns for the coated one) resulted by low-amplitude topography, calculated as the difference between the peak and the valley of the machined surface. He finally concluded that the smaller the amplitude observed by 3-D surface topography, the more uniform is the surface roughness. By examining all the machined surface samples for all

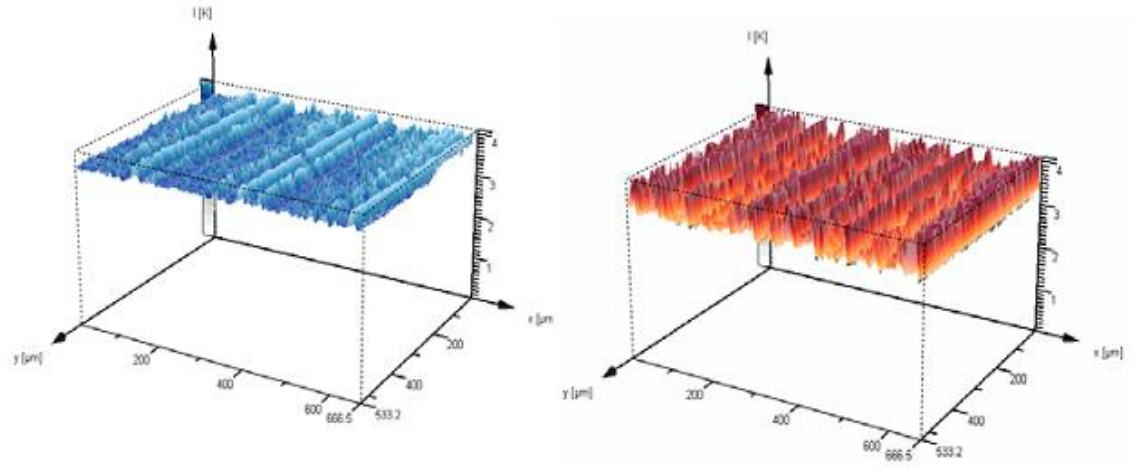

Figure 2.8 Surface Topography of turned Titanium Alloys Ti-6Al-4V ELI by using coated cemented carbide cools; (a) at cutting speed of 55 m/min and feed rate of 0.25 mm/rev (b) at cutting speed of 95 m/min and feed rate of 0.35 mm/rev [14].

the cutting conditions tested, none of them was characterised by high peak to valley amplitudes, maintaining the Ra below an average value of 0.8 microns.
Modern profilometry techniques, have been used to investigate the presence of surface defects on the machined surfaces, highlighting the presence of feed marks defects and material depositions coming from the chip flow or material particles detached from the built up layer (BUE) that is often present in machining sticky materials such as aluminium or titanium alloys.

Devilez et al. [18]used a Veeco NT 1100 (Wyco®) optical profilometer based on the white light interferometry technique with a resolution of 2nm on the optical Z axis to investigate the surface topography generated in semi-finishing turning of Inconel 718 under dry and wet lubricating conditions. Irregularities between the feed marks were observed on the 3D scanned surfaces that corresponded to portions of the BUE (Built-up Edge) and of the BUL (Built-up Layer) detached by the chip flow due to the higher cutting temperatures than wet machining and by the presence of high cutting pressures taking place on the tool tip. These thermo-mechanical conditions that are commonly generated by the absence of the coolant increase the material plasticity, thus the adhered material layers on the tool cutting surfaces can be plastically deformed more easily, provoking surface defects on the machined parts. As a proof of that, he found no material depositions on the feed marks under wet cutting conditions, because of the lower cutting temperatures, leading to a better surface integrity. Thanks to the very high resolution of modern profilometers, their use in the surface integrity characterization of machined surfaces can enhance the quality of the analysis, offering the possibility to find other kinds of surface defects that would be difficult to find by means of more traditional instrumentations, such as surface profilers. This is the case of the material side flow phenomenon that was also observed by Devilez et al. [18] in the same work, as shown in the Figure 2.9. This peculiar surface defect that can be observed in turning operations only, due to the periodic surface texture generated. It was firstly explained by Kishawy and Elbestawi et al.[19] In particular, when the chip thickness is lower than a minimum value, the workpiece material is ploughed, squeezed and deformed plastically by the tool nose, moreover it is facilitated by the wear occurring on the tool trailing edge where the plastic deformed material fills the grooves, leaving double marks. Another important technique used by researchers to characterize the surface quality of machined components, is based on the direct observations of samples by means of a Scanning Electron Microscope (SEM) at high magnifications that otherwise cannot be achieved with optical microscope techniques. The availability of different detectors to carry out the analysis, namely the ETD and BSED detectors, facilitate the researchers to find the presence of surface defects such as

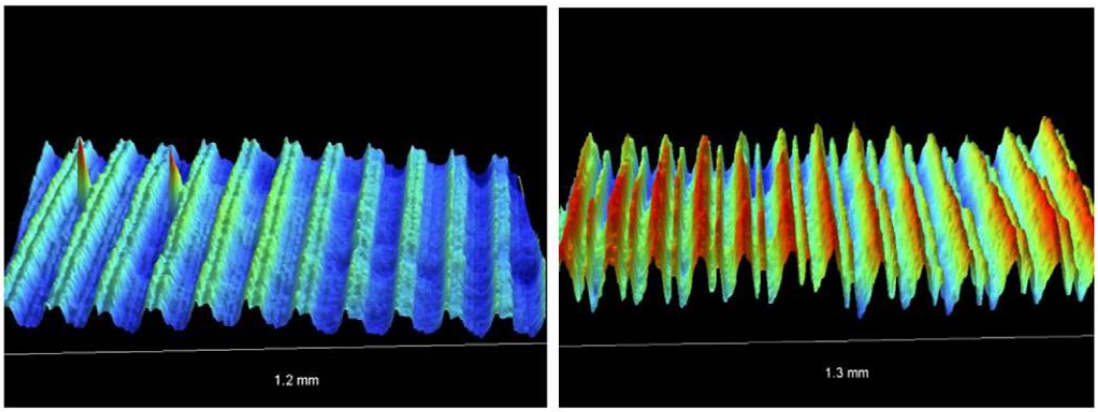

Figure 2.9 Surface quality observations under dry on the right and wet on the left lubricating condition in semi-finishing turning of Inconel 718, using the white light interferometry technique [18].

micro cracks, laps, tearings, carbide cracking, folds, smearings etc. [15]. This analysis can consequently give a qualitative indication on the affected fatigue resistance of machined surfaces, if different cutting parameters or different tool wear regimes are compared.

Gining et al. [17], performed SEM analysis to find the main defects arising during dry milling of Ti6242S alloy testing two different uncoated carbide mills under dry cutting conditions. For all the tested machining conditions, he found tearings randomly distributed on the surface texture as can be noticed in the Figure 2.10. He ascribed this surface defects to the three bodies contact generated into the tool workpiece interface because of the presence of small parts removed from the cutting tool that are peeled off forming the tool wear, and portions of the Built-Up Edge (BUE) which is deposited on the machined surface. Since both of these kind of particles are harder than the workpiece material, they cause scratches and tears on the machined surface due to the relative motion between the tool and the workpiece. In this analysis, he observed another kind of surface defect that is common when machining Titanium alloys because of their sticky tendency. He revealed the presence of chip layer formations welded on the surface when the tool wear drastically deteriorated under dry cutting conditions, that they called it BUL. Portions of the adhered workpiece material on the tool cutting surfaces are in fact detached and deposited on the machined surface by the chip flow, leaving a welded particle on the feedmarks. Usually the SEM observation of surface defects is carried out on small portions of the machined surfaces to highlight the effects of the tool wear and of the cutting parameters on their specific kind, on their average dimension and distribution. In most of the cases this analysis does not follow a structured approach but it is conducted randomly, nonetheless in very few works a comprehensive classification of the surface defects is presented. Among these works, Zhou et al. [20]investigated the surface damages in high speed turning of Inconel 718 using whisker reinforced ceramic tools under wet and dry cutting conditions. He tested three values of cutting speed: 100, 200, 300 and 400m/min respectively and two levels of feed rate: 0.1, 0.15, 0.2 mm/rev respectively adopting new, semi-worn and worn tools. He proposed a solid statistical method to quantify the presence of each kind of surface defect in a fixed scanned area of 15x10 mm, by calculating the ratio between the damaged area and the total observed area in the case of: material side flow, Built-Up-Edge, tearing and chip debris, while in the case of carbide

cracking and cavities the ratio between the number of cracked carbides and the number of total observed carbides was calculated. By doing so, he proposed a quantitative method instead of a qualitative one, which might be useful to give direct indications on the fatigue resistance of the final workpiece due to the amount of surface damage.

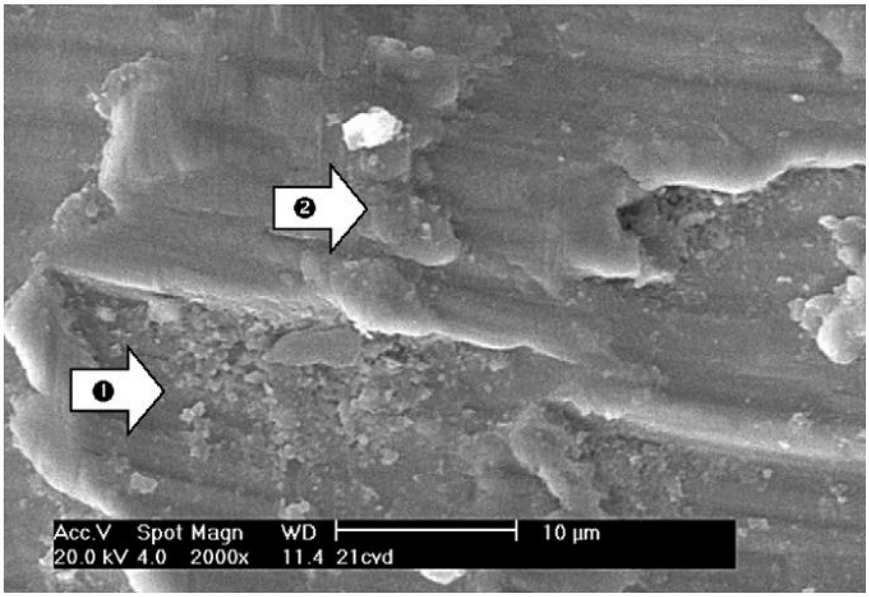

Figure 2.10 Tearing on the surface subjected to dry milling of Ti6242S [17].

Machining operations are renowned to affect the mechanical properties of machined components, altering their surface topography and their mechanical and metallurgical properties within the surface layers [21], as a consequence the fatigue resistance is affected by means of the machining process. Thus, it is of fundamental importance to investigate the effects of machining operations not only on the surface topography but even on the material microstructures. The main experimental approaches to quantify the amount of machined induced microstructural alterations are based on the measurement of the residual stresses along the main cutting directions, on the measurement of the micro or nano hardness along the radial direction beneath the machined surface and on the evaluation of the microstructural alterations such as the grain refinement, the formation of the white layer and the induced grain deformations by means of metallographic techniques. Many works that include these analyses are present in literature regarding different tested materials, different lubrication strategies and different cutting parameters [15], nonetheless among aforementioned methods, measuring the residual stresses is the most important one.

After the machining process, the workpiece material is released from the thermomechanical loads exerted by the tool, but not all of the generated energy can be retrieved. A portion of it is spent for plastic deformation, which causes the material to exhibit some stresses, especially at its surface. These stresses that remain in the material after the loading is removed are the so called residual stresses. They are considered to be caused due to mainly tensile plastic deformation in the subsurface of the workpiece material and thermal effects at the surface due to cutting and tool conditions [22]. These residual stresses present potential risk in terms of crack initiation, propagation and fatigue failure of end products, and it is necessary to remove tensile surface residual stresses or prevent them from occurring during machining processes. The most used technique to measure the residual stresses beneath the surface of metallic

portions is based on the XRD technique using the $\sin^2\psi$ method [23]. Nonetheless this method is based on a solid theory and the experimental approach is well consolidated, residual stresses profiles are nowadays still hard to measure and controversial results are found in literature. Many researchers claim that surface residuals stresses are tensile while others claim they are compressive [15]. What actually complicates the measuring method is the need to remove layers of materials as much precise as possible without altering the effective stress state present into the microstructure; hence electro-polishing methods are used. In practical the surface layers are electro polished for a certain etching time removing a desired amount of material; nonetheless the precision of this removing process is poor.

With regard of the wrought Ti6AL4V alloy, Sun and Guo et al. [24] tested the effects of the cutting parameters on the residual stresses in end milling of Ti6Al4V alloy adopting an uncoated carbide mill under water soluble cutting fluid. They measured the residual stresses along the main cutting directions that characterize the milling operation: along the feed direction, normal to the milled surface and along the cutting direction. In this work, they found that compressive residual normal stresses along cutting and feed directions increased with cutting speed and manifested a maximum around the cutting speed of 80 m/min. The compressive residual normal stress along the feed direction was about 30 % larger than the one along the cutting direction. The magnitudes of residual shear stresses were much smaller than those of the residual normal stresses. Moreover compressive residual normal stresses decreased in general with the feed rate.

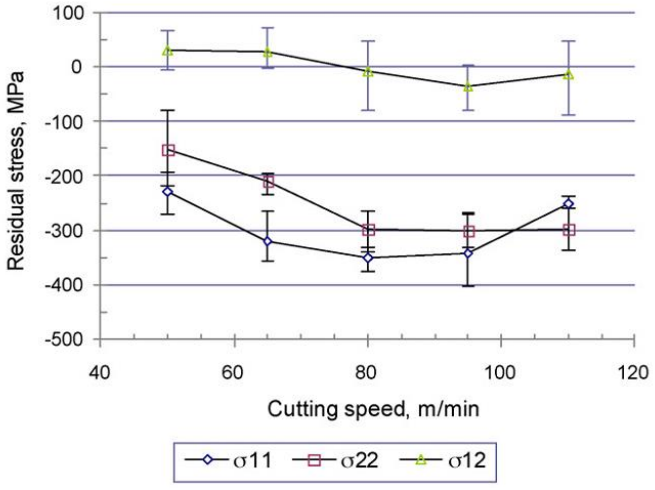

Figure 2.11 Residual stress changes with cutting speed in end milling of Ti6Al4V with coated carbide tools at V = 50 – 110 m/min, f = 0.06 – 0.14 mm/tooth, and doc = 1.5 mm [15].

The highly nonlinear coupling of mechanical and thermal loading determined the characteristics and magnitudes of residual stress profiles as showed in Figure 2.11.

Nieslony et al. [25] measured the residual stresses when turning the Ti6Al4V alloy with a coated tungsten carbide insert at the fixed cutting speed of 80 m/min, varying two levels of feed rate (0.05 and 0.2mm/rev) respectively and adopting two levels of depth of cut, equal to 0.125 and 2 mm. According to its finding, tensile residual stresses were measured on the surface layers for almost all the tested cutting parameters at a depth beneath the machined surface equal to 15 microns, the highest values resulted along the cutting direction meanwhile

lower values were always found along the tangential one. Among the cutting parameters, the depth of cut in practise did not influence the residual stresses values meanwhile on the other hand the most influential factor was the feed rate.
A faster and easier experimental investigation that can be carried out in laboratories to outline the machining effects on the material microstructure, is achieved by measuring the micro-hardness trend along a normal direction with respect to the machined surface, indenting the material at growing depths in several positions maintaining a fixed or a variable pitch. Commonly, the micro - hardness indenters provide Vickers hardness values, and thanks to the newest electronic controlled instruments, fast but reliable hardness profiles can be acquired quite easily. This analysis gives important information on possible metallurgical changes that occur during the cutting process, such as aging and work-hardening.

Che Haron et al. [13]measured the micro-hardness of turned test pieces made of Ti-6Al-2Sn-4Zr-6Mo alloy, under dry cutting conditions and setting semi-finishing cutting parameters. Two values of feed rate, 0.25 and 0.35 mm/rev and four values of cutting speed 100, 75, 60, 45 m/min were tested maintaining a fixed depth of cut equal to 2 mm. He found higher hardness than the bulk value for all the tested cutting conditions at a depth of 0.01 mm. A drop in the hardness below the bulk level was than observed at the depth of 0.02 mm. He ascribed this phenomenon to the material softening that was probably provoked by the over-ageing of the titanium alloy as result of very high cutting temperature produced at the local surface. The hardness values increased drastically at the depth of 0.07 mm below the machined surface as can be seen in Figure 2.12 meaning that strong work hardening took place under all cutting conditions in this zone. Sensible improvement of the micro-hardness was also noticed for higher values of the feed rate and when worn tools were used in the machining tests.

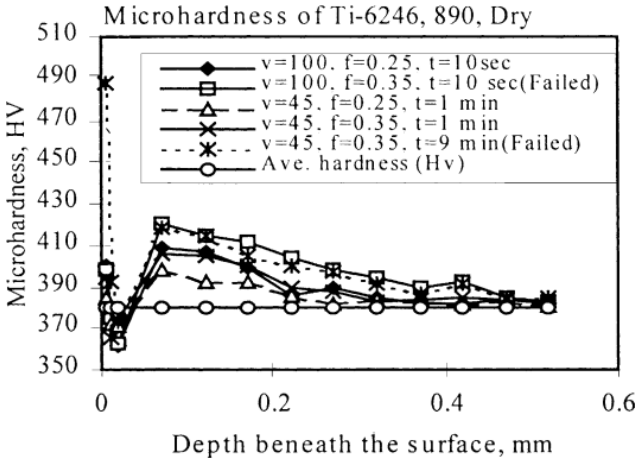

Figure 2.12 Effect of the thermal softening and of the work hardening on the micro - hardness value beneath the machined surface when turning Ti6Al4V alloy in rough machining condition [13].

Sun and Gou et al. [24], measured the Knoop micro-hardness of dry end milled Ti6AL4V alloy specimens under wet lubricating conditions, focusing the research of material alterations inside the first 100 microns beneath the machined surface. They found higher surface hardness varying from 1350 and 1500 HK than the stable bulk hardness equal to 800 HK, highlighting an increment of around 70 % induced by the surface deformation. Furthermore,

the higher the cutting speed, the lower resulted the hardness, because of the stronger thermal softening effect generated by the highest cutting temperatures.
In parallel with the micro-hardness and residual stress measurements, the visive observations and the measurement of grain deformations arose during the cutting process is necessary to accomplish a more comprehensive investigation. The thermal and mechanical loads exerted by the cutting process tend to deform the microstructure on the surface layers of the machined component, and in some cases when sever cutting conditions are applied, recrystallization and the formation of white layers are noticed. Different scale of analysis can be carried out by adopting different instrumentations such as optical microscopes, Scanning Electron Microscope (SEM) and Transmission Electron Microscopes (TEM). In the first case, etching the machined workpiece is necessary to put in evidence the grain boundaries, meanwhile on the other cases no etching is needed, but the specimen preparation requires more complex techniques. Several different cases of such kind of analysis can be found in literature with regard of microstructural analysis to highlight the material alterations occurring when machining metallic alloys [26].

Zou et al. [27] studied the surface damages caused by turning NiCr20TiAl alloy under rough cutting conditions with a coated carbide tool. He estimated the work hardened sub-surface layer by using an inverted metallurgic microscope. He found severe bending of the grain boundaries disposed in parallel along the cutting speed direction, moreover he discovered the negative effect imparted by the presence of hard carbide particles that do not deform easily and they break when the tool motion deform the surface material, or else cracks were formed around them affecting the fatigue resistance of the workpiece. Higher cutting forces were measured when the sub surface material showed higher work hardening and the microstructure was highly deformed.

Che Haron et al. [13] published one the first mile stones regarding the machinability of titanium alloys, focusing his work on the machined surface integrity. When he analysed the sub surface material microstructure, he noticed a thin layer of disturbed or plastically deformed layer immediately underneath the machined surface. The microstructure was more deformed when higher cutting parameters were adopted or when the tool wear became unstable.
A more advanced analysis of the surface layer microstructure can be achieved by conducting EBSD SEM analysis or investigate the material microstructure at nano scale by using a TEM microscope. The EBSD technique provides a quantitative analysis, providing important variables regarding the microstructural texture, such as the grain size, the grain misorientation, their strain etc. Even dough this technique is becoming more and more diffused among industries and universities, it is still rare to find its application in the research field of machining. M'Saubi et al. [28] investigated the surface integrity of Inconel 718 over multiple length scales, when machined under high cutting speed by the adoption of PCBN tools and no coolant. Aiming to improve the productivity of aerospace parts made by Nickel alloys, this extreme machining strategy was comparted with the more standardized carbide tools. The EBSD data exploited to visualize qualitatively the extent of plastic deformation in the machined sub surface layers by using the strain contouring map that provides a graphic visualization of the orientation spread within each grain and then weighted according to the

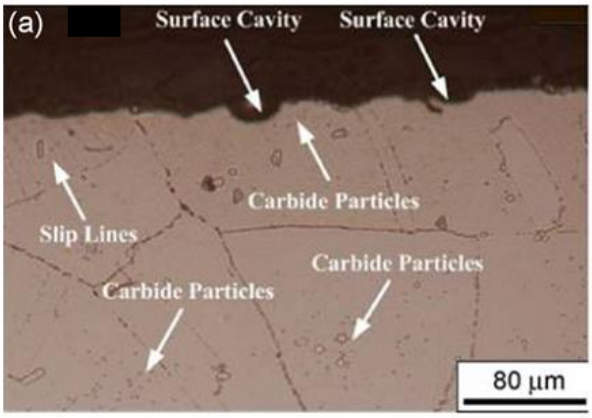

Figure 2.13 Metallographical microstructure of cross - sections of the machined surface after NiCr20TiAl nickel - based alloy was turned at the cutting speed of 60 m/min, feed of 0.15 mm/r and depth of cut of 1 mm [27].

grain size. These strain contouring maps reported in the Figure 2.14, plot yellow, green and red areas near the machined surfaces that are those most affected by deformation, on the other side, the bulk material that is not affected by the cutting process is covered by the blue areas. As can be clearly seen on the TEM images proposed in the Figure 2.15, worn tools deformed more the sub-grains in particular when a standard carbide tool was used.

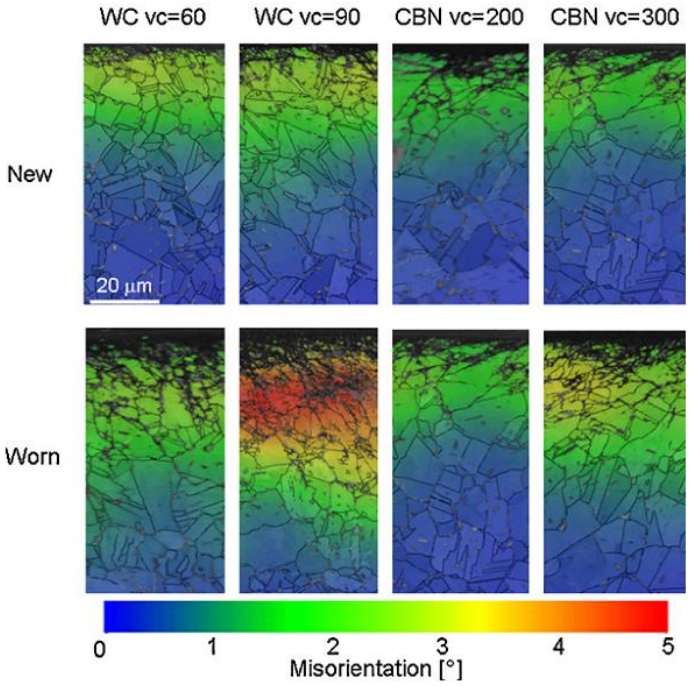

Figure 2.14 Strain contouring maps obtained from EBSD measurements on machined samples of Inconel 718 with new and worn CBN and tungsten carbide tools [28].

In the same work, M'Saubi et al. [28] revealed the presence of equiaxed ultra fine grained microstructure beneath the machined surface, with an average grain size spanning the range between 30 and 80 nm. An increment of the grain size was noticed when worn cutting tools were used in the tests.

were used in the tests.

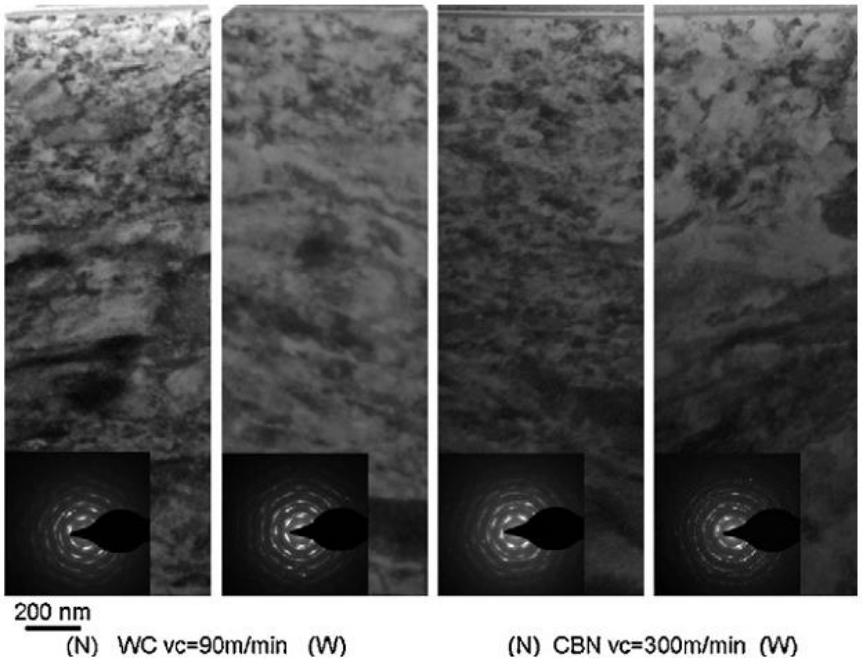

Figure 2.15 TEM images of the near surface (SPD) layers on machined samples of Inconel 718 with new and worn CBN and tungsten carbide tools [28].

2.4.2. Experimental methods used to investigate the tool wear

The tool wear is a crucial phenomenon that has to be taken into account when investigating the machinability of a material, regardless it is a metal, a plastic or a composite. It is an important phenomenon to monitor during the machining process, because the surface integrity and the product final geometry are directly influenced. The general standard that regulates the tool wear measurement in machining processes is normed by the ISO 3685 [29]. According to this standard, the two main geometrical variables measured to quantify the tool wear are: the flank wear width and the depth of the crater wear, when it is present on the tool's rake face. According the Figure 2.16 three flank wear zones are generated on the primary cutting edge flank, below the tool tip VB_C, along the straight portion of the cutting edge VB_B, and on the zone that firstly approaches the material, the so called notch wear VB_N. What is most important before starting a machinability test is the definition of a tool's rejection criterion that practically states when the tool wear reaches its maximum and becomes unstable. In correspondence to this threshold tool wear value, the machining time correspond to the tool life.
According to the standard, the following conditions define the tool life criterion:

- The maximum value of the flank wear land VB is equal to 0.6 mm if the flank wear is not regularly worn in zone B.
- The average width of the flank wear land VB is equal to 0.3 mm if the flank wear is regularly worn in zone B.

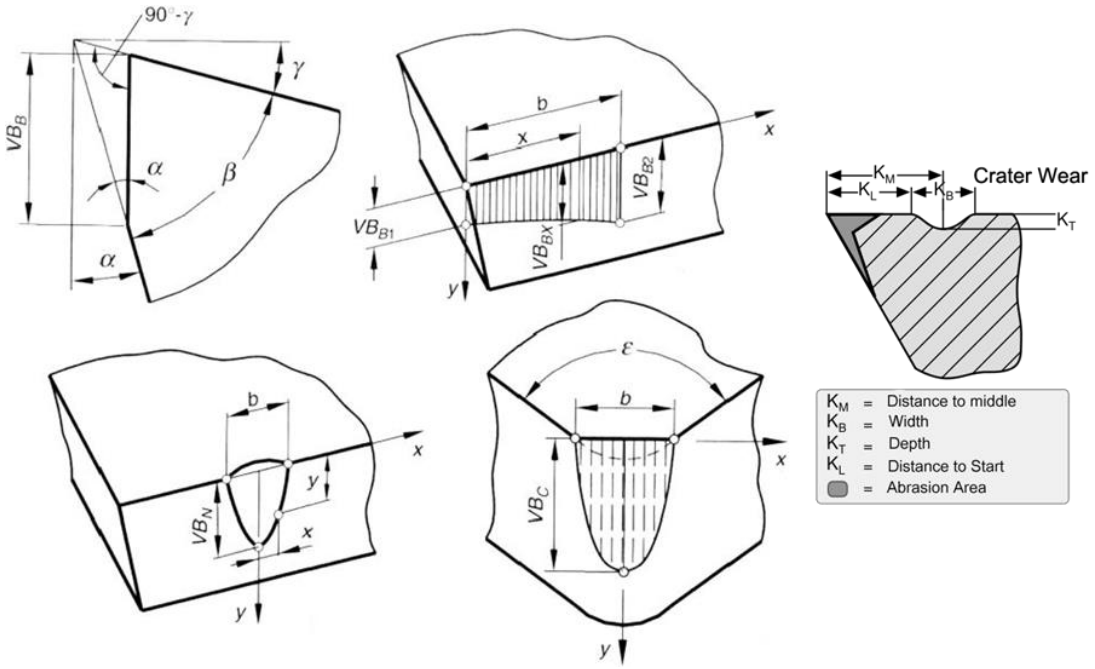

Figure 2.16 Tool wear zones and geometrical parameters according to the standard ISO 3685:1993[29].

- The depth of the crater KT, in millimetres, given by the formula (2.1) where f is the feed rate expressed in (mm/rev) is equal to one of the values listed in Table 2.3;

$$K_T = 0,06 + 0,3f \quad (2.1)$$

Table 2.3 Threshold values for feed rate and corresponding KT according to ISO3685:1993 [29].

Feed f, mm/rev	0.25	0.4	0.63
Crater depth KT, mm	0.14	0.18	0.25

- The crater front distance reduces to a value of Kf = 0,02 mm according to the Figure 2.16.
- The crater breaks through at the minor cutting edge, causing a poor finish of the machined surface.
- Catastrophic failure.

These threshold conditions for the tool wear, are often followed by the researchers, nonetheless there are exceptions in particular when finishing cutting conditions on aerospace super alloys are tested experimentally, in this case, the average value of the flank wear width is fixed at 0.1 mm [30].

The tool wear is monitored on line during the test, in the sense that to locate the tool life many stops are often needed to reach one of the above stated threshold conditions. The flank tool wear is than measured by means of simple tools maker microscopes or stereoscopic microscopes; meanwhile the depth of the crater wear is more difficult to measure, requiring a surface profiler. When the tool life criterion is reached the test is considered concluded, and

other post processing analysis can be performed afterwards such as the surface integrity characterization. From this measurement, trends plotting the flank wear width versus the cutting time are built since they can give immediate indications about the effect of different cutting parameters on the material machinability or either comparing the machinability of two different materials. In literature there are plenty of these plots, for the sake of clarity some cases are reported.

Liang et al.[31], investigated the tool wear mechanisms arising when turning wrought Ti6L4V alloy with an innovative $10Ni_3Al$ coated tungsten carbide insert, comparing its tool wear resistance with an uncoated tool under rough cutting (Vc = 50 – 100 m/min, f = 0.05 mm/rev, ap = 1mm) conditions without the coolant.

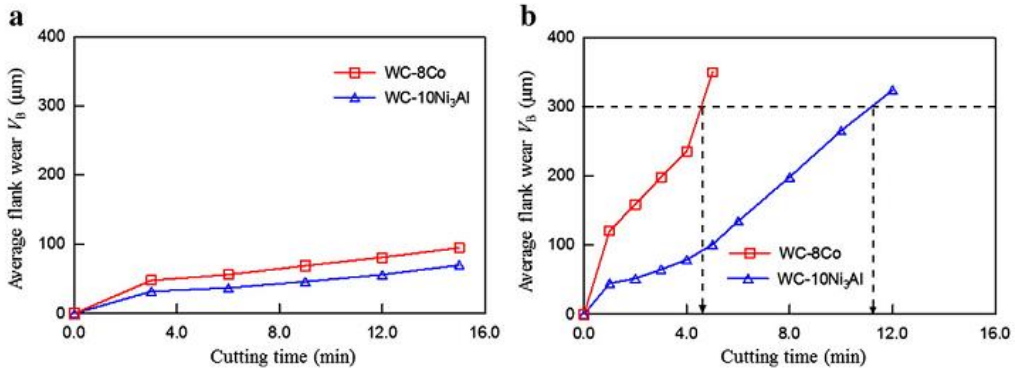

Figure 2.17 Average flank wear (VB) of WC – 10Ni3Al and WC – 8Co carbide tools in dry turning of Ti6Al4V at a cutting speed of (a) Vc = 50 m/min and (b) Vc = 100 m/min; (f = 0.05 mm/r, ap = 1.0mm) [31].

As can be seen in the Figure 2.17, the flank wear trends show a better tool wear performance of the innovative cutting tool insert in comparison to the standard uncoated one, in particular the tool life criteria is three times bigger than the one obtained with the standard tool.

Bermingham el al. [32] found an important improvement of the tool life in rough turning of wrought Ti6Al4V alloy by the adoption of cryogenic cooling instead of the standard dry cutting. For the same tested cutting conditions, the tool life was improved of more the 100% under cryogenic cooling.
Beside the quantification of the tool wear occurring during the cutting process, in the recent years many researchers have performed more and more post process analysis to clarify the tool wear mechanisms and tribological phenomena appearing between the tool-workpiece pair. In many of the most advanced tool wear analysis already published, the use of the Scanning Electron Microscope (SEM) was fundamental. In particular nowadays the adoption of Back scattered Electron Detector (BSED) and of X-Ray spectroscopy detector (EDS) are powerful tools to evidence different chemical elements present in the adhered cutting tool surfaces. The SEM analysis can be easily performed to inspect the main tool wear and tool failure modes, such as: cratering, chipping, flaking, plastic deformation, notching, thermal fatigue cracking, abrasion, adhesion of workpiece material.

Recently, Ayed et al. [33] investigated the main tool degradation modes, arising when turning the Ti17 alloy under high pressure whater jet assistance cooling under rough turning. Thanks

to the EDS and BSED analysis, he found that the notch wear was mainly caused by the adhesion wear mechanism. In the cutting zone, there was a significant release of heat, that is favourable to adhesion, but over the time and because of the volatility of the deposits, the notch is formed by tearing-off newly formed adherent layers.

M'Saoubi et al. [34] tested the tool wear performances of several different PVD coated PCBN tools in high speed turning of 16MnCr5 hardened steel. A meticulous SEM investigation of the cutting interfaces, highlighted the presence of surface cracking of the TiSiN coating, that showed remarkable tool wear resistance, but its higher hardness was counterpart of a very high brittleness.

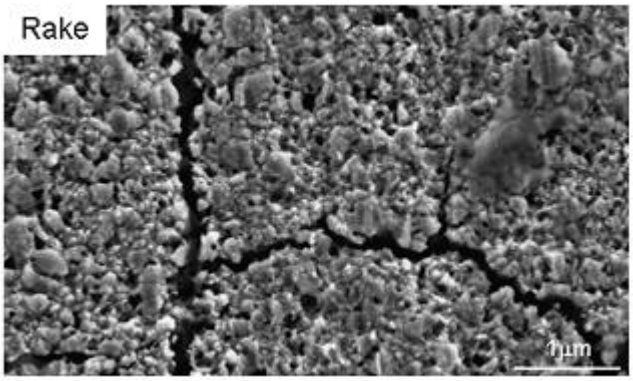

Figure 2.18 Crack in the TiSiN coating during high speed machining of 16MnCr5 hardened steel [34].

The EDS analysis allows individuating the chemical elements present in the surface layers of the scanned material, inside an analysed spot. Nowadays its adoption in characterising the tool wear modes is becoming more and more diffuse, thanks to the important information's that can be gained in particular from the EDS zone mapping mode. EDS point analysis allowed Armendia et.al [35] to find the presence of carbon elements in the BUE (Built Up Edge) formed during rough machining of Ti6AL4V under dry cutting, confirming the diffusion wear mechanism due to the activated chemical reactivity of carbon with titanium at high temperatures.

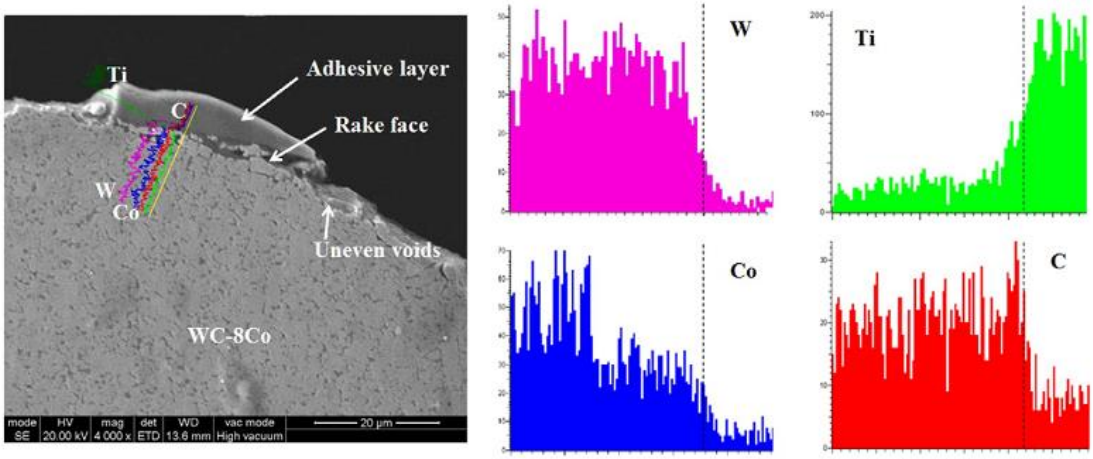

Figure 2.19 Element diffusion across the deposited layer and rake face of WC – 8Co in dry cutting of Ti6Al4V at Vc = 100 m/min. (a) The SEM micrograph of cross - sectional view of the adhesive joint interface. (b) The qualitative compositional profile of W, C, Co, and Ti diffusion across the joint interface (ap = 1.0mm, f = 0.05 mm/r, after 5min, sampling time: 150 s) [31].

The EDS analysis confirmed also the presence of tungsten carbide particles in the BUE that have been detached from the tool substrate by the abrasive action played by the chip flow.

Liang et al[31], could map the chemical elements inside the adhered workpiece layer on the tools rake face, as can be noted in Figure 2.19. Even in this work, EDS analysis confirmed the chemical reactivity of the Carbon present in tool substrate with the titanium present in the workpiece material.

2.4.3. On-line experimental approaches to investigate the machinability in cutting processes

The cutting operation involves the continuous and instantaneous variation of its main influencing variables as in many other manufacturing processes, nonetheless, the entire machining operation of a workpiece can last several minutes, and hence acquiring variables on line becomes even more crucial in this case. Furthermore, even if several post process analysis can be performed to investigate the material machinability, the acquisition of the main cutting variables on line can improve the accuracy of the analysis, allowing the identification of single variations of the tool wear. Nowadays, it is common for researchers to acquire the cutting forces and the cutting temperatures during the machinability test; thus they become the starting point for calibrating and validating the numerical models.
The cutting forces provide important information on the material machinability because they are directly correlated with: the state of the tool wear, the effect of the adopted lubricating strategy, the effect of different tool coating and of the stability of the clamping set up. There are several published works either recent or more dated that include the measurement of the three components of the cutting force. Even if several instrumentations can be adopted to achieve it, piezoelectric dynamometers are generally used because of their high sensitivity, and of their rapid dynamic response, furthermore they are easy to install in the machine tool. What of most important in measuring the cutting forces is plotting their average value at different machining time as proposed by Armendina et al. [35] to compare the machinability of the standard wrought Ti6Al4V alloy with a recent developed titanium alloy by TIMETAL®, namely the TIMETAL 54M in rough turning under standard flood cooling.

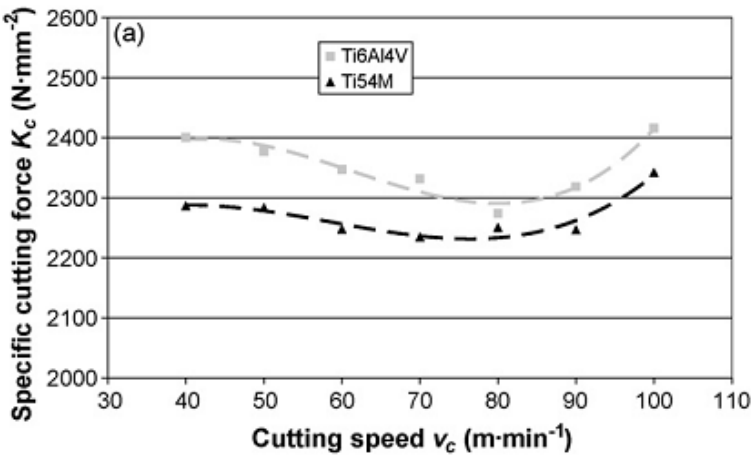

Figure 2.20 Specific cutting force measured in rough turning of Ti6Al4V and Ti55M for different cutting speeds [35].

Thanks to the on line measurement of the cutting forces, an example extracted from the paper is showed in the Figure 2.20, he could verify on the field that this new alloy present a better machinability than the standard one.

Due the high precision and the rapid response piezoelectric dynamometers, Sun et al.[24] could correlated the chip morphology produced in rough turning of wrought Ti6AL4V alloy with the measured cutting forces and with the tool holder vibrations. By analysing the spectre of the cutting forces, he could noticed the influence of the cutting parameters on the tool vibrations, by plotting the amplitude of the main cutting forces as can be noticed in the Figure 2.21, hence in order to limit the vibrations at the fixed cutting speed of 75 m/min, the feed rate should be set around 0.15 mm/rev.

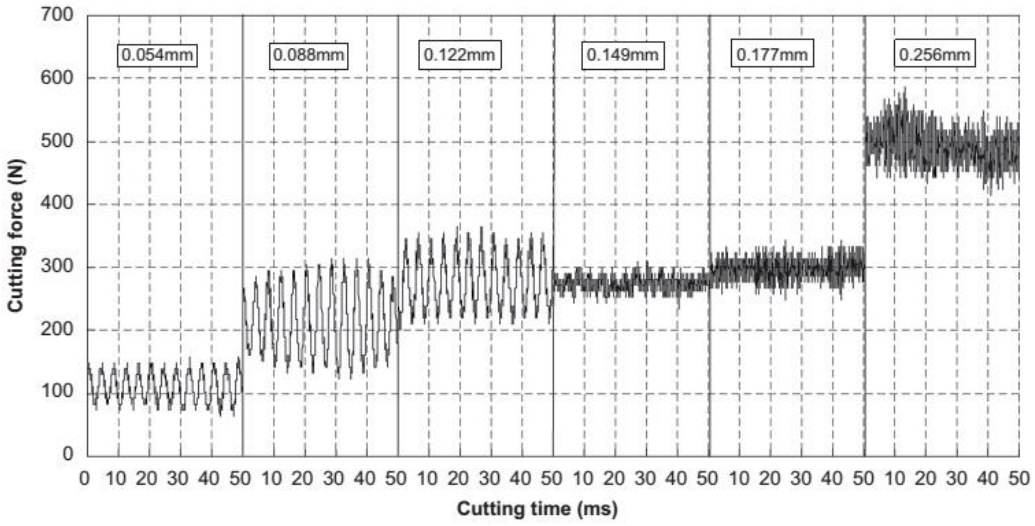

Figure 2.21 Effect of feed on the amplitude variation of cutting force at a cutting speed of 75 m/min during dry machining of Ti6Al4V alloy.

The cutting temperature is the second most important variable to acquire on line when dealing with machining operations. Being the cutting temperature strongly influencing the material plasticity, thus its easiness to be but, measuring the cutting temperature is of crucial importance to have a complete scenario correlating all the different analysis. There are several methods to measure the cutting temperature[36], nevertheless, a grade of inaccuracy is still

affecting the measurements because of the cutting mechanism that involves very high local speed, the chips cover the cutting zone, and the heated volume of the tool are in the order of the cubic millimetres. Actually, there are two main approaches to measure the cutting temperature in machining operations, the first requires the adoption of an infrared camera positioned frontally of the cutting zone hence it is more suitable for milling operations, while the second one consists in embedding a thermocouple into an hole practised in the cutting tool as close as possible to the tool tip, or stick it onto the tool rake face. Both of these methods are affected by uncertainty and it is still a challenge to be improved, in particular for the calibrating the numerical models.

Kramer et al.[37] practised an hole by EDM machining to embed a fibre-optic two-colour pyrometer into the tool insert to acquire the cutting temperature in rough machining of Ti6AL4V and Inconel 718 alloys. The temperature was measured on the bottom of a blind hole within the tool close to the cutting edge. As can be noticed in the Figure 2.23, the measurement point was positioned at a distance of 0.41 mm from the major flank face and 0.15 mm from the rake face and had a diameter of 0.5 mm.

Bermingham et al. [32] compared the cutting temperatures arising by adopting different cutting parameters in rough dry turning of Ti6AL4V alloy. He found that the feed rate was the most influencing parameter on the cutting temperature, nevertheless the measuring approach based on a glued K type thermocouple on the tool rake face (see Figure 2.22) strongly affected the measurements, because the joint of the thermocouple was positioned far from the tool tip. Thermocouples based measuring approaches provide a local temperature, but if the entire thermal field has to be acquired, an infrared camera has to be adopted. In literature, there are several examples where an infrared camera was used to measure the temperature, particularly during milling operations where there is more clear space to position the instrument beside the cutting mill, moreover and in these cutting operations the chip are short and discontinuous, hence they don't cover the cutting zone as in turning operations.

Figure 2.22 K type thermocouple glued on the tool rake face to acquire the cutting temperature during rough turning of Ti6AL4V alloy under dry and cryogenic cooling by Bermingham et al. [32].

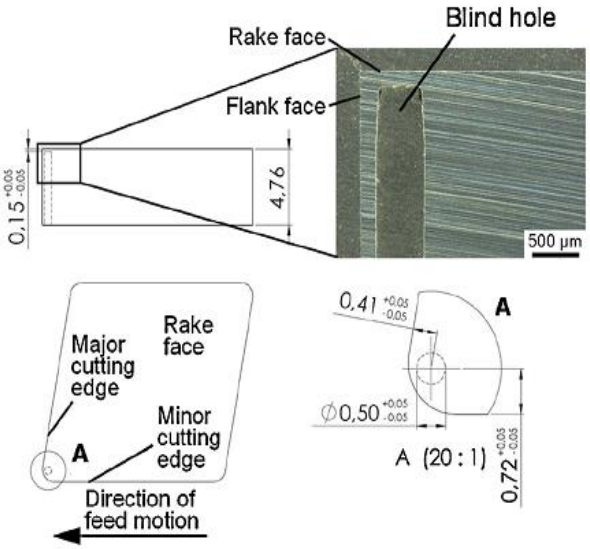

Figure 2.23 Position and dimensions of the hole practised to house a fibre-optic two-colour pyrometer to acquire the cutting temperature [37].

Armendia et al. [38], measured the cutting temperature in milling Ti6AL4V and AISI 4140 steel proposing a new technique applicable in both continuous and interrupted cutting. The adopted experimental set up is showed in the Figure 2.24 a. He found that the lower thermal conductivity and the material properties of the Ti6Al4V alloy led to higher temperatures than in milling AISI 4140 steel both in continuous and interrupted cutting. As can be seen in the Figure 2.24 b, the temperature distribution is more concentrated in a narrow area near the tool tip in the case of machining Ti6AL4V.

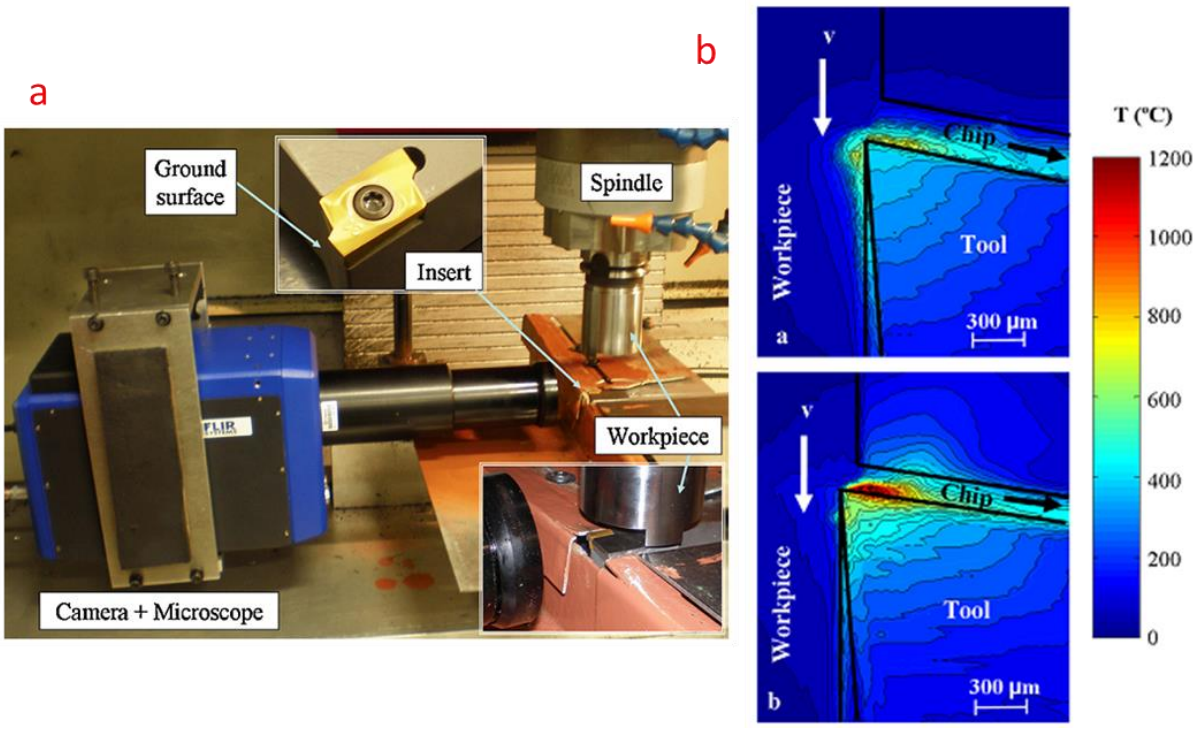

Figure 2.24 a) Experimental set-up for measuring the cutting temperature by means of the infra-red camera, b) acquired thermal field in milling AISI 4140 (in the upper figure) and in Ti6Al4V alloy (in the lower figure) [38].

2.5. Machinability of wrought Ti6Al4V alloy

Ti6Al4V widely employed for low thermal stressed [39] aircraft parts and belongs to the α/β-alloys. This alloy comprises about 45-60 % of the total titanium products in practical use and is formed by a blend of alpha and beta favouring alloying elements. The α - alloy (hexagonal close packed) is hard and brittle with strong hardening tendency. The β - alloy (body centred cubic) is ductile, easily formed with strong tendency to adhere [40].This alloy can be produced in a variety of formulations, depending on the application. The aluminium content may reach up to 6.75 % (by weight) and vanadium 4.5 %. The oxygen [8]content may vary from 0.08 % to more than 0.2 % and the nitrogen may be adjusted up to 0.5 %. Raising the content of these elements, especially oxygen and nitrogen, will help to increase the strength. Equally, the lower additions of oxygen, nitrogen and aluminium will improve ductility, stress-corrosion resistance, fracture toughness and resistance against crack growth. In order to cope with the challenge of large scale structural parts and the rising number of smaller parts, an understanding of the machining demands of titanium alloys is needed, hence dozens of experimental and numerical works have been published in the last 20 years, to respond and the higher demand for safe and reliable aerospace components. In this paragraph, a brief ordered reconstruction of the main experimental findings regarding the machinability of Ti6AL4V alloy is presented.

The recommended cutting speeds for titanium alloys of over than 30 m/min with high - speed steel (HSS) tools, and over 60 m/min with cemented tungsten carbide (WC) tools, result in rather low productivity [39]. The machining challenges can be divided into thermal and mechanical tool demands. The tool face temperature is a function of the cutting speed and exposure time to the thermal load. The longer the duration of exposure time, the larger the volume of the tool edge exposed to the critical tool temperature. The combination of titanium's low thermal conductivity and the fact that approximately 80 % of heat generated [40] is retained in the tool; result in a concentration of heat in the cutting zone (thermal stress). These issues cause complex tool wear mechanisms such as adhesion and diffusion [41]. As a prove of this, the Figure 2.24 b demonstrates the really high cutting temperatures reached in machining Ti6AL4V alloy, ranging up to 1000 °C. Other researchers [42] also measured temperatures over than 900 °C when adopting a cutting speed of 75 m/min.

Ti6Al4V exhibits segmented chip formation and the contact area of a serrated chip is found to be only a third of the contact area of a continuous chip [26]. This results in high pressure loads on the cutting edge. Catastrophic tool failure, due to vibration during the cut, is caused by self-excited chatter and forced vibrations due to the formation of shear localization [43] and the fluctuating friction force between the tool and chip flow. According to Shivpuri et al.[44] the chip segmentation phenomena significantly limits the material removal rates and causes cyclic variation of force. The combination of a low Young's modulus (114 GPa) [45], coupled with a high yield stress ratio allows only small plastic deformations[46] and encourages chatter and work piece movement away from the tool. The most challenging demands for a tool material to machine titanium alloys are the tribo-chemical and impact related wear mechanisms. Tribo-chemical wear is a combination of molecular-mechanical wear and corrosive wear and may be considered a thermally activated process whereby the work piece material and the tool material react in such a manner as to remove particles from the tool at an atomic scale. Titanium's chemical reactivity becomes

problematic at temperatures above 500 °C. Apart from diffusion wear, it has a strong affinity to adhere which leads to chip adhesion (also known as galling) onto the tool cutting surface. Once a Built-Up Edge develops, tool failure follows rapidly [47]. The unexpected reaction of titanium chips with atmospheric oxygen causing a fire hazard is also a major concern in a workshop.

The cutting tool materials often encounter extreme thermal and mechanical stresses close to the cutting edge to the poor machinability of nickel and titanium base alloys. This usually results in plastic deformation and accelerated tool wear. A major requirement of cutting tool materials used for machining these alloys is that they must possess adequate hot hardness to withstand elevated temperatures generated at high speed conditions. Most of cutting tool materials lose their hardness at elevated temperatures resulting in the weakening of the inter-particle bond strength and consequent acceleration of tool wear. The softening temperature of commercially available cutting tool materials used for machining aero-engine alloys is given in Table 2.4 while the Figure 2.25 illustrates the effect of temperature on the hardness of some cutting tool materials[47]. Coated carbide tools, ceramics, CBN/PCBN and PCD tools are generally used for high speed machining of nickel base and titanium alloys. Ceramics and CBN/PCBN tools are not usually recommended for machining titanium alloys because of their poor performance due to excessive wear rates as a result of the high reactivity of titanium alloys with ceramics. Efficient and economic machining of aero-engine alloys under high speed conditions requires a good understanding of the cutting tool materials, cutting conditions, processing time and the functionality of the machined component. Advances in cutting tool materials and machining techniques have resulted to significant increase in metal removal rate dealing with cutting difficult-to-cut aerospace superalloys. These alloys can now be economically machined at higher speed conditions with recently developed cutting tools and machining techniques.

Table 2.4 Softening temperatures of the principal tools materials.

Tool materials	**Softening point temperature (°C)**
High speed steel	600
Cemented carbide (WC)	1100
Aluminum oxide (Al_2O_3)	1400
Cubic boron nitride (CBN)	1500
Diamond	1500

The machinability of the wrought Ti6AL4V alloy in both turning and milling operations can be enhanced by acting on the lubricating strategy. Several steps ahead have been done in the last 20 years to improve the productivity of aerospace components. Nowadays, the three main cooling strategies that are being tested by the researchers in machining difficult to cut materials are: Minimum Quantity Lubrication(MQL), High Pressure Water Jet Assistance (HPWJA) and cryogenic cooling. Each of these cooling techniques, present their on peculiarity, but fundamentally they act in one the main problematic aspects that affect machining titanium alloys. Minimal Quantity Lubrication (MQL) technology involves the application of very small amount of water and soluble oil, 6 – 100 ml/h, delivered in a

compressed air stream, directed at the tool cutting edge[48]. Encouraging results had been observed in grinding, milling and turning operations. These improvements in machining can be attributed to the lubricating oil that was able to get very close to the tool – chip and tool – workpiece interfaces under pressure, therefore reducing friction and component of the forces generated during machining. Temperature reduction at the cutting zone in MQL systems is achieved mainly by the cooling effect of the compress air and partially by evaporation. Significant amount of heat is absorbed by the evaporation of the lubricants, thus contributing to a significant temperature reduction at the cutting zone. Pressure welding of chips to the cutting edge is the main cause of tool failure when milling titanium alloys with HSS tools. With MQL this failure mode can be drastically reduced causing significant improvement to surface finish of the machined components. The MQL system has shown encouraging results for precision machining at low feed and high speed conditions [49].The main disadvantage of using this system is mist generation, which possesses a health hazard to operators.
This hazard can, however, be minimised with good mist extractors.

The second powerful technique that is foreseeing a high potentiality in enhancing the machinability of aerospace super alloys is by the application of high pressure coolant onto the

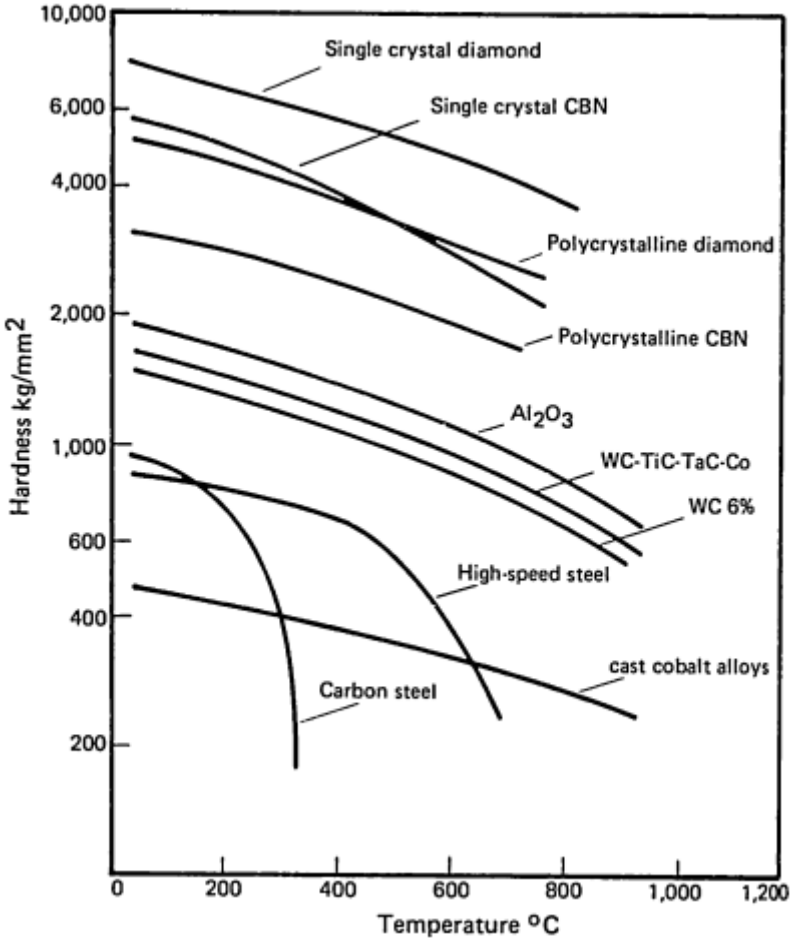

Figure 2.25 Thermal softening of the most common tools materials for a typical range of cutting temperatures.

tool's rake face(HPWJA), focusing its flow as close as possible to the tool chip interface. The idea of delivering coolant under high pressure to the cutting region in order to increase tool life during machining began in early 1950s [47]. The primary objective of this machining technique is to significantly reduce the temperature generated at the tool – workpiece and tool – chip interfaces when cutting at a higher speed conditions. This is achieved by directing coolant under high pressure at the chip – tool interface (Figure 2.26). This process can also achieve high chip breakability and control through increased chip upcurl and compressive stress. Flood cooling of the cutting zone can effectively reduce the cutting temperature when machining at lower speed conditions with significant sliding region and where relatively low cutting temperatures are generated. The coolant also acts as a lubricant, thus minimising friction and lowering component forces and consequently tool life. There is very limited access of the coolant to the tool–workpiece or tool–chip interfaces which are mainly under seizure condition when machining at high speed conditions. Coolants tend to be vaporised by the high temperature generated close to the tool edge, forming a high temperature blanket that renders their cooling effect ineffective. The film boiling temperatures of conventional cutting fluids is about 350°C[50]. Ability to deliver coolant at high pressure very close to the critical point on the secondary shear zone can improve machinability at higher speed conditions.
The credibility of this technique of coolant delivery has been thoroughly investigated over the

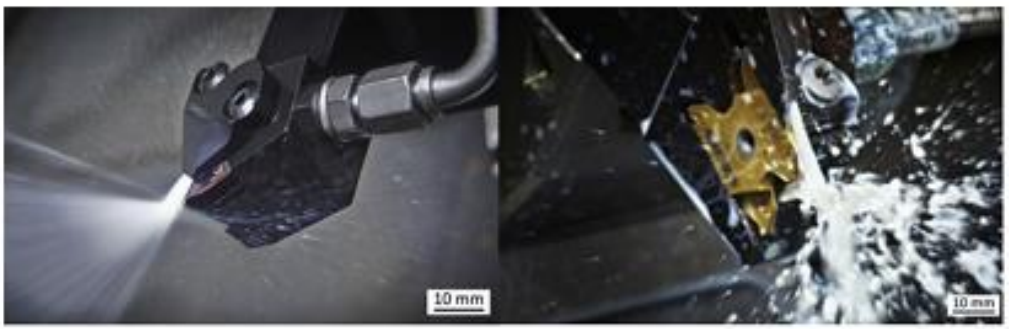

Figure 2.26 Modern commercial tool holders for external and parting turning specifically designed for High Pressure Water Jet Assistance machining.

years. Initially, this technique was unpopular because of associated equipment cost and also the fact that low speed machining was the preferred mode of production as machine tools were not capable of high speed machining applications. The manufacturing industry have recently adopted a more radical approach to increase the rate of production and high pressure coolant delivery technique is a viable means of achieving this strategy in addition to providing an effective removal (by flushing) of the chips from the cutting area. The high speed coolant jet traverses the surface faster, thus significantly lowering the film boiling action of the coolant at the cutting area. This consequently minimises heat transfer to the cutting tool. The high pressure coolant jet creates a hydraulic wedge between the tool and the workpiece, penetrating the interface with a speed exceeding that required even for high speed machining and also alters the chip flow conditions[47]. The penetration of the high energy jet into the tool–chip interface reduces the temperature gradient and eliminates the seizure effect, offering an adequate lubrication at the tool–chip interface with a significant reduction in friction. Rapid failure of ceramic tools when machining with higher pressure coolant supply and at higher cutting conditions can be associated with a significant reduction in the chip–tool contact length/area. This reduction has negligible effect on cutting forces, resulting in higher

compressive stresses on the cutting edge that tend to accelerate notching and/or tool fracture during machining. Coolant supply at high pressure tends to lift the chip after passing through the deformation zone resulting to a reduction in the tool–chip contact length/area[51]. This tend to enhance chip segmentation as the chip curl radius is reduced significantly, hence maximum coolant pressure is restricted only to a smaller area on the chip. The chip curl radius also depends on the coolant pressure and the flow rate, hence at a given power; smaller chip curl radius could be achieved at a lower coolant pressure with a high coolant flow rate. Component forces generally increase with increasing cutting speed when machining with high pressure coolant supplies. This is due to reactive forces introduced by the high pressure coolant jet. The benefits of high pressure coolant supply are more even better when machining wrought Ti6Al4V alloy and the alloy (IMI 318) with cemented carbide (coated and uncoated) tools as well as with Polycrystalline Diamond (PCD) tools. There is negligible difference between coated and uncoated carbide tools in terms of recorded tool life, hence there is no tangible benefit in machining with coated carbide tools with associated additional cost (typically 15 %). These improvements can be achieved without compromising the surface finish generated, circularity and hardness variation of the machined surfaces. Tool life generally increased with increasing coolant pressure where lower cutting temperatures are expected. Cubic boron nitride and ceramic cutting tools are not recommended for high speed machining of titanium alloys with high pressure coolant supply as they tend to suffer excessive nose wear and severe chipping and/or fracture of the cutting edge.

The third high performance cooling strategy that is nowadays being tested by several researchers to enhance the machinability of nickel and titanium alloys is cryogenic cooling which is being tested in several processes such as machining, burnishing, grinding and turning, foreseeing promising results to be implemented at an industrial scale. A detailed description of the main published works regarding this cooling strategy giving more emphasis to turning operations is presented in the next paragraph.

2.6. Cryogenic cooling and its implementation in machining operations

The first researches that tested the application of cryogenic fluids in machining operations date back to the sixties, nonetheless at that time they did not disrupted the traditional lubricating strategies adopted in industries, thus flood cooling continued to be the standard method to cool and lubricate the cutting zone in every machining operation. In the last 20 years, aerospace industry have demanded higher and higher productivity of complex parts made of exotic super alloys that are traditionally machined with very low cutting parameters, limiting the machining production rate. In the last ten years, researchers and tool's manufacturers have re-evaluated cryogenic cooling and nowadays it seems to be the right way to respond at many tasks, primarily this technology is showing great beneficial effects in improving the machinability of the most difficult to cut materials, but at the same time it responds to another or even more important issue: the sustainability of manufacturing processes.

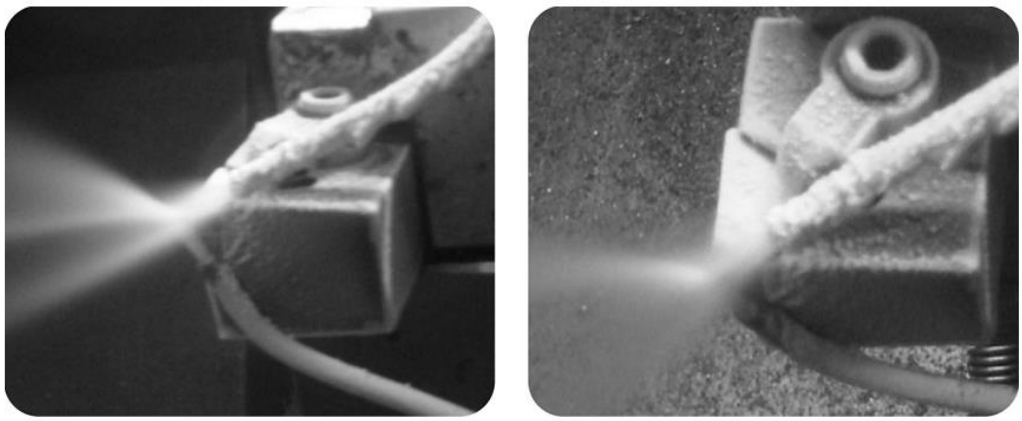

Figure 2.27 Liquid nitrogen applied on the rake and on the flank face of the tool contemporarily to enhance the cooling efficiency [55].

Cryogenic machining simply means of using a cryogenic fluid instead of a standard flood coolant to cool and to lubricate the cutting zone. Typically one of the following cryogenic fluid are adopted: liquefied nitrogen LN_2, liquefied oxygen, liquefied carbon dioxide CO_2. Cryogenic fluids can be delivered in various/different ways to the machining zone: rake, flank, both faces simultaneously, or even just to the workpiece itself. In the last specific case, the workpiece is cooled down in order to beneficially influence the material machining performances (lowering the ploughing effect, smearing prevention etc.). Cryogenic machining, with evaporation of the delivered cryogenic fluid, is a type of dry machining technology that results in dry and clean products undergoing the process.

In most cases, under the term cryogenic machining, liquefied nitrogen (LN_2) and liquid carbon dioxide (LCO_2) are proposed as C/L fluids. In both cases the C/L fluid is a refrigerant that changes phase by absorbing latent heat and cools down the zone where delivered to. In both cases, the gases or liquids are widely available[52]. Both are stored as a liquid and both are delivered to the cutting zone. The first obvious difference is the evaporation temperature, liquid nitrogen evaporates at the temperature of -195.8°C, while liquid carbon dioxide evaporates at the temperature of -78.5°C. CO_2 has one interesting characteristic that it can exist as a liquid at room temperature, but only under high pressure. Thus, there is no problem with the insulation and CO_2 is actually delivered to the nozzle through pipes in the liquid state, at room temperature and at a pressure above 6.7 MPa. When liquid CO_2 is then sprayed through the nozzle to the machining zone, there is an instantaneous drop in the pressure of the liquid to the level of the atmospheric pressure. This massive pressure reduction causes the liquid CO_2 phase to change into a mixture of a solid (dry ice) and gaseous state, at a ratio of approximately 45% of dry ice and 55% of gas [53].The gas portion of this mixture has a very low cooling capacity, so most of the cooling capacity can be expected from the solid CO_2, commonly known as "dry ice". However, dry ice can be very problematic since it can cause blocking of the delivery nozzles and, due to its size, has limited capabilities for reaching the close proximity of the machining zone. CO_2 is also problematical because it is one of the greenhouse gasses. Such gases have a negative influence on the environment since they absorb and emit infrared radiation. What is more, CO_2 has a slightly irritating odour, is colourless and heavier than air. In shop floor (at the workplace), higher density than air and the fact that CO_2 does not sustain life can cause serious problems to workers unless proper air exchange is

assured. The alternative is LN_2. It is a chemically inert, reaction inhibiting gas, which is produced in its liquid form through cryogenic air separation. N_2 is the main component of the air that we breathe (78%). Cryogenic liquefied nitrogen boils at -195°C under atmospheric pressure. Thus, the storage of it is problematic due to the need of good insulation. This is normally assured with vacuum insulated vessels (Dewars). However, with LN_2we can have lower cooling temperatures or wider cooling temperature possibilities in comparison to CO_2. Comparing both gases (CO_2 and N_2) from the operator's safety point of view, there are regulations that OSHA's carbon[54] dioxide exposure limit in the breathing atmosphere is 0.5%. In the case of nitrogen, the limit is higher. The increase of N_2levels in the air should not cross the 2%. Additionally, as an opposite of carbon dioxide, which is 1.5 times as heavy as air, nitrogen is lighter than air and is not so concentrated at low elevations (floor of the working environment).

When comparing the LN_2 and LCO_2 in machining process application, the most important characteristic is cooling capacity. The lower freezing temperatures of LN_2 mean quicker freezing, and so the amount of equipment needed to produce the same amount of product is smaller. The cooling capacity of both cryogenic fluids can be directly compared with the comparison of latent heat of vaporization and sensible heat to heat up the gas. According to Pusavec at al. [55] the refrigerant effect of LN_2 is equal to 428 kJ/Kg, while for the LCO_2 it is equal to 347 kJ/Kg, hence on this basis LN_2 is more prone to be implemented in machining difficult to cut materials, nonetheless many researches are being conducted using LCO_2 instead of LN_2.

Wang and Rajurkar et al. [56] reported a decreased tool wear in turning Ti6Al4V and Inconel 718 by using indirect LN_2 cooling of the tool. Hong and Ding et al. [57] analysed different supply strategies in turning Ti6Al4V and achieved best results when spraying the cryogenic media into the cutting zone along the tool's rake and flank face. In most research studies in the past, this supply method was preferred. In further studies of Hong et al. [58], a five times higher tool life was achieved with LN_2 compared to conventional cooling with emulsion at a cutting speed of Vc = 150 m/min, while tool life increased threefold at Vc = 90 m/min.

Bermingham et al. [59] determined a slightly lower tool wear and better chip breakage in turning Ti6Al4V using high-pressure lubricoolant supply (p = 100 bar) compared to LN_2 cooling (p = 8 bar). Klocke et al. [60]turned 45-2-2XD gamma titanium aluminide with targeted LN_2cooling of the cutting zone. Tool life and surface quality could be significantly increased by cryogenic cooling compared to MQL, conventional cooling as well as high-pressure lubricoolant supply.
Using CO_2 as cryogenic media, positive results on tool life and surface integrity during turning titanium alloys has been reported by several authors [61,62], and the current researches on milling operations that requires internal cooling of tool holder are showing a more frequent use of LCO_2 instead of LN_2 because its higher temperatures induce fewer technical problems on the structural parts of the CNC machines, due to induced thermal distortions. In brief, LN_2 is more suitable for external cooling rather than internal cooling of the tools.

Overall, it can be summarized that cryogenic cooling offers a high potential for increasing the productivity, as well as surface integrity when machining aerospace alloys. However, there is still a huge need for further research, amongst others focusing on improved supply of the cryogenic media to the cutting zone, the effect on machine tool components, as well as on dimensional and shape accuracy. A lack of literature works is present and very few papers have been published regarding the dimensional accuracy of cryogenically machined components that might encourage industries investing on these technologies in real industrial processes. On these bases a technical issue that still has to be investigated is the feasibility of cryogenic cooling to respect the dimensional accuracy, in order to complete the entire machining operation of a mechanical component and benefit of the positive effect of these cooling strategies on the final surface integrity.

Yasa et al.[63], presented a case study where they externally turned bulky cylindrical workpieces made of wrought Ti6AL4V alloy, in collaboration with the company TUSAS Engine Industries Inc. Three level of cutting speed, of feed rate and depth of cut were tested, comparing the acquired cutting forces and the final geometry of the machined component by adopting dry and standard flood cooling. The cryogenic cooling sensibly improved the tool wear than dry machining, but the improvement in comparison to wet machining was small. The company found some limitations in using cryogenic cooling in their shop floor, because the bulky equipment to supply the LN_2 on the cutting zone, impeded turning of internal diameters, regular releases of LN_2 from the safety valve installed in the system took place, that might cause health problems for the operator if he would have brought in contact having the risk to suffer severe frostbites. Furthermore, the excessive cooling of the workpiece generated geometrical distortions and the dimensional tolerances were not respected, inducing the company to rework the workpieces, with high costs dealing with expensive materials. All these limitations, forced the company to abandon the technology and continuing adopting the standard flood cooling techniques.

Islam et al. [64], published a paper concerned on the study of the dimensional accuracy achievable on cryogenically turned titanium parts comparing dry and wet cooling. He measured the geometrical discrepancies arising in external turning Ti6AL4V operations by setting three levels of feed rate and three levels of cutting speed usually adopted in rough machining of titanium. The geometrical discrepancies were quantified in terms of circularity and diameter errors comparing the final geometry with the nominal one by collecting several measurements and analysing the data using Taguchi and ANOVA statistical methods. With regard of the diameter errors, under dry and flood cooling they increased under low and medium cutting speed by increasing the feed rate. On the other hand, cryogenic cooling highlighted a different trend, when increasing the feed rate the diameter error decreased. The measured circularity was the worst in the case of cryogenic cooling. In brief cryogenic cooling provided the least diameter error when combined with higher cutting speed and medium feed rate. The circularity was more affected by the cooling strategy, and it seemed that dry machining and a contribution of feed rate and cutting speed provided the best circularity due to the local softening and chip formation mechanism.

2.7. Machinability of additive manufactured alloys

In future manufacturing processes, the use of additive manufactured alloys will be more and more diffused, even in industrial fields that traditionally employ standard production schemes. The growing demand for lighter and stiffer part to be installed in racing cars, airplanes, racing bicycles and motorbikes, or the research for innovative coating to apply on functional surfaces of surgical implants foresee a disrupting diffusion of such materials and AM technologies. As previously mentioned, machining operations are drastically reduced by using AM techniques, thus few millimetres of machining allowance is left on the as built geometry. According to that, the high tool wear and poor surface integrity that are encountered in milling and turning aerospace components made by the same alloys will not be a challenge to deal with as for producing wrought components. Nonetheless, being machining operations, in particular milling still required to achieve the product final geometry, and being the additive manufactured alloy microstructure different that the one of standard wrought or casted alloys, the machinability of these innovative materials has to be taken into account and investigated. Furthermore, with the potential incoming production of hybrid machining and additive machine tools integrated in the same body, the machinability of the generated material will be more and more important. Due to the altered mechanical properties of the surface material layers by machining that can lead to improvements of the mechanical properties rather than negative effects, tailored machining operations might carry important beneficial effects on the mechanical properties of AM alloys, improving the fatigue and the corrosion resistance. Bearing these considerations in mind, machining tests on such innovative materials should be carried out in particular for the years to come.

At the moment, there are few works published in literature concerning additive manufactured alloys, and none of them deal with biomedical alloys such as Ti6Al4V and CoCrMo alloys.
Axinte et al.[65] investigated the machinability of Nickel base alloy (PR_X) manufactured via powder route in rough and finishing turning. He analysed the tool wear and the surface integrity by means of profilometry analysis, residual stresses measurements and metallographic analysis. The turned workpiece was a disc simulating the turbine discs that are made by Inconel, Waspaloy or Udimet alloys. He proved that this material has a poorer machinability than standard Nickel alloys, nonetheless optimum parameters were found to conduct rough machining by using ceramic round tools, and finishing machining using coated carbide inserts. Narrow operation intervals of cutting parameters for finishing with coated carbide inserts were identified to satisfy a good surface quality and a reduced tool wear, however the great amount of material deposition on the machined surface at higher feed rates and low cutting tools radius reduced the range of cutting parameters. Due to the very low thermal conductivity of the material, discontinuous white layers was found through metallographic analysis. Acceptable tensile residual stresses were measured on the machined surfaces.

Priarone et al. [30] analysed the effects of the tool geometry modifications in terms of cutting edge preparation, of cutting tool angles and of different nano - structured coating in milling gamma titanium aluminide made by Electron Beam Melting. A threshold limit equal to 0.1 mm was fixed for the tool wear. The tool life was increased by using AlSiTiN insert coating rather than CrAlSiN coating. For all the tested conditions, the surface roughness was suitable

to satisfy the restrictive requirements for parts in aircraft engines, and the best result was obtained using mills with AlSiTiN coating, subjected to the polishing post-treatment. The surface hardness of the machined parts increased as the tool wear deteriorated due to the material strain hardening. Higher surface hardness was measured on the specimens machined with coated tools. Due to the peculiar microstructure of the as built material, micro craters were observed on the machined surfaces in all the tested cutting conditions.

2.8. Numerical modelling of machining Ti6Al4V

Numerical simulations are nowadays powerful engineering tools to simulate engineering problems, whether they are of structural, thermal, fluid dynamic or metal forming nature. They are offering the chance to save designing costs and time consuming experimental tests. Among the standard manufacturing processes, such as forging, sheet metal forming, drawing etc., numerical simulation of cutting processes is still far behind to be implemented at industrial scale, and few commercial FE codes have implemented packages specifically dedicated. Even in those cases, the numerical results are still affected by heavy simplifying hypothesis that are direct consequences of the physical phenomenon itself. The main challenge when dealing with cutting operations is the constitutive model of the material to be machined that cannot be easily determined by experimental testing because the common hydraulic testing presses used in laboratories are not suitable because of the limited strain rate obtainable in comparison with those reached in cutting operations. Moreover, due the high speeds, restricted contact areas, high temperatures etc., the measurements of experimental variables that govern the cutting process are still affected by important errors that limit the affordability of numerical models to set correct boundary conditions. Up to now, numerical simulations of cutting processes can be performed on commercial FE software's; nonetheless reliable results can be achieved in restricted ranges of boundary conditions that correspond to the very few validated boundary conditions calibrated in rare experimental tests. Another important limitation that affects numerical simulation of cutting processes is the possibility to simulate only short portion of standard machining operations in steady state conditions, and even the most advanced models are still far away from simulating the entire machining of a real workpiece. In brief, numerical simulations can be useful for tools designers to compare different cutting angle geometries but few manufacturing companies use them to improve their production process. Nevertheless, since the late nineties, numerical simulations of cutting operations on wrought Ti6Al4V alloy have been conducted and important findings have been achieved. Plenty of papers can be found in literature on the topic, and as a reference state of the art work the review published by Arrazola et al.[26] is nowadays one of the most comprehensive one. For sake of clarifying, an overview of the main published works since the most simplified models towards the most recent ones is presented, focusing the literature review on turning operations which will be lately developed in this thesis.

Due to the intrinsic complexity of cutting operations, most of the numerical models developed by the researches on metal cutting are simplified two dimensional FE codes implemented on commercial software's. Two dimensional cutting or so called orthogonal cutting, is easier to model and it allows an easier characterization of the chip morphology being an important process outcome to compare numerical and experimental findings.

One of the first and more relevant works on simulation of orthogonal cutting of wrought Ti6AL4V alloy was published by Umbrello et al. [66], this work was than considered as a reference for future numerical modelling developments.
In his work, he simulated an orthogonal cutting operation on wrought Ti6AL4V in conventional and high speed machining conditions, testing three different packages of experimental material constitutive model constants available in literature, suitable for being implemented in the Johnson-Cook flow stress equation. The model was implemented in the commercial software DEFORM 2D®. He calibrated and validated the model by comparing the cutting forces and the chip morphology. He adopted the original form of the Johnson-Cook flow stress equation; hence in order to precisely predict the chip morphology he also implemented the fracture criterion developed by Cockroft and Latham, in order to simulate the characteristic saw tooth chip morphology that is generally observed in machining titanium alloys. A simple Coulomb friction model was adopted and fixed cutting parameters were maintained. The numerical FE code was calibrated by optimizing the value of the friction coefficient and the damage value D of the fracture criterion. According to his findings, the better results in terms of numerical prediction of cutting forces and chip morphology was achieved by setting the Lee and Lin et al. [67] package of J-C model constants, because they were found experimentally under process conditions closer to those set in the model. He concluded his paper assessing that the FE strategy proposed can be employed to study the orthogonal process of Ti6Al4V alloy and to predict the cutting forces and the chip geometry with satisfactory accuracy.

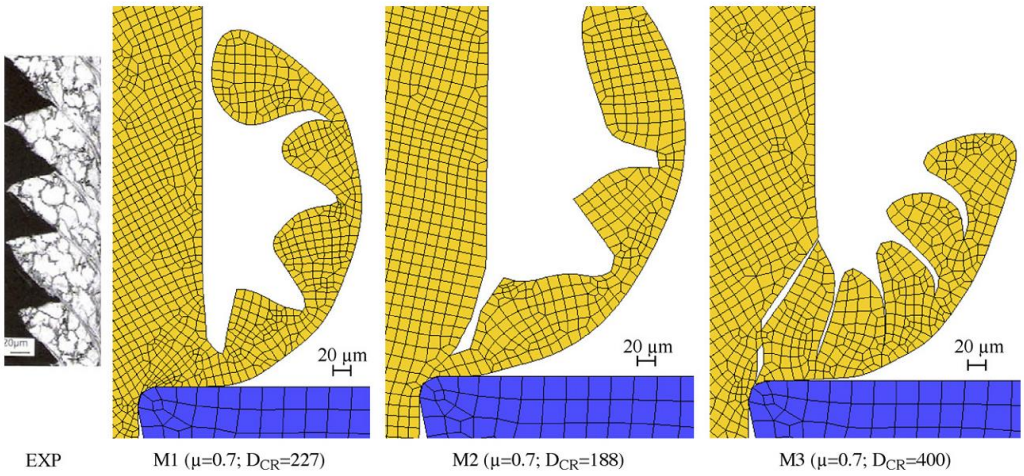

Figure 2.28 Comparison between experimental and numerical chip morphology for different values of damage value in orthogonal cutting of wrought ti6Al4V alloy [66].

Since the first researches on numerical modelling of orthogonal cutting of wrought Ti6AL4V alloy, researchers have understood the importance to improve the flow material constitutive model equation to predict accurately the chip morphology of titanium alloys. Among the flow stress equations models available in literature, the Johnson Cook was the one that due to its experimental calibration conditions was the best choice to model the thermo-mechanical phenomena arising in the cutting mechanism of low thermal conductivity alloys, in particular of titanium alloys. Despite the standard J-C model is able the represent the material behaviour by taking into account of strain and stain rate hardening as well thermal softening

phenomenon it is not applicable for all materials since different materials exhibit different behaviour, moreover it is not accurate to predict the flow stress of a material at very high strain and above all it does not couple the effects of strain, strain rate and temperature. By the consequence, several researches proposed modifications at its original equation form and in some case a benchmark among these equations was proposed, comparing their capabilities of correctly predict the cutting variables in orthogonal cutting processes.

Sima et al. [68]compared three modified J-C constitutive models presenting terms in their equations that are introduced to model the complex flow softening and strain hardening material behaviour that were found to be the origin of adiabatic shear banding and thus the saw tooth chips in machining titanium alloys. He compared a J-C material model that does not take into account temperature dependent parameters with a second J-C model including temperature dependent parameters, finally they also tested the most sophisticated J.C model [69] that contains temperature dependent strain softening parameters. Finite element analysis was performed by using the commercial FE code DEFORM-2D®. The numerical model was calibrated and validated by comparing the experimental and numerical values of the cutting forces and comparing the chip morphology. Two different rake angles, three different chip thickness values and two different cutting speeds were simulated. This work can be considered of crucial importance in the development of FE models of machining Ti6AL4V alloy because it proved the sensibility of FE models to the implemented flow stress equation. In particular, the cutting forces, the cutting temperatures and chip morphology evidenced not negligible differences due to the adopted J-C equation implemented. Another important outcome of this work was the capability to predict the correct chip morphology without the implementation of a fracture model. According to this work, the Calamaz J-C model resulted to be the more accurate one to simulate cutting processes of TI6Al4V alloy.
After several works aimed at improving the accuracy of numerical models to simulate the orthogonal cutting of wrought Ti6AL4V alloy, testing the effect of different constitutive models, friction models and numerical parameters (such as the mesh and the integration algorithm) [26], recently researchers have concentrated their efforts in proposing reliable models that would be able to predict the induced surface integrity, which is much more important to predict from an industrial point of view. It is noteworthy that the ultimate purpose of investigating the machinability of metallic alloys is improving the productivity and preserving the induced surface integrity in machining aerospace super alloys. On these bases, in the last years more and more published papers have been focused in predicting the tool wear, the residual stresses and the microstructural alterations.

Styger et al. [70] investigated the effect of the constitutive model during finite element analysis of machined induced residual stresses in Ti6AL4V alloy. Three different J-C constitutive models were used to simulate the orthogonal cutting process, they were the same tested in the work conducted by Sima et al.[68]. He predicted the residual stresses upon removal of the tool and then return of the workpiece at room temperature along with removal of the chip to allow any possible spring back that might occur. He measured the residuals stresses at the centre of the length of cut, through the thickness of the workpiece, an example of the predicted values is reported in the Figure 2.29.

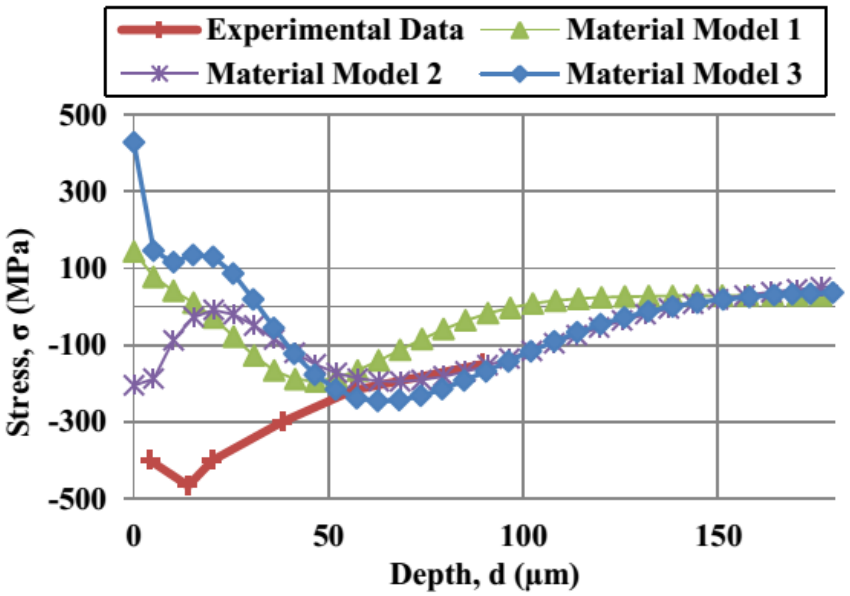

Figure 2.29 Numerically determined residual stress depth profile as compared to experimental left on the workpiece in orthogonal cutting of Ti6Al4V alloy [70].

This investigation showed that numerical modelling of induced residual stresses is deeply influenced by the adopted flow stress model, but to improve the accuracy of the numerical simulations, the constitutive models should be coupled to a kinematic model that adequately describes all aspects of the cutting process including chip morphology, cutting forces and residual stress field as a function of the various appropriate cutting parameters that should be set for titanium alloys.

A similar work was carried out by Schultze et al. [71] who tested the influence of the Jonhson-Cook material parameters on the surface integrity of wrought Ti6Al4V alloy. In developing the work, he decided to implement a self-developed continuous remeshing method using ABAQUS®, where a new mesh was created for the whole workpiece every 5 microns of relative displacement between the tool and the workpiece to avoid strong distortions of the elements. A structured mesh with different mesh densities was created for the whole workpiece, aiming at maintaining a dense mesh constantly in the primary shear zone and on the formation volume. Even in this work, after the chip was created, he lifted the chip from the surface in order to mechanically relax and cool down the workpiece to room temperature. He tested the sensitivity of the mode to four different packages of J-C constitutive equations constants. At the end of this work he assessed that the coefficients of the J-C equations influenced the predicted residual stresses. Among the cutting parameters, the cutting speed, the uncut chip thickness played the most important role.

Recently, Nieslony et al. [25] compared the numerical and experimental values of residual stresses generated in 2-D and 3-D turning of wrought Ti6Al4V alloy. In his work, he tested two different constitutive models (a power law model and a J-C model) and different sets of cutting parameters. To numerically predict the residual stresses, they used a special module available in the AdvantEdge® FEM package to change the meshing parameters in order to obtain a grid of nodes in close proximity. Numerical results of residual stresses were

compared with experimental findings measured by means of the XRD method. According to their main findings, the power law model induced more distinct changes in the RS distribution. The J-C model predicted better results of axial residual stresses than tangential stresses than the J-C one, on the other side the PL model was better in predicting tangential stresses for 3D machining. The feed rate was the most influencing cutting parameter; in contrast the effect of the depth of cut, especially in 2D simulation could be ignored. The 3D FEM model predicted better results in terms of residual stresses.

Recently few papers were published aiming to predict another and of equal important issue of machining operations: the tool wear. Zanger et al. [72] predicted the tool wear in machining Ti6Al4V alloy using FEM simulation. To reduce the complexity of the problem, two dimensional machining was tested instead of three dimensional machining. He validated the model for three different values of cutting speed and two different values of chip thickness using a tungsten carbide insert. The numerical model was implemented in ABAQUS 2D®, for the wear simulation Usui and Takeyama and Murata wear models were implemented. A quite complex hybrid numerical and experimental procedure was implemented to simulate the tool wear rate. The tool wear model was based on the assumption that the tool wear follows an Arrhenius approach, in practical the wear increases exponentially to the inverse of the absolute temperature. The validation with experimentally achieved data underlined the suitability of this model for a broad range of cutting velocities.

In a similar manner, Ducobu et al.[73] implemented a Finite Element Method of the tool wear in machining Ti6Al4V alloy in orthogonal cutting. A complex Arbitrary Lagragian Eulerian (ALE) formulation which combined the features of pure Lagragian and Eulerian analysis was implemented. No damage model was set for the simulations. Different geometrical configurations of the tools according to the experimental findings were modelled to change the tools geometry according to the removed portion of material from the flank face, allowing the simulation of the tool wear effect. The numerical study highlighted the influence of the wear of the tool on the chip formation and the machined surface. It showed that an experimental measure of the cutting forces should allow detecting a too much worn tool. Because such tool ended in an increase of the temperature and the plastic strains in the machined surface, which could induce modifications if the microstructure and increase the residual stresses.

The most recent numerical models developed include also the effects of the material microstructure alterations on the predicted cutting variables such as the cutting forces, the cutting temperatures and chip morphology. These models are thought to take into account the microstructural effect in the flow stress material equation and at the same time they can predict microstructural alterations as the micro-hardness, the grain size and the grain deformation if dynamic recrystallization occurs within the material. The most recent models have so proved that it is of primary importance to couple the flow stress equation with physical based models that describe thermo-mechanical mechanism arising in machining operations that can sensibly alter the chip formation mechanism. An example of two advanced FE numerical models have been presented by Arisoy et al. [74] and by Rotella et al. [75] in the 2014.

The FE code proposed by Arisoy et al. [74]could predict the micro hardness, the grain size and phase change of machined wrought Ti6Al4V alloy in three dimensional cutting. The model tested the effects of the tool micro geometry, of the coating and of the cutting conditions on the induced machined surface microstructure. The dynamic recrystallization was predicted using a Johnson-Mehl Avrami Kolmogrov (JMAK) model which was implemented in the DEFORM-3D® commercial FE code. They measured the recrystallized microstructure by means of self-developed imaging code implemented in Matlab®. The used flow stress model was a modified J-C model that includes temperature-dependent flow softening behaviour of high temperature titanium and nickel alloys described mathematically by the following equation:

$$\sigma = \left[A + B\varepsilon^{n} \right] \left[1 + C \ln \frac{\dot{\varepsilon}}{\varepsilon 0} \right] \left[1 - \left(\frac{T - Tr}{Tm - Tr} \right)^{m} \right] \left[D + (1 - D) \left[\tanh \left(\frac{1}{(\varepsilon + P)^{r}} \right) \right]^{s} \right] \tag{2.2}$$

$$D = 1 - \frac{T}{Tm} P = \left(\frac{T}{Tm} \right)^{s} \tag{2.3}$$

According to their findings, the numerical model predicted correctly machined induced microstructure following the experimental trends. The effects of the tool coating and of the tool radius on the material microstructure were correctly predicted by the numerical model.

In a similar work, Rotella et al.[75] coupled the modified J-C equation described in the equation 2.2 introducing the Hall-Petch equation in the first term to consider the effect of the induced material alterations on the chip formation mechanism. Furthermore they adopted the Zener-Hollomon equation introduced in an iterative procedure to determine the recrystallized grain size in the surface layers due to the cutting process. In this work, the cooling effect (dry and cryogenic) and of cutting parameters in orthogonal cutting of wrought Ti6AL4V alloy where numerically investigated. The model was calibrated and validated by comparing the cutting forces and the cutting temperatures.

It is note to point out that the literature lacks of numerical models aimed at predicting metal cutting operations on additive manufactured alloys, moreover most of the physical models that can be implemented in FE codes have been developed for globular microstructures rather than fine acicular microstructures that are more often found on AM materials such as EBM Ti6Al4V.

2.9. Weakness of literature review

The literature review empathized the copious of published papers dealing with the machinability investigation of wrought Ti6Al4V alloy. Up to now many aspects concerning machining this alloy have been cleared, and many steps ahead have been done since the last 50 years to solve the problems encountered in industry. Innovative cutting inserts, with coatings and substrates specifically designed for machining titanium alloys have been developed and

their range of cutting parameters optimized. In recent years, innovative high efficiency lubricating strategies such as HPWJA, cryogenic and MQL are improving the cutting performances of difficult to cut materials, furthermore for the case of the last two the sustainability of the manufacturing process is even improved. If giant steps have been done in this topic, few published papers are available on experimental investigations of AM alloys, and none of them deal with Ti6Al4V made by Electron Beam Melting which will be more and more diffused in the future for several applications: aero engine components, surgical implants, structural parts of racing cars motorcycles and bicycles etc. The second outcome from the literature review is the lack of papers aimed at testing the beneficial effects of cryogenic cooling on machined parts made by EBM Ti6AL4V alloy. The works present in literature asses improvement of the surface integrity of wrought Ti6AL4V alloy by the application of cryogenic cooling, nevertheless its effect on the machined part is rarely tested in terms of fatigue, wear and corrosion resistance. If these studies are important to speed up the industrialization of this innovative lubricating strategy, mechanical properties of machined components must be tested in order to validate it, especially because this material is often employed in exotic and extreme working conditions. Plenty of recent works have proved the sustainability of cryogenic machining, but all works are often oriented to enhance the productivity of aeronautic applications, rather than the biomedical one. Being a clean alternative to standard flooding, cryogenic cooling might find its ideal application in the biomedical industry where surgical implants need cleaning and sterilizing procedures after machining, hence dedicated works to biomedical surgical implants machining operations should be carried out to assess its applicability and to verify if the key surface properties for biomedical applications might be improved. A similar point that should be more investigated in literature that would persuade industries investing in cryogenic cooling is respecting the geometrical dimensions and tolerances set for the workpieces in parallel with the important researches that are currently being carried out on tool wear and surface integrity. The future researches regarding cryogenic machining must be more focused on real machining operations rather than just material testing which is more an academic exercise. According to that, geometrical accuracy has to be investigated. The last point that emerges from the literature review is the complete absence of numerical models of machining operations that have been developed for additive manufacturing alloys, or for material that presents peculiar fine acicular microstructures instead of more classical globular microstructures.
On the basis of the weaknesses of the literature review, the aims of this thesis can be summarised in the following main points:

- To investigate the machinability of Ti6Al4V alloy produced by Electron Beam Melting under dry, wet and cryogenic lubricating condition, adopting cutting parameters that are suitable for components made by AM techniques.

- To verify and validate the expected beneficial effects of cryogenic cooling on turned EBM Ti6Al4V cylindrical specimens with regard of their sliding wear resistance, in process conditions typical of biomedical applications.

- To validate the applicability of cryogenic cooling as sustainable and efficient alternative in turning acetabular cups made of EBM Ti6AL4V alloy. The geometrical accuracy of

machined acetabular cups will be evaluated, comparing cryogenic machining with standard dry and wet machining.

- To set the basis for future numerical models based on the Finite Element method to simulate the tri-dimensional machining operations on EBM Ti6AL4V alloy, or other alloys that present similar peculiar microstructures.

References

[1] Yan, M., Yu, P., An Overview of Densification , Microstructure and Mechanical Property of Additively Manufactured Ti-6Al-4V — Comparison among Selective Laser Melting , Electron Beam Melting , Laser Metal Deposition and Selective Laser Sintering , and with Conventional Po.

[2] Murr, L. E., 2015, Metallurgy of additive manufacturing : Examples from electron beam melting, Additive Manufacturing, 5:40–53, DOI:10.1016/j.addma.2014.12.002.

[3] Murr, L. E., Quinones, S. A., Gaytan, S. M., Lopez, M. I., Rodela, A., et al., 2009, Review article Microstructure and mechanical behavior of Ti – 6Al – 4V produced by rapid-layer manufacturing , for biomedical applications, 2/1:20–32, DOI:10.1016/j.jmbbm.2008.05.004.

[4] Kumar, S., 2014, Comprehensive Materials Processing. Elsevier.

[5] Murr, L. E., Gaytan, S. M., 2014, Comprehensive Materials Processing. Elsevier.

[6] Ivanova, E. P., Bazaka, K., Crawford, R. J., 2014, New Functional Biomaterials for Medicine and Healthcare. Elsevier.

[7] Froes, F. H., 2001, Titanium Alloys: Thermal Treatment and Thermomechanical Processing, Encyclopedia of Materials: Science and Technology, pp. 9369–9373, DOI:10.1016/B0-08-043152-6/01694-6.

[8] Sieniawski, J., Ziaja, W., Kubiak, K., Motyka, M., Microstructure and Mechanical Properties of High Strength Two-Phase Titanium Alloys.

[9] Murr, L. E., Esquivel, E. V, Quinones, S. A., Gaytan, S. M., Lopez, M. I., et al., 2008, Microstructures and mechanical properties of electron beam-rapid manufactured Ti – 6Al – 4V biomedical prototypes compared to wrought Ti – 6Al – 4V, Materials Characterization, 60/2:96–105, DOI:10.1016/j.matchar.2008.07.006.

[10] Facchini, L., Magalini, E., Robotti, P., Molinari, A., Facchini, L., 2010, powders Users who downloaded this article also downloaded : Microstructure and mechanical properties of Ti-6Al-4V produced by electron beam melting of pre-alloyed powders, DOI:10.1108/13552540910960262.

[11] Filip, R., Kubiak, K., Ziaja, W., Sieniawski, J., 2003, The effect of microstructure on the mechanical properties of two-phase titanium alloys, Journal of Materials Processing Technology, 133/1–/2:84–89, DOI:10.1016/S0924-0136(02)00248-0.

[12] Naves, V. T. G., Da Silva, M. B., Da Silva, F. J., 2013, Evaluation of the effect of application of cutting fluid at high pressure on tool wear during turning operation of AISI 316 austenitic stainless steel, Wear, 302/1–/2:1201–1208, DOI:10.1016/j.wear.2013.03.016.

[13] Che-Haron, C. H., 2001, Tool life and surface integrity in turning titanium alloy, Journal of Materials Processing Technology, 118/1–/3:231–237, DOI:10.1016/S0924-0136(01)00926-8.

[14] Ibrahim, G. a., Che Haron, C. H., Ghani, J. a., 2009, Surface integrity of Ti-6Al-4V ELI when machined using coated carbide tools under dry cutting condition, International Journal of Mechanical and Materials Engineering, 4/2:191–196.

[15] Ulutan, D., Ozel, T., 2011, Machining induced surface integrity in titanium and nickel alloys: A review, International Journal of Machine Tools and Manufacture, 51/3:250–280, DOI:10.1016/j.ijmachtools.2010.11.003.

[16] Darwish, S. M., 2000, Impact of the tool material and the cutting parameters on surface roughness of supermet 718 nickel superalloy, Journal of Materials Processing Technology, 97/1–/3:10–18, DOI:10.1016/S0924-0136(99)00365-9.

[17] Ginting, a., Nouari, M., 2009, Surface integrity of dry machined titanium alloys, International Journal of Machine Tools and Manufacture, 49/3–/4:325–332, DOI:10.1016/j.ijmachtools.2008.10.011.

[18] Devillez, a., Le Coz, G., Dominiak, S., Dudzinski, D., 2011, Dry machining of Inconel 718, workpiece surface integrity, Journal of Materials Processing Technology, 211/10:1590–1598, DOI:10.1016/j.jmatprotec.2011.04.011.

[19] Kishawy, H. ., Elbestawi, M. ., 1999, Effects of process parameters on material side flow during hard turning, International Journal of Machine Tools and Manufacture, 39/7:1017–1030, DOI:10.1016/S0890-6955(98)00084-4.

[20] Zhou, J. M., Bushlya, V., Stahl, J. E., 2012, An investigation of surface damage in the high speed turning of Inconel 718 with use of whisker reinforced ceramic tools, Journal of Materials Processing Technology, 212/2:372–384, DOI:10.1016/j.jmatprotec.2011.09.022.

[21] M.C.Shaw, Metal Cutting Principles, Third Edition, Massachusetts Institute of Technology Publication, Cambridge, 1954..

[22] Dudzinski, D., Devillez, a., Moufki, a., Larrouquère, D., Zerrouki, V., et al., 2004, A review of developments towards dry and high speed machining of Inconel 718 alloy, International Journal of Machine Tools and Manufacture, 44/4:439–456, DOI:10.1016/S0890-6955(03)00159-7.

[23] Noyan, I.C., Cohen, J.B. , 1987.Residual Stress – Measurement by Diffraction and Interpretation, Editor. Springer, New York..

[24] Sun, J., Guo, Y. B., 2009, A comprehensive experimental study on surface integrity by end milling Ti–6Al–4V, Journal of Materials Processing Technology, 209/8:4036–4042, DOI:10.1016/j.jmatprotec.2008.09.022.

[25] Niesłony, P., Grzesik, W., Laskowski, P., Sienawski, J., 2014, Numerical and Experimental Analysis of Residual Stresses Generated in the Machining of Ti6Al4V Titanium Alloy, Procedia CIRP, 13:78–83, DOI:10.1016/j.procir.2014.04.014.

[26] Arrazola, P. J., Özel, T., Umbrello, D., Davies, M., Jawahir, I. S., 2013, Recent advances in modelling of metal machining processes, CIRP Annals - Manufacturing Technology, 62/2:695–718, DOI:10.1016/j.cirp.2013.05.006.

[27] Zou, B., Chen, M., Huang, C., An, Q., 2009, Study on surface damages caused by turning NiCr20TiAl nickel-based alloy, Journal of Materials Processing Technology, 209/17:5802–5809, DOI:10.1016/j.jmatprotec.2009.06.017.

[28] M'Saoubi, R., Larsson, T., Outeiro, J., Guo, Y., Suslov, S., et al., 2012, Surface integrity analysis of machined Inconel 718 over multiple length scales, CIRP Annals - Manufacturing Technology, 61/1:99–102, DOI:10.1016/j.cirp.2012.03.058.

[29] ISO 3685, Tool life testing with single-point turning tools, 1993.

[30] Priarone, P. C., Rizzuti, S., Settineri, L., Vergnano, G., 2012, Effects of cutting angle, edge preparation, and nano-structured coating on milling performance of a gamma titanium aluminide, Journal of Materials Processing Technology, 212/12:2619–2628, DOI:10.1016/j.jmatprotec.2012.07.021.

[31] Liang, L., Liu, X., Li, X., Li, Y.-Y., 2015, Wear mechanisms of WC–10Ni3Al carbide

tool in dry turning of Ti6Al4V, International Journal of Refractory Metals and Hard Materials, 48:272–285, DOI:10.1016/j.ijrmhm.2014.09.019.

[32] Bermingham, M. J., Kirsch, J., Sun, S., Palanisamy, S., Dargusch, M. S., 2011, New observations on tool life, cutting forces and chip morphology in cryogenic machining Ti-6Al-4V, International Journal of Machine Tools and Manufacture, 51/6:500–511, DOI:10.1016/j.ijmachtools.2011.02.009.

[33] Ayed, Y., Germain, G., Ammar, a., Furet, B., 2013, Degradation modes and tool wear mechanisms in finish and rough machining of Ti17 Titanium alloy under high-pressure water jet assistance, Wear, 305/1–/2:228–237, DOI:10.1016/j.wear.2013.06.018.

[34] M'Saoubi, R., Johansson, M. P., Andersson, J. M., 2013, Wear mechanisms of PVD-coated PCBN cutting tools, Wear, 302/1–/2:1219–1229, DOI:10.1016/j.wear.2013.01.074.

[35] Armendia, M., Garay, a., Iriarte, L. M., Arrazola, P. J., 2010, Comparison of the machinabilities of Ti6Al4V and TIMETAL® 54M using uncoated WC-Co tools, Journal of Materials Processing Technology, 210/2:197–203, DOI:10.1016/j.jmatprotec.2009.08.026.

[36] Davies, M. a., Ueda, T., M'Saoubi, R., Mullany, B., Cooke, a. L., 2007, On The Measurement of Temperature in Material Removal Processes, CIRP Annals - Manufacturing Technology, 56/2:581–604, DOI:10.1016/j.cirp.2007.10.009.

[37] Krämer, A., Klocke, F., Sangermann, H., Lung, D., 2014, Influence of the lubricoolant strategy on thermo-mechanical tool load, CIRP Journal of Manufacturing Science and Technology, 7/1:40–47, DOI:10.1016/j.cirpj.2013.09.001.

[38] Armendia, M., Garay, A., Villar, A., Davies, M. A., Arrazola, P. J., 2010, High bandwidth temperature measurement in interrupted cutting of difficult to machine materials, CIRP Annals - Manufacturing Technology, 59/1:97–100, DOI:10.1016/j.cirp.2010.03.059.

[39] López de lacalle, L. ., Pérez, J., Llorente, J. ., Sánchez, J. ., 2000, Advanced cutting conditions for the milling of aeronautical alloys, Journal of Materials Processing Technology, 100/1–/3:1–11, DOI:10.1016/S0924-0136(99)00372-6.

[40] Symbols, G., 2010, A Review of the Machinability of Titanium Alloys, /September:43–52.

[41] Corduan, N., Himbart, T., Poulachon, G., Dessoly, M., Lambertin, M., et al., 2003, Wear Mechanisms of New Tool Materials for Ti-6AI-4V High Performance Machining, CIRP Annals - Manufacturing Technology, 52/1:73–76, DOI:10.1016/S0007-8506(07)60534-4.

[42] Narutaki, N., Murakoshi, A., Motonishi, S., Takeyama, H., 1983, Study on Machining of Titanium Alloys, CIRP Annals - Manufacturing Technology, 32/1:65–69, DOI:10.1016/S0007-8506(07)63362-9.

[43] Siddhpura, M., Paurobally, R., 2012, A review of chatter vibration research in turning, International Journal of Machine Tools and Manufacture, 61:27–47, DOI:10.1016/j.ijmachtools.2012.05.007.

[44] Shivpuri, R., Hua, J., Mittal, P., Srivastava, a. K., Lahoti, G. D., 2002, Microstructure-Mechanics Interactions in Modeling Chip Segmentation during Titanium Machining, CIRP Annals - Manufacturing Technology, 51/1:71–74, DOI:10.1016/S0007-8506(07)61468-1.

[45] Kuljanic, E., Fioretti, M., Beltrame, L., Miani, F., 1998, Milling Titanium Compressor Blades with PCD Cutter, CIRP Annals - Manufacturing Technology, 47/1:61–64, DOI:10.1016/S0007-8506(07)62785-1.

[46] Ezugwu, E. O., Wang, Z. M., 1997, Titanium alloys and their machinability, Journal of Materials Processing Technology, 68/3:262–274, DOI:10.1016/S0924-0136(96)00030-1.

[47] Ezugwu, E. O., 2005, Key improvements in the machining of difficult-to-cut aerospace superalloys, International Journal of Machine Tools and Manufacture, 45/12–/13:1353–1367, DOI:10.1016/j.ijmachtools.2005.02.003.

[48] Braga, D. U., Diniz, A. E., Miranda, G. W. ., Coppini, N. L., 2002, Using a minimum quantity of lubricant (MQL) and a diamond coated tool in the drilling of aluminum–silicon alloys, Journal of Materials Processing Technology, 122/1:127–138, DOI:10.1016/S0924-0136(01)01249-3.

[49] Machado, A. R., Wallbank, J., 1997, The effect of extremely low lubricant volumes in machining, Wear, 210/1–/2:76–82, DOI:10.1016/S0043-1648(97)00059-8.

[50] Paul, S., Chattopadhyay, A. B., 1995, Effects of cryogenic cooling by liquid nitrogen jet on forces, temperature and surface residual stresses in grinding steels, Cryogenics, 35/8:515–523, DOI:10.1016/0011-2275(95)98219-Q.

[51] Ezugwu, E. O., Bonney, J., Fadare, D. A., Sales, W. F., 2005, Machining of nickel-base, Inconel 718, alloy with ceramic tools under finishing conditions with various coolant supply pressures, Journal of Materials Processing Technology, 162–163:609–614, DOI:10.1016/j.jmatprotec.2005.02.144.

[52] Yildiz, Y., Nalbant, M., 2008, A review of cryogenic cooling in machining processes, International Journal of Machine Tools and Manufacture, 48/9:947–964, DOI:10.1016/j.ijmachtools.2008.01.008.

[53] Banerjee, S., Reidy, R. F., Mauer, L. B. R., 2008, Handbook of Silicon Wafer Cleaning Technology. Elsevier.

[54] Pusavec, F., Deshpande, A., Yang, S., M'Saoubi, R., Kopac, J., et al., 2015, Sustainable machining of high temperature Nickel alloy – Inconel 718: part 2 – chip breakability and optimization, Journal of Cleaner Production, 87:941–952, DOI:10.1016/j.jclepro.2014.10.085.

[55] Pusavec, F., Krajnik, P., Kopac, J., 2010, Transitioning to sustainable production - Part I: application on machining technologies, Journal of Cleaner Production, 18/2:174–184, DOI:10.1016/j.jclepro.2009.08.010.

[56] Wang, Z. Y., Rajurkar, K. P., 2000, Cryogenic machining of hard-to-cut materials, Wear, 239/2:168–175, DOI:10.1016/S0043-1648(99)00361-0.

[57] Hong, S. Y., Ding, Y., 2001, Cooling approaches and cutting temperatures in cryogenic machining of Ti-6Al-4V, International Journal of Machine Tools and Manufacture, 41/10:1417–1437, DOI:10.1016/S0890-6955(01)00026-8.

[58] Hong, S. Y., Markus, I., Jeong, W. C., 2001, New cooling approach and tool life improvement in cryogenic machining of titanium alloy Ti-6Al-4V, International Journal of Machine Tools and Manufacture, 41/15:2245–2260, DOI:10.1016/S0890-6955(01)00041-4.

[59] Bermingham, M. J., Palanisamy, S., Kent, D., Dargusch, M. S., 2012, A comparison of cryogenic and high pressure emulsion cooling technologies on tool life and chip

morphology in Ti-6Al-4V cutting, Journal of Materials Processing Technology, 212/4:752–765, DOI:10.1016/j.jmatprotec.2011.10.027.

[60] Klocke, F., Settineri, L., Lung, D., Claudio Priarone, P., Arft, M., 2013, High performance cutting of gamma titanium aluminides: Influence of lubricoolant strategy on tool wear and surface integrity, Wear, 302/1–/2:1136–1144, DOI:10.1016/j.wear.2012.12.035.

[61] Machai, C., Biermann, D., 2011, Machining of β-titanium-alloy Ti–10V–2Fe–3Al under cryogenic conditions: Cooling with carbon dioxide snow, Journal of Materials Processing Technology, 211/6:1175–1183, DOI:10.1016/j.jmatprotec.2011.01.022.

[62] Klocke, F., Krämer, A., Sangermann, H., Lung, D., 2012, Thermo-Mechanical Tool Load during High Performance Cutting of Hard-to-Cut Materials, Procedia CIRP, 1:295–300, DOI:10.1016/j.procir.2012.04.053.

[63] Paper, R., 2012, OVERVIEW OF CRYOGENIC COOLING IN MACHINING OF TI ALLOYS AND A, /July:1–9.

[64] Islam, M. N., Anggono, J. M., Pramanik, a., Boswell, B., 2013, Effect of cooling methods on dimensional accuracy and surface finish of a turned titanium part, International Journal of Advanced Manufacturing Technology, 69:2711–2722, DOI:10.1007/s00170-013-5223-3.

[65] Axinte, D. a., Andrews, P., Li, W., Gindy, N., Withers, P. J., 2006, Turning of advanced Ni based alloys obtained via powder metallurgy route, CIRP Annals - Manufacturing Technology, 55/1:117–120, DOI:10.1016/S0007-8506(07)60379-5.

[66] Umbrello, D., 2008, Finite element simulation of conventional and high speed machining of Ti6Al4V alloy, Journal of Materials Processing Technology, 196/1–/3:79–87, DOI:10.1016/j.jmatprotec.2007.05.007.

[67] Lee, W., Lin, C., 1998, Plastic deformation and fracture behaviour of Ti – 6Al – 4V alloy loaded with high strain rate under various temperatures, 241:48–59.

[68] Sima, M., Özel, T., 2010, Modified material constitutive models for serrated chip formation simulations and experimental validation in machining of titanium alloy Ti–6Al–4V, International Journal of Machine Tools and Manufacture, 50/11:943–960, DOI:10.1016/j.ijmachtools.2010.08.004.

[69] Calamaz, M., Coupard, D., Girot, F., 2008, A new material model for 2D numerical simulation of serrated chip formation when machining titanium alloy Ti–6Al–4V, International Journal of Machine Tools and Manufacture, 48/3–/4:275–288, DOI:10.1016/j.ijmachtools.2007.10.014.

[70] Styger, G., Laubscher, R. F., Oosthuizen, G. a., 2014, Effect of Constitutive Modeling During Finite Element Analysis of Machining-induced Residual Stresses in Ti6Al4V, Procedia CIRP, 13:294–301, DOI:10.1016/j.procir.2014.04.050.

[71] Schulze, V., Zanger, F., 2011, Numerical Analysis of the Influence of Johnson-Cook-Material Parameters on the Surface Integrity of Ti-6Al-4V, Procedia Engineering, 19:306–311, DOI:10.1016/j.proeng.2011.11.117.

[72] Zanger, F., Schulze, V., 2013, Investigations on mechanisms of tool wear in machining of Ti-6Al-4V using FEM simulation, Procedia CIRP, 8:158–163, DOI:10.1016/j.procir.2013.06.082.

[73] Ducobu, F., Arrazola, P.-J., Rivière-Lorphèvre, E., Filippi, E., 2015, Finite Element Prediction of the Tool Wear Influence in Ti6Al4V Machining, Procedia CIRP, 31:124–

129, DOI:10.1016/j.procir.2015.03.056.

[74] Arısoy, M., 2015, Journal of Materials Processing Technology Prediction of machining induced microstructure in Ti – 6Al – 4V alloy using 3-D FE-based simulations : Effects of tool micro-geometry , coating and cutting conditions, 220:1–26, DOI:10.1016/j.jmatprotec.2014.11.002.

[75] Rotella, G., Umbrello, D., 2014, CIRP Annals - Manufacturing Technology Finite element modeling of microstructural changes in dry and cryogenic cutting of Ti6Al4V alloy, CIRP Annals - Manufacturing Technology, 63/1:69–72, DOI:10.1016/j.cirp.2014.03.074.

Chapter 3

Experiments

3.1. The Approach

The most consolidated and efficient approach to investigate the machinability of an innovative material is through the conduction of machining tests under proper process conditions. These tests offer the chance to quantify important phenomena that are peculiar aspects of this kind of material characterization such as the tool wear, the surface integrity, the chip morphology, the cutting temperature etc. As a consequence, the scientific approach followed in this thesis is solidly based on the conduction of machining tests adopting real industrial conditions and equipment. The machinability is then quantified and discussed by performing dedicated experimental analysis to measure the most relevant variables. According to the literature review, no works have been published to research the machinability of Ti6AL4V alloys produced by Additive Manufacturing technologies, hence as a starting point, the main findings published on the wrought Ti6AL4V alloy machinability were taken into account as reference. As a first step, the process conditions were selected according to the literature review and to the industrial applications where machining of EBM Ti6AL4V alloy should be involved. In this phase, the cutting parameters, the proper tools and the lubricating strategies were selected. The first machining tests under standard cooling conditions were performed under these starting process conditions. After the first experimental findings, the adopted approach to characterize the machinability and the cutting parameters were exanimated and innovations were proposed in particular according to the biomedical requirements. In this second phase of the work, an innovative lubricating strategy to realise cryogenic cooling was developed, implemented and tested comparing the new experimental findings with those previously obtained to verify the effects of such innovation. An innovative approach to measure the tool wear that is suitable in particular for all the sticky materials as titanium and aluminium alloys was proposed and applied. Being the titanium alloy object of this thesis widely implemented in the biomedical industry, a deep emphasis was paid to the induced surface integrity of the machined alloy that should not be affected negatively by the process, on the contrary the machining operation could be tailored to enhance the mechanical performances of biomedical

implants. In particular, the fatigue and fretting mechanical phenomena are detrimental failure modes that affect several parts and features of the biomedical surgical implants as the taper neck joint of the hip replacement. The machining operations are renowned to alter the surface integrity hence the wear resistance of machined surfaces, on these basis, the sliding wear resistance of machined cylindrical pins made of EBM Ti6AL4V under dry and cryogenic lubricating conditions were than investigated by means of tribological wear tests under physiological environmental conditions found in the human body to verify the expected beneficial effects. A proper experimental set-up was designed and developed to characterize the sliding wear resistance of machined pins under biological environment conditions, applying the mechanical loads that are generated in the real geometrical features of implanted surgical implants. After these tests on the machinability of EBM Ti6Al4V alloy, and the characterization of the effect of cryogenic cooling on the sliding wear resistance, these findings were than applied in machining real AM Ti6Al4V surgical implants to investigate the industrial feasibility of cryogenic cooling for such specific applications. In parallel, a three dimensional cutting FE code was developed to simulate the microstructural alterations induced by the cryogenic cooling to put the basis for future numerical analysis of cutting processes on these new generation metal alloys that will be more and more diffuse in the future. In this chapter, the experimental analysis and the experimental apparatus adopted to conduct the machining tests and the measurements are described in detail. The main experimental results are discussed in the chapters 4 and 5 of this thesis.

3.2. Overview of the experimental methods

In this paragraph all the experimental methods used to characterize the machinability of EBM Ti6Al4V alloy are presented and the experimental apparatus described. The chapter is divided in two main sections with regard to the two main outcomes of the machining tests, namely the tool wear and the surface integrity characterization. A description of the cooling line designed and implemented into the CNC machine is also presented. Even dough the machining tests conducted for all the analysis presented in this thesis were carried out in different moments, having used the same experimental set-up for all the tests, it is introduced and described only in this chapter to avoid repetitions in the following part of the work.

3.3. Work material

The metal alloy investigated in this thesis is the Ti6Al4V obtained by Electron Beam Melting (EBM). The chemical composition of the as-built alloy is shown in Table 3.1: the comparison with the one of the wrought Ti6Al4V according to the ASTM F1472 [1] standard demonstrates a negligible difference in the percentage of all the chemical elements. The EBM material was produced by means of an ARCAM® A1 3D printing machine owned by the company Eurocoating S.p.a, specifically designed for the industrial production of surgical implants. Eight cylindrical specimens with a diameter of 40 mm and length of 230 mm were 3D printed having their symmetrical axis parallel to the beam direction, thus normal to the layers melting direction. The as built cylindrical specimens presented an external porous

surface generated by the AM production process as can be noted in the Figure 3.1. The microstructure of the as-built material was analysed by preparing and etching the samples with the Kroll's etchant. A detailed description of the microstructural analysis and procedure will be discussed later in this chapter. In the as-built condition, the material shows a fine acicular microstructure mainly consisting of α phase fine lamellae organized in a basket wave morphology with 7 % of bcc β phase in an hcp matrix (Figure 3.2). The microstructure is the result of the rapid solidification and subsequent annealing due to the thermal cycle of the working zone [2].

Figure 3.1 As built cylindrical workpiece made of EBM Ti6Al4V.

The microstructure analysis was conducted cutting some material samples normally and parallely to the building direction. As can be noted in Figure 3.2, the material is affected by a strong anisotropy due to profound differences in the cooling rates generated in the as printed material. Long dendrites generated along the building direction due to the epitaxial growth aligned with the main heat flow direction. No microstructural defects as cavities and cracks were detected on both the parallel and perpendicular directions with respect to the building direction in the bulk material. The mechanical properties of the EBM Ti6Al4V are presented in Table 3.2: higher values of Ultimate Tensile Stress, Hardness and a reduced elongation at fracture compared to the wrought one might foresee a reduced machinability.

The mechanical properties of the as built material were determined by tensile tests on cylindrical specimens machined from the same batch of material used to investigate its machinability. The tests were repeated three times applying the same test conditions as those expressed in [1].

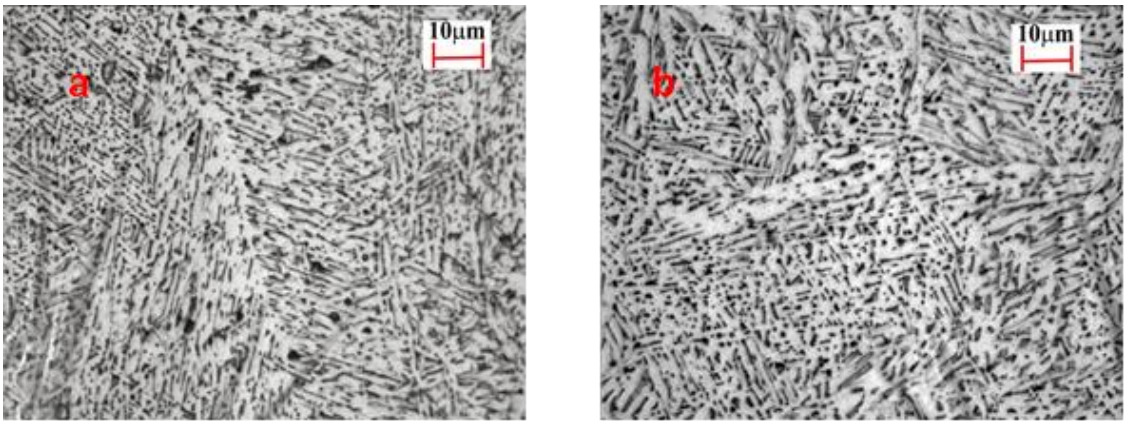

Figure 2 Microstructure of as built EBM Ti6Al4V alloy along the building direction a), and normal to the building direction b).

Table 3.1 Chemical composition of EBM Ti6AL4V alloy.

Chemical composition (wt%)							
Al	V	C	Fe	O	N	H	Ti
6	4	0.03	0.1	0.15	0.01	0.003	Bal

Table 3.2 Comparison between the mechanical properties of wrought and EBM Ti6Al4V alloys.

Material	**E [Gpa]**	**UTS [Mpa]**	**YS [Mpa]**	**Elongation (%)**	**HRC**
EBM Ti6Al4V	120	965	910	13.1	35
Wrought Ti6Al4V	118	872	790	16	31

3.4. Cryogenic cooling apparatus

The literature review highlighted the most advanced and efficient cooling strategies tested by researches and implemented in industry to enhance the machinability of difficult to cut materials as Nickel, Titanium and Cobalt base alloys. Minimum Quantity Lubrication (MQL), High Pressure Water Jet Assistance (HPWJA) and Cryogenic (Cryo) cooling strategies are without doubt the most promising strategies nowadays [3]. In this work, the possibility to implement one of these technologies to machine EBM Ti6AL4V alloy was taken into consideration by examining all the pros and cons [4]. The necessity to implement a green and clean cooling strategy suitable for machining titanium surgical implants forced the author to opt for cryogenic cooling. In the production process of surgical implants made of metal alloys, whether they are made by standard processes (casting or forging) or innovative Additive Manufacturing techniques, finishing machining operations are needed, such as turning the internal surface of the acetabular cup, external turning the taper of the modular neck hip implant etc. Traditionally these machining operations, mainly milling and turning, are

processed under standard flood cooling, adopting synthetic or more sustainable vegetable oil and water emulsions. The machined part, hence requires important cleaning and sterilizing operations that are expensive and time consuming for the companies. The ideal cooling conditions might be achieved by dry machining, because no drenching of the physiological porous metal surfaces is induced, and theoretically no cleaning operations would be needed anymore. Nonetheless, being biomedical alloys difficult to machine materials (Ti6Al4V, 17 - 4PH SS, F75CoCrMo), dry machining is nowadays still difficult to realize in practise, and it can still be considered an Utopia to pursue at the industrial scale. Bearing these considerations in mind, a clean lubricating strategy but at the same time efficient and tool safe might be the right compromise between the clean but not efficient (due to tool usage) dry machining and the hazardous and expensive wet machining. This issue can be achieved if cryogenic machining is employed, which consists in the application of high pressure cryogenic liquids as Liquified Nitrogen (LN2) or Liquified Carbon Dioxide (LCO_2) to the cutting zone. Being the intense lowering of the cutting temperature the principal beneficial effect of cryogenic cooling, which drastically reduces the tool wear and at the same time preserves the surface integrity of the machined surface. Nonetheless, thanks to the evaporation of the cryogenic fluid once in contact with the cutting interfaces, both the chips and workpieces are left dry and clean after the machining process, fulfilling the goals of reducing the costs for disposing the used coolants, cleaning the machined products and achieving a cleaner production process in comparison with standard flooding [5]. The other options were rejected because even if they might carry improvement in the machined surface integrity or an important reduction of the tool wear, they don't satisfy the sustainability issue, leaving pollutants when evaporating on the surgical implants. At the moment, even the most sophisticated and the cutting edge CNC machine available in the market, are not provided by a cryogenic cooling system, and just few industrial cases can be found in the market. As a result of that, a cryogenic cooling line have to be self-designed and built, customizing the CNC machine whether it is a lathe or a multi axis milling centre that are not designed properly for this kind of cooling technology. In this work, a cryogenic cooling apparatus was designed, built and installed in the CNC lathe used to conduct the machining tests. The author examined the cooling approaches used by the principal research groups world-wide already working on this technology by reading the literature. According to Pusavec et al.[6], that has designed a quite complicated fully automated and controlled cryogenic cooling system installed in a CNC lathe at the University of Ljubljana, the most efficient cryogenic fluid available in the market for cutting operations is the Liquide Nitrogen (LN2) due to its reduced production costs and higher cooling capacity than Liquid Carbon Dioxide (LCO2)[7]. Thanks to its thermodynamic properties, LN_2 is however more delicate to deal with because of its tendency to evaporate rapidly when supplied at pressures greater than the atmospheric value such as those needed for metal cutting processes, by the consequence, the cooling apparatus must be as much thermally insulated as possible. Many researchers have investigated different techniques and approaches to realised cryogenic cooling in metal cutting processes, trying different self-designed tool holders, modified tool inserts and different cooling directions. According to the literature review, the best results in terms of cooling capacity are achieved when supplying the LN_2 in liquid phase at high pressure and under multiple directions simultaneously. In one of the most relevant work on the topic, Bermingham et al. [8]compared the efficiencies of cryogenic and HPWJA cooling methods in rough turning of wrought Ti6Al4V alloy, using a modified tool holder that

allowed the possibility to try several LN2 cooling directions simultaneously. He assessed the delivery method as being of equal importance as the coolant itself, and the best results in terms of tool life were achieved by supplying the coolant on the rake face and on the flank face of the tool simultaneously with three separate nozzles. In agreement with these findings a cryogenic cooling apparatus dedicated for external turning of standard cylindrical specimens or internal turning of acetabular cups was designed in collaboration with the company AirLiquide Italia® S.p.a. It is note to point out that, for the purpose of this thesis which is more concerned on material testing rather than product innovation, a non-automated system was developed. The scheme of the implemented cooling line is illustrated in Figure 3.3. It consists in a vacuum insulated tank (Dewar) that is specifically designed to contain the liquid nitrogen at high pressure. The pressure of the liquid is generated by a cap of gas which consists in gasified nitrogen that pressurizes the liquid phase. The pressure is controlled and maintained at a constant level by means of a pressure control gas valve mounted on the top of the tank. When the liquid nitrogen is introduced into the Dewar, once it starts to gasify the re-pressuring system keeps the gas pressure at a constant desired value which corresponds at the pressure of the liquid emitted from the liquid phase connection. A pressure relieve valve is also installed on the Dewar to avoid the pressure to reach dangerous levels, in particular during the summer season. The liquid nitrogen is than carried towards the cutting zone through a vacuum insulated pipe specifically designed for this application, to avoid the formation of gas bubbles into the cooling line, inducing annoying fluctuations and instability in the liquid flow. Between the Dewar and the vacuum insulated pipe, an electro actuated security valve was installed to stop the flow in case of emergency.

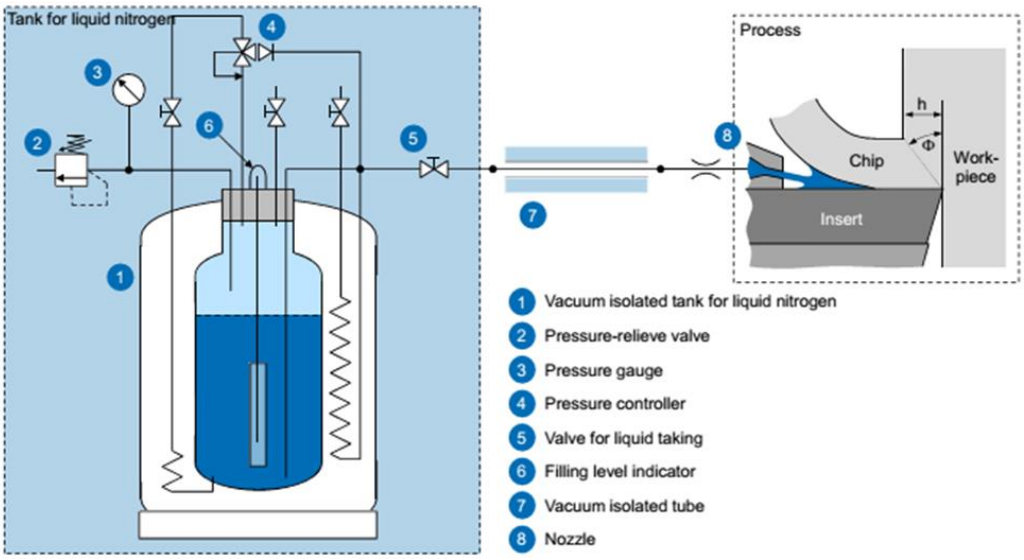

Figure 3.3 Schematic illustration of the cryogenic cooling line.

A lot of technical attention was paid to the nozzles system, because as previously mentioned, the CNC machine used for the machining tests is not designed to host a cryogenic cooling apparathus. For this work, it was decided to supply the LN_2 externally by means of external nozzles instead to design a modified tool holder with internal cooling holes[8]. In this manner, a more flexible solution might be adapted to machine other geometries rather than just cylindrical turning, or it could be used with different tool holders. A similar approach to

supply the LN_2 was used by Kynack et al.[9] in machining NiTi shape memory alloy, as can be observed in Figure 3.4.

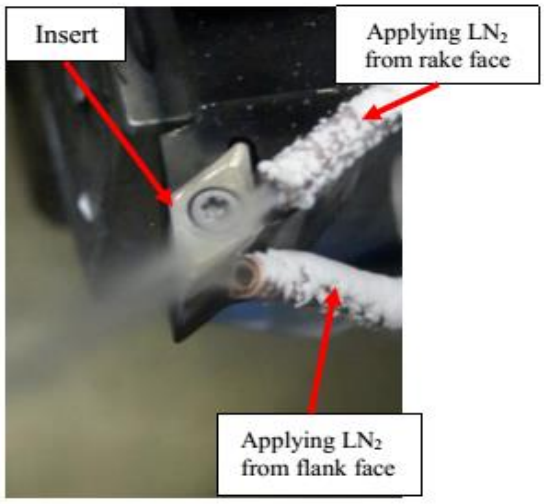

Figure 3.4 Aerosol cryogenic cooling on both the rake and the flank tool faces to enhance the cooling efficiency [9].

The tool nozzles system was designed starting from taking the dimensions by reverse engineering of the turrets that are installed on the revolver of the used CNC lathe, the Mori Seiky® NL 1500. Than an assembly made of a machined riser and a machined holed plate made of aluminium and brass respectively was designed by means of the Solidworks® design package. A 3D model of the designed assembly is visible in Figure 3.5b. The cap plate presented two holes to house two capillary copper tubes used to direct the LN_2 flow precisely towards the cutting zone.

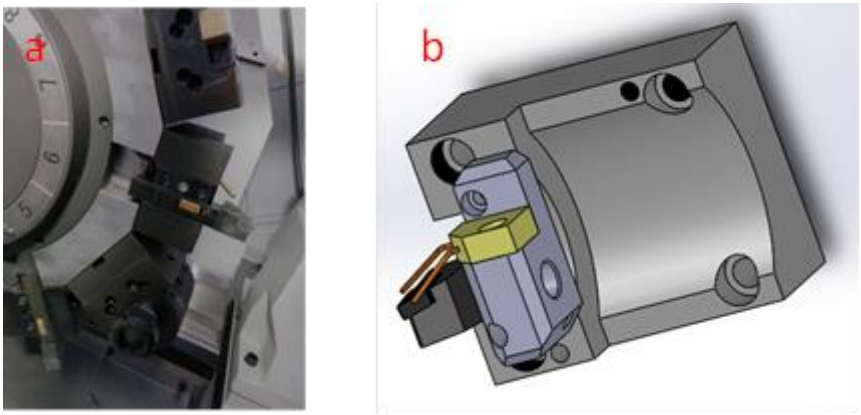

Figure 3.5 a) View of the turrets installed on the revolver of the CNC lathe and b) 3D CAD model of the nozzles system.

Thanks to the copper capillary tubes that presented an internal diameter of 0.9 mm, the LN_2 could be easily adjusted to cover the cutting zone entirely, avoiding the liquid to hit the workpiece. Due to the reduced mechanical loads and the efficiency of the thermal insulation of the vacuum insulated pipe, no FEM simulations were done to verify the dimensions of the

assembly or the fluid efficiency of the LN_2 directed on the tool tip. The complete view of the designed apparatus can be appreciated in Figure 3.6.

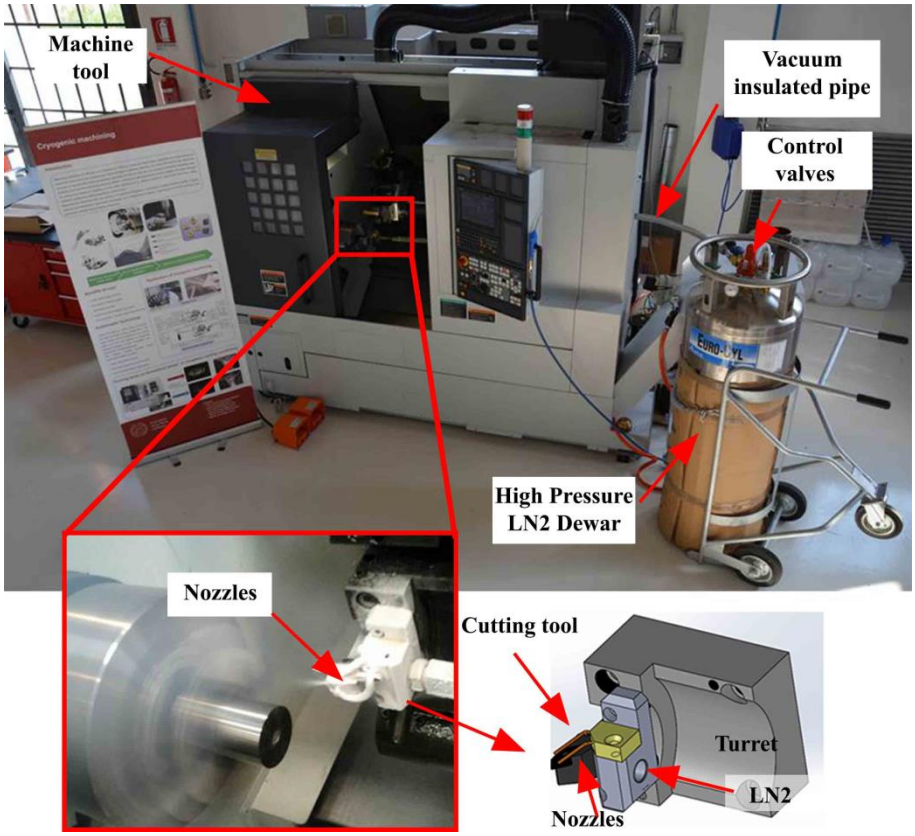

Figure 3.6 Overview of the developed cryogenic cooling apparatus implemented in the CNC lathe.

The working pressure of the Dewar was set at 15 bar, and under steady state conditions, a mass flow equal to 0.9 Kg/min of LN_2 was released. The mass flow was measured by laying the Dewar on a balance designed for motorcycles and measuring the mass reduction in a fixed time unit.

3.5.Machining tests

The machining tests were performed on a Mori Seiky® NL 1500 CNC lathe, a recent lathe that allows the possibility to perform also simple milling and drilling operations. The CNC machine was provided with different instrumentations inside according to the specific investigation to perform. As discussed in the literature review, it is important to acquire some variables in line during the machining process to refine the analysis of the material machinability. A clear view of the experimental set-up used in the machining tests can be observed in Figure 3.7. A Kistler®- type 9257 B three components piezoelectric dynamometer kindly provided by the colleagues form the University of Calabria was mounted on the lathe revolver for the acquisition of the cutting forces along the cutting speed and feed directions. An infrared camera FLIR A6000 - series provided by the colleagues from the University of Calabria was fixed on the tailstock allowing the acquisition of the thermal field from a frontal position with regard to the workpiece. The temperature near the cutting zone was measured

thanks to a 0.5 mm diameter thermocouple embedded into the turning insert: a T-type thermocouple was employed for the cryogenic cooling conditions, while a K - type one for dry and wet turning. In both cases, a hole of 0.9 mm diameter and 3 mm depth was realized by EDM at a distance from the tool nose of 1 mm. The thermocouple was maintained fixed in position during the machining operation by a thermo-conductive bound deposed into the hole, filling all the cavities. The acquisition of the cutting temperatures and forces was achieved through a LabView® based software.

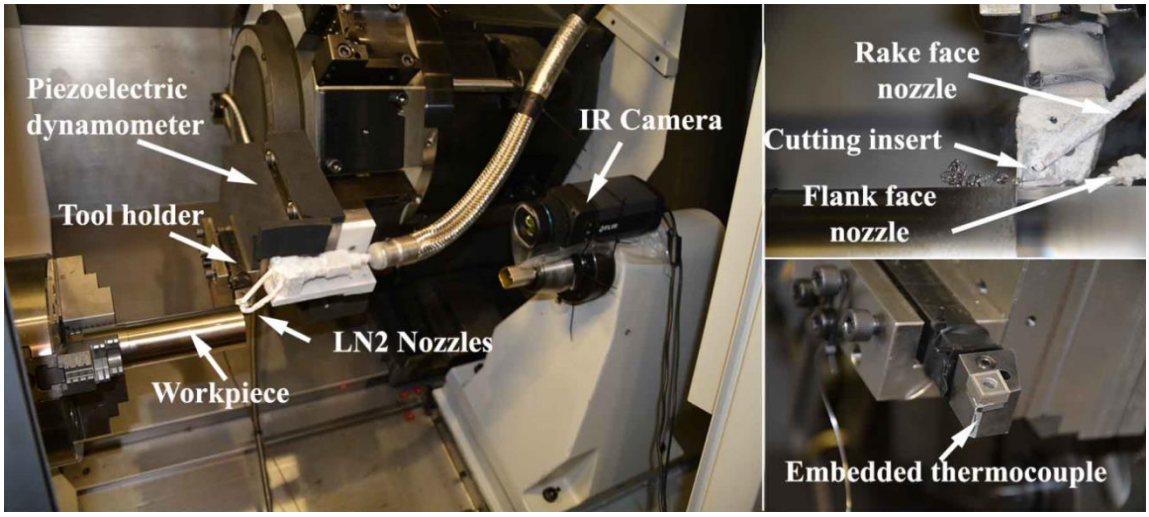

Figure 3.7 Experimental Set-Up used to acquire the cutting temperature and the cutting forces during cryogenic turning kindly provided by the colleagues from the University of Calabria.

Due to the lack of literature works and of technical data available on machining titanium alloys produced by Additive Manufacturing techniques, the choice of the cutting tools and the cutting parameters was done in collaboration with Sandvik Coromant Italy® that supported the author in the correct selection of the process parameters. It is noteworthy to spend some words about the peculiarities of the machining operations that are processed in industry on AM components. The machining allowance is the parameter that gave important indications on the cutting parameters to set in the turning tests. The adoption of AM technologies drastically reduce the volume of material to be removed by machining, if compared to bulky raw products from which traditionally mechanical components are cut out. The average machining allowance that is left on the Near Net Shape geometry of product made by AM technologies is in the order of 1mm. This value can be considered as a safe rule to completely remove the porosity in the surface layers that are philologically generated when using these forming technologies. For this entity of machining allowance, no rough machining operations are needed; meanwhile semi-finishing operations are more suitable. In order to respect this important industrial constraint, the machining tests were always carried out setting semi-finishing cutting conditions, and by the consequence the chosen cutting tool was dedicated for semi-finishing turning. Most of published works on machining wrought Ti6Al4V alloy in turning operations, report that uncoated tools perform better than coated ones as discussed by Armendia et al.[10] when he compared the machinability of two different titanium alloys. These alloys are renowned to be sticky on the cutting tool surfaces, causing problems of severe adhesion, with the formation of crater wear, of Built Up Edge and of Notch Wear. Within many of the tool coatings available in the market, the titanium is present in the form of

nitrides or carbides such as TiN, TiC, TiAlN and TiCN [11] The generation of high temperatures and high specific cutting pressures, favourites the adhesive wear due to the chemical affinity of the titanium present in the workpiece and the one in the tool coating. The absence of the coating tends to limit the occurrence of these tool wear modes that are often present in machining titanium alloys such as Ti6Al4V. Although these are precious considerations to take into account when dealing with machining titanium alloys, a coated cutting insert was used in this work, as advised by the tool manufacturer. A TiAlN coated tungsten carbide insert CNMG120404SM - GC1105 (substrate composition: 93 % WC and 7 % Co) supplied by Sandvik –Coromant® was used for all the machining tests. This cutting insert is characterized by having a radius of 0.4 mm, rake and clearance angles are of 7° and 0° respectively. The TiAlN coating is applied by the PVD technique and it allows good toughness, uniform flank wear, and overall high machining performances thanks to the mutual combination of a low friction coefficient brought by the presence of aluminium and a good thermal barrier due to the poor thermal conductivity of titanium that improves the thermal protection of the substrate. This cutting insert was mounted on a Sandvik® PCLNR/L tool holder with an approach angle Kr of 75°. The cutting parameters advised to machine wrought Ti6Al4V alloy by means of this cutting insert indicated a cutting speed range equal to 55 – 85 m/min, a feed range equal to 0.1 - 0.3 mm/rev and a depth of cut range equal to 0.2 - 2.5 mm. To realise semi-finishing cutting conditions, the depth of cut has to be limited to reduce the material removal rate at levels consistent with the goal of this turning operation. The following cutting parameters were tested in all the machining operations carried out in this thesis:

Cutting speed (Vc) = 50 - 80m/min
Feed rate (f) = 0.1 - 0.2mm/rev
Depth of cut (ap) = 0.25 mm

The following experimental plan resumed in the Table 3.3 was then followed to investigate the tool wear and the surface integrity in machining EBM Ti6Al4V alloy. The criterion chosen to consider the tool wear effect, was not based on the standard incremental machining cutting length until reaching the tool life criterion which is mainly adopted by the researches to investigate the tool wear according to the ISO 3685 standard [12], on the contrary a fixed cutting length operation approach was adopted in this thesis. The first approach is necessary to predict the tool life especially in rough cutting operations that for the case of difficult to cut materials is reached in few minutes [13]. In machining conditions set for this study, this approach could have led to very long machining times causing the waste of expensive test material to find a result that is not of primarily importance in this specific machining operation. A preliminary test conducted according to classical tool life approach led to turning operations lasting more than 200 minutes using a lot of the available material for this research. The machining tests for each cutting parameters combination were organised on three different cutting lengths of 3, 8 and 15 minutes respectively. These values are more representative of the machining operations that can be encountered in the production processes of AM surgical implants. Furthermore, this approach was already used by Armendia et al. [10] even in rough machining conditions, stating that the cutting length of 15 minutes is of industrial interest for machining wrought Ti6Al4V alloy.

Table 3.3 Experimental plan for machining tests.

Test Condition	Cutting speed [m/min]	Feed rate [mm/rev]	Depth of cut [mm]	Lubrication strategy
1	50	0.1	0.25	Dry
2	50	0.2	0.25	Dry
3	80	0.1	0.25	Dry
4	80	0.2	0.25	Dry
5	50	0.1	0.25	Cryogenic
6	50	0.2	0.25	Cryogenic
7	80	0.1	0.25	Cryogenic
8	80	0.2	0.25	Cryogenic
9	50	0.1	0.25	Wet
10	50	0.2	0.25	Wet
11	80	0.1	0.25	Wet
12	80	0.2	0.25	Wet

The machining tests were so executed with a fresh tool for each cutting condition, once the fixed cutting length was reached, the test was stopped, a portion of the machined workpiece was cut by using the parting tool available in the CNC lathe and the chips collected for the chip morphology characterization. The turning tests were repeated three times to achieve a statistical repeatability and the wet lubricating condition was realised by exploiting the lubricating embedded apparatus provided in the CNC lathe. A water and oil emulsion with a concentration of 5 % and supplied at the pressure of 5 bars was used as cutting fluid. A standard commercial semi-synthetic metalworking fluid Monroe® Astro-Cut HD XBP was mixed with water to create the adopted cutting fluid.

3.6. Characterization of tool wear mechanisms

The wear phenomenon needs different techniques to be investigated accurately. Different wear mechanisms as diffusion wear, mechanical and thermal fatigue, abrasion and adhesion wear generate several and often difficult to characterize tool wear modes. Basically these wear mechanism are reflected on the cutting process by the formation of particular tool wear modes. When machining titanium alloys, the main tool wear modes generally observed are: Built Up Edge(BUE), Notch Wear, Flank Wear, Crater Wear, Chipping due to adhesion and the Built Up Layer [11]. As in any other manufacturing process, the wear mechanism is influenced by several factors that change instantly: the specific contact pressure between the mating bodies, the temperature, the relative speed, the chemical affinity between the materials in contact, the state of the surface topography and the presence of third bodies that alter the contact conditions, such as the presence of a lubricant. It is easy to understand that, the adopted machining process parameters such as the cutting parameters, the cutting tool material, the workpiece material and the lubrication strategy play central roles in the tool wear mechanisms formation. It is important to measure the tool wear at different cutting lengths to understand its variation with time, this is generally performed in line during the cutting

process through stereoscopic microscopes or toolmaker microscopes, but at the same time at the end of each cutting step to deepen the analysis it is better to opt for the more accurate SEM microscope.
In this work, an initial qualitatively analysis of the cutting edges and cutting surfaces was carried out during the turning trials by means of a Zeiss® SteREO Discovery V8 stereomicroscope. Later on, adhesion, attrition and notch wear mechanisms were evaluated by using a FEI QUANTA 450™ Scanning Electron Microscope (SEM) equipped with the Everhart Thornley detector (ETD) and Backscattered Electron Detector (BSED). The second detector is a powerful tool for researchers in the field of machining, because it allows the identification of different materials (not the chemical elements) hit by the electron beam. As a consequence, this detector is mainly adopted [14] to investigate the adhesion wear mechanism and all the correlated tool wear modes. In this work, the BSED detector was extensively used to analyse the BUE, the crater wear and BUL on the tools rake face. An example of BSED SEM image is presented in Figure 3.9, the pastel grey areas correspond to the adhered workpiece on the cutting edge, while the white areas to the tool substrate, and the dark grey areas correspond to the virgin tool coating. A qualitative SEM analysis was so carried out to understand the evolution of the tool wear modes at the three fixed cutting lengths. In parallel the SEM microscope was also utilized to quantify the tool wear, a jig was designed and built by rapid prototyping to allow a repeatable measurement of the flank wear width, in practise being the tool mainly worn on the curved part of its flank due to the low value of depth of cut adopted, the jig positioned the cutting insert perfectly vertical on the plate of the SEM microscope, allowing the measurement of flank wear width in this portion of the tool flank, namely the VBc value according to the standard ISO3685 [12].The workpiece material adhesion on the worn cutting tools was quantified by means of an EDAX® dispersive X-Ray spectroscopy detector (EDS): both EDS mapping and point analysis were conducted by using an acceleration voltage of 20 kV. This detector allows the identification and the quantification of the chemical elements present in the analysed spot. The zone mapping function is useful to have a coloured map of the SEM image, where each pixel is coloured with the corresponding colour assigned by the software to each chemical element. A Sensofar Plu-Neox™ optical 3D profiler with a resolution of less than 20 nm on the optical Z-axis was adopted for the 3D scanning of the rake face of cutting tools. To investigate more deeply the adhesion wear mechanism, the thickness of the adhered Ti6Al4V layer onto the tool rake face was measured by an innovative procedure. A fixing reference frame designed and built by rapid prototyping, was used to orientate the cutting insert on the instrument table with a repeatable positioning manner. Thanks to the instrument software, linear sections of the acquired surfaces could be traced along any directions on the X-Y plane (the table plane), allowing plotting the surface section profile on a projected plane. The points heights, namely the Z coordinates, were then displayed at varying positions along the linear section. To better understand the position of the cutting section, the 3D sketch presented in the Figure3.8 on the left can be observed, in which the origin of the x axis is placed on the flank face. An example of acquired images of the insert rake face is presented in Figure3.8b; the lighter coloured area along the cutting edge represents the adhered material. A similar approach was used by Armendia et al. [10] to measure the depth of the crater wear when he compared the machinability of two different titanium alloys. To measure the thickness of the crater wear, there is the need to clean the

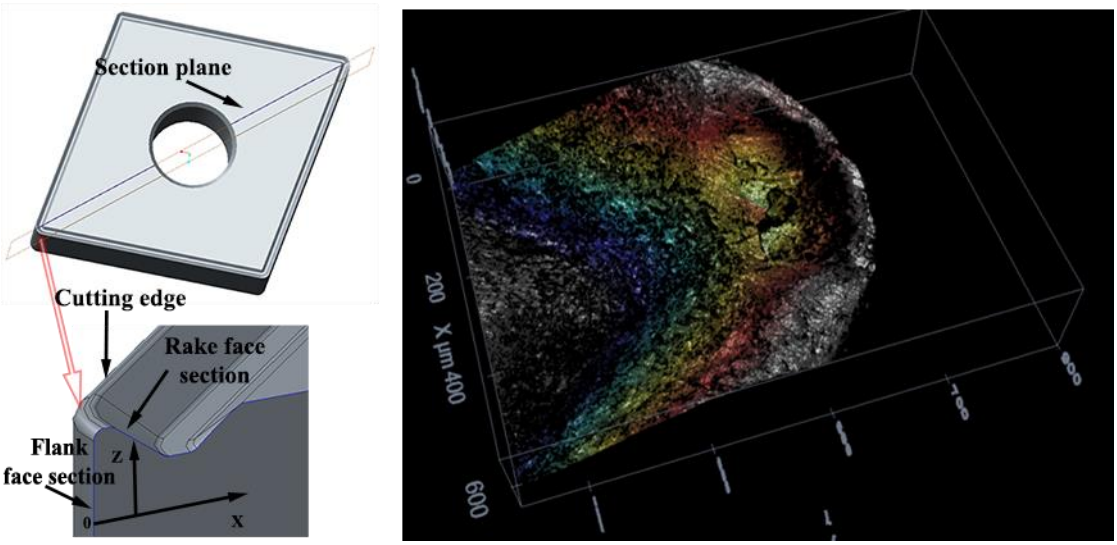

Figure 3.8 3D sketch of the tool wear measuring approach (on the left) and example of 3D scan of the tool rake face by means of the surface profilometer (on the right).

tools rake face from the great amount of material that usually adheres on the rake face of the tool. The same approach proposed to quantify the thickness the adhered layer to highlight the effect of the cooling strategy, was applied to quantify the crater wear. An hydroflouridric acid was adopted to etch the tool tip for 10 seconds, to remove the adhered material. The profilometry analysis was then repeated on cleaned tools, to measure the thickness of the crater wear. Finally the abrasive wear was investigated by means of SEM analysis, adopting the ETD detector.

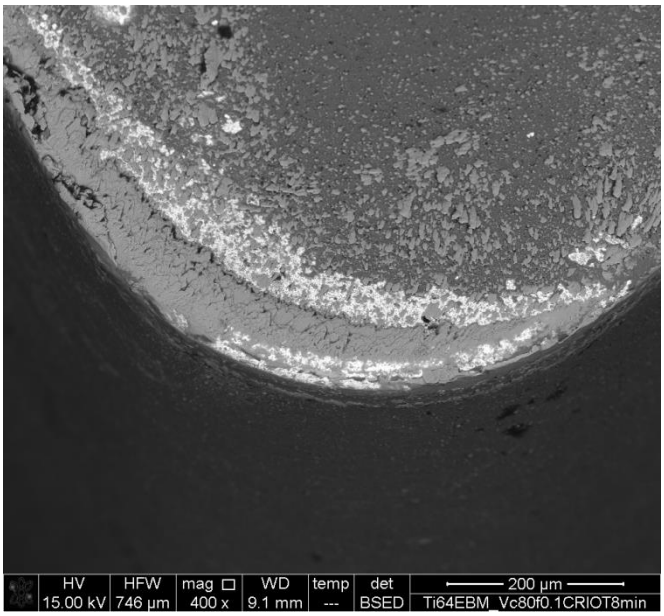

Figure 3.9 Example of SEM image of the tool rake face acquired by means of the BSED detector.

3.7. Characterization of the surface integrity

The surface integrity of the machined workpieces was quantified and analysed by several approaches according to the recent advantages as described in the literature review [15]. A cylindrical specimen of the workpiece for each of the machining test trial was cut to allow the off line analysis. According to the standard [16], the main surface roughness parameters Ra and Rt (arithmetic mean surface roughness and total height of the roughness profile) were acquired by using a Taylor Hobson-Subtronic 25™ portable roughness tester, that allowed an immediate reading of the selected parameters. For the measurements a cut off filter equal to 0.8 microns was adopted after a calibration procedure, as required by the standard [16]. These parameters are easy to measure but they allow an immediate comprehension of the cutting parameters, of the tool wear and of the cutting time effects on the surface integrity. The measurements were repeated three times on three different positions along the cylindrical surface to achieve a statistical repeatability of the measuring procedure. The surface topography of the machined surfaces, was acquired by using a Sensofar Plu-Neox™ digital profiler, by positioning the cylindrical specimens on the instrument table, and scanning the surface with a fixed matrix of 1.2 x 0.4 mm in three different positions. The surface scans were acquired in bright field light conditions with a confocal optic having a maximum zoon power in the z axis of 100 magnifications. This analysis, allowed the observation of the feed marks topography and the presence of defects as material depositions, double feed marks, craters etc. Thanks to the control software provided with the instrument, it was possible to mathematically section the three dimensional points cloud and to plot the planar section to carry out measurements of the feed marks morphology. This measuring procedure helped to investigate the effects of the main cutting parameters on the surface integrity, giving important information on the quality of the final product if machined under such conditions. An example of a profilometry scan is reported in Figure 3.10.

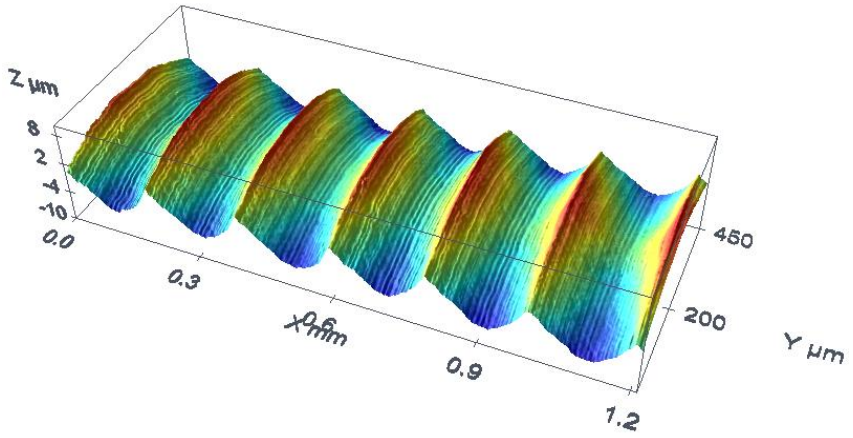

Figure 3.10 Example of turned surface topography acquired by means of the profilometer.

Machining operations are recognised to leave defects on the final surfaces, which might provoke detrimental effects on the product service life, affecting in particular its fatigue resistance [17]. In this work, a SEM analysis was carried out to qualitatively investigate the amount and main typologies of defects present on the machined surfaces by adopting dry, wet and cryogenic cooling strategies. Moreover, an EDS analysis was conducted to attest the

chemical composition of the adhered external particles on the machined surfaces, by means of an EDAX® dispersive X-Ray spectroscopy detector installed in the SEM.
Microstructural analysis was performed to evaluate the main effect of the machining process parameters on the material microstructure. In turning operations, the microstructure is mainly deformed along the cutting speed effect. Usually, these alterations are inspected by means of different instrumentations on the normal cross section with respect to the rotational axis of the workpiece. Samples of the machined test pieces for all the machining test trials, were cut using a metallographic disc cutter, hot mounted using a Struers® hot mounting press and then grinded and polished according to the procedure outlined in the Table3.4. The specimens were grinded and polished by using an automatic Struers® griding machine. After the polishing procedure, the specimens were etched to evidence the material microstructure. They were rinsed into a Kroll's reagent for 30 seconds, than cleaned by using soup and water than methanol. The microstructural analysis was conducted by using an inverted optical microscope Leica MEF4U™ equipped with a high definition digital camera. The metallographic images were acquired at 500 and 1000 magnifications. Aiming to evaluate the thermo-mechanical effects on the machined material layers, micro-hardness measurements were performed by means of a Leitz Durimet™ Vickers micro-hardness tester applying a load of 50 gr for 30 s. The micro-hardness was measured along radial profile beneath the machined surface, maintaining the same pitch between one indentation and the next one for all the analysed specimens.

Table 3.4 Procedure to polish EBM Ti6AL4V for microstructural analysis.

Step	Surface	Abrasive type	Speed (rpm)	Force (N)	Time (s)
Planar grinding	SiC-Paper	Gr. 60 Gr. 120 Gr. 320 Gr. 500 Gr. 800 Gr. 1200 Gr. 4000	300	150	150
Final polishing	MD-Chem	30% Colloidal Silica and 70% Hydrogen Peroxide	150	60	240

The residual stresses on the machined surfaces was analysed by means of the XRD technique using the $\sin^2\psi$ method [18]. The XRD analysis was carried out on an Enixè® TNX diffractometer, following the ASTM E2860 - 12 standard. The employed parameters are reported in Table 3.5. XRD is the most non-destructive way of evaluating surface residual stresses. The basic principle is based on Bragg's law, which states that when a monochromatic X - ray beam with wavelength λ is projected onto a crystalline material at an angle θ, diffraction occurs only when the distance travelled by the rays reflected from successive planes differs by a complete number n of wavelengths (Figure 3.11). Lines ABC and DEFGH represents X -ray radiation. Initially, lines AB and DE have the same

wavelength. These lines will remain in phase if EFG is an integral multiple of this wavelength. This causes reinforcement of the incident X - ray beam, which is known as constructive interference or diffraction. If EFG is not an integral multiple of the incident beam wavelength, then the lines will be out of phase resulting in destructive interference and diffraction will not occur. This can be expressed using $n\lambda = 2d\sin\theta$, where n is an integer, λ is the wavelength of a beam of X - rays incident on a crystal with lattice planes separated by distance d, and θ is the Bragg angle. XRD relies on the elastic deformation of a material to measure internal stresses. The deformation cause changes in the spacing of the lattice planes from their stress free value to a new value that corresponds to the magnitude of the applied stress. Because the wavelength is constant, the unknown parameters in Bragg's equation are the interplanar spacing d and Bragg angle θ. Thus, if θ becomes known, the d value can be obtained using Bragg's law. Complete theories and procedures for residual stress measurements by using XRD method can be found in [19] .

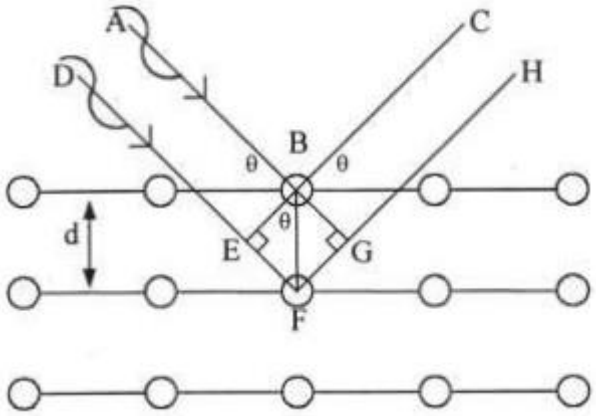

Figure 3.11 Diffraction of X-rays by a crystalline material.

Table 3.5 Parameters for measuring the residual stresses by XRD analysis.

Radiation	CuKα
Collimator Diameter (mm)	1
Detector type	40°
Filter	Nickel
Acquisition time	240s
Oscillation range	±40°
Number of ψ angles	9
Bragg Angle 2θ (Deg)	141.8
Tube current	85 μA
Tube tension	29kV
Miller's Index (hkl)	213
Selection of Ψ	Automatic
Measurements method	Static

The residual stresses were measured along axial and tangential directions, where the axial direction corresponded to the feed direction in turning, meanwhile the tangential direction corresponded to the cutting speed direction. In order to evaluate the stressed state in depth, starting from the surface, successive layers of material were removed by electro-polishing to avoid the modification of machining- induced stresses.

3.8. Chip morphology characterization

The collected chips were cut, cold mounted and polished manually according to the crystallographic procedure described above for the specimens and then etched with the Kroll's reagent to evidence the microstructure, allowing at the same time a more accurate micro-geometrical characterisation of the chip segmentation. The micro-geometry of the chips was measured by using the imaging software supplied with the optical microscope Leica MEF4U® used also to observe the microstructure of the chips.

References

[1] ASTM F1537-11, Standard Specification for Wrought Cobalt-28Chromium-6Molybdenum Alloys for Surgical Implants (UNS R31537, UNS R31538, and UNS R31539), ASTM International, West Conshohocken, PA, 2011, www.astm.org

[2] Facchini, L., Magalini, E., Robotti, P., Molinari, A., Facchini, L., 2010, powders Users who downloaded this article also downloaded : Microstructure and mechanical properties of Ti-6Al-4V produced by electron beam melting of pre-alloyed powders, DOI:10.1108/13552540910960262.

[3] M'Saoubi, R., Axinte, D., Soo, S. L., Nobel, C., Attia, H., et al., 2015, High performance cutting of advanced aerospace alloys and composite materials, CIRP Annals - Manufacturing Technology, 64/2:557–580, DOI:10.1016/j.cirp.2015.05.002.

[4] Debnath, S., Reddy, M. M., Yi, Q. S., 2014, Environmental friendly cutting fluids and cooling techniques in machining: a review, Journal of Cleaner Production, 83:33–47, DOI:10.1016/j.jclepro.2014.07.071.

[5] Deiab, I., Raza, S. W., Pervaiz, S., 2014, Analysis of lubrication strategies for sustainable machining during turning of titanium ti-6al-4v alloy, Procedia CIRP, 17:766–771, DOI:10.1016/j.procir.2014.01.112.

[6] Pušavec, F., Kopač, J., 2011, Sustainability assessment: Cryogenic machining of inconel 718, Strojniski Vestnik/Journal of Mechanical Engineering, 57/9:637–647, DOI:10.5545/sv-jme.2010.249.

[7] Pusavec, F., Deshpande, A., Yang, S., M'Saoubi, R., Kopac, J., et al., 2014, Sustainable machining of high temperature Nickel alloy - Inconel 718: Part 1 - Predictive performance models, Journal of Cleaner Production, 81:255–269, DOI:10.1016/j.jclepro.2014.06.040.

[8] Bermingham, M. J., Palanisamy, S., Kent, D., Dargusch, M. S., 2012, A comparison of cryogenic and high pressure emulsion cooling technologies on tool life and chip morphology in Ti-6Al-4V cutting, Journal of Materials Processing Technology, 212/4:752–765, DOI:10.1016/j.jmatprotec.2011.10.027.

[9] Kaynak, Y., Karaca, H. E., Noebe, R. D., Jawahir, I. S., 2013, Tool-wear analysis in cryogenic machining of NiTi shape memory alloys: A comparison of tool-wear performance with dry and MQL machining, Wear, 306/1–/2:51–63, DOI:10.1016/j.wear.2013.05.011.

[10] Armendia, M., Garay, a., Iriarte, L. M., Arrazola, P. J., 2010, Comparison of the machinabilities of Ti6Al4V and TIMETAL® 54M using uncoated WC-Co tools, Journal of Materials Processing Technology, 210/2:197–203, DOI:10.1016/j.jmatprotec.2009.08.026.

[11] Ezugwu, E. O., Wang, Z. M., 1997, Titanium alloys and their machinability, Journal of Materials Processing Technology, 68/3:262–274, DOI:10.1016/S0924-0136(96)00030-1.

[12] ISO 3685, Tool life testing with single-point turning tools, 1993.

[13] Wang, Z. Y., Rajurkar, K. P., 2000, Cryogenic machining of hard-to-cut materials, Wear, 239/2:168–175, DOI:10.1016/S0043-1648(99)00361-0.

[14] Naves, V. T. G., Da Silva, M. B., Da Silva, F. J., 2013, Evaluation of the effect of application of cutting fluid at high pressure on tool wear during turning operation of

AISI 316 austenitic stainless steel, Wear, 302/1–/2:1201–1208, DOI:10.1016/j.wear.2013.03.016.

[15] Arrazola, P. J., Özel, T., Umbrello, D., Davies, M., Jawahir, I. S., 2013, Recent advances in modelling of metal machining processes, CIRP Annals - Manufacturing Technology, 62/2:695–718, DOI:10.1016/j.cirp.2013.05.006.

[16] ISO 4287, Geometrical Product Specifications (GPS) Surface texture: Profile method, Terms, definitions and surface texture parameters.

[17] Ulutan, D., Ozel, T., 2011, Machining induced surface integrity in titanium and nickel alloys: A review, International Journal of Machine Tools and Manufacture, 51/3:250–280, DOI:10.1016/j.ijmachtools.2010.11.003.

[18] Noyan, I.C., Cohen, J.B. , 1987.Residual Stress – Measurement by Diffraction and Interpretation, Editor. Springer, New York

[19] Umbrello, D. (2004). FE – Analysis of machining processes: innovative experimental techniques for results assessing. PhD, University of Calabria

Chapter 4

Experimental results: Machinability of EBM Ti6Al4V

4.1. Introduction

The literature review revealed the complete lack of works regarding the study of the machinability of Electron Beam Melted (EBM) Ti6Al4V alloy. At the moment, in industrial applications the technical guidelines to machine wrought Ti6Al4V alloy are followed, nonetheless differences in mechanical properties generated by a different microstructure (see Table 2.2) foresee discrepancies in their machinability that have to be investigated to improve the efficiency of the manufacturing process and the reliability of components. Even if the tool wear cannot be considered the primarily driving parameter when dealing with additive manufactured alloys, its physical deterioration has to be investigated to keep under control its effect on the surface integrity that as reported in several experimental studies[1] is influenced by the state of the tool and how it interacts with the material being cut. Due to the very limited amount of machining allowance to remove from the near net shaped raw products achieved by the use of these technologies, different machining strategies might result to be efficient in milling and turning AM super alloys. Even after more than 50 years of research aimed to improve the machinability of wrought Ti6Al4V, tools manufacturers' advice the use of great flows of lubricoolant, keeping low cutting parameters to machine aerospace and biomedical components. Dry turning has been tested several times for standard titanium products manufacturing, but even by adopting high performance cutting tool materials, its feasibility in real production processes is still far to be efficiently implemented [2]. However, sustainable cooling strategies such as dry and cryogenic might find their ideal application in

machining AM surgical implants because of the very short cutting times (lengths), the limited necessity to speed up the machining process to enhance the productivity (low volumes of AM products) and above all to reduce the cleaning and sterilizing costs.
Nowadays the applied cutting fluid for metalworking applications is the crucial factor regarding the sustainability of machining processes [3], being considered as one of the main environmental hazards in the context of manufacturing [4]. The conventional cutting fluids are not biodegradable but environmental contaminants; moreover, the biocides, which are used to control coolants bacteria and microbial activity, as well as to extend the coolant life, are extremely hazardous additives. Such fluids can damage water and soil resources when wrongly handled, therefore, as a consequence, rigid and expensive disposal procedures have been recently imposed to the manufacturing companies [5]. Furthermore, a prolonged exposure of the operators to standard emulsion coolants is scientifically proved to cause serious skin and breathe illnesses [6].
Bearing these considerations in mind, testing the machinability of EBM Ti6Al4V alloy under sustainable lubricating conditions can be considered more important for future industrial applications in particular for the biomedical industry. By the consequence, more emphasises to dry and cryogenic turning was given in this work, starting with the investigation of the EBM Ti6Al4V machinability. In this chapter the main experimental findings regarding the tool wear and the machined surface integrity are presented according to the experimental approaches described in chapter 3. The tool wear is characterized by measuring the flank wear width at different cutting times for all the tested lubricating conditions, than a SEM analysis regarding the main tool wear mechanisms and modes is presented to put in evidence the effects of the lubricating condition. Subsequently, a profound investigation of the tool wear by means of SEM and EDS analysis is proposed to assess the feasibility of the tested sustainable turning procedures under dry and cryogenic cooling. In the second part of this chapter, a comparison regarding the machined surface integrity in terms of surface roughness, residual stresses, surface defects and microstructural alterations under semi-finishing cutting conditions by adopting dry, wet and cryogenic lubricating strategies is presented.

4.2. Tool Wear analysis

The machinability of EBM Ti6AL4V was investigated under the process conditions summarised in Table 3.3. This paragraph resumes the main tool wear modes and mechanisms; the first part provides a general overview of the tool wear, highlighting the main differences induced by the adopted lubricating strategy, meanwhile in the second part a detailed description of the tool wear is presented by means of sophisticated analysis. Due to the higher industrial interest for sustainable cooling strategies to implement in the biomedical field, a deeper emphasis to dry and cryogenic cooling is given.

4.2.1. Characterization of tool wear mechanisms arising by the application of different lubricating strategies

This paragraph summarises the main tool wear mechanisms and tool wear modes observed on the adopted TiAlN coated tungsten carbide insert under different process conditions, namely

the cutting parameters and the lubrication strategy. The trends of the nose wear parameter VBc at fixed machining times are shown in Figure 4.1 when a cutting speed of 80 m/min and a feed rate of 0.1 mm/rev (Figure 4.1a) and of 0.2 mm/rev (Figure 4.1b) are adopted, respectively. It is noteworthy that for all the turning trials, the tool rejecting criterion was never reached being set a threshold limit of 0.1 mm for the VBc parameter. Furthermore, the Figure 4.1 shows that consistent lower tool wear values can be appreciated when cryogenic cooling is applied, which are evident also with a cutting speed of 50 m/min. On the other side, higher nose wear resulted in comparison with standard wet turning when no coolant was applied, in particular for the feed rate of 0.2 mm/rev. The flank and nose wear of the tool is usually connected with the abrasive action of the workpiece against the tools flank face, removing first the tool coating and then particles of the substrate [7]. The addition of mineral oil to the water to generate the emulsion coolant has the proper function of reducing the friction coefficient that generates at the cutting interfaces, and, by the consequence, of lowering the cutting temperature.

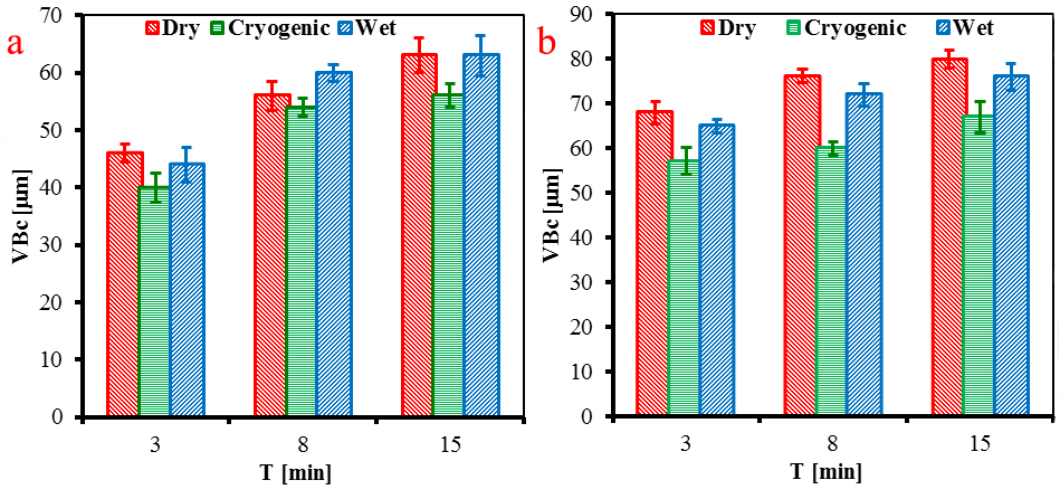

Figure 4.1 Nose wear VBc as a function of the machining time when adopting a cutting speed of 80 m/min and a feed rate of: (a) 0.1 mm/rev and (b) 0.2 mm/rev.

It is not surprising that for such cutting parameters, higher values of flank wear resulted under dry turning when the most severe cutting parameters were adopted. Conversely, dry turning becomes competitive with the wet one when the lowest feed rate is applied, leading to comparable or lower values of VBc (see Figure 4.1a): this might be ascribed to the lower

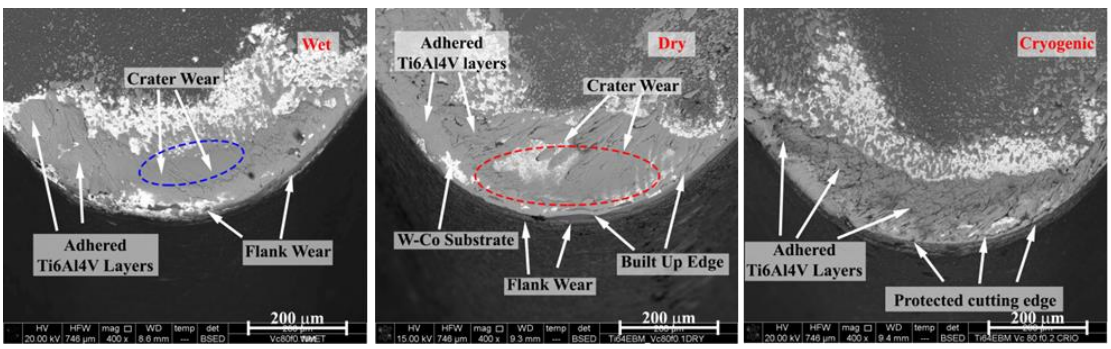

Figure 4.2 SEM images of the worn tools after 15 minutes of turning when adopting a cutting speed of 80 m/min and a feed rate of 0.2 mm/rev.

friction forces and temperatures generated at the tool workpiece interface in comparison to those obtained for the higher feed rate.

The SEM analysis of the worn tools highlighted the main tool wear mechanisms occurring when turning EBM Ti6Al4V under wet, cryogenic and dry lubricating conditions. Adhesive wear was the principal one, confirming the sticky tendency of the EBM Ti6Al4V even if its mechanical properties and its microstructure is quite peculiar if compared to the wrought alloy. It was noticed in all the test trials, as shown in Figure 4.2 where worn tools are presented when a cutting speed of 80 m/min and a feed rate of 0.2 mm/rev were adopted, after 15 minutes of turning. Even if the microstructure of EBM Ti6Al4V is quite different than the wrought Ti6Al4V one, the affinity among its main chemical elements with those composing the tool insert (mainly Ti, Al, W, Co), its low thermal conductivity and the high specific cutting forces reached during the machining process, favour the adhesive wear mechanism [8].

Adhesion of Ti6Al4V layers on the tool faces when machining with coated or uncoated tungsten carbide inserts have been extensively investigated in literature also when using different lubricating strategies are generally employed such as cryogenic [9], High Pressure Water Jet Assistance (HPWJA) and MQL[10]. In this study, the occurrence of adhesion can be noticed by the presence of the pastel grey areas on the SEM images obtained with the BSED detector. This tool wear mechanism led to the formation of the Built-Up-Edge (BUE) and the crater wear on the tool rake face in case of wet and dry machining. Since the early stages of the cutting process, cratering occurred during dry and wet turning when the most severe cutting parameters were employed because of the higher specific cutting forces applied on the tools rake face and cutting temperatures, on the contrary it was never observed with the application of LN_2. Even if no measurements of the cutting temperature were carried out in this preliminary study of the machinability, it can be reasonably assumed that its values under wet turning might position between those reached under dry and cryogenic cooling conditions. Cratering is a well-known adhesion-diffusion wear process provoked by the continuous formation and breakage of strong bonds between the sliding surface of the chips and already adhered workpiece layers or fresh tool substrate particles. Their formation is strongly dependent on the temperatures reached at the tool workpiece interface rather than the specific normal pressure [11]. Thus, the higher the temperatures the higher the tendency of the workpiece material adhesion on the tool cutting faces. On this basis, the higher amounts of adhered material noticed on the tool faces and the occurrence of cratering during dry and wet turning are directly correlated to the high temperatures reached in the cutting zone, in particular the avoidance of the application of a cutting fluid sped up the adhesive wear rate, leading to wider craters as visible in Figure 4.2. The SEM analysis of the worn tools revealed an intense presence of adhered layers even on the cutting edge and on the rake face, with more regular and intact geometries when applying the LN_2. The presence of these layers tend to protect the exposed WC-Co substrate when the coating is abraded during the early stages of the machining process, providing at the same time a thermal barrier for the substrate. Nonetheless, higher wear rates were reached during dry and wet cooling conditions due to the higher temperatures; hence the cutting edge was more subjected to unpredictable detachments of fragments suffering more severely the rubbing effect of the rotating workpiece against the tools substrate, affecting the tool flank wear resistance as showed in Figure 4.1. The main tool wear modes observed in dry, wet and cryogenic turning of the EBM Ti6Al4V are summarized

in Figure 4.3. Abrasion, chipping and adhesion of the workpiece material are the main tool flank face wear mechanisms (see Figures 4.3a and 4.3b), while for the rake face, crater wear, Built-Up-Layer (BUL) and Built-Up-Edge (BUE) are observed (see Figures 4.3c and 4.3b). Chipping is generated by the instable cutting edge fragment detachment under adhered workpiece material layers that weld onto the tool surfaces since the cutting beginning, proving that even the chipping process is initially activated by the adhesion wear mechanism [12]. Fig. 4.3d shows the BUL and BUE generated by the plastic deformation of the workpiece material bonded on the cutting surfaces.

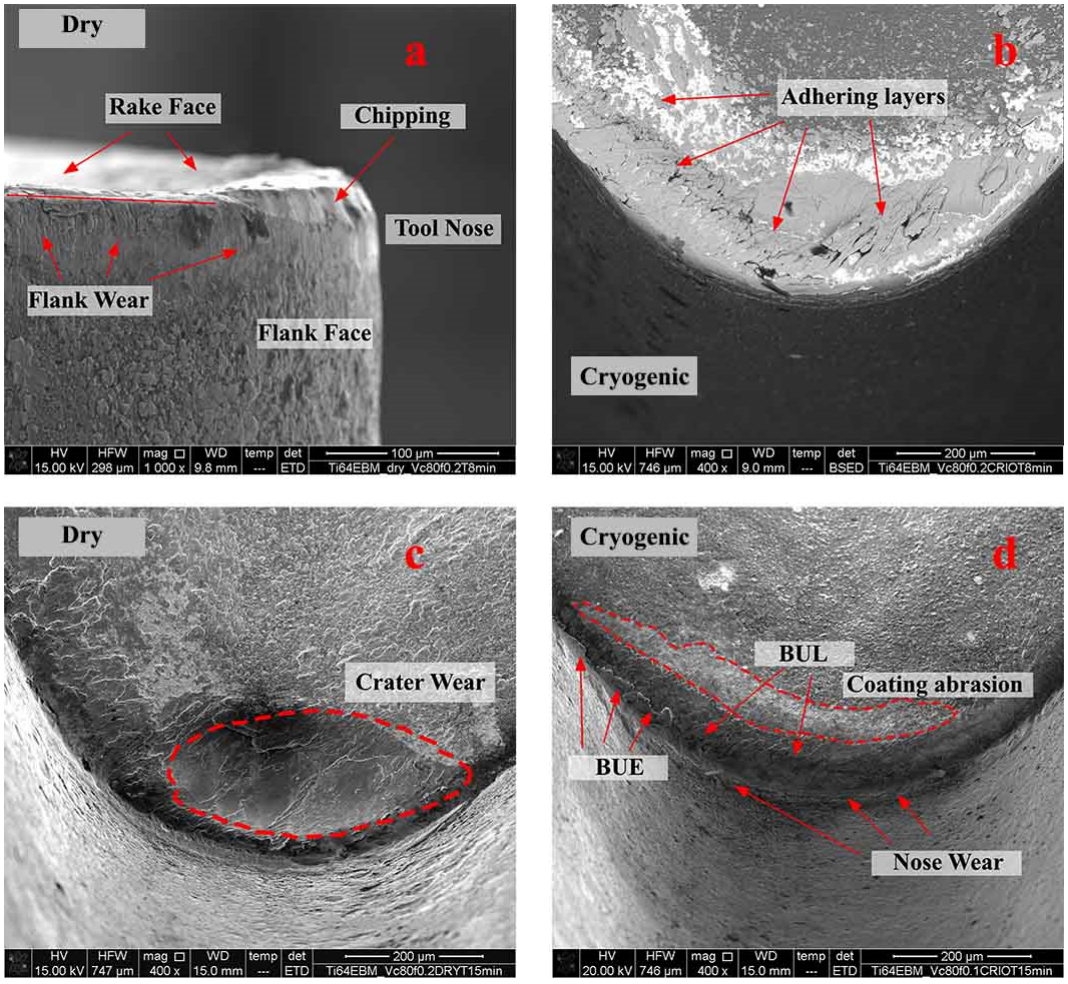

Figure 4.3 SEM images of the main tool wear modes generated in dry and cryogenic turning after 8 minutes when adopting a cutting speed of 80 m/min and a feed rate 0.2 mm/rev.

In machining Titanium alloys, high values of cutting temperatures and specific cutting pressures can be reached as reported experimentally in several papers [13,14], this might provoke the thermal softening of the welded layers thus allowing the plastic deformation by extrusion on the rake face due to the friction tangential loads applied by the flowing chips, as a result BULs are generated as shown in Figs 4.3b and 4.3d. From an environmental point of view, cryogenic cooling meets the increasing demand for cleaner manufacturing with regard to the tool wear by increasing the tool life, and thus limiting the amount of cutting tools used in the manufacturing process. When a feed rate of 0.1 mm/rev is set, dry turning becomes a sustainable alternative to the standard wet machining thanks to comparable values of the nose wear. Aiming to implement sustainable cooling strategies, from an industrial point to view it is

more interesting to investigate the machinability of EBM Ti6Al4V alloy under dry rather than wet lubricating condition, because for such low turning parameters the differences between dry and wet turning are very narrow. In the next sections, the tool wear modes under dry and cryogenic turning of the EBM Ti6Al4V are investigated and quantified more in detail, by means of different criteria.

4.2.2. Adhesion wear

The dominant wear mechanism of tungsten-carbide tools during turning titanium alloys is the adhesion one, due to dissolution – diffusion [11,15]. The large forces and high temperature arising during cutting, together with the high titanium chemical reactivity, produce the ideal environment for the diffusion and adhesion of the tool elements into the Ti6Al4V chips and similarly for the workpiece material elements to bond onto the tool surfaces. Clear evidence that the adhesion mechanisms occurred during the tests previously described is appreciable thanks to the SEM and EDS analysis (see examples in Figures 4.4a and 4.4b), proving that, also with the application of the cryogenic cooling strategy, the chemical and mechanical conditions arising during cutting are favourable to initiate the adhesion process. According to the data reported in Table 4.1, EDS1 and EDS 3 (regions in Figures 4.4a and 4.4b) spots show high concentration of titanium, aluminium and vanadium, which are the main chemical elements of the EBM Ti6Al4V, while the EDS 2 and EDS 4 spots indicate higher concentration of tungsten and cobalt, namely the main tool substrate elements. Considering the percentages of workpiece material elements found by the EDS point analysis in the spots 1 and 3, a decrease of Ti, Al and V is appreciable by adopting cryogenic cooling, suggesting that lower temperatures reached during the cooled environment tend to inhibit the adhesion wear mechanism. The adhesion wear mechanism affected strongly the tool flank wear avoiding the direct exposure of the tool material to the rotating test piece, thus limiting the rubbing effect and abrasion wear mechanism: a prove of this is given by the nose wear values summarized in the Figure 4.1. The TiAlN insert coating was removed by attrition and by the adhesion wear mechanisms in the very first stages of the turning process, leaving the uncoated

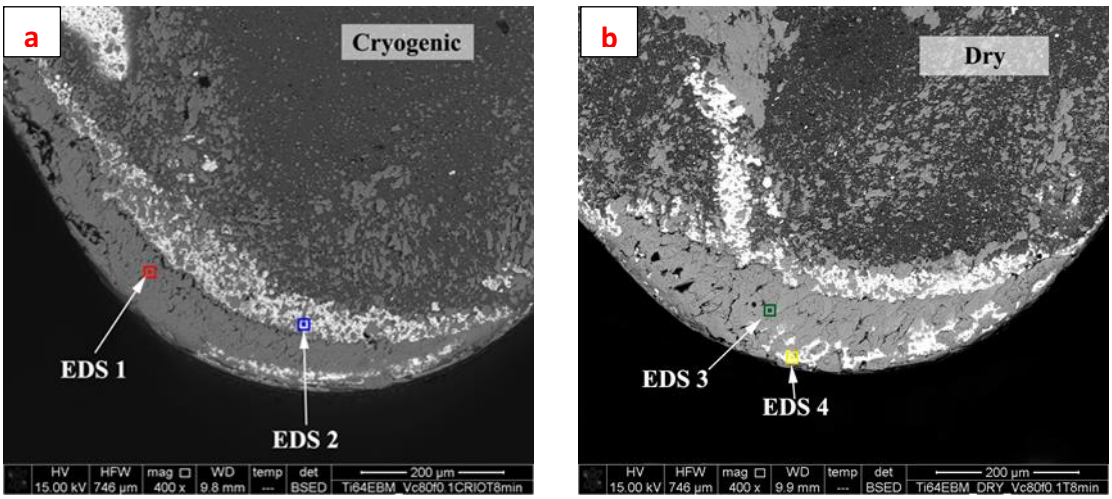

Figure 4.4 BSED analysis of the insert rake face after 8 minutes of turning under a) cryogenic cooling and b) dry turning when adopting a cutting speed of 80 m/min and a feed rate of 0.1 mm/rev.

Table 4.1 EDS results (%wt) of the point analysis presented in Figures 4.4 a and 4.4 b.

EDS spot	**W**	**Co**	**Al**	**V**	**Ti**	**C**
1	0.89	0.33	5.52	5.34	85.9	1.01
2	88.10	3.61	0.01	0.02	6.29	1.52
3	0.91	0.44	4.21	4.42	81.31	2.50
4	87.21	4.21	0.03	0.04	6.04	2.21

substrate exposed to the intimate contact with the workpiece and the flowing chips. With the increase of the cutting time, further workpiece material adhered to the previous one forming strong bonds on the rake face. The rate of the adhesion-diffusion mechanism depends by the temperature and specific pressure acting on the sliding interface. Both of these variables are influenced by supplying LN_2 on the cutting zone, provoking a reduction of workpiece material elements adhered and a contraction of the zone of strong adhesion and sticking of the chips on the tool rake face, as evidenced in Table 4.2 where it is shown a reduction of the tool chip contact length in case of cryogenic machining. The tool chip contact length is an important parameter that gives information on the intimate contact between the chip and the rake face, as for the heat generated due to the friction along the secondary deformation zone, hence the lubricating capability of the cooling mean. A shorter value of the tool-chip contact length will result in a greater coolant penetration, reduced friction and a greater cooling efficiency, thus longer tool life.

Table 4.2 Tool chip contact length measurements during dry and cryogenic turning.

	Dry	**Cryogenic**			
Time [min]	**Tcl [μm]**	**Tcl[μm]**	**Tcl*d*-Tcl*c*[%]**	**DevSt (Tcl*d*-Tcl*c*) [%]**	**Cutting Conditions**
3	100	78	22.0	3.0	**Vc50m/min f0.1mm/rev**
8	98	91	7.1	2.0	
15	88	95	6.0	2.8	
3	181	145	19.9	3.1	**Vc50m/min f0.2mm/rev**
8	200	142	29.0	2.1	
15	167	127	24.0	2.6	
3	111	99	10.8	2.8	**Vc80m/min f0.1mm/rev**
8	103	96	6.8	2.6	
15	116	87	25.0	3.6	
3	212	145	31.6	4.1	**Vc80m/min f0.2mm/rev**
8	235	158	32.8	3.2	
15	243	139	42.8	2.6	

Observing the Figures 4.5 and 4.6, the presence of three main zones on the tool worn rake faces can be identified according as found in similar works in literature [13,16,17]. The first

zone corresponds to the sliding area of the chips onto the uncoated rake face as proven by the EDS spots 1 and 3 presented in Table 4.1, and delimitated by the black dotted line in the Figures 4.5 and 4.6. The second zone is delimited by the green dotted line and corresponds to the delaminated and abraded tool coating characterized by abrasion and tearing off of tungsten particles where high percentage of tungsten is found (EDS spots 2 and 4) along with chip fragments welded on the insert substrate as can be observed in Figure 4.6 in the right upper snapshot. Finally, the last zone is the area that remains intact, characterized by a high percentage of Al.

In the Figures 4.5 and 4.6, a clear effect of cryogenic cooling on the Built Up Layers and on the abraded coating area is visible. The BUL falls into the seizure region at where the coolant cannot penetrate, outside a region of chip slipping. The border that separates the two zones is the end of the tool chip contact length. The flow of LN_2 directed onto the rake face lifts the chip upward making it separating earlier from the tool surface, thus reducing the chip curvature as can be seen in Figure 4.7. In this figure an example of the chips obtained when turning EBM Ti6Al4V under dry and cryogenic lubricating conditions is presented. Supplying the LN_2 by two nozzles directed onto the rake and flank faces changes the chip morphology: long tubular helical chips were obtained for the cryogenic case, whereas snarled washer type helical chips resulted for the dry one. The chip morphology did not change significantly at increasing the tool wear or at varying the cutting parameters, but at reducing the test piece diameter chips entanglements were observed in particular for dry turning, in which a higher chip curvature resulted for all the tested cutting conditions.

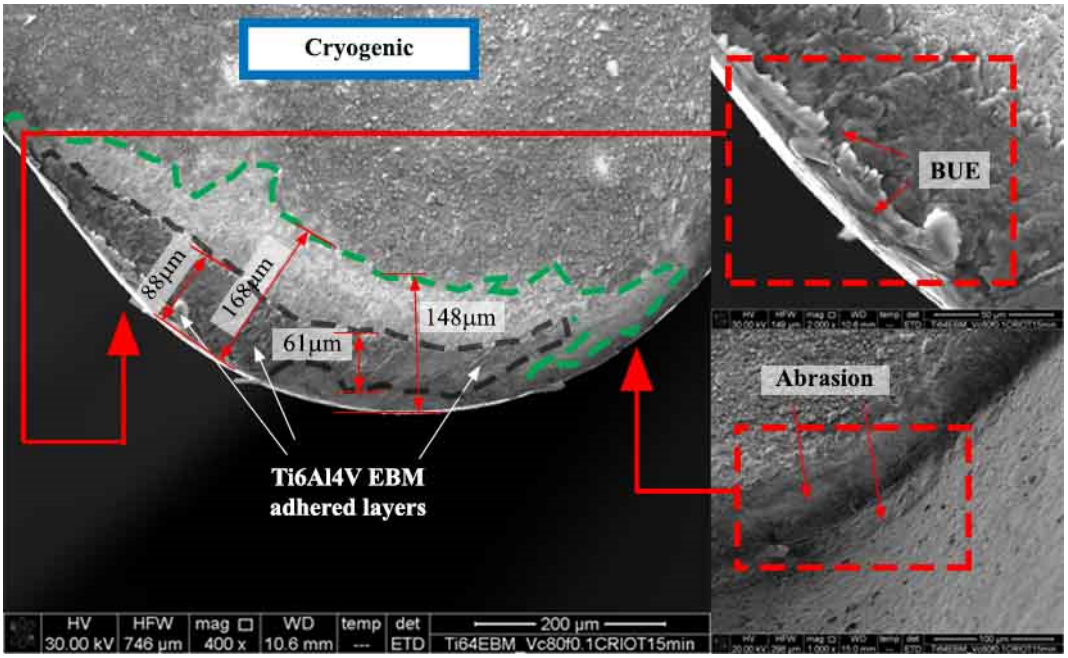

Figure 4.5 Rake face wear and tool chip contact length in cryogenic turning of EBM Ti6Al4V when adopting a cutting speed of 80 m/min a feed rate of 0.1 mm/rev after 15 minutes.

Whether the LN_2 flow influenced the curvature of the chip, it did not possess the energy momentum to break the chip as for the application of HPWJA. According to the experimental results presented by Bermingham el al. [13] the tool chip contact length is reduced by the

application of LN_2, as for the dry turning a higher reduction can be found for a feed rate of 0.2 mm/rev than for 0.1 mm/rev. The percentage reduction of tool chip contact length when adopting the LN_2 overtakes the 20% for a feed rate of 0.2 mm/rev, reaching the value of 42.8 % after 15 minutes of turning when adopting a cutting speed of 80 m/min at 15 minutes.

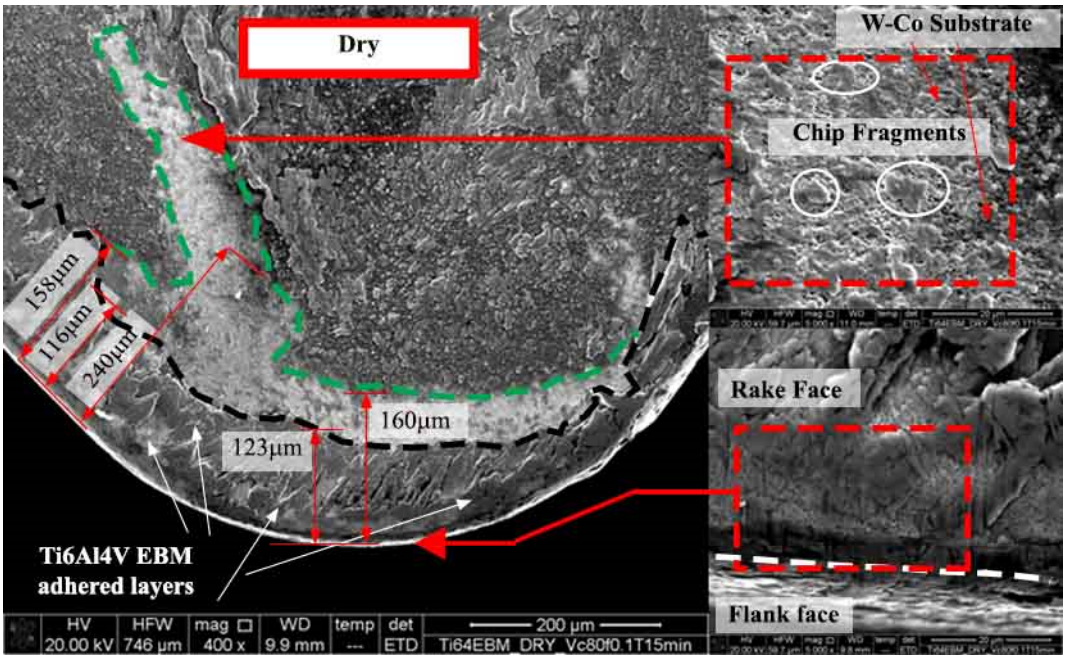

Figure 4.6 Rake face wear and tool chip contact length in dry turning of EBM Ti6Al4V when adopting a cutting speed of 80 m/min a feed rate of 0.1 mm/rev after 15 minutes.

A slight reduction resulted when a feed rate of 0.1 mm/rev was adopted without a consistence trend. For both lubricating conditions, the cutting speed effect is weaker than the feed rate one, and a slight increase in the tool chip contact length is measured when passing from 50 to 80 m/min.

To investigate more deeply the adhesion wear mechanism, the thickness of the adhered Ti6Al4V layer onto the tool rake face was measured in a fixed position by using the Sensofar Plu-Neox™ profiler as described in the chapter 3, adopting a fixing reference frame for a repeatable positioning of the tool on the instrument table.

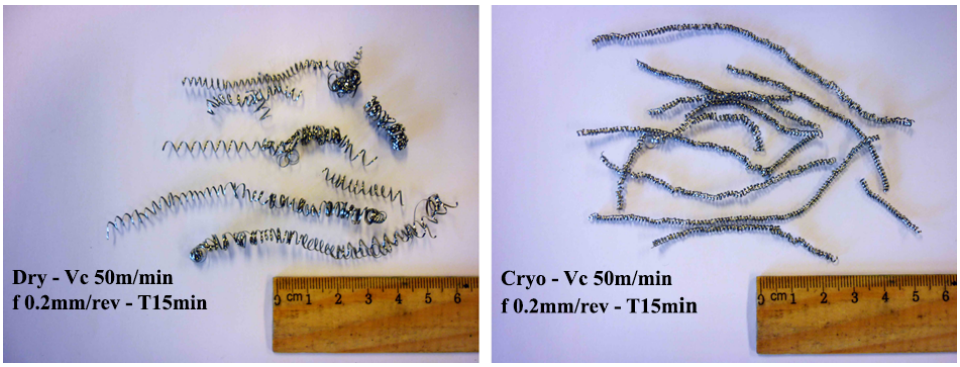

Figure 4.7 Effect of the cryogenic cooling on the chip morphology for fixed turning time and cutting parameters.

Thanks to the instrument software, linear sections of the acquired surfaces can be traced along any directions on the X-Y plane, allowing plotting the surface section profile on a projected plane. The points heights, namely the Z coordinates, are then displayed at varying position along the linear section. To better understand the position of the cutting section, the 3D sketch presented in the Figure 4.8 can be observed, in which the origin of the X axis is placed on the flank face.
An example of acquired images of the insert rake face is presented in Figures 4.9; the lighter coloured area along the cutting edge represents the adhered material.

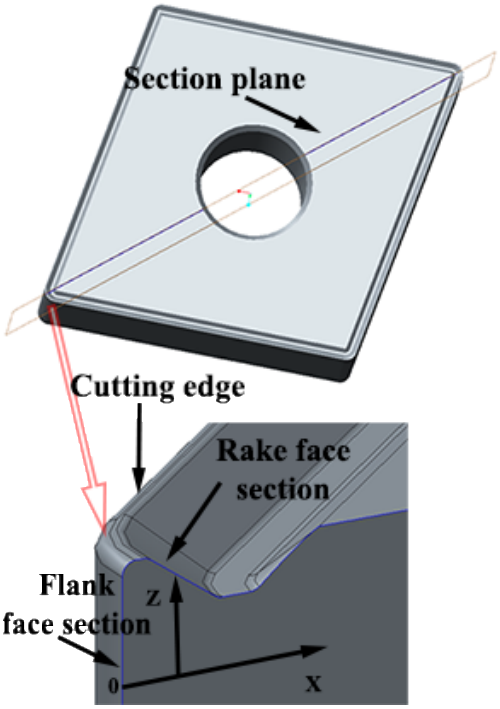

Figure 4.8 Schematic representation of the reference coordinates defined to evaluate the thickness of the adhered layer on the tool rake face.

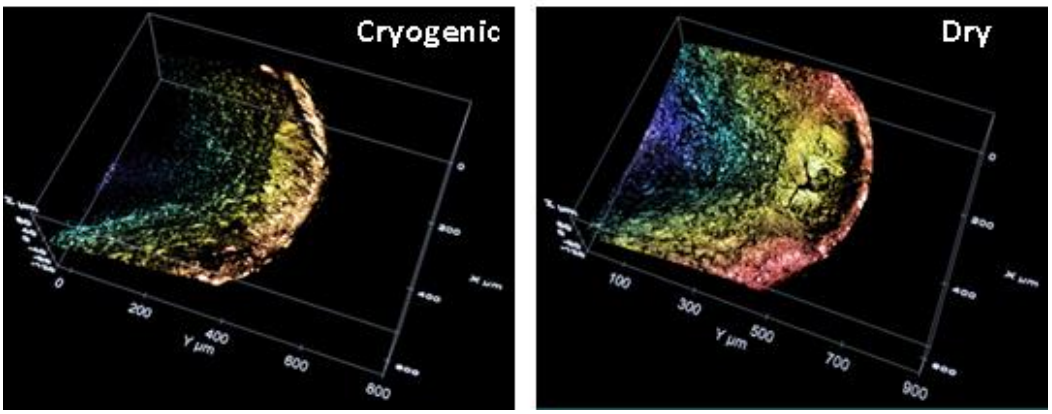

Figure 4.9 3D Optical images representing the tool rake face and the cutting edge when adopting a cutting speed of 80 m/min and a feed rate of 0.2 mm/rev after 15 minutes.

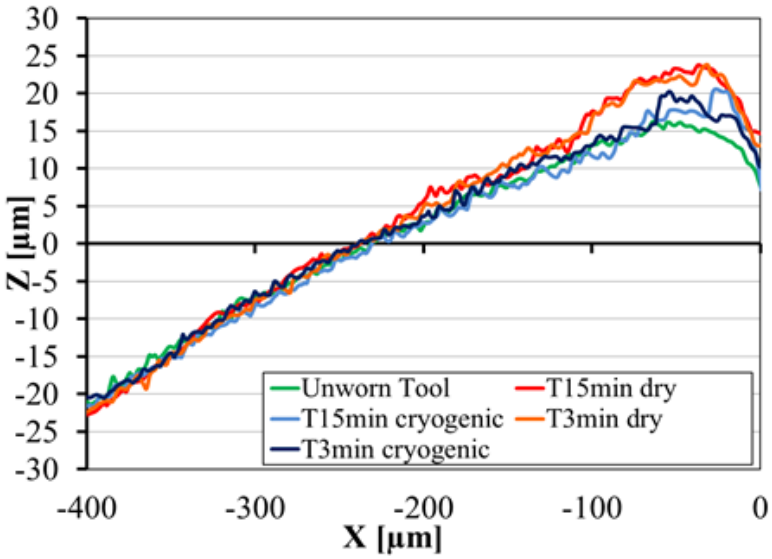

Figure 4.10 Rake face profile heights in dry and cryogenic turning when adopting a cutting speed of 80 m/min and a feed rate of 0.1 mm/rev after 3 and 15 minutes.

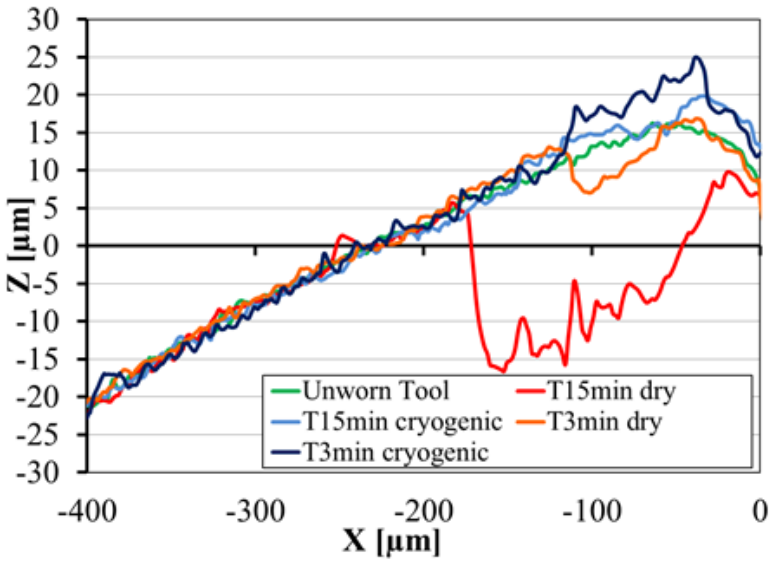

Figure 4.11 Rake face profile heights in dry and cryogenic turning when adopting a cutting speed of 80 m/min and a feed rate of 0.2 mm/rev after 3 and 15 minutes.

The Figures 4.10 and 4.11 illustrate the section profiles of the tool worn rake faces, showing the effects of the feed rate and cutting time when turning EBM Ti6Al4V under dry and cryogenic lubricating conditions. The Z-axis represents the profile height of the tool rake face, and the X-axis the distance from the flank face on the tool nose, being zero the position of the flank surface. In general, the adhesion wear evolution is not clearly predictable due to the instability and non-linearity of the mechanism itself with respect of time and space [18], making the accumulation of the workpiece material on the tool surfaces and the wear rate not uniform. Nevertheless, the adopted approach of measuring the layer thickness permits a qualitative overview of the adhesion wear mechanism, evaluating the sticking tendency of the EBM Ti6Al4V on the tools surfaces at varying cutting parameters and lubrication. By observing the Figures 4.10 and 4.11, the green profile represents the unworn tool rake face, whereas the blue and red profiles the cryogenic and the dry conditions, respectively. In case of

an adopted feed rate of 0.1 mm/rev (Figure 4.10), the maximum thickness of the adhered layer results equal to 10 μm after 15 minutes falling at a distance from the cutting edge that varies between 50 and 75 μm, whereas in case of cryogenic cooling the workpiece material adhesion is lower for each cutting time. In the Figure 4.11, the red and orange profiles relevant to dry conditions show the occurrence of the crater wear when adopting a feed rate of 0.2 mm/rev. The cutting parameter that played the major role in the adhesion mechanism results to be the feed rate, but also the cutting speed induced an increase of the adhered workpiece material for both the dry and cryogenic conditions due to the higher cutting temperature that could be reached when increasing the cutting speed [19].
The adhesion process mainly depends on the specific pressure, the temperature at the mating interface and the chemical affinity among tool and workpiece materials. Generally, their effects manifest themselves with different intensities, in particular for high speed processes as for cutting of metals [20]. Observing the plots in the Figures 4.10 and 4.11, different influences of temperature and specific pressure can be appreciated despite no direct measurements of these quantities was taken. According to several numerical and experimental works present in literature [21], the position at which the maximum temperature occurs is located at a greater distance from the cutting edge then the position where the maximum cutting pressure is applied. The presence of the crater wear on the tool rake face when turning with a feed rate of 0.2 mm/rev under dry conditions is an indicator of the position at which the maximum temperature is reached according to literature [11]. The maximum crater depth is observed at distance of 100 μm from the flank face, whereas for all the turning trials the maximum adhered material layer thickness is found into a range of distances from the flank face that varies from 25 to 50 μm. This position might correspond to the area at which the maximum cutting pressure was reached, proving that the bonding process of workpiece material layers might be more affected by the cutting pressure than by the temperature in dry turning of EBM Ti6Al4V. Cryogenic cooling reduces the temperature in the cutting zone [15], and as a consequence, the influence of the chemical affinity of Titanium with Cobalt and Tungsten present in the tool substrate is reduced [22,23] along with the plasticity and the thermal conductivity of the workpiece material [24]. The main consequence of the temperature reduction can explain the different stickling behaviour that was observed with the application of LN_2. During dry turning the bonded layer thickness tended to increase at increasing the turning time or remaining stable along the 15 minutes as showed in Figure 4.11 by the red curves. The accumulated material is then smeared down along the rake face by the chip flow, favoured by the increased plasticity of the workpiece material. In the case of cryogenic machining, thicker adhered layers were measured after only three minutes of turning as can be seen in the Figures 4.10 and 4.11 for different levels of feed rate; but the reduced material plasticity, thermal conductivity and chemical affinity of Titanium inhibited the adhesion process to go further, removing the welded layers by the chip flow earlier than in the case of dry turning.

4.2.3. Crater Wear

The crater wear formation during machining operations on Ti alloys is frequently observed as a tool wear mode when using coated and uncoated tungsten carbide inserts, representing the

main tool failure mode in the worst cases . As the crater wear formation is a thermally activated mechanism, it is affected by the cooling strategy. Venugopal et al. [25] published one of the first works on cryogenic turning of Ti6Al4V and in that case even supplying LN_2 on the cutting zone could not prevent the crater formation along the cutting edge. During machining titanium alloys, the crater wear is consequence of an aggressive removal process of the substrate tungsten particles by the flowing chips when adhesion and diffusion rates between the workpiece and the tool substrate elements are very high due to the environment conditions. In the present study, the crater depth was measured by means of the Sensofar Plu-Neox™ optical profiler following the same procedure illustrated in the previous section, after etching the insert nose. Cratering was observed only during dry cutting conditions when a feed rate of 0.2 mm/rev was adopted. In Figure 4.12, the crater wear evolution during dry turning for a cutting speed of 80 m/min and a feed rate of 0.2 mm/rev is presented. The maximum crater depth resulted to be of 25 μm for a turning time of 15 minutes. Comparing the profiles presented in Figure 4.10 with those shown in Figure 4.12 corresponding to the etched inserts, it is clearly visible that the peaks present on the initial profiles correspond to stuck material on the crater surface. The cutting speed effect had a weaker influence on the crater wear than the feed rate, even if sensible effects were appreciated due to its variation. More in detail, when adopting a cutting speed of 50 m/min, cratering occurred only after 15 minutes of cutting, while for a cutting speed of 80 m/min the loss of tool particles from the rake face started from the first turning stages. This aspect can be explained as consequence of the high temperatures that can be reached when higher cutting speeds are adopted [26]. Due to the reduced temperatures that are generated in the cutting zone by supplying the LN_2, the crater wear was inhibited. The crater surfaces, resulted to be smooth (SEM image shown in Figure 4.3c), meaning that severe rubbing took place between the sliding chips and the tool rake face. Looking at the SEM image presented in Figure 4.3c, the crater spanned the entire tool nose radius after 15 minutes of turning, but neither the cutting edge depression nor the tool failure occurred due to the crater deepening at increasing cutting time.

4.2.4. Abrasion and Notch Wear

The SEM analysis conducted on the worn tools using both the ETD and BSED detectors evidenced the presence of abrasion marks and erosion grooves onto the insert flank faces for both the dry and cryogenic lubricating conditions. The abrasion of the flank face at the nose area gave rise to the flank wear evolution (VBc) shown in Figure 4.1, but the tool life criterion was not reached in any of the machining trials. In fact, during the machining tests, a significant amount of adhered EBM Ti6Al4V was detected on the tool primary and secondary cutting edges as well as on the tool nose, protecting the tool against the rubbing action induced by the workpiece. The presence of this protective layer makes the flank wear less sensitive to the adopted cutting parameters than the rake wear, since no appreciable differences can be ascribed in terms of VBc passing from dry to cryogenic machining. The protection role played by the adhered material for both the lubricating conditions can be confirmed in the images shown in Figure 4.13, where the abrasion marks are visible on the pastel grey areas representing the adhered EBM Ti6Al4V; moreover, it is worth to note that the density and width of the abrasion marks did not change significantly at varying cutting parameters. The LN_2 supply on the tool rake face resulted to limit the amount of adhered material, and, as a

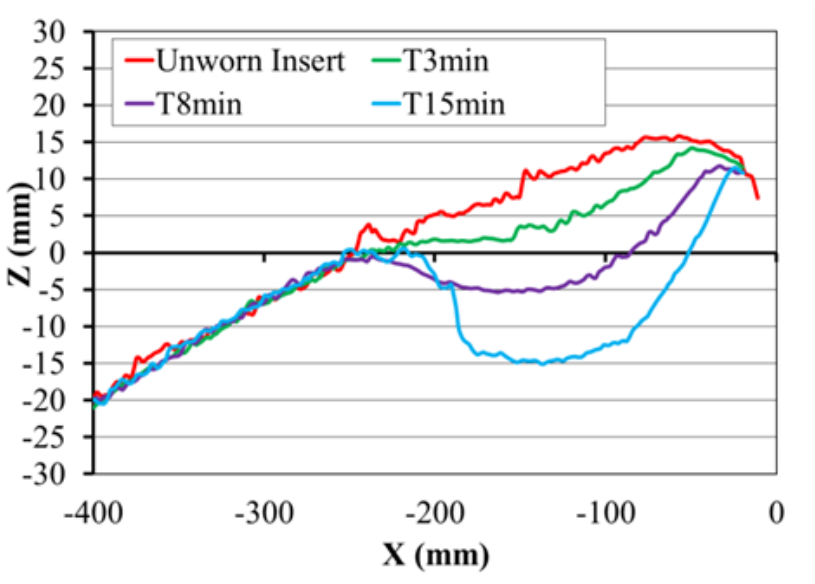

Figure 4.12 Rake face profile heights of etched insert in dry turning when adopting a cutting speed of 80 m/min and a feed rate of 0.2 mm/rev after 3 and 15 minutes.

consequence, the cutting edge chipping caused by the instable detachment of fragments from the substrate. On the contrary, the chipping of the cutting edge, caused by abrasion and erosion, can be observed in Figure 4.13 on the left for the dry cutting conditions, whereas in the case of cryogenic turning the cutting edge is still well protected by the adhesion of Ti6Al4V (Figure 4.13 on the right). By adopting the cutting parameters proposed in the present work, no wear in terms of V-shaped notch was detected for both the lubricating conditions, possibly as a consequence of the absence of burrs generation as shown in Figure 4.14 where the abrasion marks are clearly visible at the depth of cut zone.

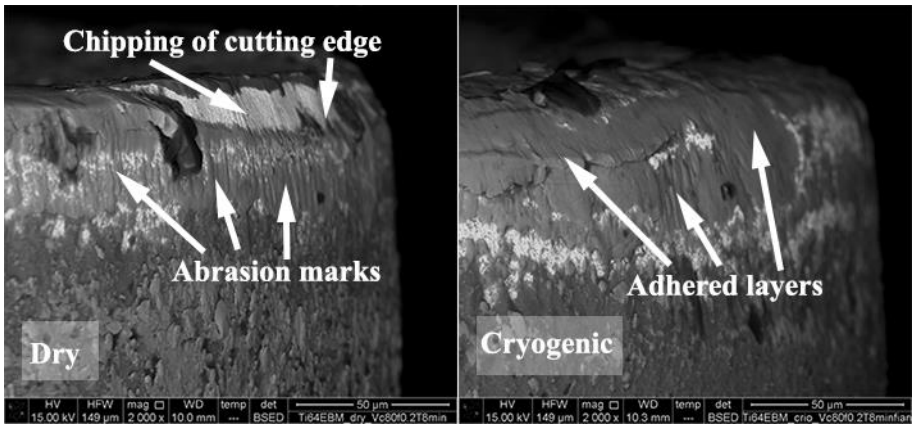

Figure 4.13 Abrasion marks when turning EBM Ti6Al4V when adopting a cutting speed of 80 m/min and a feed rate of 0.2 mm/rev after 15minutes.

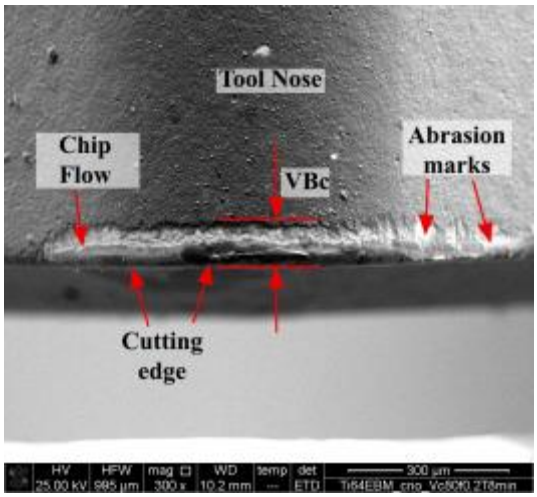

Figure 4.14 Flank wear when turning EBM Ti6Al4V under cryogenic cooling when adopting a cutting speed of 80 m/min and feed rate of 0.2 mm/rev after 8 minutes.

4.3.Surface Integrity

The surface integrity of a machined component is the result of many cutting conditions arising during the manufacturing process. Tool wear, cutting parameters, stiffness of the clamping and tool set-ups and the lubrication strategy are the process parameters that continuously influence the interaction between the tool tip and the material being cut, determining the so called surface integrity. In machining surgical implants or more in general metal components obtained by AM techniques, the surface integrity can be considered the most important machining issue to monitor. Up to now, the classical investigation of the surface integrity based on experimental testing is still the most reliable and complete approach. This paragraph outlines the main experimental findings concerning the surface integrity generated in semi-finishing turning of EBM Ti6AL4V alloy, by testing the effects of three different lubricating strategies (wet, dry and cryogenic) and of different values of cutting speed and feed rate according to experimental plan listed in the Table 3.3. The effect of the tool wear is also considered by analysing the surface integrity at three different turning lengths: 3, 8, 15 minutes. The principal aim of this work is assessing the feasibility of sustainable cooling approaches (dry and cryogenic) for a future implementation in machining surgical implants such as acetabular cups, to improve the material reliability in terms of its mechanical properties and at the same time to reduce the costs of manufacturing processes of biomedical components. A detailed critical analysis of the main findings obtained by the measurement of surface roughness parameters, of residual stresses and on the main surface defects is presented.

4.3.1. Surface Roughness parameters

The average values of the mean surface roughness Ra, of the total height of the roughness profile Rt are listed in Table 4.3, whereas in Figure 4.15 the cooling strategy effect on the mean surface roughness after 8 minutes of turning is shown. It comes evident a reduction of

the Ra values when the cryogenic cooling is applied at the most severe cutting parameters, namely a cutting speed of 80 m/min and a feed rate of 0.2 mm/rev, whereas negligible differences result for the lowest applied feed rate, being the only cutting condition provoking sensible differences in terms of flank and crater wear occurred when applying different cooling strategies, as discussed in the previous paragraph. Under such cutting conditions, cratering occurred under wet and dry turning, furthermore SEM analysis revealed more abrasion scratches and fresh substrate areas on the tool flank face after a machining time of 8 and 15 minutes. Generally, the more severe the tool wear the poorer the surface quality, thus lower values of Ra and Rt were measured for cryogenic cooling machined samples as can be noticed in Table 4.3. These results confirm the main findings present in literature [27] concerning the beneficial effects of cryogenic machining on the surface integrity in machining difficult to cut materials. If the cutting speed is reduced to 50 m/min, the application of LN_2 still leads to beneficial effects inducing lower values of Ra and Rt, nonetheless closer differences with wet and dry turning are found, since nose wear and no cratering under wet turning occurred. The surface roughness is deeply influenced by the tool flank wear developing during machining; however the tool wear analysis points out no direct contact between the workpiece and the tool flank by the presence of great amounts of adhered workpiece material, thus limiting the occurrence of the abrasive wear mechanism. This phenomenon strongly flattens the effects of the adopted lubricating strategies in case of semi-finishing machining compared to most of the published works about machining the wrought Ti6Al4V that deal with rough machining operations [10]. In case of rough machining, the rapid wear rate provokes significant differences among the different lubricating conditions, while in the case of semi-finishing machining negligible differences are found for the lowest feed rate, even for longer turning lengths. From an environmental perspective, dry and cryogenic cooling are feasible strategies with regard to the roughness parameters, but more comprehensive analyses are needed to further assess their possible implementation in the biomedical field.

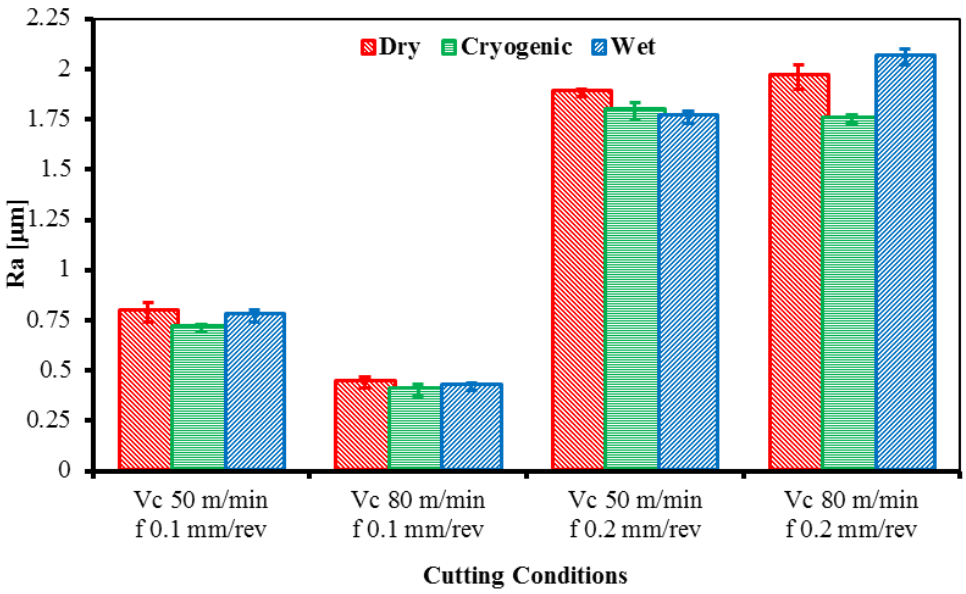

Figure 4.15. Effects of the lubricating strategies on the mean surface roughness Ra after 8 minutes of turning.

Table 4.3 Average values of the roughness parameters Ra and Rt.

Cutting Parameters	Time [min]	Ra_{dry} [µm]	Ra_{cryo} [µm]	Ra_{wet} [µm]	Rt_{dry} [µm]	Rt_{cryo} [µm]	Rt_{wet} [µm]
Vc 50 m/min f 0.1 mm/rev	3	0.76	0.82	0.64	3.48	4.15	2.88
	8	0.79	0.81	0.71	3.53	3.85	3.12
	15	0.77	0.81	0.74	3.56	3.89	3.46
Vc 50 m/min f 0.2 mm/rev	3	1.86	1.78	1.49	7.01	7.13	6.56
	8	1.88	1.79	1.75	7.84	8.46	6.90
	15	1.81	1.72	2.13	7.61	7.37	7.99
Vc 80 m/min f 0.1 mm/rev	3	0.49	0.39	0.74	2.98	2.09	3.55
	8	0.44	0.42	0.42	2.06	4.29	2.54
	15	0.46	0.61	0.55	2.71	3.43	2.20
Vc 80 m/min f 0.2 mm/rev	3	2.06	1.32	2.10	7.03	6.18	7.90
	8	1.96	1.75	2.06	8.54	7.03	8.08
	15	2.10	1.82	2.14	8.45	6.94	8.22

4.3.2. Surface defects and surface topography

The SEM analysis of the surface damages resulting from the turning process was then carried out for all the cutting conditions tested by using both ETD and BSED detectors. The extent of the surface damage that occurs during machining and how it develops are important

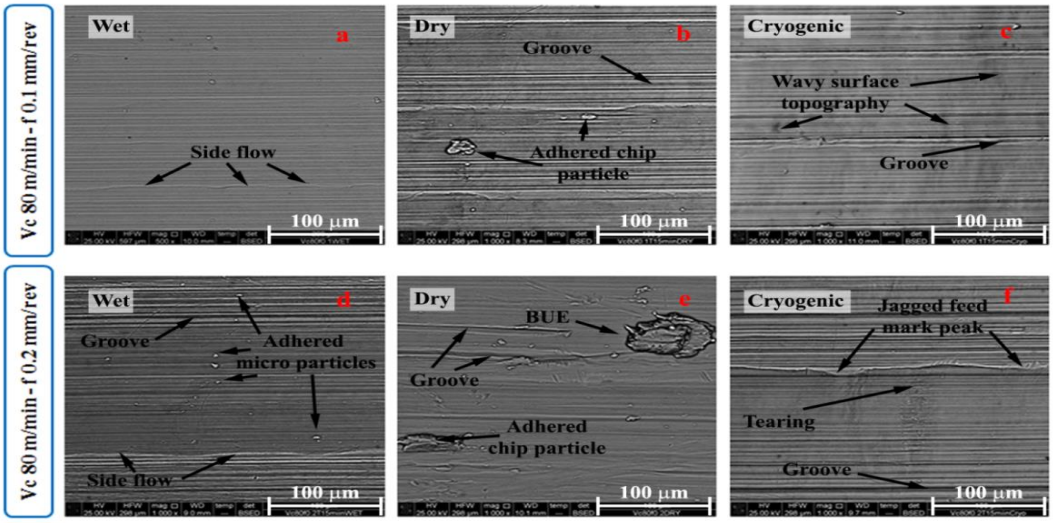

Figure 4.16 Main surface damages after 8 minutes of turning adopting wet, dry and cryogenic cooling strategies.

information since the fatigue resistance of a component is strongly influenced by the state of the surface layers, giving rise to crack sources [18].
In literature, a strong emphasis has been paid to characterize surface damages generating during rough milling and turning of wrought titanium and nickel alloys [1,29] but very few works are available on finishing turning of AM alloy [30]. Many variables are involved, such as the ductility of the workpiece material, its microstructure, the tool mechanical properties, and the thermo-mechanical conditions arising during the process; furthermore, strong effects were proved to be played by the tool wear and cutting parameters [31]. An overview of the main typologies of surface defects generated under the tested lubricating conditions is presented in the Figure 4.16.

In general, material side flow, double feed marks, long grooves and micro-particles adhered on the machined surface were found under wet turning as can be seen in Figures 4.16 a and d, with a greater density for the highest feed rate and for longer turning lengths, meanwhile the influence of the cutting speed is weak. The material side flow can be ascribed to the plastic deformation of the surface material induced by the feed motion of the tool nose, enhanced by an increased plasticity provoked by the higher temperatures reached when the most severe cutting parameters are set. Long strait grooves could be also noticed between two consecutive feed marks for all the scanned samples under wet turning, meaning that a ploughing action by the cutting edge took place. According to Zhou et al. [32], these grooves are generated by small fragments of the BUE that are randomly detached by the rubbing action, hence, when they pass below the tool flank face, they leave grooves on the softer underlying material being cut. Moreover, the great amount of adhered material developing in all the turning tests left particles welded on the surface, as can be noted in Figure 4.17. On the same figure, randomly oriented micro-scratches are visible, generated by the chip entanglements occurred during wet turning. Cleaner and more undamaged surfaces resulted when a feed rate equal to 0.1 mm/rev was set as showed in Figure 4.16 a.

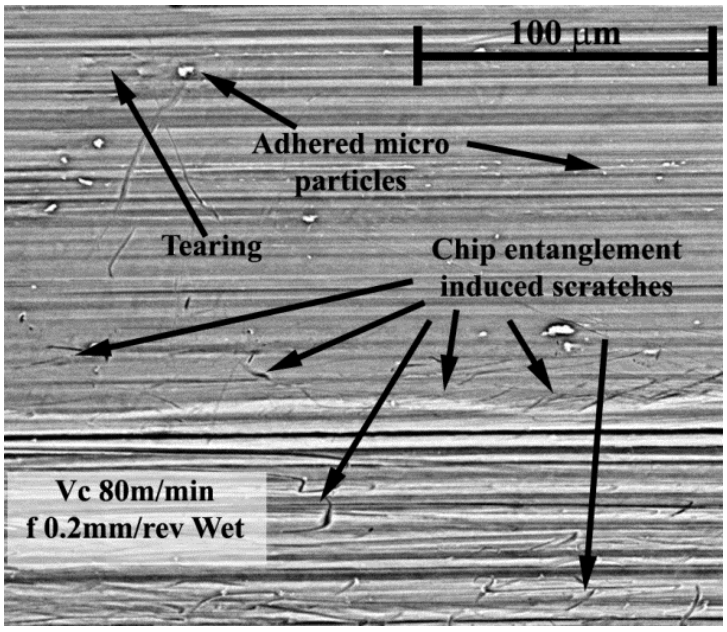

Figure 4.17 Scratches and adhered particles provoked by chip entanglements in case of wet turning after 8 minutes of cutting.

Ti6Al4V is renowned for having a poor thermal conductivity in comparison with other metal alloys [14]: as a consequence, the thermal flux that is dissipated through the workpiece encounters more resistance, and higher temperatures are concentrated on its surface in particular in case of short machining operations. If no coolant is applied, higher temperatures are reached at the workpiece–tool interface making the material softer, thus leading to more surface defects in comparison to wet turning with the same cutting parameters. In Figure 4.16 b and e, wider adhered chip fragments attached on the machined surfaces are present, especially for the most severe cutting parameters. Under dry cutting, BUE, adhered chip fragments, long grooves, folds, severe material side flow and smeared material were found as main surface damages; furthermore the feed rate played more a detrimental role, increasing their size and density compared to wet turning. Figure 4.16 e shows a portion of the BUE adhered on the machined surface and the EDS analysis reported in Figure 4.18 confirms its chemical composition, being the same of the workpiece material. When portions of BUE were deposed on the surface, they were dragged on the fresh surface leaving long grooves as can be seen in Figure 4.16 e. During dry turning, chip entanglements occurred, and due to the higher temperatures that developed, chip fragments tended to weld onto the surface as shown in Figure 4.16 b. The Figures 4.16 c and f shows the machined surfaces generated under cryogenic cooling conditions evidencing the effect of the feed rate when a cutting speed of 80 m/min was set. The main peculiarity is the wavy surface topography along the cutting speed direction (normal to the feed marks) and the jagged feed marks peaks compared to the other lubricating strategies. These findings were generally observed even for the lowest cutting speed and regardless the tool wear condition. Since the workpiece was frozen during the machining tests due to the application of LN_2 on the cutting zone for long stages, the plasticity of the alloy was then noticeably reduced limiting its capacity to be deformed by the tool nose pass and forming regular feed marks. This low plasticity of the surface layers is further proved by the presence of tears and wrinkles inside the feed mark valleys where tensile stresses applied by the friction forces lead the surface to break forming tears. A snapshot of these surface damages occurred when applying cryogenic cooling is presented in Figure 4.19. In comparison to the surface damages found in case of wet and dry turning, cleaner surfaces were observed in case of cryogenic cooling, revealing fewer adhered particles and chip fragments, less side flow and BUE, due to the reduced material plasticity provoked by the cryogenic thermal conditions.

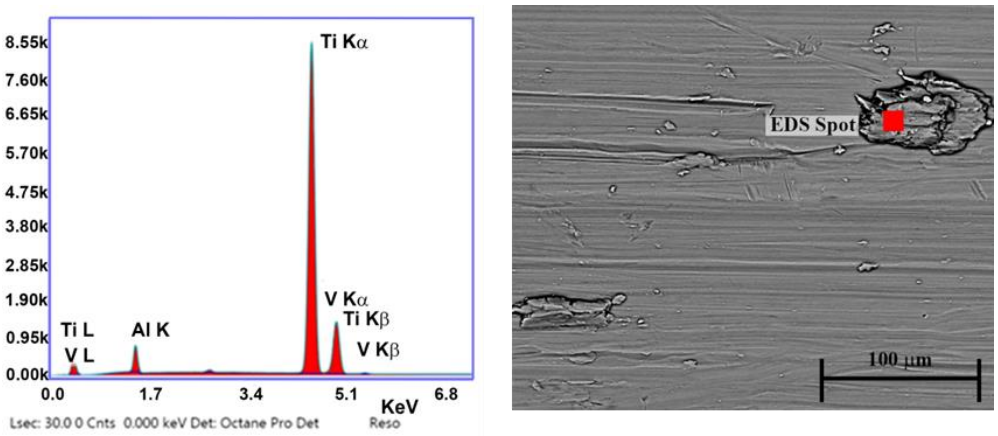

Figure 4.18 EDS analysis of BUE fragments adhered on the machined surface after 8 minutes of dry cutting.

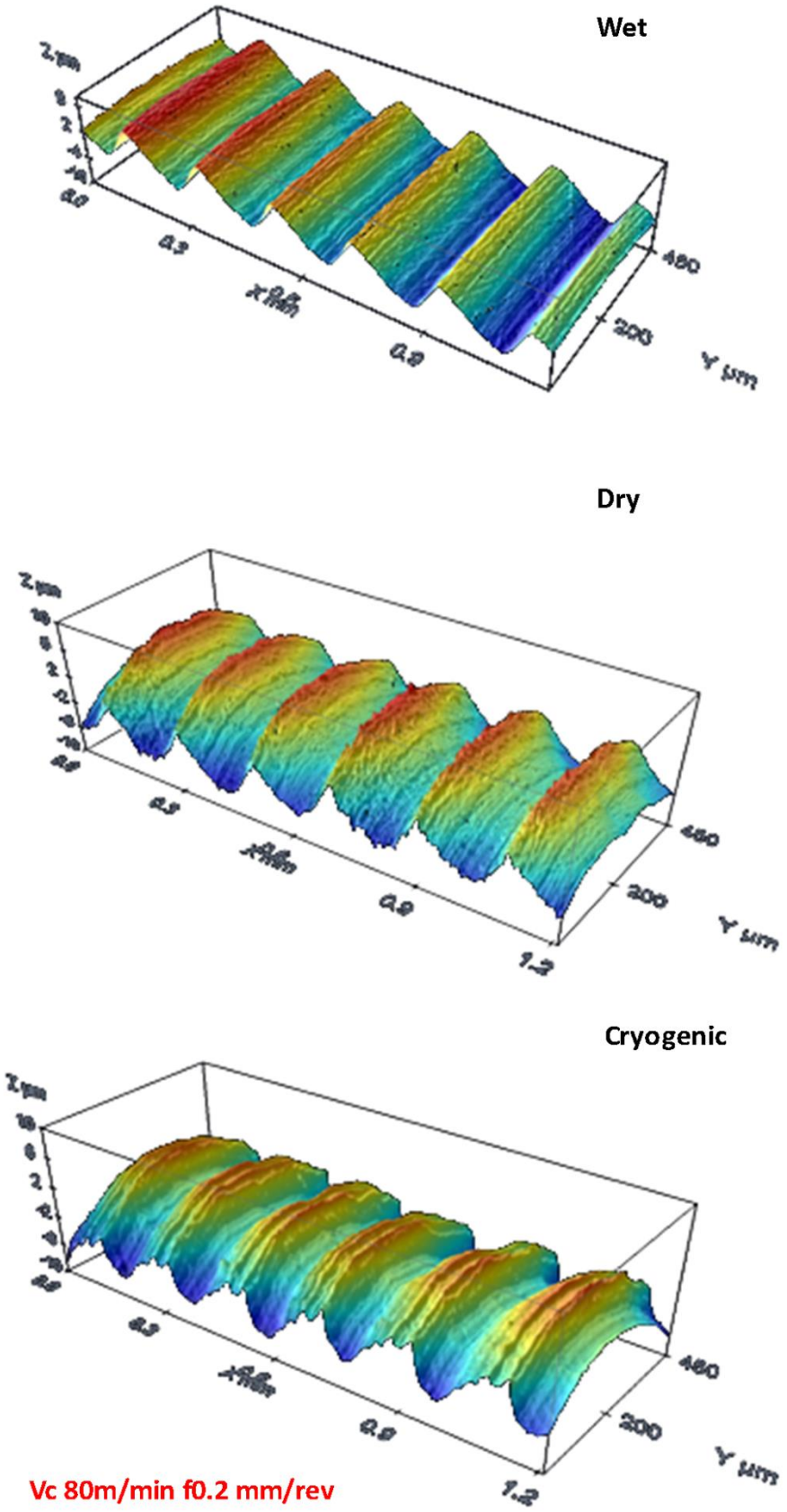

Figure 4.20 Coolant effect on machined surface topography when adopting a cutting speed of 80 m/min and a feed rate of 0.2 mm/rev after 15 minutes of turning.

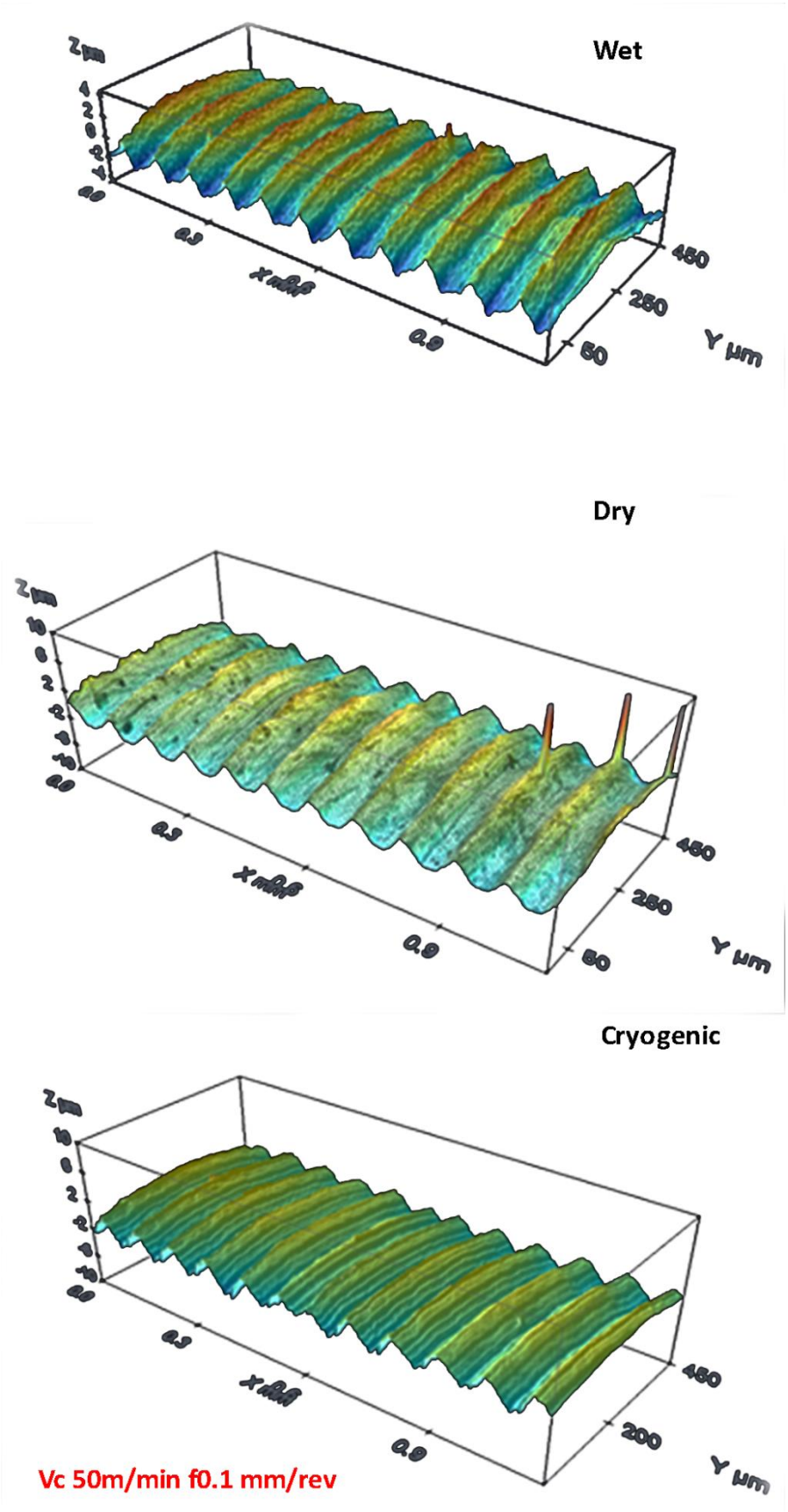

Figure 4.21 Coolant effect on machined surface topography when adopting a cutting speed of 50 m/min and a feed rate of 0.1 mm/rev after 15 minutes of turning.

In order to reduce the waviness of the machined surface, shorter machining operations would limit cooling of the workpiece: this is feasible in case of machining AM components since very few cutting passes are necessary to finish the already near-net-shape geometries.

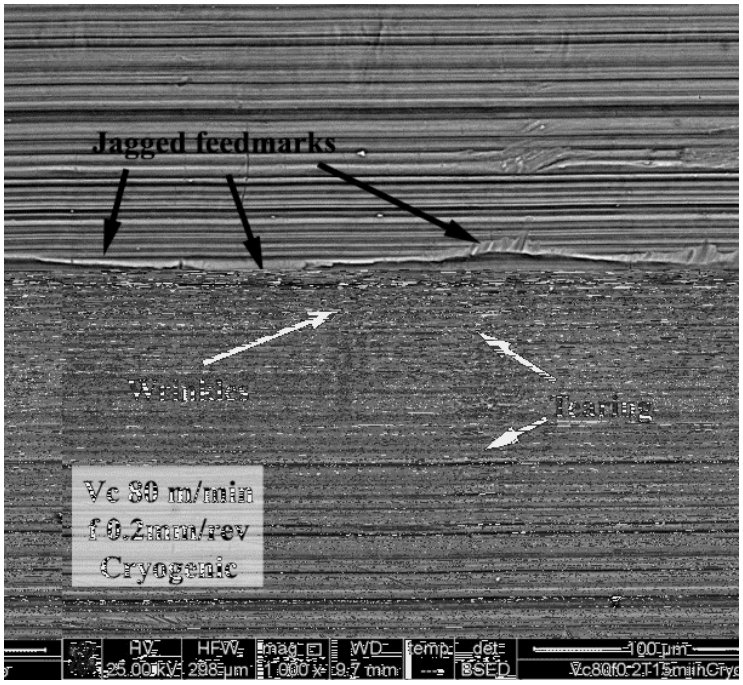

Figure4.19 Main surface damages provoked by applying cryogenic cooling after 8 minutes of cutting.

The analysis of surface topography conducted by the profilometer on the machined samples for all the cutting conditions tested confirmed the SEM analysis above described. The Figures 4.20 and 4.21 reports two examples of how the lubricating strategy affected the surface topography. The most clean and regular surface textures were achieved by the application of standard flood cooling, because the surface temperature of the material being deformed by the turning process was more stable and it reasonably reached values that stay between the two extreme conditions provoked by dry and cryogenic machining. The surface topography analysis, evidenced the complete absence of double feed marks and material side flow that might occur for the low depth of cut adopted in comparison with the tool radius. Dry turning generated more regular feed mark profiles and valleys than cryogenic machining, that as previously mentioned determined wrinkles and jagged feed marks. The surface topography deteriorated for higher feed rates during cryogenic machining, with the formation of irregular profiles. These conditions might be influenced by the reduced material plasticity on the surface layers and by the altered stiffness of the tool holder that became completely frozen by the application of LN_2, hence its stiffness and its modal behaviour could be altered due to the lower temperatures. Further analysis, with the application of accelerometers might help to understand the jagged feed marks arose during cryogenic machining.

4.3.3. Micro-hardness and microstructural alterations

The thermomechanical loads applied on the surface layers of the newly generated machined

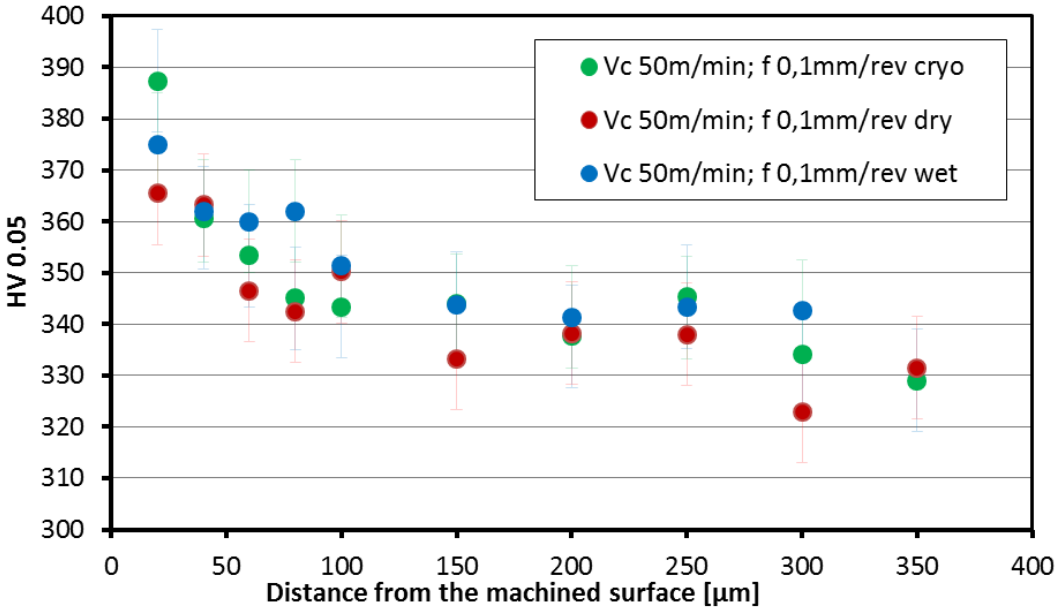

Figure 4.22 Effects of the adopted lubricating strategy on the micro-hardness trend after 8 minutes of turning with a cutting speed of 50 m/min and a feed rate of 0.1 mm/rev.

surface are renowned to alter the microstructure of the material. In particular, the strain hardening and the strain softening are the most important phenomena that alter the mechanical resistance of the wrought Ti6AL4V alloy when it is subjected to cutting operations. Strain hardening induces the material to become more resistance increasing its flow stress, on the other side, the strain softening plays an opposite role at higher strains [33]. The intensity of these phenomena depends on the adopted cutting parameters and on the lubricating strategy that determine the applied stresses and temperatures on the surface layers of the material. Measuring the micro-hardness trend along a radial direction beneath the machined surface is a simple but quite efficient approach to evidence their occurrence during the machining process. The Figures 4.22 and 4.23 report the micro-hardness trend measured for the extreme tested combinations of cutting parameters, highlighting the effect played by the lubricating strategy. In both the cases, a lowering trend of the micro hardness is clearly visible starting from the machined surface towards the inner layers of the material. These trends are a proof of the material work hardening occurred during the cutting process. Even dough the cutting parameters used should determine variations on the material alteration; the trends don not show significant variations in terms of micro-hardness. In general the higher the cutting parameters, the higher values of micro-hardness are measured. For both the presented cutting parameters combinations, the effect of the coolant is not significant on the point clouds measured, nonetheless a sensible difference is appreciable within the first twenty microns beneath the machined surface. The cryogenic effect rose the micro hardness for all the tested cutting parameters because of the lower temperatures reached on the workpiece

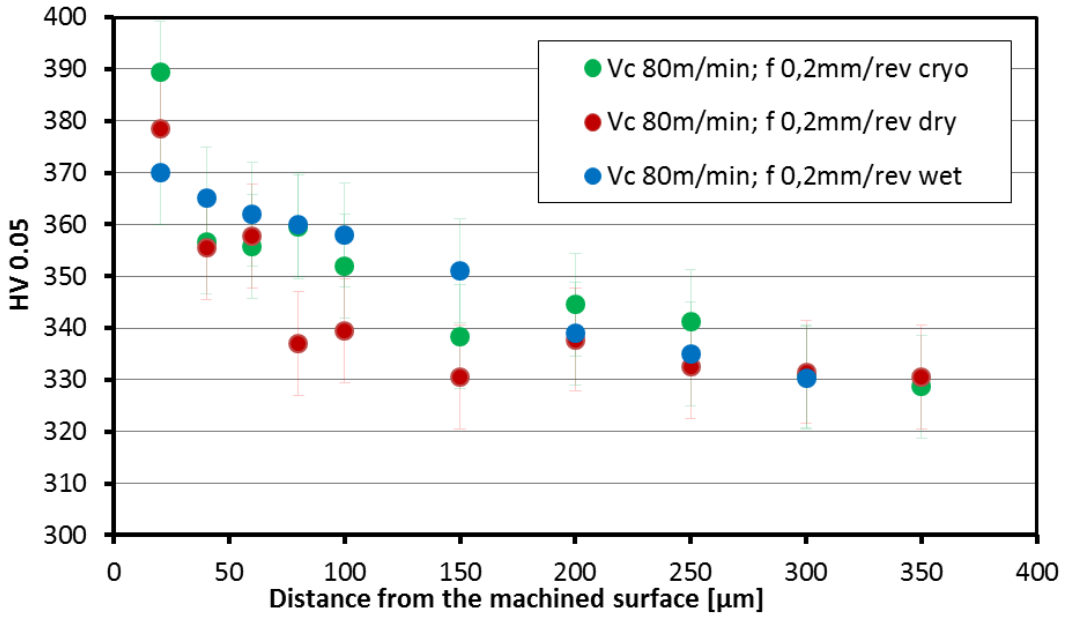

Figure 4.23 Effects of the adopted lubricating strategy on the micro-hardness trend after 8 minutes of turning with a cutting speed of 80 m/min and a feed rate of 0.2 mm/rev.

surface under this lubricating condition. In fact, during the turning tests the surface of the workpiece was completely frozen before the cutting insert pass. By the consequence, the material tends to require more energy to be cut, showing a more fragile behaviour. Similar findings were obtained by Pusavec et al. in cryogenic machining of Inconel 718 [34]. These results, are however important findings with regard to the wear resistance, because the higher the hardness the higher is the wear resistance offered by the surface against sliding wear or fretting wear mechanisms. On this basis, cryogenic machining might be efficiently adopted to improve the fretting resistance of those surfaces affected by this damaging mechanism in biomedical applications, such as the turned taper neck surface.

The main differences in terms of microstructural alterations induced by the turning process beneath the machined surface are reported in Figure 4.24. Even if the basket wave morphology (peculiar characteristic of the EBM Ti6AL4V alloy) complicates the identification of clear evidences, the α phase lamellae are bended towards the cutting speed direction. Furthermore, they are refined inside the severe plastic deformed layer as consequence of the material dynamic rearrangement [35]. The width of the severe plastic deformed layer (SPD) was measured for all the cutting conditions tested and it resulted to be equal to 20 microns, with no sensible variations determined by the cutting parameters. However, the cryogenic effect generated a less disturbed microstructure within the SPD layer, as can be seen in the Figure 4.24 on the left. Due to the very peculiar microstructure, in some cases the microstructure presented bended lamellae even under cryogenic machining, hence this can be considered as a generalised observation with some exceptions. Negligible differences were noticed in the resulting microstructure of dry and wet machined specimens. This phenomenon can be ascribed to the smaller differences of cutting temperatures that were reached during these turning processes.

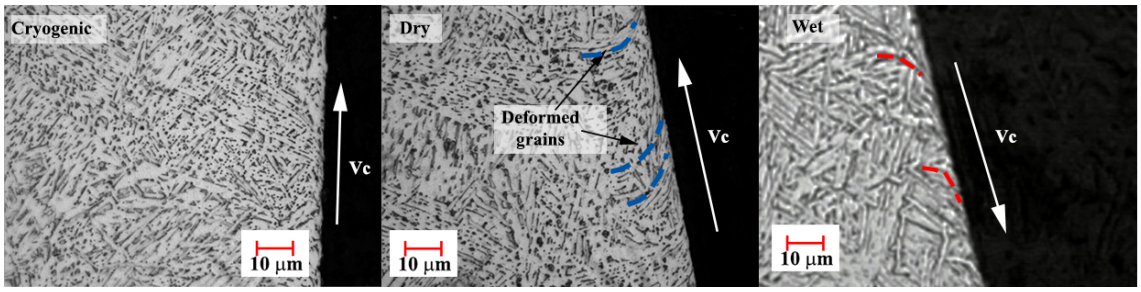

Figure 4.24 Microstructural alterations provoked by the machining process under dry, cryogenic and wet cooling conditions after 15 minutes of cutting.

4.3.4. Residual stresses

Aiming to quantify the microstructural alterations provoked by a cutting process, whether it is a milling, a turning or a drilling operation, the measurement of the residual stresses left in the surface layers of the material can be considered the most important investigation. During machining (milling, turning or grinding), the near-surface region of the work-piece is deformed plastically. Thus volume elements in this region are extended when the tool passes by and the constraints of the bulk material should introduce compressive stresses near the surface. Indeed, this does not occur for shallow, slow, well-lubricated cuts with a sharp tool. However, extensive studies of the stress pattern have shown that the actual situation is usually much more complex [36]. If strong work hardening occurs only near the surface, this produces tensile residual stresses due to the greater elastic relaxation of this region compared to the bulk. Local compressive plastic deformation due to the pressure applied by the tool will cause tensile residual stresses and if the sum of external stresses and residual stresses exceeds the local yield strength, plastic recovery will take place in this region. Even when there is no cross-feed of the tool, a biaxial stress state is observed. Heating, due to the lack of lubrication or a dull tool or high down feed, produces tensile stresses because locally heated regions are upset by the cooler surroundings. According to the literature, residual stresses are generated by mechanic and thermal loads applied on the surface layers by the tool pass. Their combination that depends by the cutting parameters, by the lubrication and by the tool radius and coating, determines the amount of the residual stresses left into the surface of the machined workpiece. Even if many works have been published in literature, it is still a complex phenomenon to explain. In this work, the residual stresses induced by the semi-finishing turning operation on EBM Ti6Al4V alloy under three different lubricating conditions were measured along the feed and the tangential direction for an adopted cutting speed equal to 80 m/min and an adopted feed rate equal to 0.1 mm/rev. This condition was selected among those tested because more interesting according to the previous finding. In fact, the higher cutting speed improved the material removal rate and the lower feed rate guaranteed a better surface integrity according to the previous findings. The Figures 4.25 and 4.26 report the residuals tresses trends below the machined surfaces along the axial and tangential directions when a cutting speed of 80 m/min and feed rate of 0.1 mm/rev were adopted after 8 minutes of turning. Both graphs prove that the cooling strategy has a deep influence on the residual stresses trend below the machined surface. For both the directions, cryogenic cooling generates higher compressive residual stresses on the surface. Along the axial direction, the

residual stresses remain more compressive for cryogenic machining inside the first 50 microns of material decreasing to a stress relaxed condition at a depth equal to 50 microns. On the other side, dry machining determines compressive axial residual stresses until 27 microns of depth becoming tensile up to 140 MPa at a depth equal to 100 microns. Wet machining generates a trend closer to cryogenic cooling as can be seen in Figure 4.25.

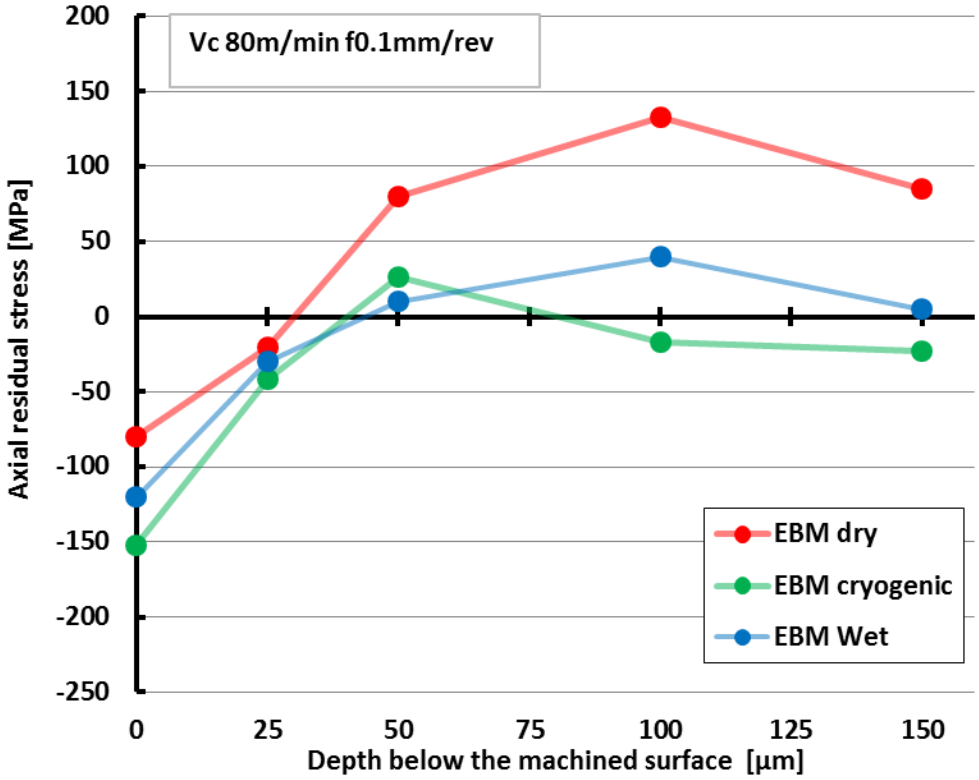

Figure 4.25 Effect of the lubricating strategy on the axial residual stresses when adopting a cutting speed of 80m/min and a feed rate of 0.1 mm/rev after 8 minutes of turning.

By observing the tangential direction, higher compressive residual stresses were measured on the surface for all the tested lubricating condition. Nonetheless dry machining unexpectedly generated a more compressive surface volume leading to the stress relaxation at the depth of 150 microns; meanwhile wet and cryogenic cooling raised steeply the stresses towards the relaxation state before a depth equal to 50 microns. These trends cannot be compared to similar works published in literature by Pusavec et al.[34] and by Devilez et al. [37] when they investigated the surface integrity in semi-finishing turning of Inconel 718 under different lubricating conditions. However, dry turning is renowned to promote tensile residual stresses in the surface layers, because of the higher thermal loads applied during cutting [36]. Hence, higher residual stresses found under wet and cryogenic machining on the surface of the workpieces might be the result of the lower cutting temperatures reached thanks to the application of a coolant mean, by the consequence with the goal to improve the surface integrity, dry machining even if it does not provoke tensile stresses, might reduce the fatigue resistance of the final product. In order to clarify the feasibility of sustainable dry and cryogenic cooling strategies to machine surgical implants made of EBM Ti6Al4V alloy, further analysis were carried out.

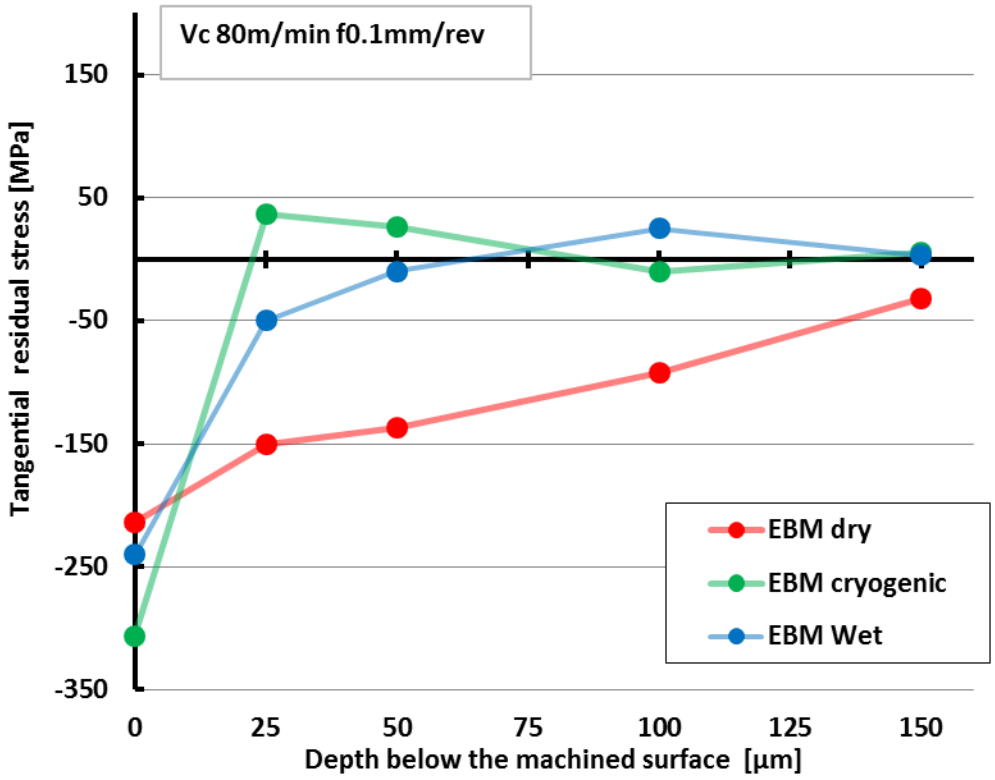

Figure 4.26 Effect of the lubricating strategy on the tangential residual stresses when adopting a cutting speed of 80 m/min and a feed rate of 0.1 mm/rev after 8 minutes of turning.

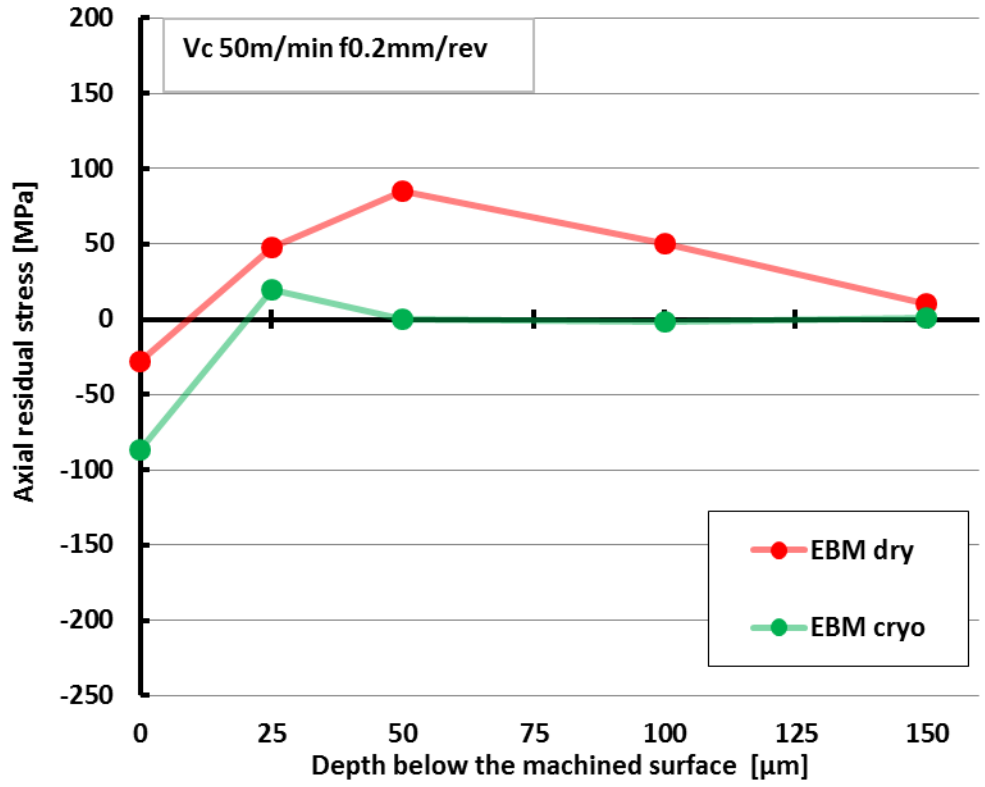

Figure 4.27 Comparison between dry and cryogenic cooling on the axial residual stresses measured on the specimens turned with a cutting speed equal to 50 m/min and a feed rate equal to 0.2 mm/rev.

The Figures 4.27 and 4.28 report the axial residual stresses due to dry and cryogenic cooling, evidencing the effect of the cutting speed for a feed rate equal to 0.2 mm/rev. It is clearly appreciable that if compared to the values plotted in Figure 4.25, the higher feed rate provokes lower values of the residual stresses for both the tested cutting speed. This aspect might be correlated to the higher amount of heat generated by adopting higher feed rate that tends to limit the beneficial effect of the cryogenic cooling. By comparing the values reported in Figure 4.27 to those plotted in Figure 4.28, this hypothesis can be confirmed. Higher cutting speeds generate higher amount of heat in the cutting zone, by the consequence tensile residual stresses are measured on the machined surface. For the highest feed rate, the cryogenic cooling is less efficient for improving the compressive residual stress layer.

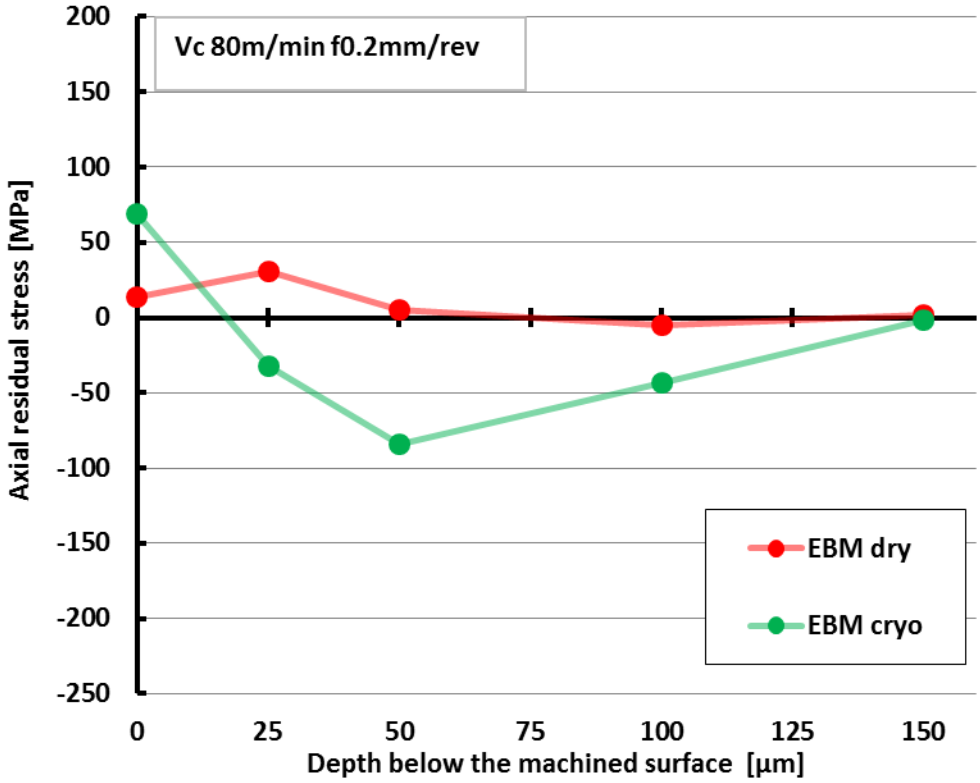

Figure 4.28 Comparison between dry and cryogenic cooling on the axial residual stresses measured on the specimens turned with a cutting speed equal to 80 m/min and a feed rate equal to 0.2 mm/rev.

If the tangential direction is considered (see Figures 4.29 and 4.30), the higher shear loads exerted by the tool nose on the machined surface for an adopted feed rate equal to 0.2 mm/rev, higher compressive residual stresses are measured in the surface layers for both dry and cryogenic turning (see Figure 4.25) than those measured for a feed rate equal to 0.1 mm/rev. Under such cutting conditions, the mechanical loads seem to prevail on the thermal loads. Similar trends were measured under dry and cryogenic turning, and when the most severe cutting parameters were set, cryogenic cooling induced higher compressive stresses on the machined surface, moreover, the compressive stress state material volume was wider than the one found for the lower feed rate applied, reaching the relaxation condition at a depth equal to 150 microns. These findings are however crucial for evaluating the feasibility of dry and cryogenic turning of EBM Ti6Al4V biomedical components, because high tensile residual stresses were never measured on the machined samples. In brief, cryogenic turning improved the compressive residual stresses more than dry turning for almost all the tested cutting

conditions and its efficiency was more explicated within the first 50 microns of the machined material. On the basis of these findings, dry turning might be implemented with a weaker effect because it did not lead to drastic increment of the residual stresses to dangerous tensile values.

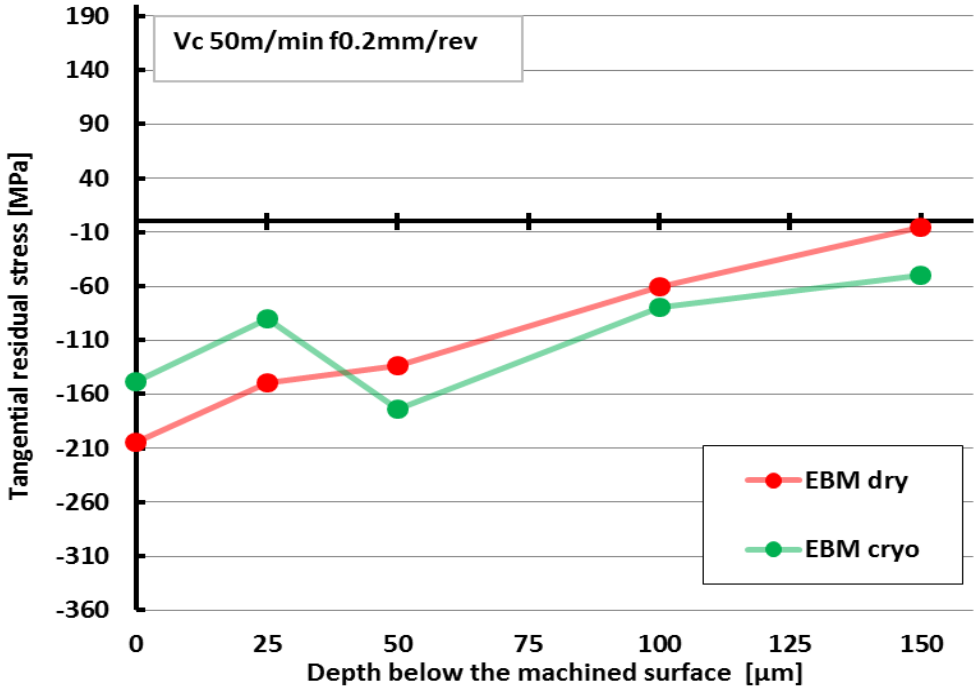

Figure 4.29 Comparison between dry and cryogenic cooling on the tangential residual stresses measured on the specimens turned with a cutting speed equal to 50m/min and a feed rate equal to 0.2 mm/rev.

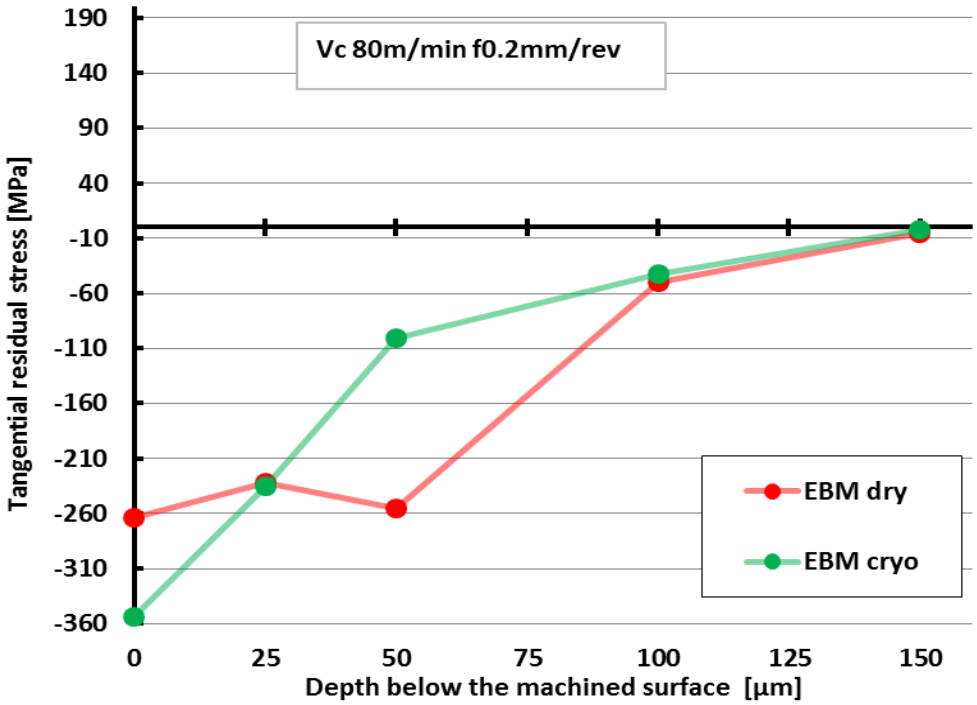

Figure 4.30 Comparison between dry and cryogenic cooling on the tangential residual stresses measured on the specimens turned with a cutting speed equal to 80m/min and a feed rate equal to 0.2 mm/rev.

4.4.Chip morphology

The chip control is of paramount importance during a machining process in order to achieve both a stable breakability and an easy disposal of the chips. In general, long chips should be avoided to prevent unpredictable entanglements around the workpiece or along the chip conveyor leading to workpiece and machine tool damages or even production stops to clear the chip evacuation. Further information about the feasibility and the sustainability of dry cutting and cryogenic cooling strategies can be gained by the chip morphology analysis. Figure 4.31 shows the chips morphology after 8 minutes of cutting, for the two levels of the feed rate at a fixed cutting speed of 80 m/min.

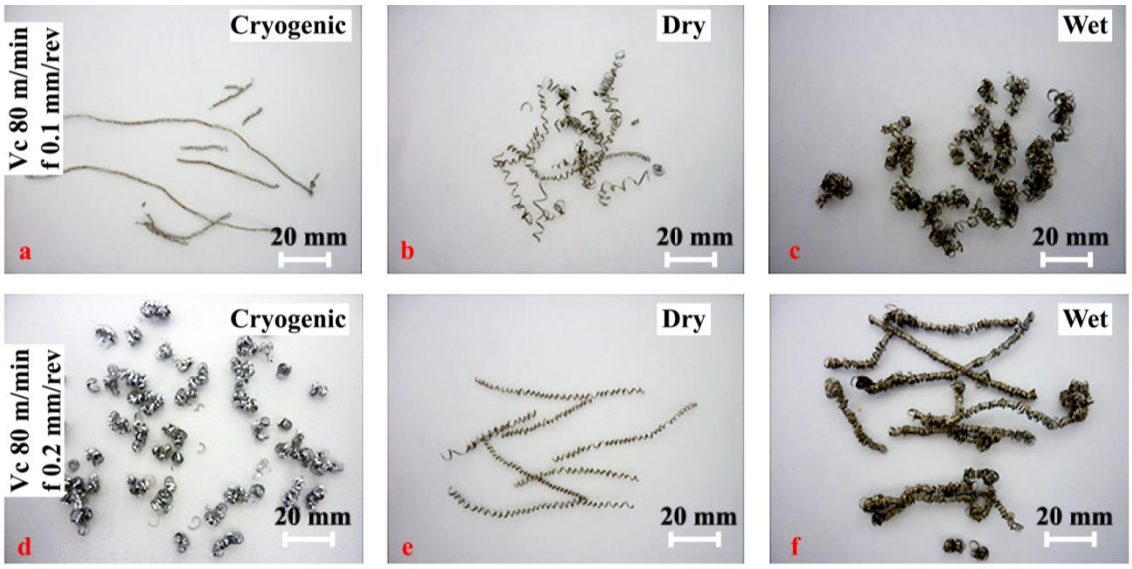

Figure 4.31Chip morphology under cryogenic, dry and wet turning conditions after 8 minutes of cutting and for a cutting speed of 80 m/min.

Since the tool wear was limited for all the cutting parameters tested in this work, no significant variations in terms of chip morphology were noticed at different turning stages. On the contrary, what is most noticeable is a significant variation of both the chip size and morphology when varying the cooling conditions. Frequent chip entanglements occurred during dry turning because the chip breaker exerted no breaking action due to the low depth of cut. The chips presented snarled ribbon morphology for the lowest feed rate that changed to a long helical one for the highest feed rate, as shown in Figure 4.31 b and e. The cutting temperatures reached under these conditions facilitated adhesion of chip fragments on the machined surface as discussed in the previous paragraph. It is noteworthy that under semi-finishing turning, the chip cross section is generally small hence for ductile alloys such as the Ti6Al4V alloy, they show a great bending capacity leading to a poor breakability[38]. In case of wet turning, the chip morphology changed noticeably as can be seen in Figure 4.31 c and f appearing as snarled tubular for a feed rate of 0.1 mm/rev while almost long tubular chips resulted for the value of 0.2 mm/rev. Thanks to the mechanical action exerted by the coolant flow stream, shorter chips were generated than in case of dry turning when the smallest feed rate was adopted, but less beneficial effects were noticed for the highest value due to the higher chip thickness, leading to the formation of 200 mm long chip segments. In addition,

the chip radius drastically increased in comparison to dry turning provoking more damages to the cutting tool and machined surface, as shown in Figure 4.1.

A better chip control was achieved when applying the cryogenic cooling, because of the material plasticity drop due to the lower cutting temperatures, which reduced the ductility and the bending capacity of the material portion involved in the chip formation. Figure 4.31 a and d shows that long helical chips with an average diameter of 2 mm were formed for the lowest feed rate, while 20 mm long snarled helical chips were collected for the highest one. In both cases, no chip entanglements formed around the tool holder enhancing the chips disposability and evacuation from the working area. Even dough no comparable works can be found in literature about machining the EBM Ti6Al4V, these findings are in accordance with other published works available on the effect of cryogenic temperatures on chip morphology when turning wrought Inconel 718 and Ti6Al4V alloys. In a recent work, Pusavec et al. [38]found a better chip breakability when turning the wrought Inconel 718 when applying LN_2 as a lubricant with even better results if coupled with MQL, whereas Pradeep and Dilip [40] noticed a better chip control and breakability during turning the wrought Ti6AL4V when applying the LN_2 rather than the CO_2 as cryogenic cutting fluid. In both works, the authors primarily imputed the lower temperatures reached during cutting as the main driving force for a better chip breakability. With the aim to better understand the effect of the cooling strategy on the chip morphology, the chips were collected, mounted, polished and etched to characterize their cross section geometry. A total amount of 30 measurements of the distance between serrations d_s (see Figure 4.32), of the primary shear band angle ϕ and, of the chip thickness c_t were carried out for each cutting condition. The averaged measurements are summarised in Figures 4.33 - 4.35 for a cutting length of 8 minutes. Serrated chips resulted for all the applied cooling strategies and the microstructural analysis proved that the chip segmentation consisted of a cracking – shear banding mechanism, as can be noticed in Figure 4.32 where a crack and an Adiabatic Shear Band (ABS) are highlighted between two consecutive chip peaks. The serrated chips were more regular for the highest feed rate of 0.2 mm/rev and for all the tested cooling strategies. The chip segmentation mechanism in machining Ti6Al4V is boosted by the cutting temperature and by the amount of deformation induced on the primary shear zone [41], hence for the low depth of cut applied in this work, an higher segmentation tendency for the highest cutting parameters is consistent with the literature records. The application of flood coolants in turning the EBM Ti6Al4V did not significantly affect the cross section geometry of the chip, and no significant discrepancies can be found if the error bands of the results are taken into account. Apart from the scatter in the measurements, which is common in this type of investigation[15], the marginal differences in the cutting temperatures between dry and wet turning for the low depth of cut here adopted could have limited the effects of the flood coolant on the chip segmentation mechanism. On the other hand, the cryogenic cooling influenced this phenomenon as can be appreciated by the measurements (see Figures 4.33 and 4.34) of the chip thickness c_t, and of the distance between serrations d_s. A chip thickness reduction is noticed mainly for the highest feed rate, whereas for all the cutting parameters combinations, greater distances between serrations are found.

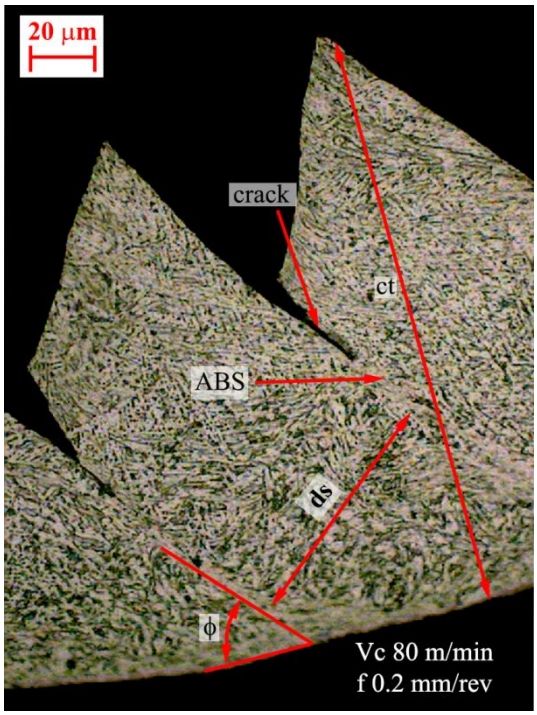

Figure 4.32 Cross section of the chip generated during machining under cryogenic cooling with indicated the measured chip features.

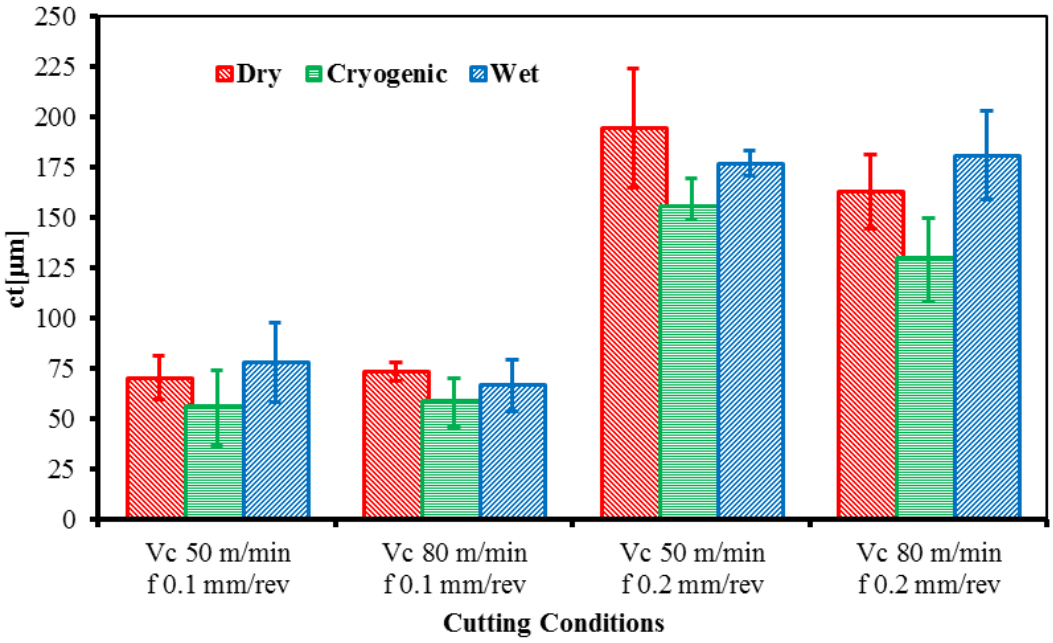

Figure 4.33 Effect of the cooling strategies on the chip thickness after 8 minutes of cutting.

From a sustainable point of view, a reduction of the chip thickness is important because thinner chips allow more space for cooling the cutting zone compared to thicker chips that tend to insulate the cutting zone from external coolants. Moreover, reminding that shorter chips were produced under cryogenic cooling, they are less hazardous to machine operators and are more convenient to dispose.

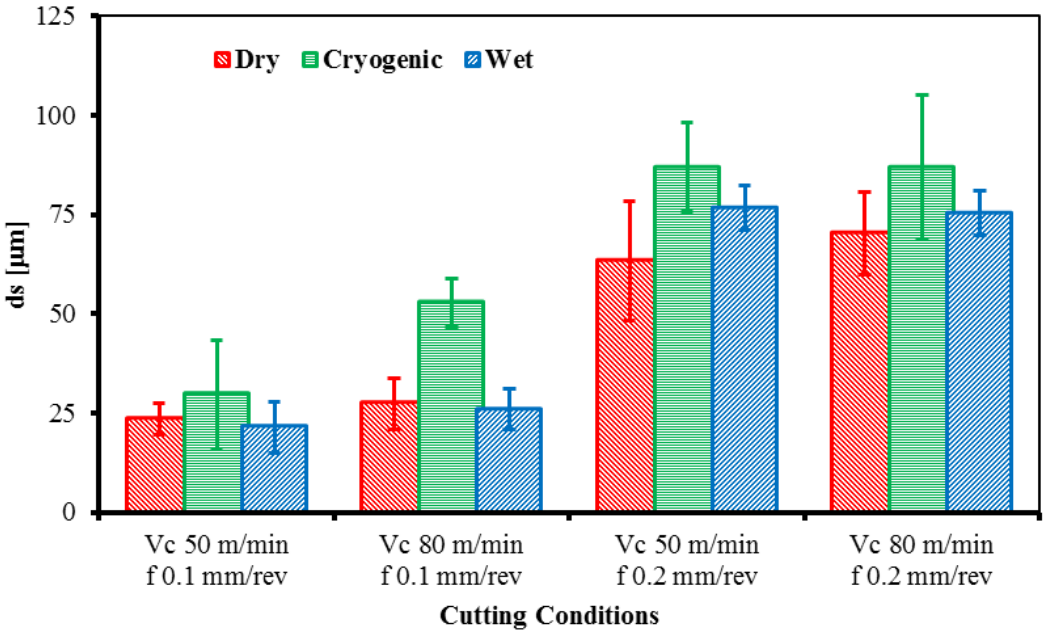

Figure 4.34 Effect of the cooling strategies on the distance between serrations for the chip formed after 8 minutes of cutting.

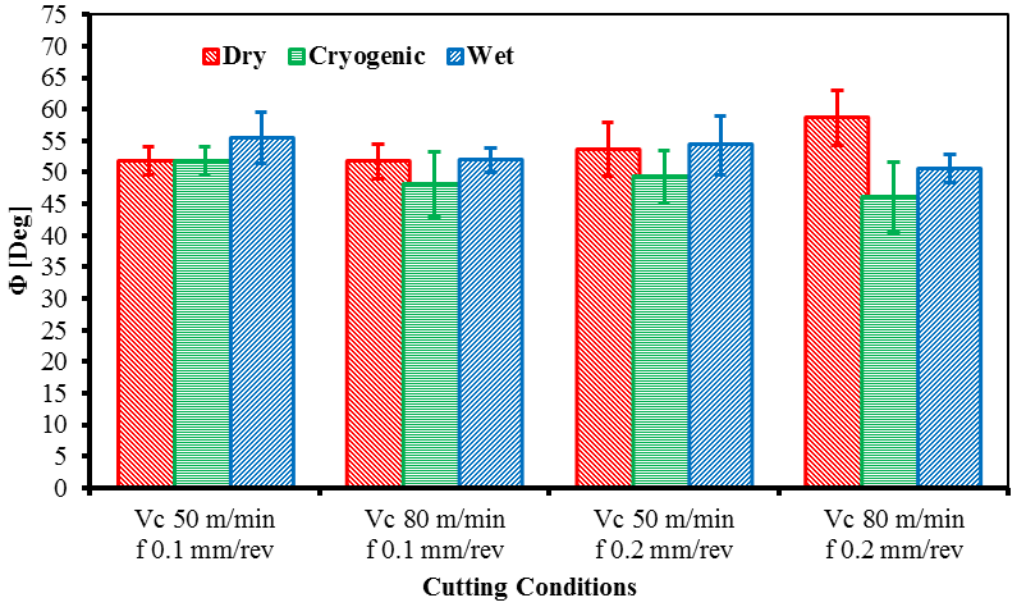

Figure 4.35 Effect of the cooling strategies on the primary shear band angle for the chip formed after 8 minutes of cutting.

4.5. Chapter concluding remarks

The machinability of the Ti6Al4V alloy produced by the additive manufacturing technique of Electron Beam Melting in semi finishing turning operation was investigated for the first time in this work through an experimental approach. The effects of the turning parameters and of three different lubricating strategies, namely dry, wet and cryogenic were tested. The machinability was determined by inspecting the tool wear, the surface integrity and the chip morphology with the aid of different experimental analysis.
The most important findings from this study are summarised below:

- Regardless of the lubricating strategy adopted to machine EBM Ti6AL4V alloy, adhesion wear was the principal tool wear mechanism in semi finishing turning due to its chemical affinity with most of the chemical elements composing the tool coating. Even dough the microstructure of the alloy produced by EBM is quite different than the one characterizing wrought alloys, a sticky tendency of Ti6AL4V on the tool cutting surfaces is still confirmed. Nevertheless the adopted lubricating strategy has a deep influence on adhesion wear rates due to different thermal fields arose during the cutting process.

- The application of LN_2 reduced the tool wear for all the tested cutting parameters due to its higher cooling capacity of the cutting zone. The lowest values of the nose wear VBc were achieved and no cratering of the tool rake face was generated although the most severe cutting conditions were adopted.

- The feed rate resulted to be the most influential cutting parameter on the tool wear. When the feed rate was limited, dry turning led to tool wear values comparable to those of wet turning, thanks to the severe adhesion of the workpiece material on the tool cutting faces that limits the effect of the abrasive wear; on the contrary, when the feed rate was increased, dry machining led to severe cratering, confirming a poor machinability of Ti6AL4V and the need to apply a cooling mean when the cutting parameters are increased to preserve the tool wear. The higher cooling capacity of wet turning retarded the formation of crater wear when the highest feed rate and cutting speed were set in comparison to dry turning.

- The abrasion wear was limited on both the tool cutting edge and flank face thanks to the presence of a significant amount of adhered material limiting the extension of the flank wear width (nose wear). A slight reduction of the nose wear was measured when adopting the cryogenic cooling, with more appreciable effects for the most severe cutting parameters.

- As a prove of the beneficial effects of cryogenic cooling on the adhesion wear mechanism, a reduction of the tool-chip contact length and reduced thickness of the

adhered layer on the rake face at increasing the cutting time were achieved in comparison to dry turning.

- Concerning the surface integrity, the cooling conditions did not affect the roughness parameters Ra and Rt of the machined surfaces when the lowest feed rate was set and regardless of the cutting speed, whereas sensible improvements were assured by the application of LN_2 for the most severe cutting parameters, thanks to lower nose wear.

- Cryogenic cooling led to cleaner machined surfaces with fewer adhered particles than dry and wet turning, but due to the lower plasticity of the material induced by the lower cutting temperatures, the surfaces were wavier with the presence of jagged feed marks.

- Cryogenic cooling improved the mechanical properties of final workpiece within the superficial machined affected layer. Higher values of micro-hardness and higher compressive residual stresses were achieved up to a depth of 25 microns beneath the machined surface than dry and wet turning, foreseeing improvements of fatigue and wear resistance of the final product, furthermore the microstructure appeared less disturbed by the cutting process. Dry turning led to the worst results in terms of residual stresses and surface micro-hardness.

- The chip morphology changed considerably with the applied lubricating/cooling strategy. Cryogenic cooling enhanced the chip breakability due to the low ductility of the chips cooled by the LN_2 flow streams, thus avoiding frequent entanglements around the tool holder, which, instead, occurred during wet and dry turning, being more hazardous for the operator and less convenient to dispose.

- From an environmental point of view, cryogenic cooling was more prone than dry machining to be implemented in machining EBM Ti6Al4V, fulfilling a potential reduction of the production costs and environmental impact if applied in the biomedical field, nonetheless further researches need to be carried out by considering real industrial cases and the consequences of applying the LN_2 on the machined component geometrical tolerances.

References

[1] Ulutan, D., Ozel, T., 2011, Machining induced surface integrity in titanium and nickel alloys: A review, International Journal of Machine Tools and Manufacture, 51/3:250–280, DOI:10.1016/j.ijmachtools.2010.11.003.

[2] Symbols, G., 2010, A Review of the Machinability of Titanium Alloys, /September:43–52.

[3] Debnath, S., Reddy, M. M., Yi, Q. S., 2014, Environmental friendly cutting fluids and cooling techniques in machining: a review, Journal of Cleaner Production, 83:33–47, DOI:10.1016/j.jclepro.2014.07.071.

[4] Dudzinski, D., Devillez, A., Moufki, A., Larrouquère, D., Zerrouki, V., et al., 2004, A review of developments towards dry and high speed machining of Inconel 718 alloy, International Journal of Machine Tools and Manufacture, 44/4:439–456, DOI:10.1016/S0890-6955(03)00159-7.

[5] Hosseini Tazehkandi, A., Pilehvarian, F., Davoodi, B., 2014, Experimental investigation on removing cutting fluid from turning of Inconel 725 with coated carbide tools, Journal of Cleaner Production, 80:271–281, DOI:10.1016/j.jclepro.2014.05.098.

[6] Ozcelik, B., Kuram, E., Huseyin Cetin, M., Demirbas, E., 2011, Experimental investigations of vegetable based cutting fluids with extreme pressure during turning of AISI 304L, Tribology International, 44/12:1864–1871, DOI:10.1016/j.triboint.2011.07.012.

[7] Dutta, S., Kanwat, a., Pal, S. K., Sen, R., 2013, Correlation study of tool flank wear with machined surface texture in end milling, Measurement: Journal of the International Measurement Confederation, 46/10:4249–4260, DOI:10.1016/j.measurement.2013.07.015.

[8] Hartung, P. D., Kramer, B. M., von Turkovich, B. F., 1982, Tool Wear in Titanium Machining, CIRP Annals - Manufacturing Technology, 31/1:75–80, DOI:10.1016/S0007-8506(07)63272-7.

[9] Courbon, C., Pusavec, F., Dumont, F., Rech, J., Kopac, J., 2013, Tribological behaviour of Ti6Al4V and Inconel718 under dry and cryogenic conditions - Application to the context of machining with carbide tools, Tribology International, 66:72–82, DOI:10.1016/j.triboint.2013.04.010.

[10] Ezugwu, E. O., 2005, Key improvements in the machining of difficult-to-cut aerospace superalloys, International Journal of Machine Tools and Manufacture, 45/12–/13:1353–1367, DOI:10.1016/j.ijmachtools.2005.02.003.

[11] Venugopal, K. a., Paul, S., Chattopadhyay, a. B., 2007, Growth of tool wear in turning of Ti-6Al-4V alloy under cryogenic cooling, Wear, 262/9–/10:1071–1078, DOI:10.1016/j.wear.2006.11.010.

[12] Cantero, J. L., Díaz-Álvarez, J., Miguélez, M. H., Marín, N. C., 2013, Analysis of tool wear patterns in finishing turning of Inconel 718, Wear, 297/1–/2:885–894, DOI:10.1016/j.wear.2012.11.004.

[13] Bermingham, M. J., Palanisamy, S., Kent, D., Dargusch, M. S., 2012, A comparison of cryogenic and high pressure emulsion cooling technologies on tool life and chip morphology in Ti-6Al-4V cutting, Journal of Materials Processing Technology, 212/4:752–765, DOI:10.1016/j.jmatprotec.2011.10.027.

[14] Krämer, A., Klocke, F., Sangermann, H., Lung, D., 2014, Influence of the lubricoolant

strategy on thermo-mechanical tool load, CIRP Journal of Manufacturing Science and Technology, 7/1:40–47, DOI:10.1016/j.cirpj.2013.09.001.

[15] Bermingham, M. J., Kirsch, J., Sun, S., Palanisamy, S., Dargusch, M. S., 2011, New observations on tool life, cutting forces and chip morphology in cryogenic machining Ti-6Al-4V, International Journal of Machine Tools and Manufacture, 51/6:500–511, DOI:10.1016/j.ijmachtools.2011.02.009.

[16] Ayed, Y., Germain, G., Ammar, a., Furet, B., 2013, Degradation modes and tool wear mechanisms in finish and rough machining of Ti17 Titanium alloy under high-pressure water jet assistance, Wear, 305/1–/2:228–237, DOI:10.1016/j.wear.2013.06.018.

[17] Gekonde, H. O., Subramanian, S. V., 2002, Tribology of tool–chip interface and tool wear mechanisms, Surface and Coatings Technology, 149/2–/3:151–160, DOI:10.1016/S0257-8972(01)01488-8.

[18] Gómez-Parra, a., Álvarez-Alcón, M., Salguero, J., Batista, M., Marcos, M., 2013, Analysis of the evolution of the Built-Up Edge and Built-Up Layer formation mechanisms in the dry turning of aeronautical aluminium alloys, Wear, 302/1–/2:1209–1218, DOI:10.1016/j.wear.2012.12.001.

[19] M.C.Shaw, Metal Cutting Principles, Third Edition, Massachusetts Institute of Technology Publication, Cambridge, 1954.

[20] E.M. Trent, P.K. Wright, Metal Cutting, Fourth Edition, Butterworth-Heinemann, New York (USA) (2000).

[21] Xue, C., Chen, W., 2011, Adhering layer formation and its effect on the wear of coated carbide tools during turning of a nickel-based alloy, Wear, 270/11–/12:895–902, DOI:10.1016/j.wear.2011.02.018.

[22] Molinari, A., Nouari, M., 2002, Modeling of tool wear by diffusion in metal cutting, Wear, 252/1–/2:135–149, DOI:10.1016/S0043-1648(01)00858-4.

[23] Hua, J., Shivpuri, R., 2005, A Cobalt Diffusion Based Model for Predicting Crater Wear of Carbide Tools in Machining Titanium Alloys, Journal of Engineering Materials and Technology, 127/1:136, DOI:10.1115/1.1839192.

[24] Calamaz, M., Coupard, D., Girot, F., 2008, A new material model for 2D numerical simulation of serrated chip formation when machining titanium alloy Ti–6Al–4V, International Journal of Machine Tools and Manufacture, 48/3–/4:275–288, DOI:10.1016/j.ijmachtools.2007.10.014.

[25] Venugopal, K. a., Paul, S., Chattopadhyay, a. B., 2007, Tool wear in cryogenic turning of Ti-6Al-4V alloy, Cryogenics, 47/1:12–18, DOI:10.1016/j.cryogenics.2006.08.011.

[26] Xie, J., Luo, M. J., Wu, K. K., Yang, L. F., Li, D. H., 2013, Experimental study on cutting temperature and cutting force in dry turning of titanium alloy using a non-coated micro-grooved tool, International Journal of Machine Tools and Manufacture, 73:25–36, DOI:10.1016/j.ijmachtools.2013.05.006.

[27] Umbrello, D., Micari, F., Jawahir, I. S., 2012, The effects of cryogenic cooling on surface integrity in hard machining: A comparison with dry machining, CIRP Annals - Manufacturing Technology, 61/1:103–106, DOI:10.1016/j.cirp.2012.03.052.

[28] Jouini, N., Revel, P., Mazeran, P. E., Bigerelle, M., 2013, The ability of precision hard turning to increase rolling contact fatigue life, Tribology International, 59:141–146, DOI:10.1016/j.triboint.2012.07.010.

[29] Zhang, S., Li, J. F., Wang, Y. W., 2012, Tool life and cutting forces in end milling

Inconel 718 under dry and minimum quantity cooling lubrication cutting conditions, Journal of Cleaner Production, 32:81–87, DOI:10.1016/j.jclepro.2012.03.014.

[30] Axinte, D. a., Andrews, P., Li, W., Gindy, N., Withers, P. J., 2006, Turning of advanced Ni based alloys obtained via powder metallurgy route, CIRP Annals - Manufacturing Technology, 55/1:117–120, DOI:10.1016/S0007-8506(07)60379-5.

[31] Zou, B., Chen, M., Huang, C., An, Q., 2009, Study on surface damages caused by turning NiCr20TiAl nickel-based alloy, Journal of Materials Processing Technology, 209/17:5802–5809, DOI:10.1016/j.jmatprotec.2009.06.017.

[32] Zhou, J. M., Bushlya, V., Stahl, J. E., 2012, An investigation of surface damage in the high speed turning of Inconel 718 with use of whisker reinforced ceramic tools, Journal of Materials Processing Technology, 212/2:372–384, DOI:10.1016/j.jmatprotec.2011.09.022.

[33] Sima, M., Özel, T., 2010, Modified material constitutive models for serrated chip formation simulations and experimental validation in machining of titanium alloy Ti–6Al–4V, International Journal of Machine Tools and Manufacture, 50/11:943–960, DOI:10.1016/j.ijmachtools.2010.08.004.

[34] Pusavec, F., Hamdi, H., Kopac, J., Jawahir, I. S., 2011, Surface integrity in cryogenic machining of nickel based alloy—Inconel 718, Journal of Materials Processing Technology, 211/4:773–783, DOI:10.1016/j.jmatprotec.2010.12.013.

[35] Motyka, M., Kubiak, K., Sieniawski, J., Ziaja, W., 2007, Hot Plasticity of Alpha Beta Alloys.

[36] Christian Schlauer, Near-surface Residual Stress and Microstructural Changes after Turning of a Nickel-based Superalloy, Linköping Studies in Science and Technology Licentiate Thesis No. 1002, 2003.

[37] Devillez, a., Le Coz, G., Dominiak, S., Dudzinski, D., 2011, Dry machining of Inconel 718, workpiece surface integrity, Journal of Materials Processing Technology, 211/10:1590–1598, DOI:10.1016/j.jmatprotec.2011.04.011.

[38] Pusavec, F., Deshpande, A., Yang, S., M'Saoubi, R., Kopac, J., et al., 2014, Sustainable machining of high temperature Nickel alloy - Inconel 718: Part 1 - Predictive performance models, Journal of Cleaner Production, 81:255–269, DOI:10.1016/j.jclepro.2014.06.040.

[39] Pusavec, F., Deshpande, A., Yang, S., M'Saoubi, R., Kopac, J., et al., 2015, Sustainable machining of high temperature Nickel alloy – Inconel 718: part 2 – chip breakability and optimization, Journal of Cleaner Production, 87:941–952, DOI:10.1016/j.jclepro.2014.10.085.

[40] M, P. K., 2012, Effect of Cryogenic Cutting Coolants on Cutting Forces and Chip Morphology in Machining Ti-6Al-4V Alloy, 2012:1–7.

[41] Ye, G. G., Xue, S. F., Jiang, M. Q., Tong, X. H., Dai, L. H., 2013, Modeling periodic adiabatic shear band evolution during high speed machining Ti-6Al-4V alloy, International Journal of Plasticity, 40:39–55, DOI:10.1016/j.ijplas.2012.07.001.

Chapter 5

Effects of lubricating strategy on wear performance of turned EBM Ti6Al4V alloy

5.1. Introduction

The experimental research conducted to investigate for the first time the machinability of the EBM Ti6Al4V alloy, under different process conditions described in chapter 4, highlighted that the surface integrity of turned test pieces can be improved by the adoption of cryogenic cooling. More in detail, the residual stresses and the surface hardness resulted to be efficiently improved thanks to the cryogenic effects: higher surface micro-hardness and higher compressive residual stresses were measured for cryogenically turned pins for most of the tested process conditions, in comparison to dry and wet turning (see the Figures 4.22, 4.23, 4.26 and 4.27). Starting from these important findings, the following step expects to validate these beneficial effects through a technological test that replicates real working conditions of a surgical replacement. When dealing with machined induced surface integrity, the fatigue performance of the workpiece and the wear resistance of the surface are those properties more ideal to be tested aiming to validate the effects of machining conditions. Among all the most used surgical implants, few of them requires turning operations, rather they are produced by standard forging and machining or by additive manufacturing technologies. The taper of the modular neck hip replacement is subjected to turning operations and their effects on the

surface layers of the material determine its fatigue and its fretting resistance. This particular turned feature is taken into account in this work, aiming to verify in close real working conditions if the cryogenic cooling effectively improves the workpiece performances by carrying out sliding wear tests applying loads and displacements as close as possible as those present in the real surgical joint interface composed by the taper neck replacement and the femoral head as can be seen in the Figure 5.1.

Figure 5.1 Examples of different modular neck designs on the left, and of acetabular sphere made of ceramic and CoCrMo on the right.

Compared to iron and cobalt-based alloys, titanium alloys are nowadays the most attractive solution for biomedical applications thanks to their chemical (i.e. corrosion resistance, biocompatibility) and mechanical properties (i.e. stiffness, density) [1,2]. Furthermore, the possibility to manufacture components with tailored porosities and different degrees of surface roughness has been attracting a broad interest in the scientific community, since it may allow reducing the stiffness mismatch with the human bones [3,4], obtaining the prosthesis fixation through complete bone ingrowth[2], as well as improving the cell adhesion, viability, differentiation and growth [5]. However, at the same time, titanium alloys present low wear resistance to the combined action of body fluids and micro-motions [6–9], which usually accelerates the release of metal debris and reduces the lifetime of implants due to adverse tissue reactions. Apart from these few studies, a survey of the scientific literature reveals that the correlation between the use of lubrication strategies different from conventional cutting fluids and the wear resistance performances of the machined functional surfaces remains largely unknown, and requires a deeper investigation. Samples machined adopting the cutting parameters set to analyse the machinability of the material under dry and cryogenic cooling conditions were tested by using a reciprocating sliding wear testing set-up, specifically developed to carry out in-vitro temperature-controlled wear tests. The machined EBM Ti6AL4V samples, were subjected to sliding wear on CoCrMo alloy as counterpart material[10], in order to reproduce one of the typical tribological couplings of human prosthesis. The wear resistance of the turned specimens were quantified by measuring in line the friction coefficient and the weight variation due to the wear phenomenon. Moreover, a detailed SEM and EDS analysis helped to assess the main wear mechanisms and modes arising during sliding wear of EBM Ti6AL4V alloy on wrought CoCrMo alloy.

5.2. Experimental methods

In this chapter, the experimental approaches followed to investigate the sliding wear resistance of EBM Ti6AL4V alloy turned pins on CoCrMo are presented, giving more emphasis to the tribological tests and the scientific approach to set the appropriate conditions.

5.2.1. Materials

In the present work, a couple of two biomedical alloys were investigated under reciprocating sliding wear conditions, respectively a wrought ASTM F1537 CoCrMo was considered for the flat plate and an Electron Beam Melted Ti6AL4V alloy for the cylindrical pin. Their chemical composition and mechanical properties are presented in Table 5.1 and Table 5.2 respectively. The Ti6Al4V pins were obtained by cylindrical billets manufactured by electron beam melting (EBM) process using an ARCAM® A1 EBM platform. Each billet was manufactured with the symmetry axis parallel to the growing direction, with a diameter of 14 mm and a height of 180 mm. The CoCrMo alloy chosen for the flat plate is widely employed in the biomedical field to realise artificial metal on metal joints due to its high wear and corrosion resistance [11] particular for the production of spherical heads of the hip replacement as can be seen in the Figure 5.2. Being the material object of this investigation coming from the same batch of billets used to investigate the machinability, more information's regarding the material properties and its microstructure can be found in the chapter 3 of this thesis.

Table 5.1 Chemical composition of the tested materials (%weight).

EBM Ti6AL4V							
Al	**V**	**C**	**Fe**	**O**	**N**	**H**	**Ti**
6	4	0.03	0.1	0.15	0.01	0.003	Bal
ASTM F1537							
Cr	**Mo**	**C**	**Fe**	**Ni**	**N**	**Si**	**Co**
26	6	0.14	0.75	1	0.25	≤ 1	Bal

Table 5.2 Mechanical characteristics of the tested alloys in the as built condition.

Material	**E [Gpa]**	**UTS [Mpa]**	**YS [Mpa]**	**Elongation (%)**	**$HV_{0.05}$**
EBM Ti6Al4V	114	914	830	13.1	335
ASTM F1537 CoCrMo	240	1172	827	12	505

Figure 5.2 Femoral heads made of CoCrMo alloy for metal on metal (MOM) hip replacement.

5.2.2. Reciprocating wear tests

The reciprocating wear tests were carried out on the Bruker-UMT-3™ tribometer using a cylinder-on-plate configuration, whereby a 5 mm long and 10 mm of diameter Ti6Al4V pin was made to slide against a CoCrMo plate in a linearly reciprocating path. Such type of configuration was selected as it was the most suitable to investigate the behaviour of cylindrical shapes obtained by turning, as it was reported in [12–14]

Micromotions at stem-neck interfaces could range from approximately 10 μm to approximately 50 μm [15]. In this study, displacement has to be kept at higher values due to the limitations of the tribometer used to conduct the wear tests: the adopted half-stroke length was 500 μm. The test frequency was set equal to 10 Hz, since to avoid interfering with the re-passivation of the titanium alloy surface the maximum test frequency has to be kept below 15 Hz [16].The test duration was fixed in 10^5 cycles. Actually if the time between two load cycles is smaller than the repassivation time, penetrant corrosion can be induced. Ti6AI4V alloy passivates very quickly: about 60 ms in Hanks solution at 37°C[17]. Unfortunately, the cyclic surface oxidation may reduce the O_2 level in the crevice solution, decelerating the passivation process. On the other hand, Bobyn et al. [18] demonstrated that the damage produced in the head-stem modularity tested in vitro at frequency of 10 Hz was similar to that retrieved from patients. Moreover 10 Hz is also the upper frequency limit imposed by the ISO 7206/3 standard for endurance tests. So with the aim to reduce test duration and to do not interfere with titanium's repassivation time it has been decided to run tests at the highest level that does not interfere with the experiment.

The test loading conditions were chosen on the basis of a non-linear 3-D Finite Element (FE) stress analysis carried out to determine the contact loads at the interfaces between stem and femoral heads. The FE model was developed in PTC Creo Parametric® modelling the stem neck with tetrahedral solid elements of an average element size of 0.5 mm, while the stem and the head prosthesis were meshed using tetrahedral solid elements of an average size of 2 mm. The 3000 N load was applied at the centre of the femoral head, following the ISO 7206-7 standard recommendations. It was found a maximum compressive stress acting on the taper surface equal to 100 MPa as can be seen in the Figure 5.3, in close agreement with the findings of other numerical studies [13].

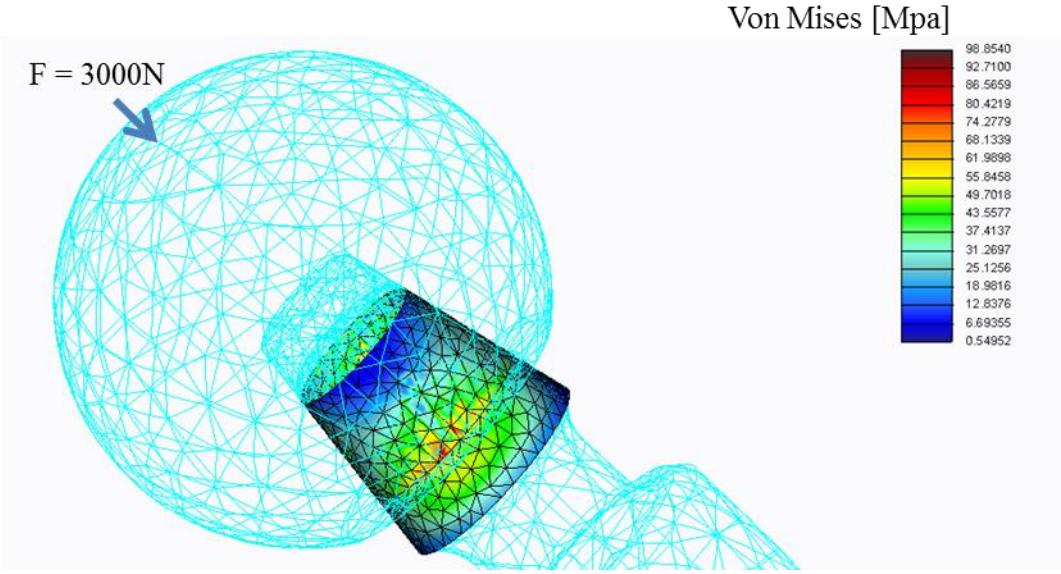

Figure 5.3 Stress field (contact pressure) applied on the taper junction of the hip replacement, due to the application of a vertical load equal to 3000 N.

The shape and dimensions of the wear tests components as well as the loading conditions were designed in order to replicate the results of the 3-D FE stress analysis following the Hertz's theory [19]. Therefore, a load of 7 N was applied during the wear tests to obtain an average contact pressure of 100 MPa that was kept constant for all the tests. The wear tests were performed under a saline solution (0,9% NaCl in distilled water) in a temperature-controlled environment by using a commercially heating element that was set at body temperature. The temperature was held at 37 $\pm$ 2°C in order to simulate as much realistic as possible the environmental conditions acting on a human hip implant. A thermometer, immersed in the water basin, was used in order to have a feedback of the real temperature set in the water. The tests parameters imposed for the wear tests are summarised in Table 5.3. **Errore. L'origine riferimento non è stata trovata.** shows the scheme of the experiment and some details about the testing set-up.

Table 5.3 Reciprocating sliding wear testing parameters (nominal values).

Half stroke	500 μm	**Frequency**	10 Hz
Normal load	7 N	**Environment**	Saline Solution
Maximum contact pressure	100 Mpa	**Repeatibility**	n=3
Number of cycle	10^5		

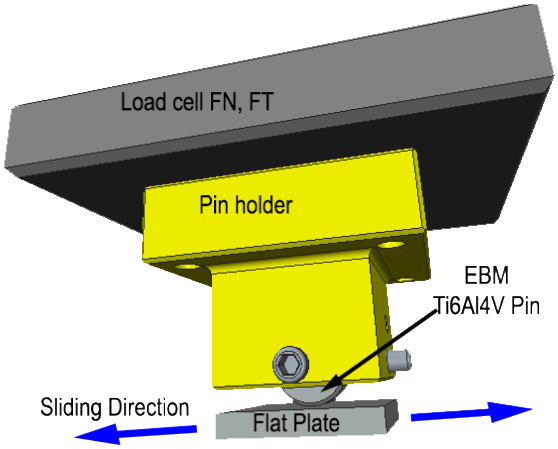

Figure 5.4 Schematic representation of the reciprocating sliding wear testing set-up.

The cylinder, with a diameter of 10 (±0.02) mm and length of 5 (±0.02) mm, is clamped to its holder by means of a screw and both are connected to a vertical and horizontal translation system in order to allow handling. The cylinder-holder is mounted on a load cell to acquire the tangential and normal forces during the tests; the normal load sensor provides an in-line feedback control for the vertical movement, which is actively adjusted in order to ensure a constant load during testing.

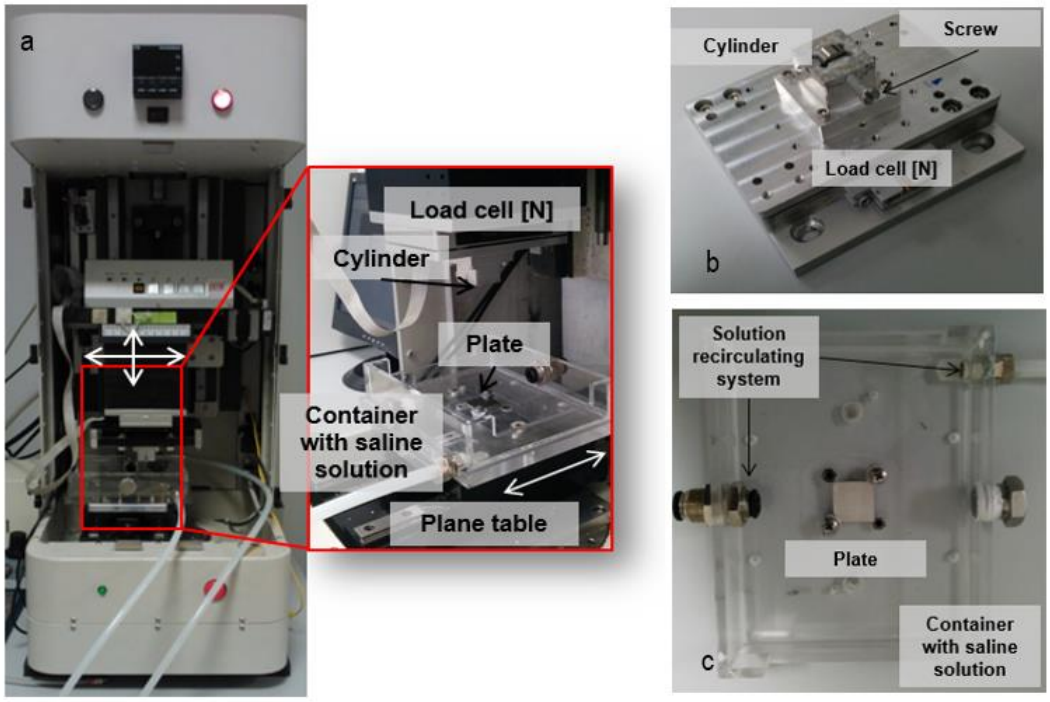

Figure 5.5 a) Photos of the tribological test apparatus with a magnified image of the overall system. b) Magnification of the cylinder-holder mounted on the load cell. c) Magnification of the plate fixed on the container assigned to contain the saline solution.

The plate, with an area of 20x20(±0.02) mm^2 and thickness of 2(±0.02) mm, is positioned within a container filled with the saline solution and clamped to it by means of two screws; the container in turn is placed on a plane table controlled by a servo motor, that allowed the alternative linear motion with a speed up to 60 (±0.5) mm/s. **Errore. L'origine riferimento**

non è stata trovata. shows the experimental set-up with details of the cylinder, load cell, plate and container fixed to the plane table. In **Errore. L'origine riferimento non è stata trovata.** b and **Errore. L'origine riferimento non è stata trovata.** c is possible to observe the system load cell-suspension and locking cylinder in order to ensure perfect locking and the plate immersed in the saline solution.

5.2.3. Machining tests

The cylindrical pins made of EBM Ti6Al4V, 10 mm dia. and 5 mm long, were machined respecting as much as possible a real scenario that could be encountered in the manufacturing process chain of Additive Manufactured surgical implants. By implementing AM technologies as forming strategies of metallic parts, the machining allowance usually left on the raw product design is in the range between 0.1 and 0.5 mm to minimize the number of machining steps required to obtain the final shape, thus only semi-finishing or finishing operations are needed. Considering the overall dimensions of the as-built cylindrical specimens that presented an external diameter of 14 mm and a length of 180 mm, they were pre-turned under dry cutting conditions to reach a diameter of 11 mm. By doing so, the machining allowance required to achieve the expected diameter resulted to be of 0.5 mm on the radius, limiting the number of the turning passes to a range that is in accordance with machining of Additive Manufactured parts. Furthermore, this pre-sizing operation allowed obtaining a reference surface topography for all the pins, with a resulting surface roughness Ra of 0.6 μm. The turning operations were performed on a Mori Seiki™ CNC lathe equipped with the cryogenic cooling apparatus described in the paragraph 3.5. With the goal of reproducing the same surface integrity patterns and do not alter the microstructural alterations described in the paragraph 4.2.2, the turning conditions described in the paragraph 3.5 were repeated in this work, setting the same cutting parameters, adopting the same tool holder and tool insert.

Table 5.4 Experimental plan for the machining tests.

Test Number	Cutting speed [m/min]	Feed rate [mm/rev]	Depth of cut [mm]	Lubrication
1	50	0.1	0.25	Dry
2	50	0.2	0.25	Dry
3	80	0.1	0.25	Dry
4	80	0.2	0.25	Dry
5	50	0.1	0.25	Cryogenic
6	50	0.2	0.25	Cryogenic
7	80	0.1	0.25	Cryogenic
8	80	0.2	0.25	Cryogenic

The experimental plan is reported in Table 5.4; three pins were realised for each of the cutting condition tested to take into account the repeatability of the experimental results. The cylindrical pins were turned clamping the pre-turned workpieces only at the spindle: as a consequence, the unsupported machined length was limited to a maximum value of 30 mm to reduce the vibrations (see Figure 5.6). 24 square plates were machined from a 29 mm diameter round bar made of the ASTM F1527 CoCrMo alloy with nominal edge length and thickness equal to 20 mm and 3 mm, respectively, dedicating a flat plate for each of the wear tests. After the milling operation, both the plate faces were ground in order to achieve a geometrical planarity tolerance of ±0.005 mm and a smooth surface topography. The surface topography of the pins and plates was measured through a Sensofar Plu-Neox™ optical 3D profiler with a resolution of less than 20 nm on the optical Z-axis. The average roughness Ra of the turned pins was evaluated along the perpendicular direction with respect to the feed marks, whereas the average surface roughness Sa of the flat plates was evaluated considering the directions parallel to their edges. The measured surface roughness values are indicative of actual machining operations carried out on biomedical implants, as encountered in several literature records [20,21].The mechanical characteristics of the pins machined surface were evaluated through Vickers micro-hardness measurements performed using a Leitz Durimet™ micro-hardness tester with a load of 50(±0.5) gr for 30 s; five values were recorded for each cylindrical pin and then the average value calculated. In order to investigate the microstructural alteration below the machined surface to verify the general replication of the experimental findings regarding the machinability investigation described in the chapter 3.7, the residual stresses on the cylindrical pins machined surfaces were measured by means of the X-Ray Diffraction (XRD) technique using the $\sin^2\psi$ method. The XRD analysis was carried out on an Enixè™ TNX diffractometer, using the parameters reported in Table 5.5. Being the wear resistance influenced by the surface layers properties, the residual stresses along the axial and circumferential directions with respect to the cylindrical pin axis were measured on the surface and at a depth of 25 μm below the surface, by removing the material layers through an electro polishing process to avoid modifications of the machining-induced stresses.

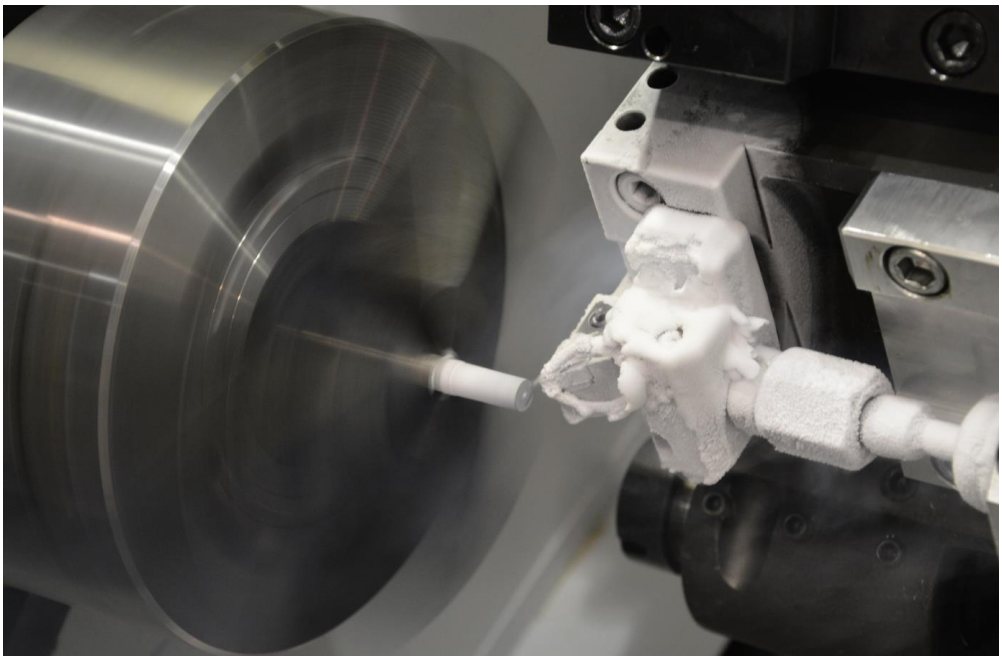

Figure 5.6 Cryogenic turning of the pins for sliding wear testing.

Table 5.5 XRD analysis parameters.

Radiation	CuKα
Collimator Diameter (mm)	1
X-Ray elastic constants2θ (MPa^{-1})	S1-1.21x10^{-6} S2-5.42x10^{-6}
Number of ψ angles	9
Bragg Angle 2θ (Deg)	141.8
Current	85 μA

5.2.4. Wear analysis

Before and after the wear tests, both the pins and the plates were ultrasonically cleaned for 15 minutes. After cleaning, they were weighed three times by using a KERN TM ABT 1205DM balance (sensitive to 0.01 μg), and the average weight calculated. The surface topography of the worn surfaces was evaluated using the Sensofar Plu–Neox™ optical 3D profiler. The average surface roughness parameters Ra and Sa of the worn pins and flat plates were evaluated accordingly, by adopting the same criteria of the measurements of the as-machined workpieces. After the wear tests, the roughness measurements were taken in the correspondence of the area characterized by the maximum pressure, which is located at the middle of the reciprocating sliding path. A FEI QUANTA 450™ Scanning Electron Microscope (SEM) equipped with the Everhart - Thornley Detector (ETD) and Backscattered Electron (BSED) detectors was used to examine the surface characteristics of the worn samples. The Energy Dispersive X-ray analysis (EDX) was carried out to identify the surface chemical composition after wear testing.

5.3.Experimental results

5.3.1. Characterization of machined samples

A comparison between the surface topographies of the pins machined under dry and cryogenic cooling conditions when adopting a cutting speed of 80 m/min and a feed rate of 0.2 mm/rev is presented in **Errore. L'origine riferimento non è stata trovata.**a, whereas the results of the surface integrity characterization are presented in **Errore. L'origine riferimento non è stata trovata.**. Higher micro-hardness values measured at a fixed depth of 15 μm below the machined surface, combined with higher compressive residual stresses, characterize the metallurgical alterations induced by the turning process when cryogenic cooling is applied compared to dry cutting, foreseeing sensible increases of the sliding wear resistance of EBM Ti6Al4V pins when machined under cryogenic cooling. Despite the lubricating strategy affected the mechanical properties of the machined surface, negligible differences in terms of the surface Roughness Ra were induced by the application of LN_2, since a fresh cutting edge was used to machine each pin hence the negligible tool wear did not significantly affect the surface integrity. These experimental findings are consistent with other works published in literature concerning the experimental investigation of surface integrity induced by cryogenic machining on different alloys. Pusavec et al. [22] found that under cryogenic cooling, higher values of surface hardness and higher compressive residual stresses along both axial and tangential directions are induced in the workpiece surface layers in comparison with dry machining when turning Inconel 718 adopting comparable cutting parameters than those adopted in this work. Pu et al. [23] proved that cryogenic cooling might consist in an efficient method aimed at improving functional properties of the final product, by increasing the hardness and compressive residual stresses along axial directions when LN_2 is applied as a cooling mean in machining AZ31B Mg alloy. In so doing, cryogenic machining might substitute surface treatments aimed at improving both fatigue and wear resistance as shoot-peening and electro polishing; nonetheless more researches have to be done along this direction. With respect to the CoCrMo flat plates, an average value of the Sa parameter equal to 0.234 ± 0.025 μm was calculated: an example of the surface topography resulting after milling and grinding is showed in Figure 5.7c.

Table 5.7 Surface integrity characterization of the EBM Ti6Al4V pins after the turning process.

		Surface Roughness		Micro-hardness		Residual Stresses			
Turning parameters	**Lubrication**	**Ra [µm]**	**DevSt (Ra) [µm]**	**$Hv_{0.05}$**	**DevSt (H_V)**	**σa_s[MPa]**	**σa_d[MPa]**	**σt_s[MPa]**	**σt_d[MPa] ***
V_c= 50 m/min f= 0.1 mm/rev	Dry	0.829	0.093	378.5	6.0	-64	-15	-276	-149
V_c= 80 m/min f= 0.1 mm/rev	Dry	0.942	0.127	369.5	4.2	-28	49	-205	-250
V_c= 50 m/min f= 0.2 mm/rev	Dry	2.339	0.049	371.8	7.4	-80	-20	-214	-150
V_c= 80 m/min f= 0.2 mm/rev	Dry	2.278	0.069	367.1	4.6	14	31	-264	-232
V_c= 50 m/min f= 0.1 mm/rev	Cryogenic	0.891	0.059	409.4	8.3	-123	-156	-156	-80
V_c= 80 m/min f= 0.1 mm/rev	Cryogenic	0.936	0.043	400.2	4.6	-87	20	-148	-90
V_c= 50 m/min f= 0.2 mm/rev	Cryogenic	2.328	0.045	389.0	7.2	-152	-42	-307	37
V_c=80 m/min f= 0.2 mm/rev	Cryogenic	2.294	0.049	385.0	4.5	-69	-32	-354	-235

σa: along axial direction, **σt:** along tangential direction, **σx_s**: residual stress measured on the surface (depth = 0 µm), **σx_t**: residual stress measured at the depth of 15 µm.

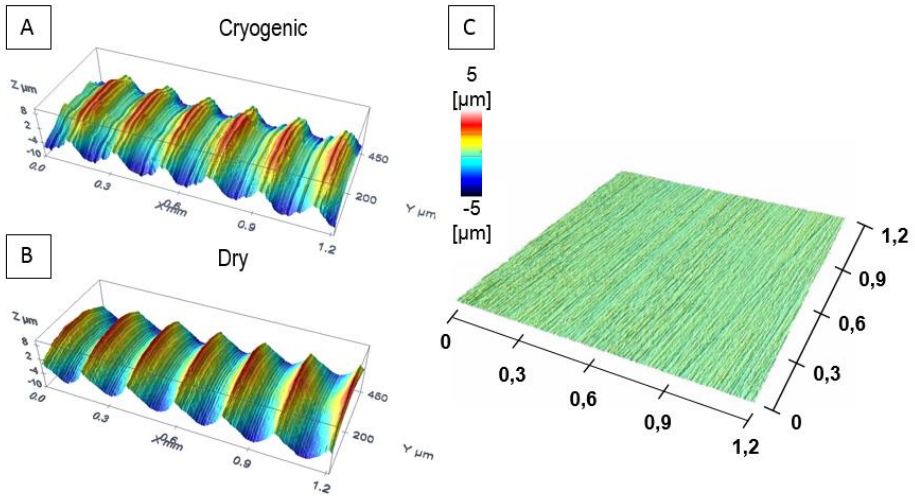

Figure 5.7 Comparison between the surface topography of the machined pin under: a) cryogenic and b) dry cooling conditions when adopting a cutting speed of 80 m/min and a feed rate of 0.2 mm/rev. c) Surface topography of the as grinded CoCrMo flat plate.

5.3.2. Friction analysis

Table 5.8 reports the average values of the steady-state Coefficient Of Friction (COF) and the total accumulated energy through all the cycles for each test trial. The COF was calculated as the ratio between the measured tangential and normal forces. In addition, from the experimental data, the force-displacement plot called hysteresis loop could be drawn to

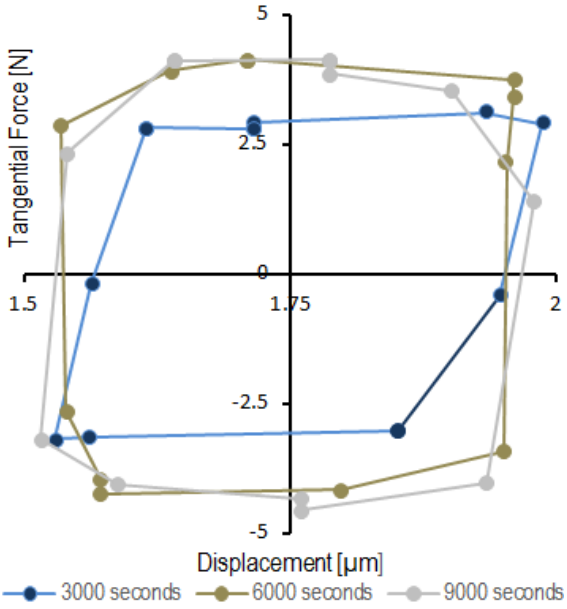

Figure 5.8 Development of the Hysteresis loop at different test lengths for the machined pin at Vc 50m/min and f 0.1 mm/rev.

evaluate graphically the dissipated energy through a single sliding cycle that corresponds to the area of each closed loop.

An example as the hysteresis loop evolved at increasing number of sliding cycles is presented in Fiure5.8. As for all the test trials, it proves that the test was carried out under gross slip conditions; furthermore, its quasi-rectangular shape reveals the dissipated energy was the biggest portion of the total energy and it reveals that the tests are being performed within the wear - dominated regime[24].

Table 5.8 Average values of the steady-state COF and dissipated energy as a function of the pins turning conditions.

Test. No	Lubrication	Vc [m/min]	f [mm/rev]	Average COF	DissipatedEnergy(*10^{-5}) [N*mm]
1	Dry	50	0.1	0.54	2.9
2	Dry	80	0.1	0.46	2.7
3	Dry	50	0.2	0.51	2.9
4	Dry	80	0.2	0.42	2.5
5	Cryogenic	50	0.1	0.36	1.9
6	Cryogenic	80	0.1	0.41	2.3
7	Cryogenic	50	0.2	0.37	1.9
8	Cryogenic	80	0.2	0.42	2.5

The COF values were calculated at fixed time lengths for all the tests. The COF tends to increase abruptly in the first 100 seconds of motion, and then it stabilizes after roughly 1000 seconds before smoothly increasing up to the final targeted sliding length. An example of such trend is given in Figure 5.9 in which the COF is plotted against time, showing the effects of the adopted feed rate and lubricating strategy at fixed cutting speed of 50 (m/min) (a similar trend was found for the highest cutting speed).

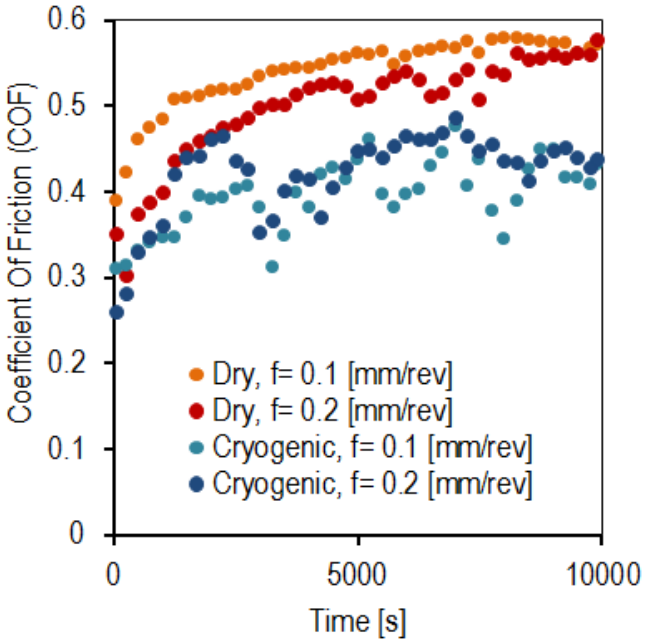

Figure 5.9 Influence of the feed rate and lubricating strategy on the COF in case of EBM Ti6Al4V pins machined at Vc= 50 (m/min).

The cryogenic cooling assures in general lower values of the COF, even if it increases the COF fluctuations during the test. This behaviour can be justified if a third body wear mechanism due to formation and oxidation of the mating surface layers of the EBM Ti6Al4V is taken into account as explained in literature by Qu et al. [25], who investigated the dry sliding wear behaviour of the Ti6Al4V against alumina, and found a higher oscillation of the COF when periodic localized fracture of the transferred layers took place.

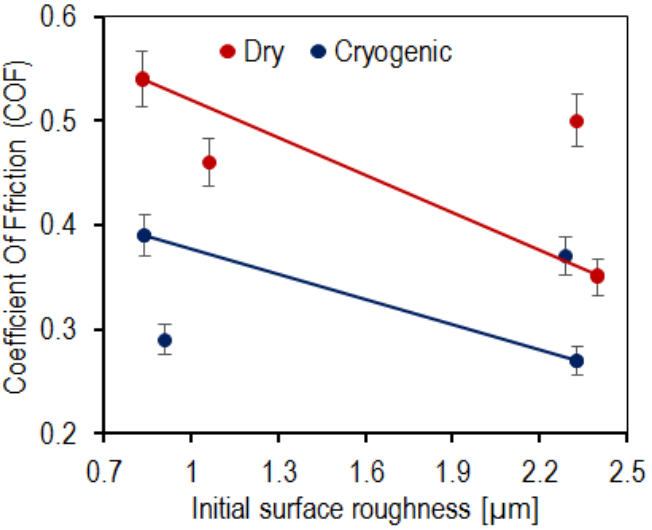

Figure 5.10 Effect of the initial roughness on the COF.

Figure 5.10 shows the influence of the pins surface roughness after semi-finishing turning on the average calculated COF for all the tested experimental conditions: the higher the surface roughness after machining, the lower the COF, in accordance to similar findings reported by Kubiak et al. [26]. Even if no sensible variations in terms of surface roughness are induced by the lubrication strategy, as evidenced in Table 5.8, the cryogenic cooling seems to

considerably affect the COF values by having a direct influence on the surface layer mechanical properties.

5.3.3. Sliding wear characterization

Tables 5.9 and 5.10 summarise the pins and plates weight loss due to wear phenomena, listing also the average values of the pin and plates initial and final weights as a function of the pins turning conditions. Since the experiments were conducted in an aqueous environment, the measure of the weight loss includes the effects of both the corrosion and wear. Nevertheless, the time between two successive load cycles is higher than the repassivation time of the Ti6Al4V alloy, which is found to be about 60 ms in Hanks solution at 37°C [27] Therefore, the Ti6Al4V surface can reach the passive state during sliding with a consequent negligible contribution of the corrosion to the total wear loss. On the basis of the wear map developed by Jiang and Stack et al. [28], the experimental conditions adopted in this research study can be assumed being in the corrosion-induced wear regime, and the wear loss due to corrosion considered negligible.
In Figure 5.10, a clear difference in the wear behaviour can be observed between dry and cryogenic machined worn pins: a weight decrease is noticeable for the dry machined pins whereas a weight increase is detected for the cryogenic ones. This can be ascribed to the

Table 5.9 EBM Ti6Al4V pins initial and final average weights, relative standard deviation and weight loss as a function of the pins turning parameters.

Lubrication	f [mm/rev]	Vc [m/min]	Initial Weight [g]	Final Weight [g]	ΔWeight [g] (*10^{-5})
Dry	0.1	50	1.76009	1.76007	-1.6
Cryogenic	0.1	50	1.87361	1.87369	8.2
Dry	0.1	80	1.83844	1.83837	-7.0
Cryogenic	0.1	80	1.83732	1.83739	6.9
Dry	0.2	50	1.84207	1.84203	-4.3
Cryogenic	0.2	50	1.80864	1.80872	8.5
Dry	0.2	80	1.83104	1.83101	-3.0
Cryogenic	0.2	80	1.86580	1.86585	4.6

Table 5.10 CoCrMo plates initial and final average weights, relative standard deviation and weight loss as a function of the pins turning parameters.

Lubrication	f [mm/rev]	Vc [m/min]	Initial Weight [g]	Final Weight [g]	ΔWeight [g]
Dry	0.1	50	9.87151	9.91047	0.03896
Cryogenic	0.1	50	9.88455	9.87131	-0.01324
Dry	0.1	80	9.87176	9.91102	0.03926
Cryogenic	0.1	80	9.87169	9.87156	-0.00013
Dry	0.2	50	9.91047	9.94874	0.03827
Cryogenic	0.2	50	9.87166	9.87155	-0.00011
Dry	0.2	80	9.91102	9.94224	0.03122
Cryogenic	0.2	80	9.87134	9.87109	-0.00025

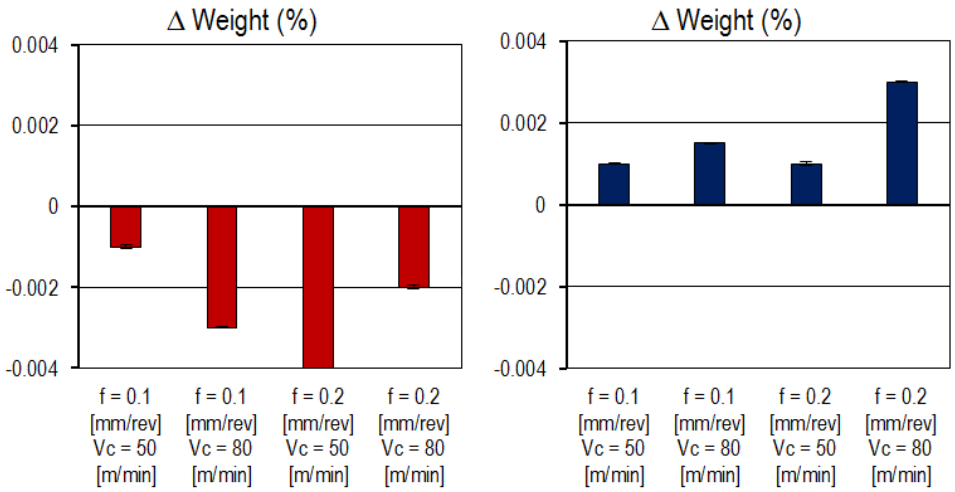

Figure 5.10 Effect of the dry (on the left) and cryogenic (on the right) machining strategies on the weight loss of the EBM Ti6Al4V pins after wear testing.

different superficial conditions: the cryogenic machined pins presented both higher superficial hardness and compressive residual stresses (see Table 5.7) than the dry machined ones; therefore, in accordance with the Archard's wear rate equation[29], their higher initial hardness determines lower wear volumes in comparison with the dry machined pins. The opposite behaviour, in term of weight measurements, was detected for the CoCrMo plates: those that were in contact with the dry machined pins showed an increase in weight , which can be ascribed to an adhesion of the counterpart material.

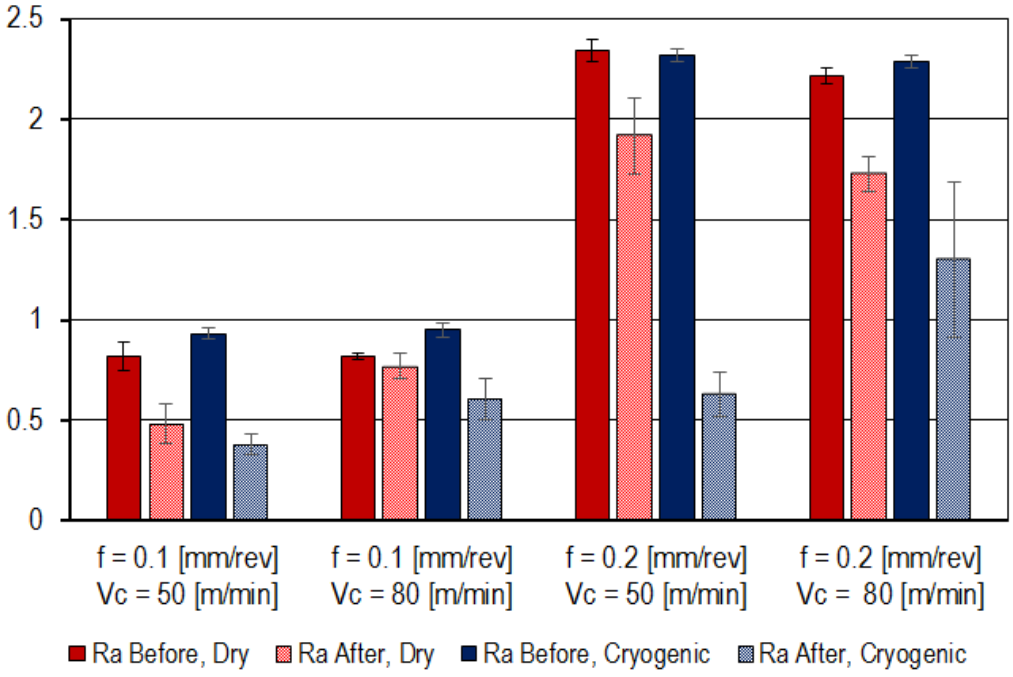

Figure 5.11 Surface roughness values of the EBM Ti6Al4V pins before and after wear testing.

Figure 5.11 shows the comparison between the average values of the surface roughness of the EBM Ti6Al4V pins before and after wear testing. Regardless the pins machining condition, the surface roughness decreases after wear testing as a consequence of the flattening of the sliding interfaces. When two surfaces are mating together, the real contact area is established

only at the surfaces asperities causing higher local contact pressure; afterwards, in case of smoother mating surfaces, these specific loads reduce. As a result, higher contact pressures can lead more readily to the formation of the Tribological Transformed Structure TTS layer and wear debris generation, decreasing the amount of energy needed to activate the wear phenomenon. The sliding surface of the EBM Ti6Al4V pins was also investigated through SEM analysis. As shown in Figure 5.12, wear scars were generally produced as a consequence of the wear testing, with a progressive smoothing of the feed marks peaks induced by turning. The comparison between the SEM images of the dry and cryogenic machined pins (see Figure 5.12) proves that the scars formed on the dry machined pins are wider and more fragmented. Furthermore, non - uniform grooves can be observed on the scars of the dry machined pins, especially in case of an adopted feed rate equal to 0.1 [mm/rev]. The observed differences in the scars topography and amplitude can be ascribed to the different initial state of the surface layer of the pins machined with different cutting parameters and lubricating strategy, namely the cryogenic pins present higher surface hardness that increases the surface damage resistance. Figures 5.13A and 5.13 B show detailed images of the worn surfaces of the EBM Ti6Al4V pins machined with the same cutting parameters under dry cutting and cryogenic cooling, respectively. Long continuous uniform grooves are observable in both cases, which indicate the occurrence of the abrasion wear mechanism. In correspondence of the peaks of the feed marks, flaking is also present. In addition, some fine wear debris, characterized by a bright colour that rise from charging, can be noticed on the worn surfaces, which are residuals

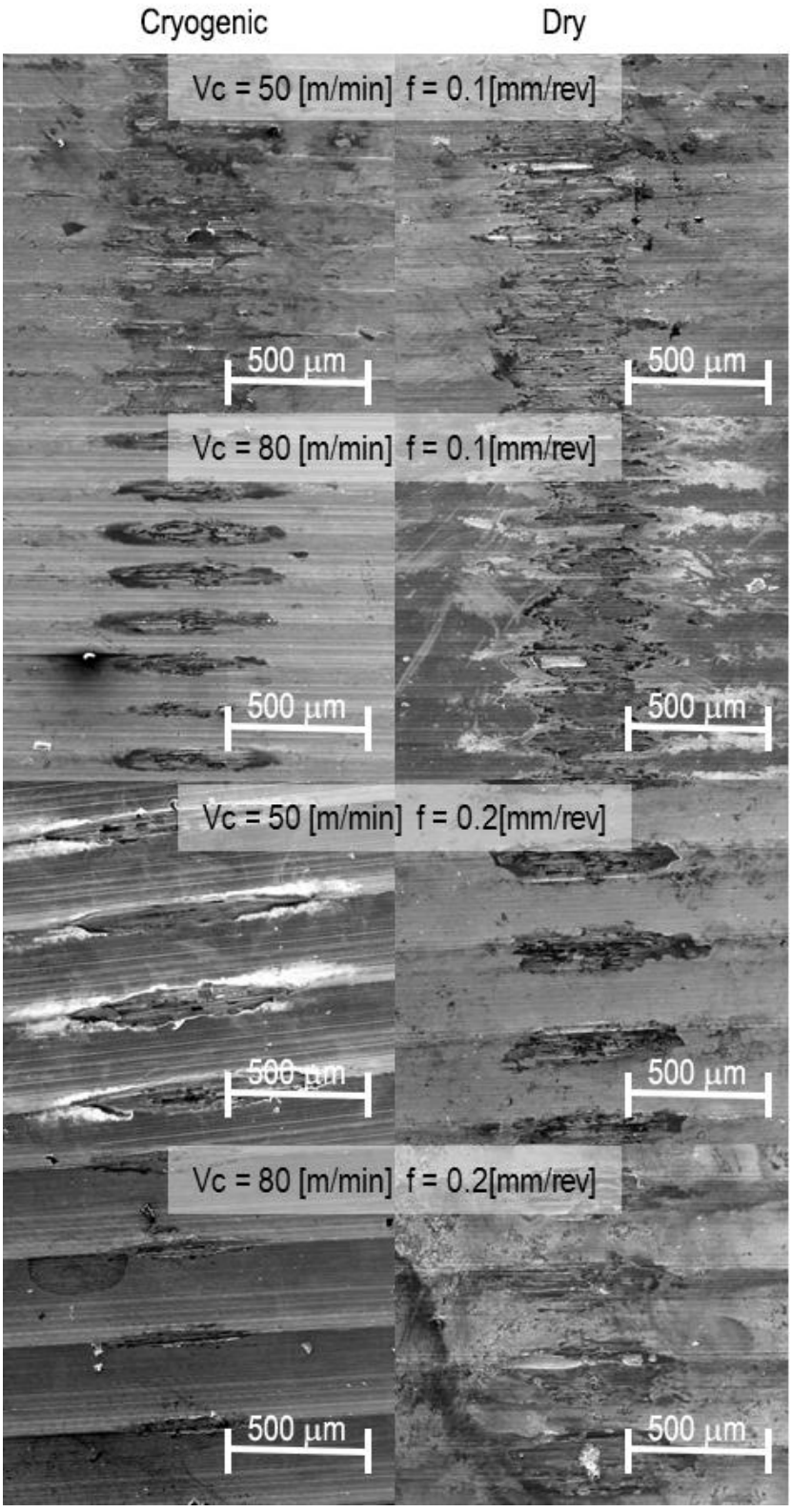

Figure 5.12 SEM images of wear scars in the EBM Ti6Al4V pins.

of titanium oxides formed on the sliding surface. The presence of particles made of oxide fragments, which are in general more fragile and harder than the substrate, can favour the formation of the three-body abrasion phenomenon that may significantly increase the wear rate, see Figure 5.13C. In case of the cryogenic machined pins, severe adhesion of the flat

plate material was found on the pins surface, as shown in Figure 5.13D, and cracks orthogonal to the sliding direction were also observed for all the tests. An EDS zone mapping analysis was conducted aiming at identifying the chemical elements adhered onto the pins worn interface. Figure 5.14a and b report the coloured maps corresponding to the main chemical elements of the pin and of the flat plate, when a cutting speed of 50 m/min and a feed rate of 0.2 mm/rev were used in dry and cryogenic turning, respectively.

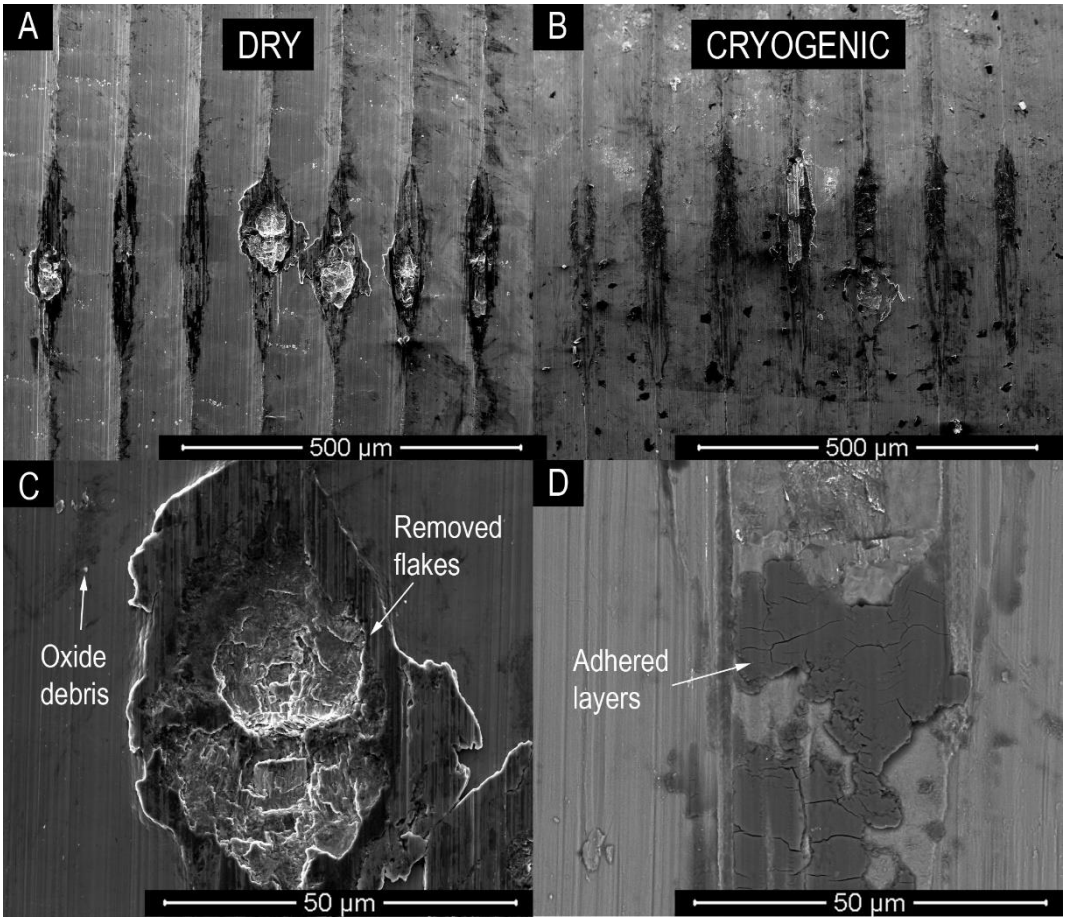

Figure 5.13 A) SEM images of the wear scars of the EBM Ti6Al4V pin dry machined with a cutting speed of 80 [m/min] and a feed rate of0.2 [mm/rev]. B) SEM images of the wear scars of the EBM Ti6Al4V pin cryogenically machined with a cutting speed of 80 [m/min] and a feed rate of 0.2 [mm/rev]. C) Detail of A: the crater indicates severe abrasion. D) Detail of image B: the adhered layer indicates adhesive wear.

For both the presented cases, the formation of patches due to the CoCrMo continuous transfer from the flat plate to the pin is noticeable. Nonetheless, higher amounts of the chemical elements characterizing the flat plate, namely Co, Cr and Mo, were found on the scars generated in the case of cryogenic machined pins, as can be noticed in the right top corner of the Figure 5.14. The presence of a higher amount of adhered material, as confirmed also by the SEM images, plays as protective layer against further abrasive wear that tends to remove particles from the pin due to its lower hardness in comparison with that of the flat plate. Therefore, as confirmed by the SEM and EDX analyses, the main wear mechanisms

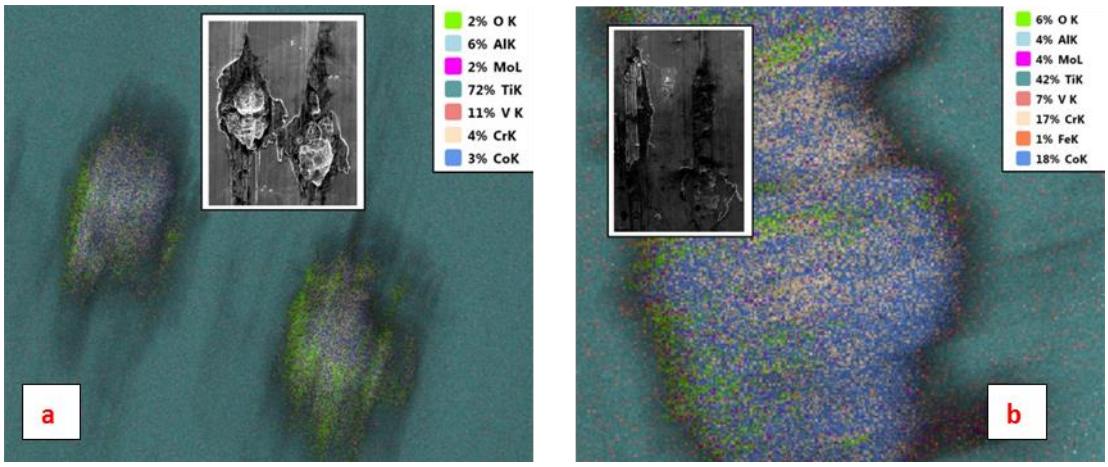

Figure 5.14 EDX map acquired from the marked area EBM Ti6Al4V pin machined at Vc = 50 [m/min] and f = 0.1 [mm/rev] under a) dry and b) cryogenic cooling condition.

that affected the EBM Ti6Al4V pins turned under dry and cryogenic cooling conditions were abrasion and adhesion. However, the dry machined pins were subjected more to abrasion of the surface layers undergoing a weight loss, whereas the cryogenic machined pins underwent a weight increase due to a stronger adhesion of the CoCrMo counterpart material. This different behaviour is reasonably provoked by the different surface mechanical properties of the EBM Ti6Al4V as a result of the different machining process conditions.

5.4. Chapter concluding remarks

On the basis of the improved surface integrity led by cryogenic turning on EBM Ti6Al4V alloy, sliding wear tests of cylindrical pins on flat plate of wrought CoCrMo were carried out in this work, to verify the feasibility of this cooling method to limit the wear mechanism arising in the service life of surgical implants manufactured with the same alloys. Sliding wear tests were performed by means of a tribometer, reproducing loads, displacements and environmental conditions as close as possible to those present in the human body; the effects of turning parameters and lubricating condition (dry and cryogenic) were investigated.
The most important findings from this study are summarised below:

- Cryogenic machining is an efficient strategy to limit the release of wear particles from the mating interfaces, fulfilling potential applications in the biomedical field, since the minimization of the metal particles release from surgical implants is one of the main goals in this field.

- Different wear mechanisms between the cylindrical pin and the flat plate appeared according to the machining cooling strategy that was found to alter more the surface material properties rather than the initial surface roughness state. Hence, the feed rate influenced the initial surface roughness of the pins, and rougher surfaces resulted for the highest feed rate set.

- Cryogenic cooling assured in general lower values of the friction coefficient (COF) than dry turning, but more fluctuating trends were noticed within the test duration, due to periodic localized fracture of a greater amount of oxidized layers formed in the sliding interface caused by different surface layer mechanical properties. For both the tested lubricating strategies, the higher the initial surface roughness of the pins, the lower COF resulted.

- For all the machining parameters set to turn the pins, cryogenic cooling generated a weight increment of worn pins; on the contrary a weight loss was measured on worn pins turned under dry conditions, because of the different principal wear mechanism taking place. This aspect can be translated to the positive reduction of wear particles losses within the sliding interface, fulfilling the necessity to limit this phenomenon in metal on metal surgical replacements.

- Abrasion and adhesion wear mechanism were found to be the EBM Ti6Al4V pins main wear mechanisms; the cryogenic machined pins were characterised by a remarkable adhesion of CoCrMo protective layers on the peaks of the feed marks that induced an increment of their weight, whereas the dry machined pins were subjected to a loss of weight due to a more severe abrasive action.

References

[1] Barranco, V., Escudero, M. L., García-Alonso, M. C., 2007, 3D, chemical and electrochemical characterization of blasted TI6Al4V surfaces: Its influence on the corrosion behaviour, Electrochimica Acta, 52/13:4374–4384, DOI:10.1016/j.electacta.2006.12.031.

[2] Long, M., Rack, H. ., 1998, Titanium alloys in total joint replacement—a materials science perspective, Biomaterials, 19/18:1621–1639, DOI:10.1016/S0142-9612(97)00146-4.

[3] Harrysson, O. L. a, Cansizoglu, O., Marcellin-Little, D. J., Cormier, D. R., West, H. a., 2008, Direct metal fabrication of titanium implants with tailored materials and mechanical properties using electron beam melting technology, Materials Science and Engineering C, 28/3:366–373, DOI:10.1016/j.msec.2007.04.022.

[4] Parthasarathy, J., Starly, B., Raman, S., Christensen, a, 2010, Mechanical evaluation of porous titanium (Ti6Al4V) structures with electron beam melting (EBM), J Mech Behav Biomed Mater, 3/3:249–259, DOI:10.1016/j.jmbbm.2009.10.006.

[5] Haslauer, C. M., Springer, J. C., Harrysson, O. L. A., Loboa, E. G., Monteiro-Riviere, N. A., et al., 2010, In vitro biocompatibility of titanium alloy discs made using direct metal fabrication., Medical engineering & physics, 32/6:645–52, DOI:10.1016/j.medengphy.2010.04.003.

[6] Molinari, A., Straffelini, G., Tesi, B., Bacci, T., 1997, Dry sliding wear mechanisms of the Ti6Al4V alloy, Wear, 208/1–/2:105–112, DOI:10.1016/S0043-1648(96)07454-6.

[7] Straffelini, G., Molinari, A., 1999, Dry sliding wear of Ti–6Al–4V alloy as influenced by the counterface and sliding conditions, Wear, 236/1–/2:328–338, DOI:10.1016/S0043-1648(99)00292-6.

[8] Budinski, K. G., 1991, Tribological properties of titanium alloys, Wear, 151/2:203–217, DOI:10.1016/0043-1648(91)90249-T.

[9] Niinomi, M., 2008, Mechanical biocompatibilities of titanium alloys for biomedical applications., Journal of the mechanical behavior of biomedical materials, 1/1:30–42, DOI:10.1016/j.jmbbm.2007.07.001.

[10] Tigani, D., Fosco, M., Ben Ayad, R., Fantasia, R., 2013, Wear of Orthopaedic Implants and Artificial Joints. Elsevier.

[11] Reclaru, L., Brooks, R. A., Zuberbühler, M., Eschler, P.-Y., Constantin, F., et al., 2014, Evaluation of taper joints with combined fatigue and crevice corrosion testing: comparison to human explanted modular prostheses., Materials science & engineering. C, Materials for biological applications, 34:69–77, DOI:10.1016/j.msec.2013.10.005.

[12] Mohd Tobi, A. L., Ding, J., Bandak, G., Leen, S. B., Shipway, P. H., 2009, A study on the interaction between fretting wear and cyclic plasticity for Ti–6Al–4V, Wear, 267/1–/4:270–282, DOI:10.1016/j.wear.2008.12.039.

[13] Zhang, T., Harrison, N. M., McDonnell, P. F., McHugh, P. E., Leen, S. B., 2013, A finite element methodology for wear-fatigue analysis for modular hip implants, Tribology International, 65:113–127, DOI:10.1016/j.triboint.2013.02.016.

[14] Alam, M. O., Haseeb, A. S. M. A., 2002, Response of Ti–6Al–4V and Ti–24Al–11Nb alloys to dry sliding wear against hardened steel, Tribology International, 35/6:357–362, DOI:10.1016/S0301-679X(02)00015-4.

[15] Kim, K., Geringer, J., Pellier, J., Macdonald, D. D., 2013, Fretting corrosion damage of total hip prosthesis: Friction coefficient and damage rate constant approach, Tribology International, 60:10–18, DOI:10.1016/j.triboint.2012.10.008.

[16] Baxmann, M., Jauch, S. Y., Schilling, C., Blömer, W., Grupp, T. M., et al., 2013, The influence of contact conditions and micromotions on the fretting behavior of modular titanium alloy taper connections., Medical engineering & physics, 35/5:676–83; discussion 676, DOI:10.1016/j.medengphy.2012.07.013.

[17] Viceconti, M., Cavallotti, G., Andrisano, A. O., Toni, A., 1996, Discussion on the design of a hip joint simulator, Medical Engineering & Physics, 18/3:234–240, DOI:10.1016/1350-4533(95)00026-7.

[18] J. D.Bobyn, A.R.Dujovne, J.J Kryger and D.L.Young. Surface analysis of the taper junctions of retrieved and in vitro tested modular hip prostheses. Biological, Material, and Mechanical Considerations of Joint Replacement. 1993, 287-301.

[19] Contact Mechanics. Johnson, Kenneth Langstreth. 1987, Cambridge University.

[20] Sporer SM, Callaghan JJ, Olejniczak JP, Goetz DD, Johnston RC. The effects of surface roughness and polymethylmethacrylate precoating on the radiographic and clinical results of the Iowa hip prosthesis. A study of patients less than fifty years old. J Bone Joint Surg Am 1999;81:481–92.

[21] Barril, S., Mischler, S., Landolt, D., 2004, Influence of fretting regimes on the tribocorrosion behaviour of Ti6Al4V in 0.9wt.% sodium chloride solution, Wear, 256/9–/10:963–972, DOI:10.1016/j.wear.2003.11.003.

[22] Pusavec, F., Hamdi, H., Kopac, J., Jawahir, I. S., 2011, Surface integrity in cryogenic machining of nickel based alloy—Inconel 718, Journal of Materials Processing Technology, 211/4:773–783, DOI:10.1016/j.jmatprotec.2010.12.013.

[23] Pu, Z., Outeiro, J. C., Batista, A. C., Dillon, O. W., Puleo, D. A., et al., 2012, Enhanced surface integrity of AZ31B Mg alloy by cryogenic machining towards improved functional performance of machined components, International Journal of Machine Tools and Manufacture, 56:17–27, DOI:10.1016/j.ijmachtools.2011.12.006.

[24] Hintikka, J., Lehtovaara, A., Mäntylä, A., 2016, Normal displacements in non-Coulomb friction conditions during fretting, Tribology International, 94:633–639, DOI:10.1016/j.triboint.2015.10.029.

[25] Qu, J., Blau, P. J., Watkins, T. R., Cavin, O. B., Kulkarni, N. S., 2005, Friction and wear of titanium alloys sliding against metal, polymer, and ceramic counterfaces, Wear, 258/9:1348–1356, DOI:10.1016/j.wear.2004.09.062.

[26] Kubiak, K. J., Liskiewicz, T. W., Mathia, T. G., 2011, Surface morphology in engineering applications: Influence of roughness on sliding and wear in dry fretting, Tribology International, 44/11:1427–1432, DOI:10.1016/j.triboint.2011.04.020.

[27] Fraker AC, Ruff AW, Sung P, Van Orden AC, Speck KM. SURFACE PREPARATION AND CORROSION BEHAVIOR OF TITANIUM ALLOYS FOR SURGICAL IMPLANTS. ASTM Spec. Tech. Publ., ASTM; 1983, p. 206–19.

[28] Jiang, J., Stack, M. M., 2006, Modelling sliding wear: From dry to wet environments, Wear, 261/9:954–965, DOI:10.1016/j.wear.2006.03.028.

[29] Archard JF. Single Contacts and Multiple Encounters. J Appl Phys 1961;32:1420. doi:10.1063/1.1728372.

Chapter 6

Finite Element Modelling of 3D turning of EBM Ti6Al4V alloy under dry and cryogenic cooling

6.1. Introduction

In the recent years more and more sophisticated numerical models based on the Finite Element method have been developed to simulate cutting operations, as evidenced by the literature review in the chapter 2. The latest works aims to predict some of the most relevant effects of the cutting process on the resulting surface integrity, such as residual stresses and microstructural alterations. Among most of the works present in literature, wrought Ti6Al4V is without doubt the most investigated alloy by means of numerical approaches, due to the industrial demand for enhancing its machinability. Aiming to set the basis for future works and speculations on EBM Ti6AL4V alloy, a numerical model of three dimensional turning is set in this work. A numerical model for semi-finishing turning was implemented in the commercial FE code STFC® DEFORMS 3D. The work was conducted in collaboration with Professor Domenico Umbrello and Dr. Stano Imbrogno of the University of Calabria. It is fundamental to underline that the numerical model was developed for dry and cryogenic cooling conditions only, because they revealed to be more interesting for a sustainable application in machining AM titanium alloys, nonetheless the approach could be extended to

wet lubricating conditions quite easily. Due to the lack of literature works dealing with numerical simulations of turning the EBM Ti6Al4V alloy, the work was structured in two main steps. In the first step the material constitutive model and the friction model was calibrated to predict the cutting forces and temperatures during the semi-finishing turning operation on EBM Ti6Al4V alloy under dry and cryogenic cooling. In fact, being the material microstructure of the analysed AM material quite different than the one present in the wrought alloy, a material flow stress equation usually adopted to simulate cutting processes (modified Johnson-Cook model) for wrought Ti6AL4V alloy was calibrated by inverse numerical simulations, comparing experimental and numerical results of cutting forces and temperatures. Later on, the numerical model was improved to predict the microstructural alterations arising during the cutting process, under different cutting conditions. Due to the absence of physically based models developed to predict microstructural alterations for basket wave morphologies within the typical thermomechanical process conditions, an empirical model based on a mathematical fitting of experimental measurements conducted on the material microstructure was implemented. The thickness and the strain of the α phase lamellae and the nano-hardness trends within the severe plastic deformed layer (SPD) were predicted by the FE code, under different cutting process conditions: three levels of cutting speed and two levels of feed rate. Moreover, the flow stress equation was coupled with the thickness of the altered α phase lamellae that have been proved in some literature works to modify the mechanical properties of the EBM Ti6AL4V alloy, in order to consider the effects of the altered material near the cutting zone. The developed numerical model, even if it is based not on physical equations, is the first work present in literature regarding the numerical modelling of the microstructural alterations induced by a machining process on a Widmanstätten microstructure that is renowned to be difficult to characterize. In fact, most of the published works on the topic concern on more standard equiaxed biphasic microstructures such as wrought Ti6AL4V alloys. Being AM technologies more and more diffused in the years to come, the proposed approach might set the basis for a pioneer work on numerical simulations of cutting processes conducted on AM titanium alloys, with a particular interest in predicting their effects on the surface integrity rather than the tool wear that can be considered of minor importance when dealing with these innovative manufacturing processes.

6.2.Experimental tests

Turning trials were conducted to acquire the main cutting variables used to calibrate the implemented FE code, namely the cutting forces and the cutting temperatures. The experimental set up used in this work is presented in Figure 3.7 to carry out cryogenic turning, the same tool holder and cutting insert as the one used to investigate the machinability were adopted during these turning trials, hence the chapter 3 of this thesis can be considered as a reference with regard to the turning trials set up and experimental testing preparation. The cutting forces were acquired by means of A Kistler®- type 9257 B three components piezoelectric dynamometer mounted on the lathe revolver for the acquisition of the cutting forces along the cutting speed and feed directions. An infrared camera FLIR® A6000-series was fixed on the tailstock allowing the acquisition of the thermal field from a frontal position

with regard to the workpiece. The material emissivity calibration was realised by heating up a test piece into a temperature-controlled electrical furnace. It is noteworthy that the developed numerical model does not take into account the tool wear that is renowned to influence the process [1], by the consequence a fresh cutting edge was used for each of the turning trial. Furthermore, one turning pass was performed for each turning trial, allowing a minimum turning length of 20 seconds, in order to reach a steady state thermo-mechanical condition, so the fastest turning conditions were machined firstly, proceeding towards the slowest turning condition with a step turning procedure leaving a 20 mm machined free surface between one pass and the next one to allow following material characterization. The followed approach can be easily understood by observing the machined workpiece showed in the Figure 6.1: the biggest turned diameter corresponds to the highest feed rate and cutting speed tested, whereas the smallest one corresponds to the lowest values of cutting speed and feed rate. One EBM Ti6Al4V workpiece was used for dry turning trials and one for cryogenic turning trials. Three levels of cutting speed and two level of feed rate were adopted, maintaining a fixed depth of cut equal to 0.2 mm in order to remain into a semi - finishing turning condition. The experimental plan set for the turning trials is summarised in Table 6.1.

Table 6.1 Experimental plan followed to perform the turning trials.

Test Trial N°	Cutting speed [m/min]	Feed rate [mm/rev]	Depth of cut [mm]	Lubrication
1	110	0.2	0.2	Dry
2	80	0.2	0.2	Dry
3	50	0.2	0.2	Dry
5	110	0.1	0.2	Cryogenic
6	80	0.1	0.2	Cryogenic
7	50	0.1	0.2	Cryogenic

A disc corresponding to each turning trial (see the Figure 6.1) was cut in order to extract a portion of surface for metallographic characterization and XRD analysis. These portions of machined surfaces, were hot mounted, polished and etched for metallographic analysis repeating the procedure described in the paragraph 3.7.

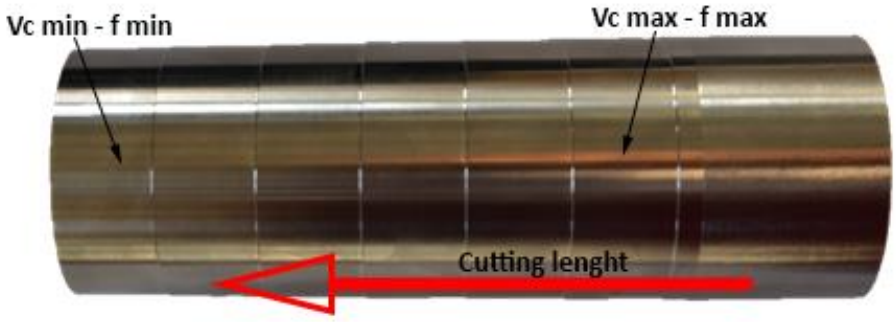

Figure 6.1 Machined workpiece after the six turning trials conducted under dry cooling condition.

The microstructure was analysed by means of a FEI QUANTA 450™ Scanning Electron Microscope (SEM). X-ray diffraction (XRD) analysis was conducted on the machined surfaces

and on a bulk portion of EBM Ti6Al4V samples, acquiring patterns between 30° and 90° 2θ to highlight possible phase transformations induced by the machining operation. Moreover, the effects of the machining process on the mechanical properties were investigated through nano-indentation tests by means of a FISCHERSCOPE® HM2000 nano-indenter provided with a Vickers tip. The parameters (dwell time and load) set for measuring the nano-hardness were chosen after some preliminary tests. The load and dwell time were respectively varied from 10 mN to 200 mN and from 5 s to 30 s. More reliable results (with no creep effects) were obtained setting 20 mN and 15 s. Three matrix spots of sixty indentations, each one from the top machined surface toward the bulk material, were performed for each sample.

6.3.Numerical model Set-Up

In this paragraph, all the main steps followed to set up the numerical model in the commercial FE code STFC Deform 3D®, are discussed. In particular the flow stress equation, the boundary conditions and the calibration variables are described. The work was conducted in two different stages, in the first the friction model and the flow stress equation were calibrated by comparing experimental and numerical values of the cutting forces and temperatures. In the second stage, the developed empirical numerical model for predicting the microstructural alterations is described. Part of the main findings obtained in the first stage, in particular the friction model, was used in the second numerical campaign without the necessity of a second calibration.

6.3.1. Flow stress equation and friction model to predict cutting forces and temperatures

The proposed numerical procedure developed in this work is aimed at testing the feasibility of a consolidated material constitutive model for the wrought Ti6Al4V when implemented in a 3D FE model of a turning operation conducted on the EBM Ti6Al4V under dry and cryogenic conditions. Most of the material constitutive models for simulating the thermo-mechanical behaviour of the wrought Ti6Al4V are based on the renowned J-C flow stress rule [2–4]. When the dynamic recovery (DRV) is the predominant restoration process during plastic straining, the dislocation rearrangement and annihilation (softening) always counterbalance the effect of work hardening and the resulting flow stress curve always increases up to a saturated value at very high strain values. This material behaviour is well described by the standard J-C equations, nonetheless it cannot adequately predict the adiabatic phenomenon responsible for chip segmentation at low speeds because the strain softening is not considered. Based on previous works about Ti6Al4V machining simulation [5] , the J-C material model modified by Calamaz in [6] was implemented into the numerical model. This modified material model proved its capability of predicting the chip morphology and cutting forces more accurately than the classic Johnson-Cook model coupled when with a damage criterion, such as the Cockroft and Latham, Brozzo ones [7]. This new flow stress model has shown to be successful in predicting serrated chip in machining Ti6Al4V alloy at cutting speeds and feed rates conditions where dynamic

recrystallization (DRX) may be active [8]. In fact, when the dynamic recrystallization (DRX) prevails, the work hardening drives the flow stress curve up to a peak value, usually lower than the saturation value occurring for the dynamic recovery. After this critical value, the stress decreases at increasing the strain up to a value when it reaches the steady state value. An accurate description of the singular parameters of the flow stress model and their physical meaning can be found in dedicated published works [6], nonetheless the equations implemented in the model can be written as:

$$\sigma = \left[A + B\varepsilon^{n} \right] \left[1 + C \ln \frac{\dot{\varepsilon}}{\varepsilon_0} \right] \left[1 - \left(\frac{T - Tr}{Tm - Tr} \right)^{m} \right] \left[D + (1 - D) \left[\tanh \left(\frac{1}{(\varepsilon + P)^{r}} \right) \right]^{s} \right] \tag{6.1}$$

$$D = 1 - \frac{T}{Tm} \tag{6.2}$$

$$P = \left(\frac{T}{Tm} \right)^{s} \tag{6.3}$$

where the constants A, B, C, n and m are listed in the Lee-Lin work [9], while r and S are the material parameters introduced by Özel et al. [10]. The material constants are summarized in the Table 6.2. The room temperature Tr was set equal to 20° for both dry and cryogenic cooling. The assumption of implementing a flow stress model that has demonstrated accurate numerical predictions in 2D and 3D turning of the wrought Ti6Al4V was considered by evaluating the tiny differences in terms of chemical composition and mechanical properties

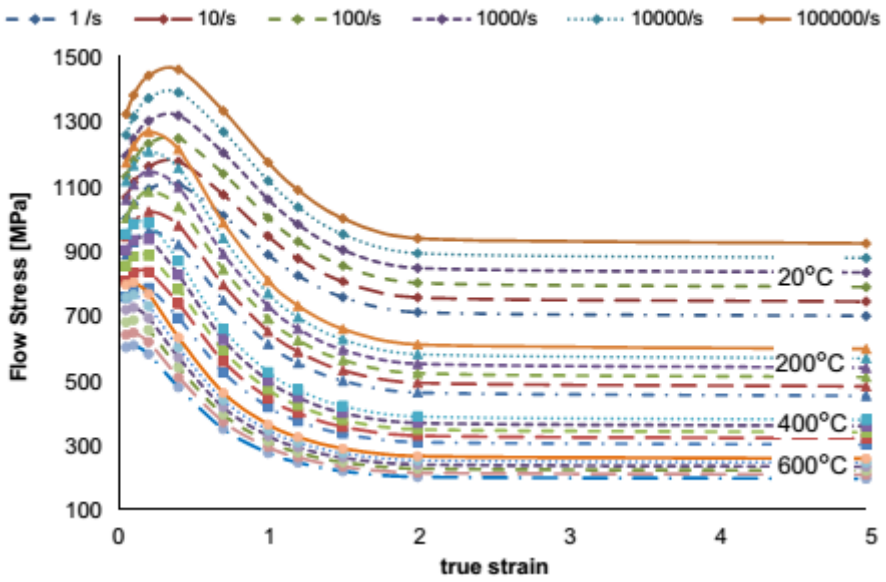

Figure 6.2 Flow stress curves using the Calamaz modified material model at different temperatures, strain rates and strains [6].

between the EBM and wrought alloys as evidenced in Table 3.2. Moreover, the chip morphology characterization (see paragraph 4.3) highlighted the occurrence of the chip segmentation under semi-finishing turning process conditions. The trend of the Johnson-

Cook equation modified by Calamaz, for different values of strain rate, strain and temperature is visible in the Figure 6.2.

Table 6.2 Set of coefficient for the material constitutive model adopted in the FE analysis.

A [MPa]	B [MPa]	n	C	m	r	s
724.7	683.1	0.47	0.035	1	1.2	2.7

Finally the sticking-sliding friction model (sticking governed by the shear model $\tau = m\tau_0$; sliding governed by the Coulomb model $\tau = \mu\sigma$) was also implemented; the friction coefficients m and μ were chosen equal to 0.8 and 0.9 respectively, according to Rotella et al. [7].
This flow stress equation (equation 6.1), was used for the first simulation campaign to calibrate the friction coefficients of the hybrid sticking and sliding model and to set the material coefficients of the Johnson and Cook equation. Later on, the Calamaz equation model was updated to include the microstructural alterations in the material behaviour, as it is described in the paragraph 6.3.4.

6.3.2. Boundary conditions

The commercial FEA code SFTC DEFORM 3D® was utilized to simulate the semi-finishing turning operation. The cutting tool was modelled as a rigid body (divided into 38000 tetrahedral elements), and an isotropic hardening behaviour was assumed for the material of the workpiece, which was divided into 85000 tetrahedral elements. The thermal and the mechanical properties of both the tool and the workpiece material were chosen among those present in the software library a part for the constitutive equation model for the Ti6Al4V alloy. Regarding the mesh density, the elements around the tool nose and along the machined surface were fifty times as dense as the other ones that presented an average length of 7 μm. The cutting tool and the workpiece were allowed exchanging heat with the environment, by setting a convection coefficient equal to 20 W/(m^{2}K), which is a standard value for free-air convection in DEFORM®, whereas an environmental window for heat exchange was defined between the machined surface and the flank side of the tool, near the tool radius to simulate cryogenic cooling effect, by setting a local temperature of -196°C and a convection coefficient, namely h_{cryo}. As demonstrated in a previous work [5], a good agreement between measured and predicted temperatures under cryogenic cooling is achieved for an h_{cryo} equal to 20 kW/(m^2/K). Aiming at reaching a thermal steady state condition at the tool chip interface in a short computational time, with the assumption of a thermally perfect contact, a global heat transfer, $h_{int,}$ was set equal to 100000 kW/(m^2/K), according to the literature results [3]. The thermal boundary conditions applied for simulating the cryogenic cooling can be seen in the Figure 6.3.

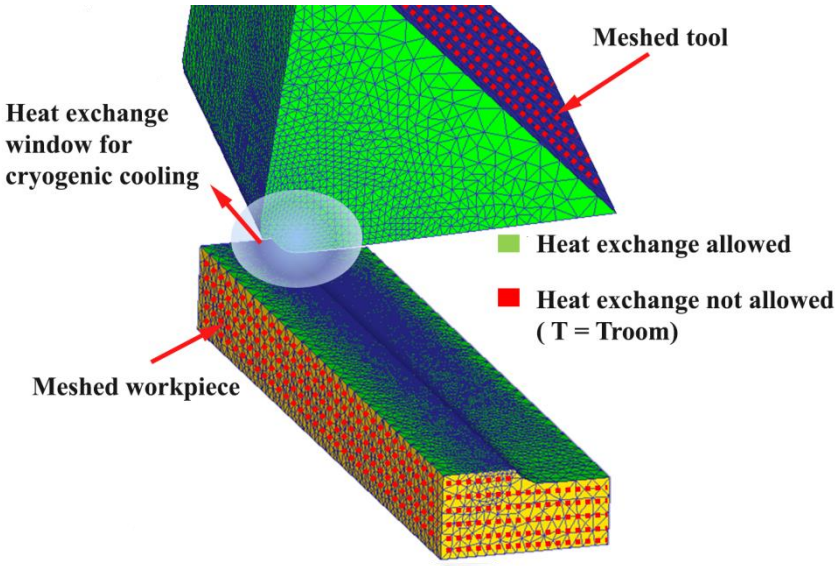

Figure 6.3 FE model and thermal assumption for simulating cryogenic cooling.

6.3.3. Microstructural modelling for predicting grain deformation

Microstructural alterations such as grain refinement, grain growth, dynamic recrystallization etc., are metallurgical phenomena that often take place within the surface layer of the machined component due to the severe thermomechanical conditions generated by the cutting operation. If such phenomena have to be taken into account in a numerical model, some adaptions at the default functions provided into commercial FE codes have to be realised. In practise a user defined function has to be implemented in a common programming language to require the numerical solver to compute other defined variables rather than the standard thermomechanical outputs such as strain, strain rate, temperature and stress in each node. In this work, the numerical model was modified after the first calibration stage, to consider the deformation of the α phase lamellae and to couple its effects with the flow stress equation model. Furthermore, some empirical equations have to be implemented in the FE code to require the numerical model to compute other microstructural variables, such as the nano-hardness trend within the severe plastic deformed layer (SPD). In this paragraph, the main passages and the experimental approach that led to the implementation of such empirical equations are discussed. Based on main experimental findings regarding the surface integrity and the microstructural alterations induced by the turning process, the material microstructure beneath the machined surface is altered due to the thermo-mechanical loads exerted on the machined surface. A consistent bending, stretching and grain refinement was noticed (see Figures 4.24). The mechanical properties of the EBM Ti6Al4V alloy are influenced by the thickness of the alpha phase lamellae [11,12]. As a result, the lamellae deformation and thickness variation across the SPD layer were experimentally measured through an image analysis tool of the SEM control software. The plastic strain of the lamellae was calculated according to the following equation:

$$\varepsilon = \tan(\theta) = l / \delta \tag{6.4}$$

where δ and l are the components of the lamellae deformation along and across the machined surface as illustrated in Figure 6.4b. These dimensions were measured in three different positions on the analysed section, repeating each measurement five times to achieve a statistical repeatability. Being the lamellae progressively bended towards the machined surface, becoming almost tangent to the cutting speed vector, their deformation was calculated in fifteen positions along the radial direction, setting a fixed pitch equal to 1 μm. The thickness of the alpha phase lamellae was measured at the same positions considered for measuring their deformation, repeating the same approach. It is noteworthy that only the machined induced lamellae deformation of the alpha phase was considered because of the relative volume fraction of the beta phase found by means of the XRD analysis. In fact, the average beta phase fraction of the as-built material resulted equal to 5 %, whereas the machined samples showed values ranging from 4.7 to 5.3 %, proving that the machining process and cooling strategy did not provoke any phase variations. Furthermore, since the beta transus temperature (980°) was never reached during the machining tests, the microstructure of the EBM Ti6Al4V alloy maintained its original morphology. Therefore, considering all the above mentioned evidences and that alpha phase is approximately three times harder than beta phase, only the relative volume fraction of alpha phase and its microstructure can have a significant effect on the flow stress of the machined EBM Ti6Al4V alloy.

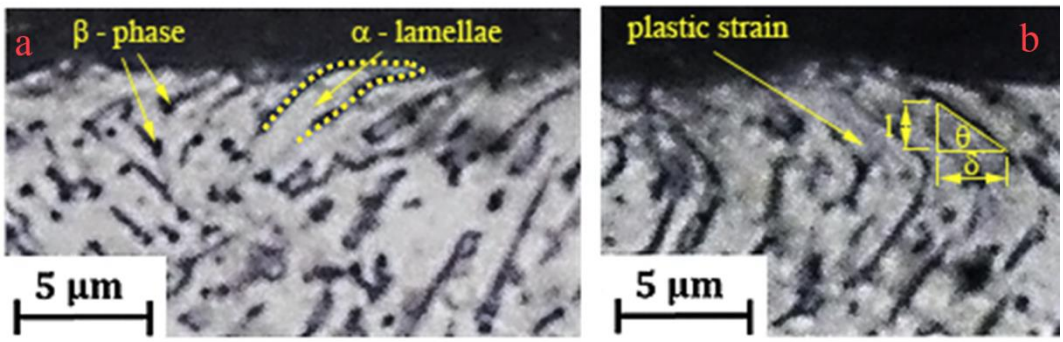

Figure 6.4 (a) Microstructure after machining; (b) experimental procedure to evaluate the plastic strain near the machined surface.

6.3.4. Numerical modelling of microstructural alterations

The JC equation was further modified to take into account the influence of the alpha phase lamellae thickness, according to Blackmore et al. [11] that showed the variation of the lamellae thickness mostly influencing the material mechanical behaviour. In particular, he found that the yield strength of EBM Ti6Al4V decreased for higher values of the alpha lath size characterizing the microstructure [8]. Thus, the final modified J-C material constitutive equation was written as:

$$\sigma = \left[\left(a + \frac{k}{\sqrt{t}}\right) + B \cdot \varepsilon^{n}\right] \cdot \left[1 + C \cdot ln\left(\frac{\dot{\varepsilon}}{\dot{\varepsilon}_0}\right)\right] \cdot \left[1 - \left(\frac{T - T_r}{T_m - T_r}\right)^{m}\right] \times \left[D + (1 - D)\left[tanh\left(\frac{1}{(\varepsilon + P)^{r}}\right)\right]^{s}\right] \quad (6.5)$$

Where the material constants are the same as those previously mentioned for the equation 6.1. The variable t represents the alpha phase lamellae thickness, while a (708.73 MPa) and k (265.57 MPa*$\mu m^{0.5}$) are two constants calculated from experimental evidences [11]. Due to the lack of physical models available in literature that describe the lamellae thickness variation, especially when DRX phenomena are absent, an empirical model was proposed for modelling the microstructural alterations. The model was developed fitting by Matlab® regression script the experimental lamellae thickness (t) near to the surface with the temperature (T) and strain-rate ($\dot{\varepsilon}$) data provided by FE simulations for each testing condition. The following second order polynomial regression model was chosen to represent the lamellae thickness:

$$t = 0.8735 + 0.0319 \cdot \dot{\varepsilon} - 0.03436 \cdot T + 0.1561 \cdot \dot{\varepsilon}^2 + +0.05892 \cdot \dot{\varepsilon} \cdot T + 0.1112 \cdot T^2 \quad (6.6)$$

This equation, couples the effects of microstructural alterations, namely the thickness of the α phase lamellae t, with the main variables that describe the plastic behaviour of the material subjected to the cutting process, namely the strain rate and the temperature. In this manner, the numerical model is can compute the value of t for each node of the mesh at any step during the deformation according to the level of T and $\dot{\varepsilon}$. This value, continuously update the flow stress expressed by the equation 6.5.
According to Murr et al. [13], a Hall Petch-based equation was used to predict the hardness variation along the machined-altered layer. In particular, the following equation was implemented into the FE code by a User Subroutine:

$$HM = C_0 + \frac{C_1}{\sqrt{t}} \quad (6.7)$$

where HM is the Martens hardness (GPa), t the alpha phase lamellae thickness, while C_0 and C_1 are two numerical constants evaluated by fitting the experimental data of the nano-indentations tests for one selected case (V_c = 80 m/min, f = 0.1 mm/rev, dry condition), used as calibration test.

6.3.5. FE calibration

The calibration of the FE model consisted in determining the friction coefficients that characterize the implemented sticking - sliding friction model, namely m for the sticking friction and μ for the sliding friction. Furthermore, even the coefficient A of the J - C equation (see Eq. 6.1), that governs the YS exhibited by the Ti6Al4V alloy, was calibrated to better fit the higher mechanical properties of the EBM Ti6Al4V in comparison with the wrought one (see Table 3.2). Based on recent works devoted at measuring the friction coefficients when machining under cryogenic cooling [14], the adoption of LN_2 provokes a variation on the friction mechanisms, hence on the friction coefficients. According to that, two parallel calibration procedures were performed to evaluate the friction coefficients, while the coefficient A was computed under dry condition. The calibration procedure was carried out for two cutting conditions tested, corresponding to the following cutting parameters: cutting speed of 50 m/min and feed rate of 0.1 mm/rev for the first condition, and cutting speed of 110 m/min and feed rate of 0.2 mm/rev for the second one. An iterative inverse

analysis was implemented, based on error minimization by comparing experimental and predicted results of the main cutting force Fc, fixing a threshold value of 10 % as an acceptable error. At the end of the calibration procedure, the friction coefficients resulted of being equal to 0.2 and 0.3 for μ and m respectively, whereas on the other side higher values resulted under cryogenic cooling being equal to 0.3 and 0.4. The coefficient A of the J - C equation was raised to 940 MPa instead of the initial value assumed equal to 782.7 MPa.
This first calibration phase, as stated several times, allowed the implementation of the second J-C equation (Eq. 6.5) without performing a novel calibration of the friction coefficients. Furthermore, being the novel FE code developed for predicting the microstructural alterations by means of empirical equations (Eqs. 6.4 -6.6) that fitted the experimental measurements, the model does not require coefficients to calibrate. As an example, Rotella et al. [7] calibrated 4 constants in her innovative FE code developed for simulating the recrystallized grain size in dry and cryogenic turning of wrought Ti6AL4V alloy, a couple of them governed the Hall Petch equations and the second one the Zener - Hollomon equation model. Nevertheless, lots of simulations were performed to set the user sub routines written in Fortran®, adding constraints to the scalar fields of the predicted nano - hardness and of grain deformation, to avoid nonphysical phenomena. Aiming to achieve an accurate prediction of the process variables within the machined surface layers, a dynamic local remeshing window was set following the tool motion. This remeshing criterion permits to obtain a continuously refining of the mesh only in the portion of the machined workpiece behind the tool, maintaining unchanged the mesh size of the machined surface and consequently the predicted results. Before the presentation of the main results, it is fundamental to point out that the chip

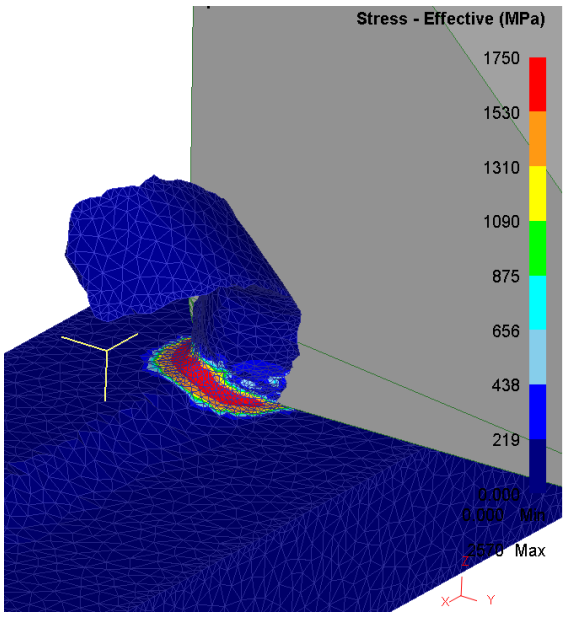

Figure 6.5 Simulated chip formation mechanism of semi-finishing turning of EBM Ti6AL4V alloy.

morphology was not taken into (see Figure 6.5) account during the calibration phase, due to the intrinsic limit to characterize the three dimensional helical chip morphology that is usually observed in standard turning, with a solid approach. On the other hand, in studying

orthogonal cutting, the chip morphology is a fundamental aspect to control, but due to its spiral shape it is easier to characterize through a an engineering approach.

6.4.FE results

6.4.1. FE simulations of cutting forces and temperatures

In this paragraph, the main results of the predicted cutting forces and temperatures under dry and cryogenic turning of EBM Ti6Al4V alloy are compared with the experimental values. The comparison was achieved by computing the average values of the cutting forces and temperatures during the steady state trend, so the initial ramp up was not considered for the calculation. The cutting temperature was calculated by averaging the values calculated by the FE code on 40 points equally distributed on a straight line positioned on the tool rake face as can be observed in the Figure 6.6. These first numerical results, were obtained by adopting the Calamaz modified J-C equation (Eq. 6.1), setting the values of the constant A and of the friction coefficient μ and m found in the calibration phase, as described in the paragraph 6.3.5. Figure 6.8 shows the comparison between the measured and predicted cutting forces for dry and cryogenic machining. The predicted main cutting force fits correctly the experimental data for all the tested cutting condition under both dry and cryogenic cooling conditions.

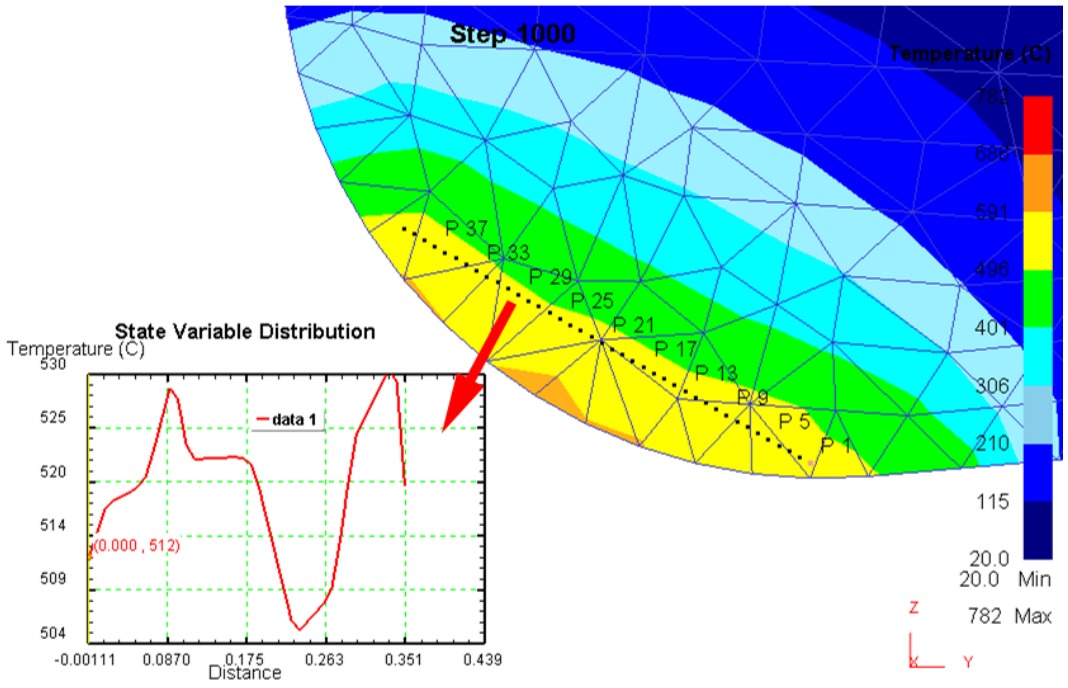

Figure 6.6 Straight distribution of 40 points on the tool rake face to acquire the cutting temperature.

The highest errors were equal to -8.7 and -6.8 % for dry and cryogenic cooling conditions, respectively, when, in both the cases, the more severe cutting parameters were adopted, namely cutting speed equal to 110 m/min and feed rate equal to 0.2 mm/rev. The Figure 6.8 shows that even the radial and feed forces trend is correctly predicted although the differences between predicted and experimental data are higher than for the main cutting force. These discrepancies might be related to the used friction models that are well validated for

orthogonal machining but not yet for 3D machining. More in detail, other important parameters might be taken into account and related to the friction coefficient as the tool geometry (tool nose radius, angles, etc.) and the grain size. It is worth to point out that for both the components of the cutting force, a progressive decrement is observed at increasing the cutting speed for the tested lubricating conditions. This aspect might be related to the thermal softening of the Ti6Al4V alloy that is provoked by the major heat generated into the cutting zone when increasing the cutting speed.

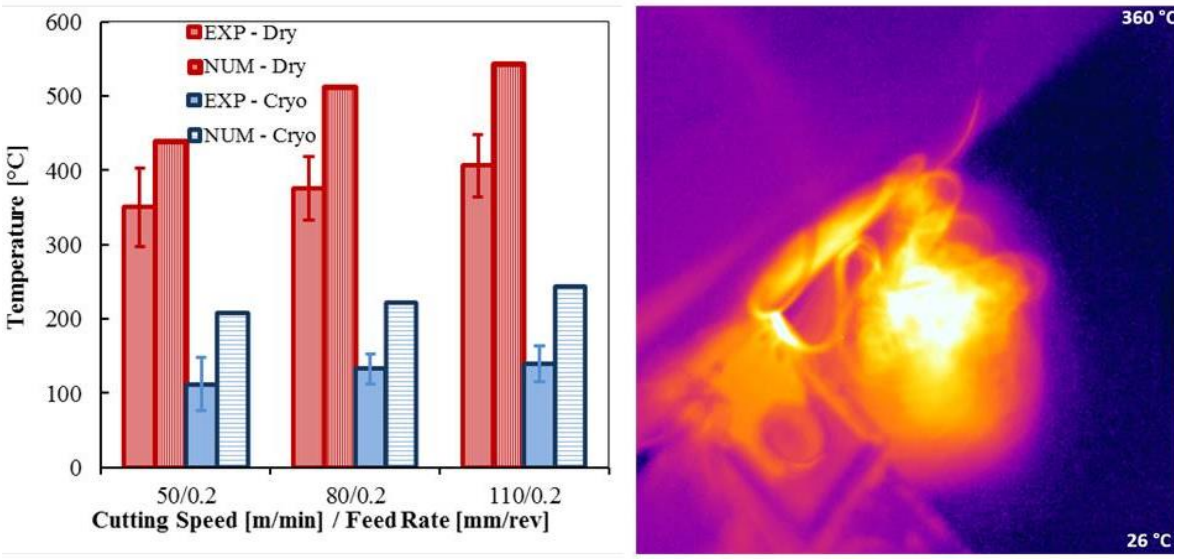

Figure 6.7 Comparison between predicted and experimental values of cutting temperature (on the left) and an acquired temperature filed during dry turning of EBM Ti6AL4V alloy.

Another important variable considered in validating the numerical model was the cutting temperature. The comparison between the measured and predicted cutting temperatures is showed in Figure 6.7 on the left, in which the cutting temperature measured by means of the IR Camera is compared with the average value computed on the tool rake face. The FE model simulates correctly the trend of the cutting temperatures at varying the cutting speed for both lubricating conditions tested even dough some discrepancies are denoted between numerical and experimental values. It is worth to note that the discrepancies might be partially induced by the high sensitivity of the temperature measurements with the selected position on the FE model and on the IR image. Nonetheless, the proposed model predicts correctly the increasing trend of the temperature with the cutting speed for both dry and cryogenic conditions.

Figure 6.9 on the right shows a coloured FE map representing the spatial distribution of the strain in the portion of material being turned along the radial direction. The model predicts correctly the strain gradient along the radial direction in the portion of the material being cut under the tool nose, indicated as the valid zone in Figure 6.9. It is of fundamental importance to underline that only the portion of the FE model that presents the correct mesh setting can be considered for evaluating the numerical results, being the portion not totally affected by the remeshing steps. One of the main parameters to consider when evaluating the effects of machining operations on the material is the thickness of the severe plastic deformation layer, namely SPD as indicated in Figure 6.10. The average thickness of the SPD layer was evaluated in three different positions into the as defined valid zone.

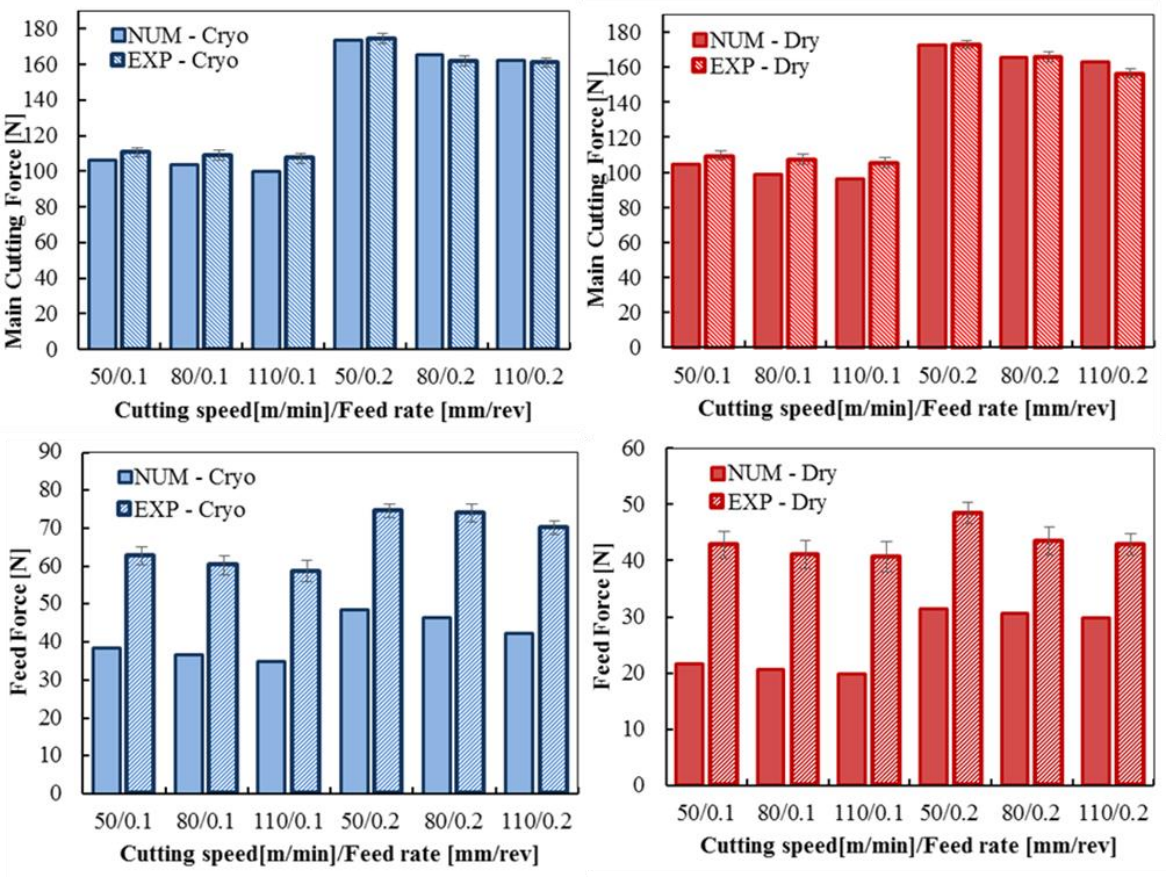

Figure 6.8 Comparison between measured and predicted main cutting forces during dry and cryogenic machining.

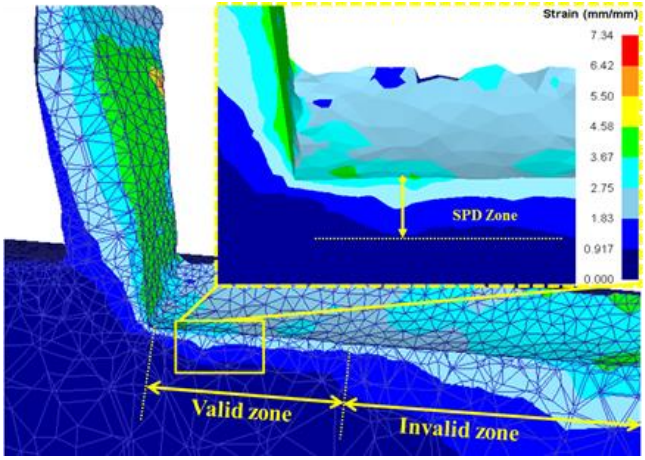

Figure 6.9 Map of strain distribution during FEA simulation along the radial direction under the machined surface.

The proposed FE model predicts correctly the trends of the SPD thickness, where an increment is observed when increasing the cutting speed, moreover higher values of SPD are found when adopting the cryogenic cooling.

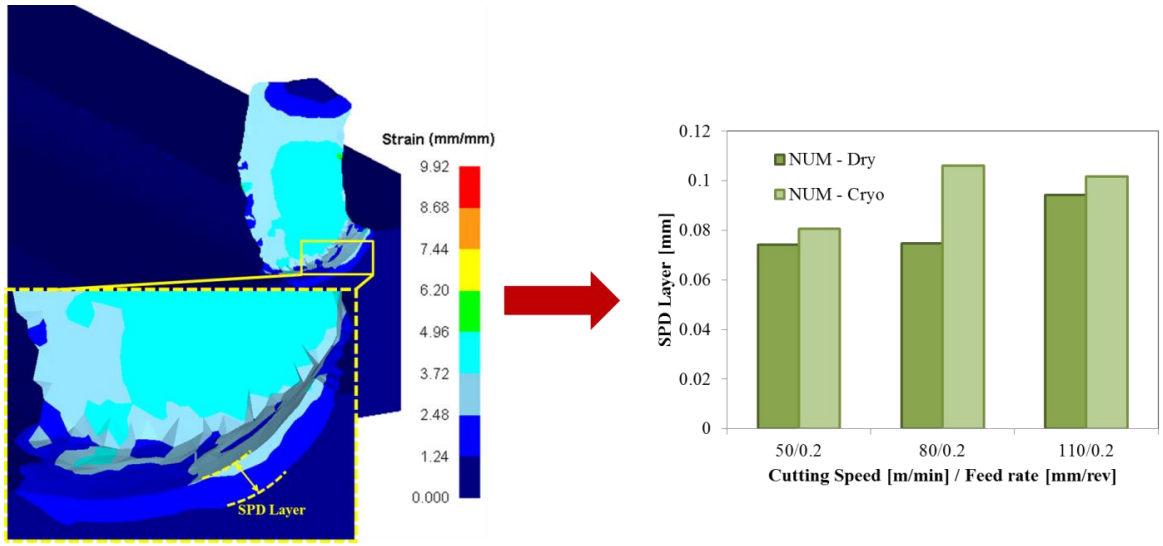

Figure 6.10 Position of the severe plastic deformation layer (SPD) in the FE model on the right. Average SPD layer thickness on the left.

6.4.2. FE simulations of microstructural alterations

Figure 6.11 shows the FE numerical prediction at the machined surface and sub-surface (a cutting plane was set to show the results into the affected layer) for the alpha lamellae strain, their thickness and the nano - hardness variation. The proposed FE model aims to predict those variables relevant to evaluate both the metallurgical and quality performance when the EBM Ti6Al4V alloy is machined under dry and cryogenic conditions. Figure 6.12a highlights increasing values of the alpha lamellae strain when higher cutting speeds are adopted due to the higher shear friction forces at the machined surface, regardless of the cooling condition. However, higher strain values were observed in case of cryogenically machined samples. The use of the LN_2 inhibits in fact the localised strain softening of the surface layers due to the microstructure rearrangement. During dry machining, cutting temperatures higher than 400°C were measured as can be noticed in the Figure 6.7 on the right, hence the material surface layers underwent a localised rearrangement with bending and breakage of the existing lamellae in sub-lamellae. In contrast, as the cutting temperatures in cryogenic machining had maximum values around 200°C (Figure 6.7 on the left), this phenomenon was inhibited leading to higher bending of the surface lamellae favoured also by the higher flow stress of the material at lower temperatures. Figure 6.11 shows the alpha lamellae thickness results. As can be observed, the lamellae thickness is slightly affected by the cutting speed since its variation from 50 m/min to 110 m/min during a semi-finishing operation generates a slight increment of the temperature, with a consequent nearly negligible grain growth. In contrast, when the LN2 is supplied during the machining operation, lower lamellae thicknesses are observed. In fact, as the cooling rates increases, the length and thickness of the lamellae decrease. Thus, the ability of the cryogenic cooling to stop the regrowth phase plays the major role in the grain refinement process. All these aspects also lead to higher yield strength and hardness.

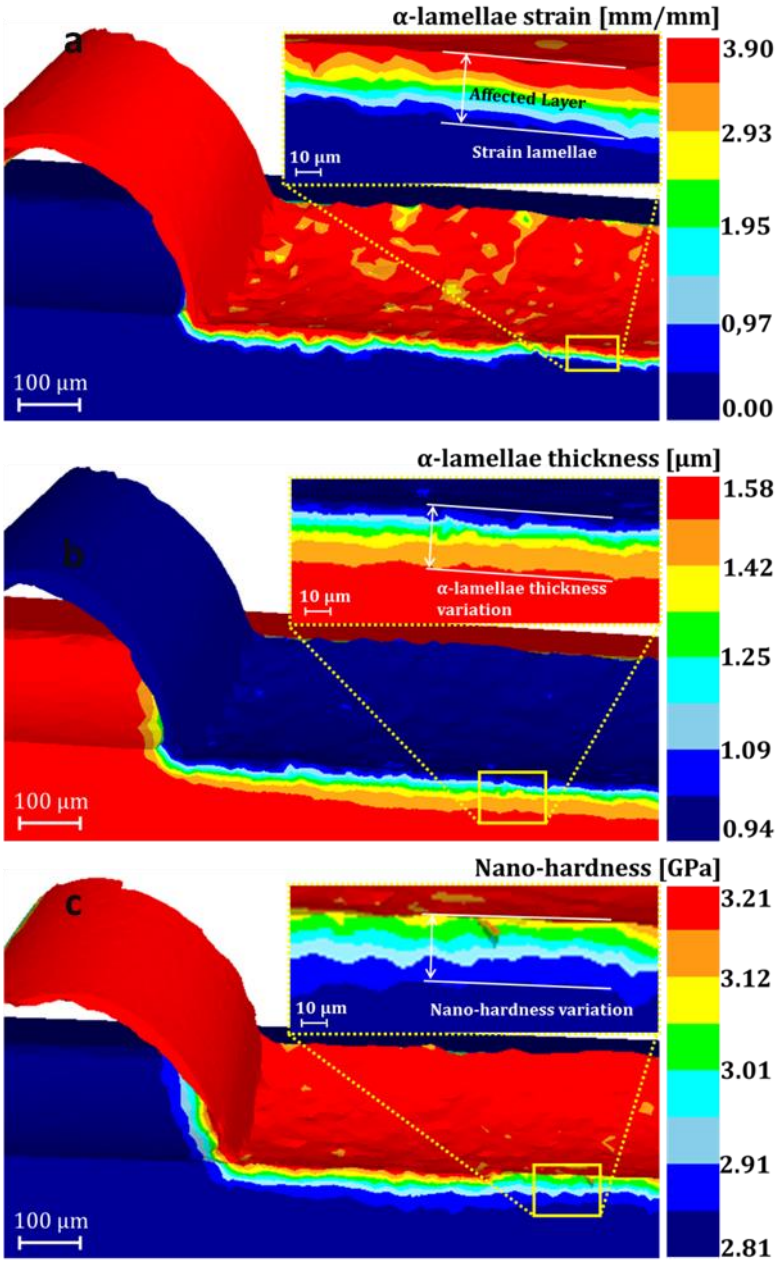

Figure 6.11Predicted (a) alpha lamellae plastic strain, (b) alpha lamellae thickness, and (c) nano-hardness variation on the workpiece dry machined at 80 m/min and 0.1 mm/rev.

The nano-hardness near the machined surface is particularly influenced by both thickness and strain hardening effect. Higher alpha lamellae strain due to the increasing of cutting speed in dry machining permits to increase the machined surface and sub-surface nano-hardness as illustrated in Figure 6.12a. Indeed, higher nano-hardness values are always detected on cryogenically machined samples, as shown Figure 6.12b, due to the lower lamellae thickness.

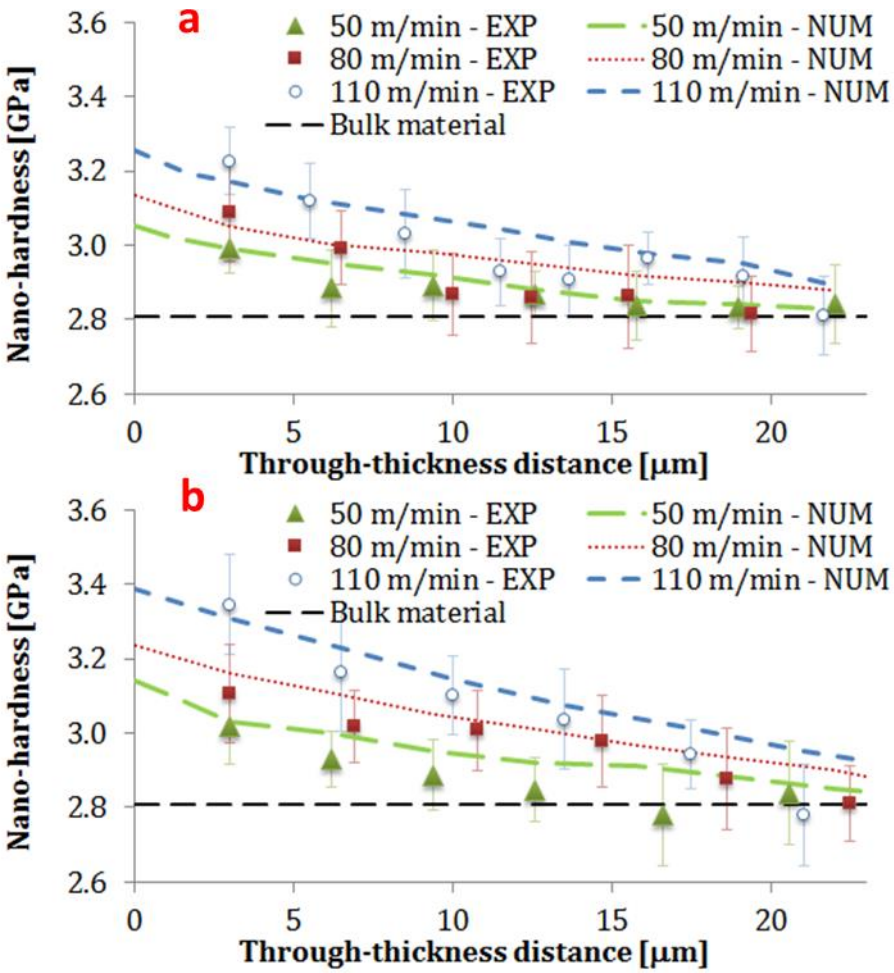

Figure 6.12 Comparison between measured and predicted (a) alpha lamellae plastic strain and (b) alpha lamellae thickness.

The effectiveness of the proposed FE strategy is confirmed by the good agreement in the prediction of the alpha lamellae strain and thickness (Figure 6.11), as well as the nano-hardness on the machined surface and sub-surface (Figure 6.12) for all the investigated testing conditions. The predicted results also highlight that the thickness of the affected deformed layer in the sub-surface varies from 15 to 25 µm. The numerical results are in good agreement with those experimentally deducted by analysing the nano-hardness variations (the machined affected layer experimentally varies from 10 to 18 µm). As overall, the obtained results highlight the beneficial and positive effects of the cryogenic application when machining AM metal parts made in Ti6Al4V alloy. Furthermore, the newly developed FE model permits to predict and numerically analyse the microstructural changes and surface integrity details varying the cooling conditions (dry and cryogenic) and under the cutting speeds conventionally adopted in semi-finishing cutting operations.

6.5. Chapter concluding remarks

A numerical model based on the Finite Element Method (FEM) was developed in this work, to simulate the cylindrical turning of EBM Ti6Al4V alloy under different process conditions: cutting parameters and lubricating strategy (dry and cryogenic). The work was subdivided in two main phases: in the first a numerical model implemented in the commercial FE code STFC DEFORM 3D® was developed to predict the principal cutting variables, namely the cutting forces and the cutting temperature, while in the following phase the model was improved to predict the microstructural alterations arising in the severe plastic deformed layer (SPF) due to the cutting operation. For both the developing phases, the numerical model was calibrated and validated comparing experimental and numerical results. The main purpose of this work was to propose for the first time a numerical model of turning Ti6Al4V alloy produced by additive manufacturing (EBM), giving emphasis to the induced surface integrity rather than the tool wear.

Due to the lack of literature works and experimental data available to model mathematically the material behaviour of EBM Ti6Al4V alloy subjected to cutting operations, a modified Johnson-Cook constitutive equation validated for the wrought Ti6Al4V was implemented and coupled with an hybrid sticking – sliding friction model for simulating the friction forces on the cutting tool. The model was calibrated and validated by comparing the predicted main cutting force with the experimental one under a couple of cutting conditions. The numerical results showed a very good prediction of the main cutting force for all the tested cutting conditions under dry and cryogenic machining. The predicted feed force showed a trend that respected the experimental findings but wider discrepancies between the values were present. The FE model simulated correctly the trend of the cutting temperatures when varying the cutting speed for both lubricating conditions tested even dough some discrepancies were denoted between the numerical and the experimental values. These discrepancies were ascribed to the friction model that was well validated for orthogonal cutting operations but it did not take into account some important variables such as the tool nose radius. However the first developed numerical model was capable to predict correctly the cryogenic effect on the turning process. The FE model was improved by implementing an empirical equation and an Hall-Petch based equation via user-subroutine to predict the alpha lamellae thickness and the hardness variation within the sever plastic deformed layer. The original J-C constitutive model equation was lately modified to take into account the effect of the lamellae thickness variation on the material behaviour. Good agreements between experimental and numerical data were found in terms of alpha lamellae strain, thickness and nano-hardness trend. In brief, the developed numerical approach proved the capacity to predict the main cutting variables and the induced surface integrity, evidencing the strong effect of the cooling strategy.

References

[1] Arrazola, P. J., Özel, T., Umbrello, D., Davies, M., Jawahir, I. S., 2013, Recent advances in modelling of metal machining processes, CIRP Annals - Manufacturing Technology, 62/2:695–718, DOI:10.1016/j.cirp.2013.05.006.

[2] Johnson G.-R., Cook W.-H., A constitutive model for metals subjected to large strains, high strain rates and high temperatures, in: Proceedings of the Seventh International Symposium on Ballistics, Hague, Netherlands, vol. 54,1983, pp. 1–7.

[3] Umbrello, D., M'Saoubi, R., Outeiro, J. C., 2007, The influence of Johnson–Cook material constants on finite element simulation of machining of AISI 316L steel, International Journal of Machine Tools and Manufacture, 47/3–/4:462–470, DOI:10.1016/j.ijmachtools.2006.06.006.

[4] Shrot, A., Bäker, M., 2012, Determination of Johnson–Cook parameters from machining simulations, Computational Materials Science, 52/1:298–304, DOI:10.1016/j.commatsci.2011.07.035.

[5] Pu, Z., Umbrello, D., Dillon, O. W., Jawahir, I. S., 2014, Finite Element Simulation of Residual Stresses in Cryogenic Machining of AZ31B Mg Alloy, Procedia CIRP, 13:282–287, DOI:10.1016/j.procir.2014.04.048.

[6] Sima, M., Özel, T., 2010, Modified material constitutive models for serrated chip formation simulations and experimental validation in machining of titanium alloy Ti–6Al–4V, International Journal of Machine Tools and Manufacture, 50/11:943–960, DOI:10.1016/j.ijmachtools.2010.08.004.

[7] Rotella, G., Umbrello, D., 2014, CIRP Annals - Manufacturing Technology Finite element modeling of microstructural changes in dry and cryogenic cutting of Ti6Al4V alloy, CIRP Annals - Manufacturing Technology, 63/1:69–72, DOI:10.1016/j.cirp.2014.03.074.

[8] Calamaz, M., Coupard, D., Girot, F., 2008, A new material model for 2D numerical simulation of serrated chip formation when machining titanium alloy Ti–6Al–4V, International Journal of Machine Tools and Manufacture, 48/3–/4:275–288, DOI:10.1016/j.ijmachtools.2007.10.014.

[9] Lee, W., Lin, C., 1998, Plastic deformation and fracture behaviour of Ti – 6Al – 4V alloy loaded with high strain rate under various temperatures, 241:48–59.

[10] Özel, T., Sima, M., Srivastava, a. K., Kaftanoglu, B., 2010, Investigations on the effects of multi-layered coated inserts in machining Ti-6Al-4V alloy with experiments and finite element simulations, CIRP Annals - Manufacturing Technology, 59/1:77–82, DOI:10.1016/j.cirp.2010.03.055.

[11] Blackmore, M. L., Zhang, W., Todd, I., 2010, The Origin of Microstructural Diversity , Texture , and Mechanical Properties in Electron Beam Melted Ti-6Al-4V, DOI:10.1007/s11661-010-0397-x.

[12] Sieniawski, J., Ziaja, W., Kubiak, K., Motyka, M., Microstructure and Mechanical Properties of High Strength Two-Phase Titanium Alloys.

[13] Murr, L. E., Esquivel, E. V, Quinones, S. A., Gaytan, S. M., Lopez, M. I., et al., 2008, Microstructures and mechanical properties of electron beam-rapid manufactured Ti – 6Al – 4V biomedical prototypes compared to wrought Ti – 6Al – 4V, Materials Characterization, 60/2:96–105, DOI:10.1016/j.matchar.2008.07.006.

[14] Rotella, G., Umbrello, D., 2014, Numerical simulation of surface modification in dry and cryogenic machining of AA7075 alloy, Procedia CIRP, 13:327–332, DOI:10.1016/j.procir.2014.04.055.

Chapter 7

Case study: Feasibility of cryogenic cooling in machining acetabular cups made of EBM Ti6Al4V alloy

7.1. Introduction

Cryogenic cooling, whether it is realised in turning or milling operations is showing a great potentiality to improve the productivity of machining operations, where difficult to cut materials are employed for producing aeronautic parts. However, its application is still circumscribed at an academic level and it is far to be widely industrialized, since many issues regarding fast and reliable cryogenic implants, its safety usage on the shop floor and more technical problems regarding its effect on the machine tools structure and the accuracy of the final workpiece still have to be assessed[1]. Nevertheless, there are some machine tools manufacturers that are now providing complex CNC multi axis machining centres with the cryogenic cooling line[2]. Among many of the unclear aspects that still have to be assessed regarding the applicability of cryogenic machining at an industrial scale, the geometrical accuracy obtainable by applying cryogenic cooling to turn an industrial workpiece is afforded in this work. In the previous paragraphs, the investigation of the machinability of EBM Ti6Al4V alloy and the sliding wear tests have proved this cooling strategy might find its ideal application in the biomedical field, satisfying technical, environmental and economic aspects. Nonetheless, being the manufacturing process of biomedical surgical implant made by AM techniques to require semi-finishing operations only, to assess the applicability of this cooling

strategy for this specific application, the geometrical accuracy issue has to be estimated. In the following paragraphs, a biomedical machining case study is presented. The company Eurocoating S.P.A, partner of the research project, has provided Near Net Shaped acetabular cups made of Ti6Al4V EBM. These surgical implants require the turning operation to finish the internal surface in order to house the insert that is in contact with the femoral head as can be seen in the Figure 7.1.

Figure7.1 Machined acetabular cup, internal polymeric insert and femoral head.

As can be understood by observing the Figure 7.1, the internal surface of the acetabular cup requires strict geometrical and form tolerances to be achieved by the machining operation. Hence, the lubricating strategy does not have to induce thermal distortions. The feasibility of cryogenic cooling to machine the internal surface of the acetabular cup is investigated in this work, a comparison with standard emulsion cooling and dry turning is assessed. This research, is subdivided in two main stages, during the first, a discretized cup shape of the same material is turned to identify the main critical aspects that provoke deviations on the final diameters. According to the main findings reached in this preliminary work, a machining strategy is than set to turn the cups, aiming to limit the final geometrical deviations. This work aims to fill the lack of literature works regarding the thermal issues and the consequential geometrical deviations that inevitably arise when applying cryogenic cooling to machine a real workpiece. Since this work is a preliminary study of this topic, a simplified geometry of the cup is machined by realising primitive geometries that are easier to characterize, furthermore the geometrical characterization has been concentrated on the dimensional errors only to simplify the problem, hence further investigations need to be carried out aiming to assess the feasibility of this innovative and quite exotic cooling strategy in biomedical applications. A comparison between the component geometry after dry, wet and cryogenic machining is presented and discussed.

7.2.Experimental approach

The turning tests were realised by means of a Mori Seiki® NL 1500 CNC lathe already employed in the previous works presented in this thesis. A detailed description of the cryogenic cooling line can be found in the paragraph 3.4.
A Sandvik Coromant® A20M-SDXCR 11-R boring bar with a DCGT 11 T3 08-UM GC1105 coated carbide insert supplied by the same manufacturer was used as cutting tool.
Turning the internal profile of the acetabular cup can be considered a quite simple operation; nonetheless, its geometry complicates the identification of each individual effect on the geometrical deviations played by the following main factors: the lubrication, the geometry, and the cutting length. Aiming to accomplish that, a simplified test specimen made of EBM Ti6Al4V alloy (the same material of the acetabular cup) was initially machined starting from a cylindrical rod, realizing three internal steps with nominal diameters equal to: D1=33 mm, D2=28 mm, D3=20 mm respectively, with a constant step depth equal to 6 mm as shown in Figure 7.2b. The range of diameters was chosen accordingly to the internal dimensions of the near-net-shape acetabular cup shown in Figure 7.2a and manufactured through the EBM technology. The test specimens were also machined externally to reach the same mass of the acetabular cup equal to 70 g. A schematic illustration of the test specimen in its initial state is shown in Figure 7.2b. Two strategies were then followed to separate the effect of the turning length of the complete internal profile of the test specimen (which has a direct influence on the thermal effect played by the lubrication strategy) from the turning length required to machine each step equal to 40 seconds that corresponds to the time required to machine one pass of the internal surface of the investigated acetabular cup when setting the following cutting parameters: a cutting speed equal to 60 m/min a feed rate equal to 0.1 mm/rev and a depth of cut equal to 0.25 mm as advised by the tools manufacturer.

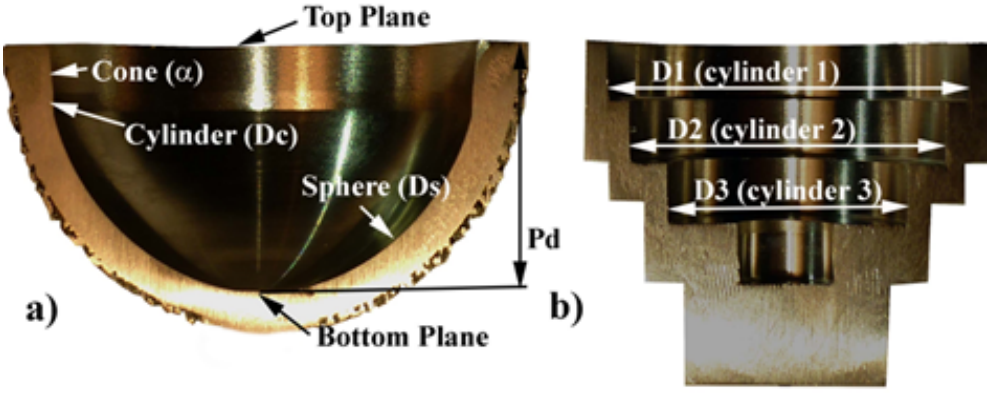

Figure 7.2 Nominal geometry machined on the: (a) acetabular cup; (b) test specimen.

Through the first turning strategy, the three steps composing the internal profile of the test specimen were cut one after the other, evidencing the thermal effect led by the application of cryogenic cooling on the dimensional accuracy.
As regards the second strategy, the same steps were turned one at a time setting the same nominal diameters and letting the specimens return to room temperature. By doing that, the geometry effect was uncoupled with the turning length effect. In fact, it is renowned that thermal distortions of metals are directly proportional to the nominal dimension (or initial

dimension), hence for the same thermal load applied, different diameters could suffer different geometrical deviations. Furthermore, the thermal coefficient in forced convection thermal transfer mechanism, depends to the second power of the rotating speed, as a consequence, the thermal exchange with free air due to the workpiece rotation, could sensibly vary from one diameter to another affecting the final thermal distortions due to the geometry effect. A fresh cutting edge was used to carry out each turning operation, thus avoiding the tool wear effect on the final dimensional accuracy. The tool wear, is in fact one of the most important causes of geometrical deviations of the final workpiece, so to exclude its effect in this preliminary work, a fresh cutting edge for each machining operations was adopted.

The geometry of the machined parts was measured using a Zeiss® Prismo 7 VAST coordinate measuring machine (MPE 2.2+L/300 μm). A single stylus with a 3 mm diameter rubidium tip was used. The measurements were carried out in a temperature-controlled room at a nominal temperature of 20 °C. Moreover, the workpiece temperature stability was ensured by laying it in the measuring room for 24 hours before measuring. To investigate the geometrical distortions correlated with the cryogenic cooling on the test specimen, three different cylinders were evaluated (two different circles on each cylinder were measured). The least squares method was used for the extraction of the fitting circles. For the acetabular cups it was decided to evaluate the following geometrical elements (highlighted in Figure 7.2a: the top plane (machined exclusively for fine alignment), a cone, a cylinder, a sphere, and the bottom plane. To compare the obtained geometrical quality the following characteristics were selected: diameter of the cylinder (Dc), aperture angle of the cone (α), distance between the top and bottom planes (Pd), and the diameter of the sphere (Ds). The mean value and standard deviation were calculated on the basis of 3 repetitions.

Being the geometrical deviations arisen in machining operations influenced by temperature, it is of fundamental importance to monitor its variations within the workpiece and the tool holder. An infrared camera FLIR® Thermovision A40 was therefore fixed on the tailstock of the lathe to acquire the temperature field generated after turning both the specimen and the acetabular cup in a reproducible manner as shown in Figure 7.3. In fact, since the tail stock of the CNC machine is controlled axis, it is possible to position it with ac accuracy of 0.001 mm. The tool holder temperature was acquired embedding a k-type thermocouple into the lubricating hole inside the tool stem (as designed by the manufacturer) at a distance of 35 mm from the tool tip as showed in the schematic illustration on the left upper corner of Figure 7.3. A LabVIEW® based software was used to acquire the temperature from the thermocouple signal.

Three test specimen for each lubricating strategy, namely: dry, wet and cryogenic were machined to assess the repeatability of the process. Wet turning operations were conducted by means of the cooling line provided with the machine tool. A standard commercial semi-synthetic metalworking fluid Monroe® Astro-Cut HD XBP was mixed with water to create the adopted cutting fluid, a water emulsion having a concentration of 5%, supplied at the pressure of 5 bar. Three acetabular cup were than machined for each tested lubricating strategy, maintaining fixed cutting parameters and the nominal dimension set on the CAM program. In order to turn the internal surface of the acetabular cup, a clamping device was designed in Solidworks 3D®, a 3D view of the assembly is visible in Figure 7.4.

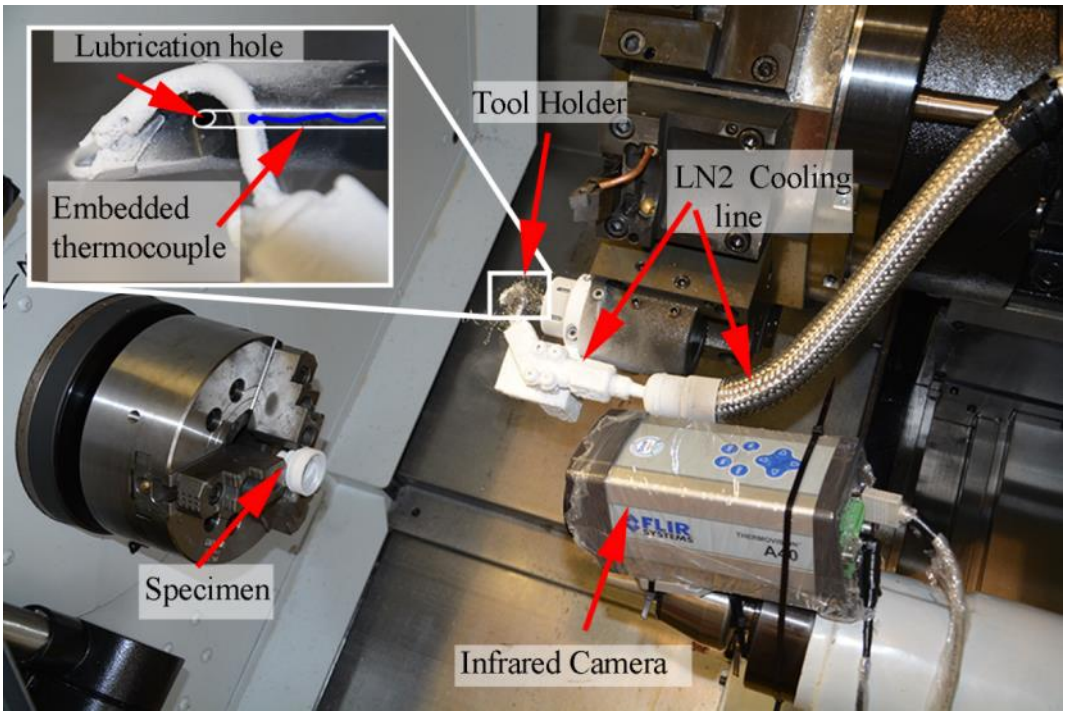

Figure 7.3 Experimental set up used to machine the test specimen and the acetabular cup, allowing the acquisition of the tool holder and the workpiece temperature.

Before conducting the turning tests, an estimation of the geometrical errors due to the precision of the adopted machine tool was carried out. In this work, the research was focused on diameter measurement; hence the precision of the machine tool was validated by comparing the nominal and the measured final diameters, due to the internal turning

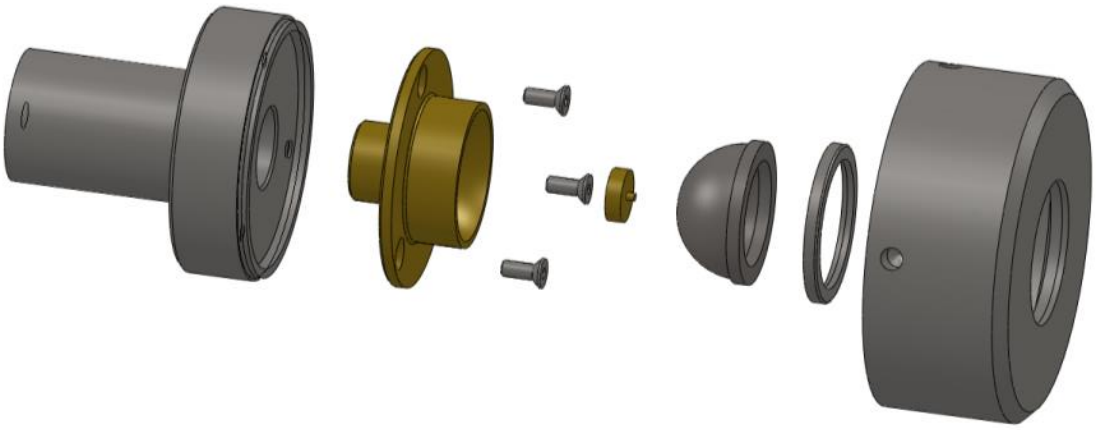

Figure 7.4 Exploded view of the clamping device adopted to machine the acetabular cup.

operation required to prepare the initial dimension of the test specimen having the following nominal diameters: D1=33 mm, D2=28 mm, D3=20 mm. Nine test specimens were cut starting from a cylindrical rod of EBM Ti6AL4V alloy. Rough machining was carried out using the same solid mill and the same cutting insert, but the finishing pass for each internal step was achieved with a fresh cutting edge under wet cooling condition, in order to avoid the tool wear effect on the geometrical deviations. The final geometry of the test specimens was measured according to the measuring approach described above. These preliminary

qualification process, led to the following geometrical discrepancies between nominal and actual dimensions, summarized in Figure 7.5. Geometrical discrepancies are present between the nominal and the machined surfaces. By analyzing the data plotted in Figure 7.5, the first three specimens have to be neglected because no tool radius compensation was set for the turning operation, determining errors around 0.2 mm that are not acceptable for a modern CNC machine tool. If the remaining 6 test pieces are taken into account, the following average

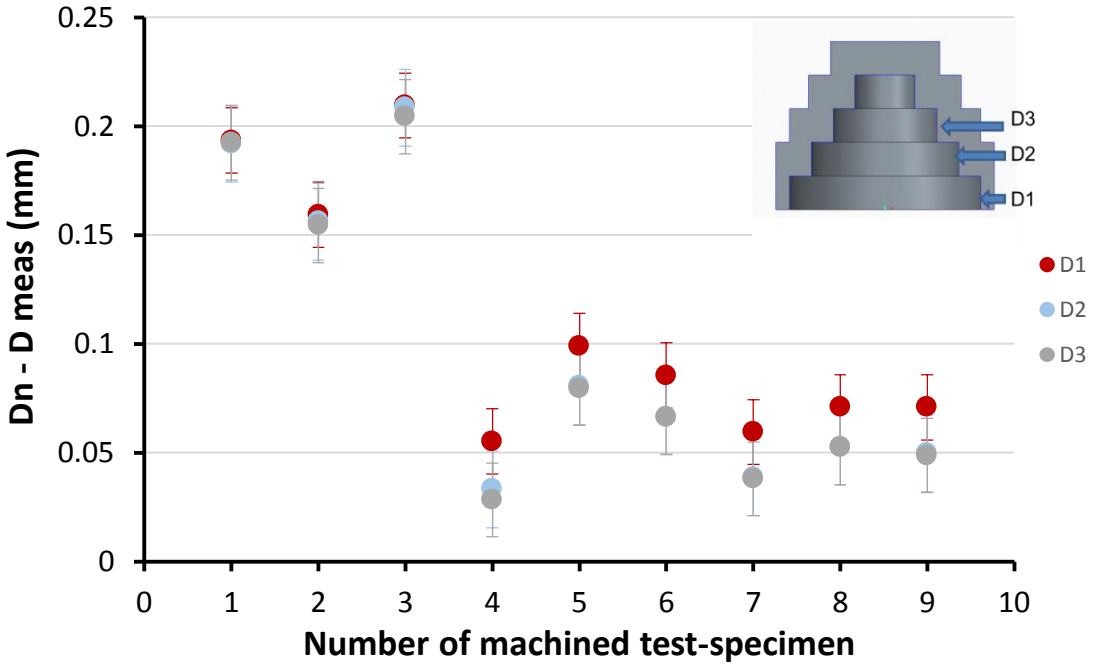

Figure7.5 Geometrical deviations between nominal and measured internal diameters due to the intrinsic error of the machine tool.

errors have been measured for D1,D2,D3 respectively: 0.073, 0.053, 0.052 mm. Understanding the technical causes of these important deviations is a difficult issue to solve, since several factors affects the precision of turning operations, such as the stiffness of the tool holder, the stiffness of the clamping set up (for the tool holder and for the workpiece), and more over the precision of the pre-setting stylus adopted to set the zero position of the tool tip according to the machine reference frame. Anyhow, the measured errors tends to increase for higher turned diameters (D1 > D3) according to the adopted scheme. The average errors occurred in turning each diameter were than considered to evaluate the final dimension of the test specimens.

7.3.Experimental results

7.3.1. Turning tests on test specimens

Figure 7.6 resumes the average differences between the nominal and measured values of D1 and D3 turned one at a time, for each lubricating condition at the fixed turning time of 40

seconds. The test specimens were turned immediately after the LN2 flow became stable and completely in liquid phase. Under such conditions, the short turning length of 40 seconds inhibited the time effect on the geometrical deviations for each measured diameter, and no significant differences were observed regardless the adopted lubricating strategy in particular for the highest diameter, meanwhile for smaller diameter cryogenic cooling tends to enlarge the errors. The presented results, can be explained if the geometry of the workpiece is considered and how the thermal loads are exchanged by varying the diameter. For higher diameter, it is reasonably to suppose that due to higher circumferential (or tangential) speeds, the test specimen exchange het by forced convection more easily than smaller diameters because the peripheral speed is smaller, hence the convection heat exchange with free air is reduced, adding less heat to the cooler workpiece (the free air can be considered at 20° and the workpiece reaches sub-zero temperatures during cryogenic machining). Furthermore, another important consideration about the LN_2 flow interaction with the workpiece have to be done. A part of the LN_2 cooling flow, inevitably hits the internal surface of the workpiece, and being the test specimen a closed geometry, in tends to point towards the smallest diameter of the selected geometry rather than skimming the wider circumferential surfaces. In few words, the inner part of the test specimen is more cooled by the liquid nitrogen hitting the surface.

Nevertheless, the diameter effect is weak if the data variability is taken into account. In brief, the results shown in this graph encourage the LN_2 adoption if short turning lengths, thus short cooling expositions, are involved.

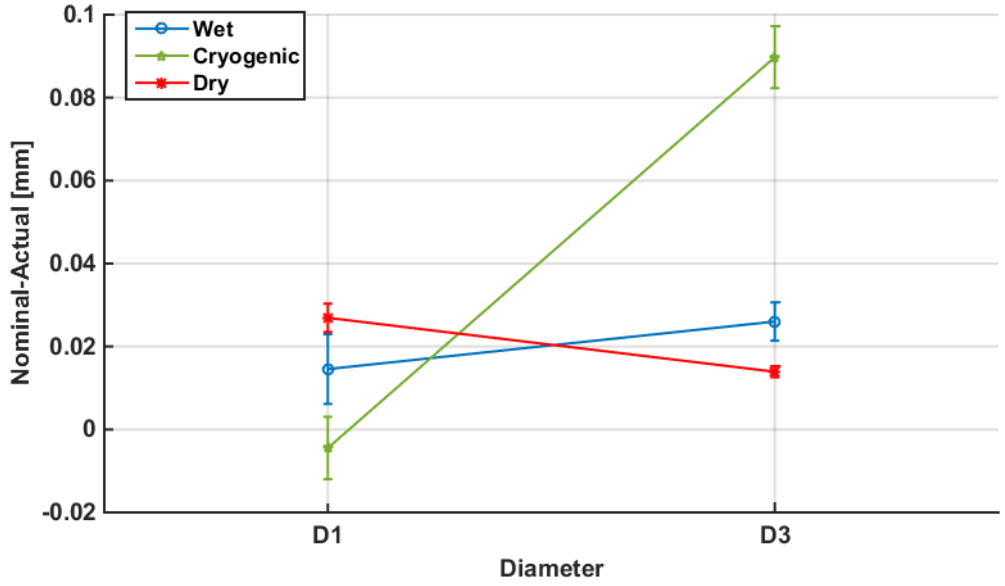

Figure 7.6 Geometrical deviations occurred after turning the diameters D1, D2 and D3 one at a time under dry, wet and cryogenic cutting conditions.

If the same final diameters are turned consecutively, a substantial different scenario emerges as revealed by Figure 7.7. A significant change arises regarding the cryogenic turned test specimen that exhibits an increment of the deviations for the smallest diameter, namely D3, from 0.02 mm up to 0.08 mm on an average. On the other side negligible differences are still present between the dry and wet machined geometries. The temperature measurements of the workpiece and tool help to clarify these findings.

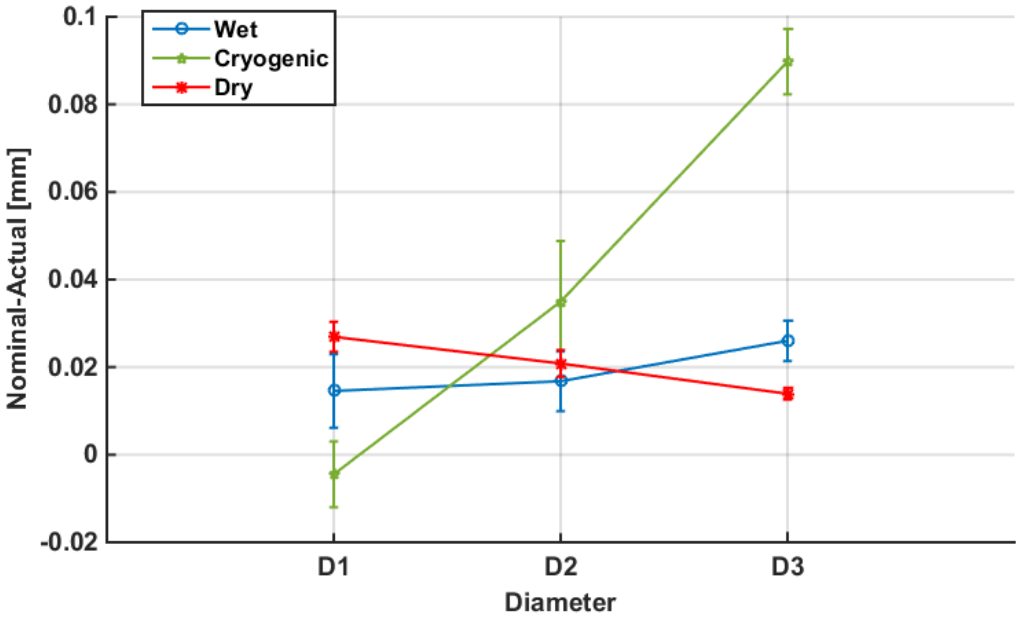

Figure 7.7 Geometrical deviations occurred after turning the diameters D1, D2 and D3 in sequence under dry, wet and cryogenic cutting conditions.

Even though the highest geometrical deviation is expected for the biggest diameter, namely D1, under this turning strategy the highest one resulted in correspondence to D3. The acquired thermographic images of the test specimens reveal that no substantial differences in the temperature field are induced by the higher turning length imposed during these turning operations, and the same average temperature of almost -20°C was measured as can be seen in Figure 7.8a. This thermal field suggests that even after 40 seconds of turning a thermal steady state condition is reached in the test specimen due to the thermal exchange with the environment at room temperature by the rotating motion. On the contrary, the tool holder is heavily cooled down during the turning process of the three subsequent diameters, because it is directly hit by the LN_2 flow.

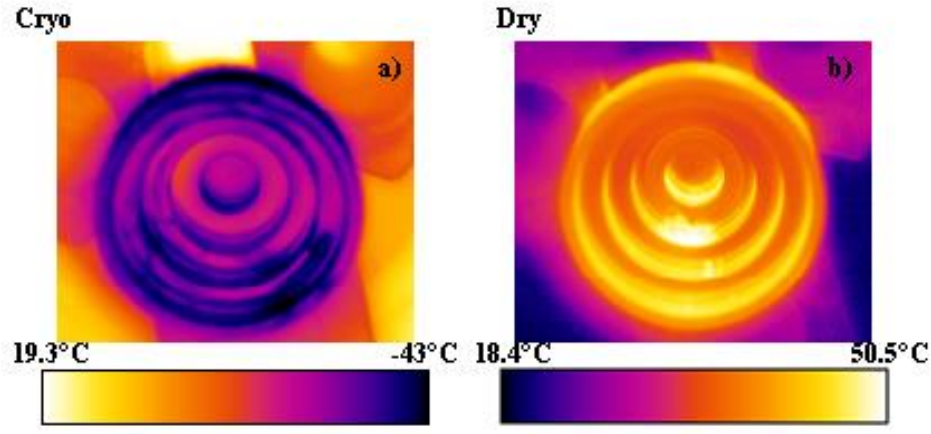

Figure 7.8 Thermographic images of the test specimen turned under: a) cryogenic and b) dry cooling conditions.

As a prove of that, the Figure 7.9 illustrates a completely frozen tool holding set up, during cryogenic machining after the initial cooling ramp from room temperature. As a consequence,

the tool holder progressively contracts starting from the machining of the first diameter, namely D1, reaching its minimum during the turning of the last diameter, namely D3. Thermal simulations of the contraction of the tool holder might help to clarify if within this process time between the first turning step to the last one, the tool holder contracts of the same order of magnitude of the measured errors between D3 and D1.

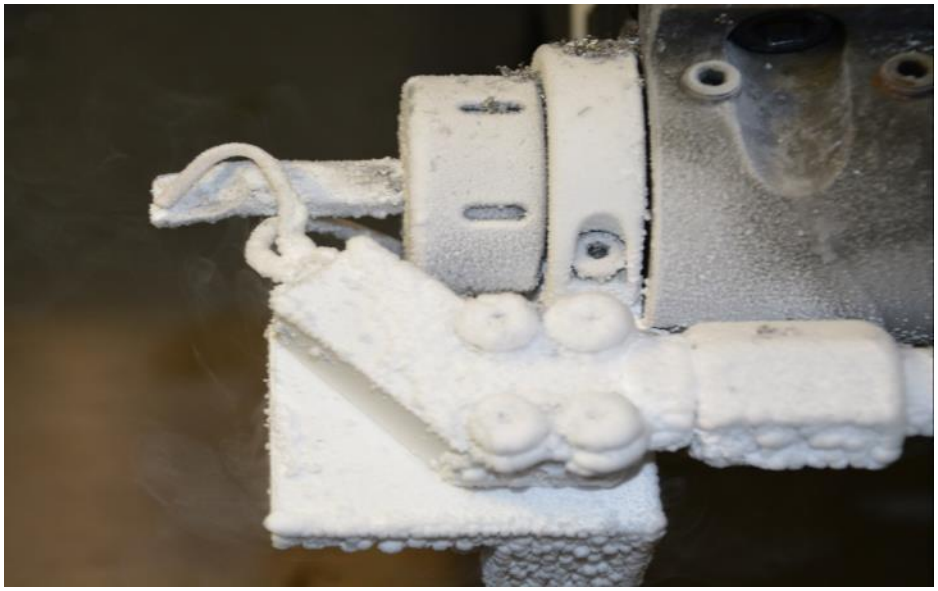

Figure 7.9 Tool holder and nozzles set up completely frozen during cryogenic machining.

As a proof of that, the temperature measured inside the tool holder in Figure 7.10 shows a lowering blue trend when machining the test specimens starting from the conditions of stable

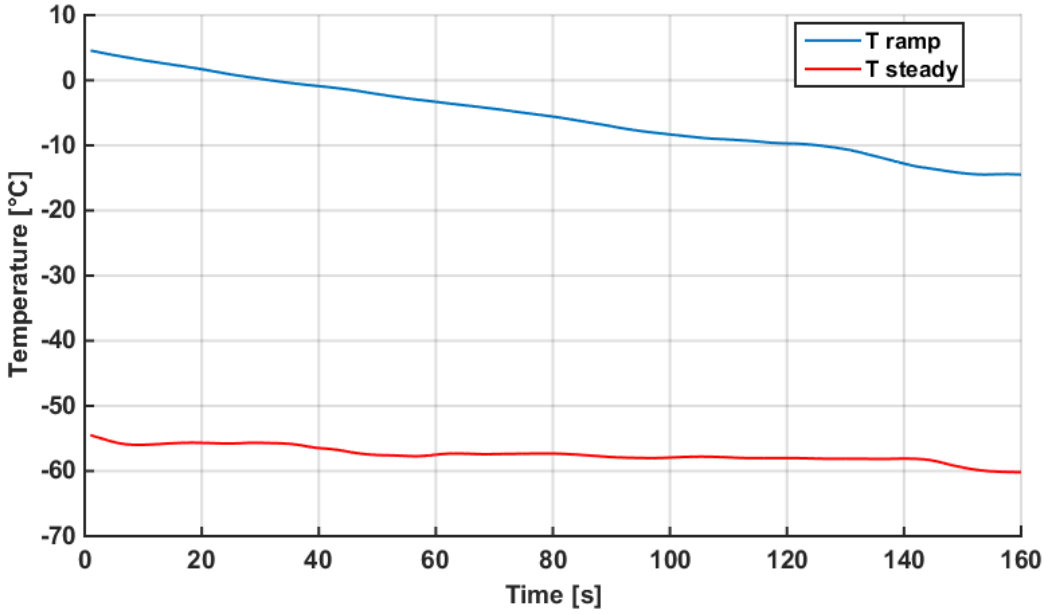

Figure7.10 Tool holder (inner) temperature evolution during a cooling ramp (blue trend) and thermal steady state condition (red trend).

LN_2 flow, and the clamping jaws laying at room temperature. The green data presented in Figure 7.7 were acquired under these thermal conditions. The tool holder suffered a severe

cooling down during machining three specimens one after the other, reaching a thermal steady state condition at the temperature of around -60 °C.

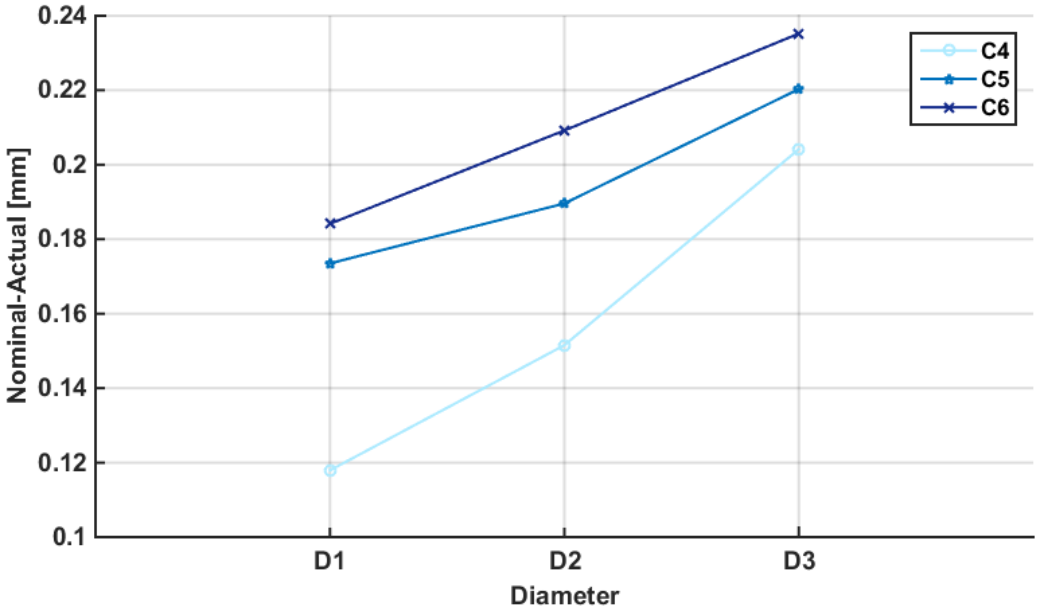

Figure 7.11 Effect of the tool holder progressive cooling on the geometrical deviations of three subsequent machined test specimens.

Because of the progressive cooling of the tool holder, a worsening in the accuracy of the geometry was found starting from the first test specimen to the third one, as proved by the presented deviations plotted in Figure 7.11. The temperature measurements of the entire thermal field generated onto the inner surface of the test specimens, showed repeatable average values of -20°, hence the such worsening of final diameters arising by turning three test specimens in a sequence can be ascribed to the progressive contraction of the tool holder. When observing Figure 7.7, negligible variations can be noticed among the three diameters, but the most stable trend is achieved under standard flood cooling. Under such cooling condition a constant temperature of around 18 °C was maintained during the turning process, as a result there is no cutting length effect for this cooling strategy. Due to the small temperature increment provoked by the absence of a flood coolant that rose the average temperature of the freshly machined surfaces at around 43 °C as can be seen in Figure 7.8b, negligible geometrical distortions occurred during dry turning of the three diameters one after the other as confirmed in Figure 7.7. Even for dry machining, the cutting length effect is still negligible. By comparing the results presented in the Figures 7.6 and 7.7, an important consideration can be drawn regarding the LN_2 application in turning. If the test specimens are cryogenically machined, the cutting length plays a crucial role because it affects the cooling rate thus the contraction of the tool holder, while the workpiece cooling is less critical. If the cutting length is equal to 120 seconds, the highest deviation with the nominal diameter of 24 mm reaches its maximum of 0.085 mm, on the contrary the error on the first machined diameter equal to 36 mm is negligible. In the case of short cutting lengths of around 40 seconds, the cryogenic machined test specimen present dimensional deviations with the nominal geometry that are comparable with those obtained under dry and wet turning.

7.3.2. Turning tests on acetabular cups

According to the main findings described in the previous paragraph, three acetabular cups for each lubricating strategy were turned to realize the nominal dimensions indicated in Figure 7.2a. Aiming to minimize the cooling contractions on both the workpiece and tool holder that arises during cryogenic turning, the LN_2 flow was stopped for two minutes between one turning pass and the next one, allowing the tool holder not to cool down at the thermal steady state temperature of -60°C found during machining the test specimens. The temperature filed generated inside the acetabular cups after the turning operation was acquired in the same manner as for the test specimen. Even dough to turn the acetabular cups a bulky steel clamping device was used, that might heat up the workpiece more than the jaws used to machine the test specimens, no substantial differences in terms of surface temperature were reached, hence thermal loads applied to the system can be considered repeatable. This machining strategy was in fact implemented to replicate the thermal field arisen during machining the test specimens for a restricted time of 40 seconds (testing the effect of the geometry presented in Figure 7.6), which, as previously described, made cryogenic turning be competitive with dry and wet machining. In Table 7.1 the average measured dimensions for the chosen characteristics composing the internal profile of the acetabular cup are summarized: differences of less than 0.05 mm are found between cryogenically and wet turned acetabular cups, foreseeing that the applied turning strategy might be implemented to machine an entire batch. Even dough an overall dead time of 4 minutes per part is added with respect to dry and wet machining, due to the low volumes produced by AM technologies the proposed strategy can be successfully implemented to apply cryogenic machining in such particular industrial case. Aiming to clarify the tool holder contraction effect on the geometrical deviations between nominal and measured dimensions a batch of 5 acetabular cups was machined under cryogenic cooling only. The cups were turned starting from a condition of stable LN_2 mass flow in liquid state, turning one after the other, with a repeatable procedure. The LN_2 was started after having mounted a new cup on the clamping device, and stopping it at the end of the turning operation of each cup, avoiding a too sever cooling of all the cutting set-up during the set up time. To trace the internal temperature of the tool holder, the acquisition was started before turning the first cup and stopped at the end of the entire batch, in doing so the tool holder temperature is monitored even during the set-up times required to remove the machined cup and install the next one. This procedure, allows simulating a more realistic machining approach that might be found in industry, evidencing the problems regarding the thermal distortions arising during cryogenic machining by applying a standard manufacturing approach. Even in this new test, the tool wear has been neglected by substituting the cutting tool insert with a fresh one after having turned a cup. Future developments will take into account the tool wear.

Aiming to improve the accuracy of the measurement approach, the internal surface of the EBM Ti6Al4V acetabular cup was further simplified removing the cone, turning a straight cylindrical surface until starting the spherical surface and then the final plane. An illustration sketch of the simplified geometry is represented in the Figure 7.13.

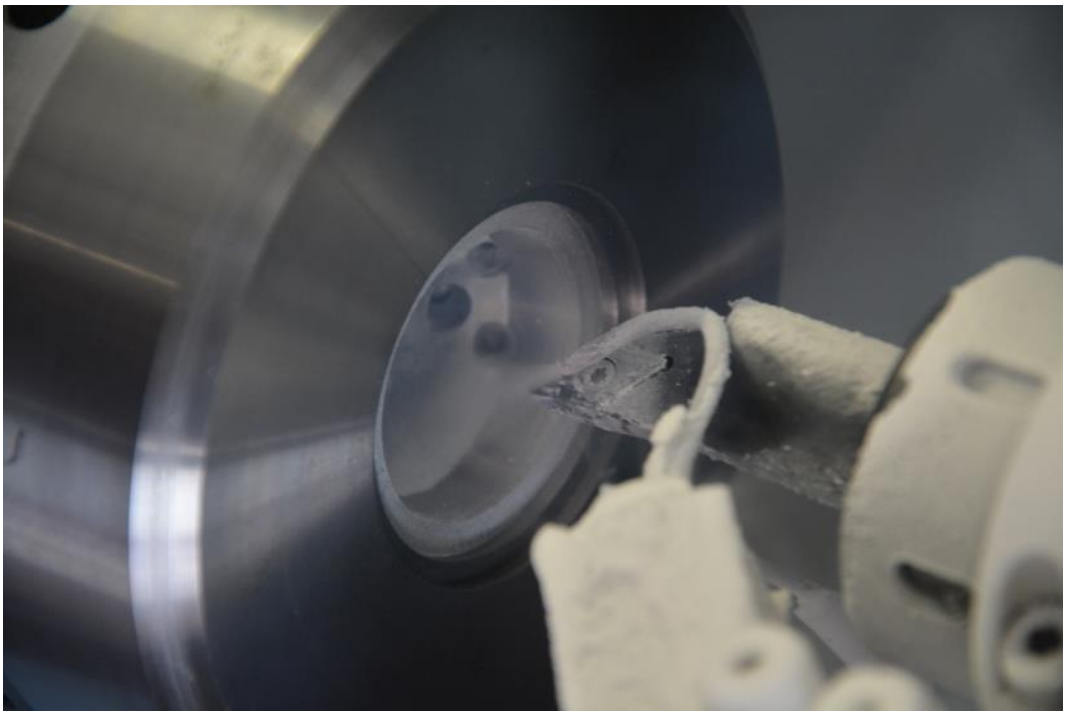

Figure 7.12 Cryogenic turning of the acetabular cup.

Table 7.1 Average measurements of the chosen characteristics composing the internal profile of the machined acetabular cups.

Lubrication Strategy	Dc (mm)	α (Deg)	Pd (mm)	Ds (mm)
Dry	41.325	10.042	23.496	42.217
Cryogenic	41.334	10.138	23.451	42.199
Wet	41.414	10.164	23.624	42.292

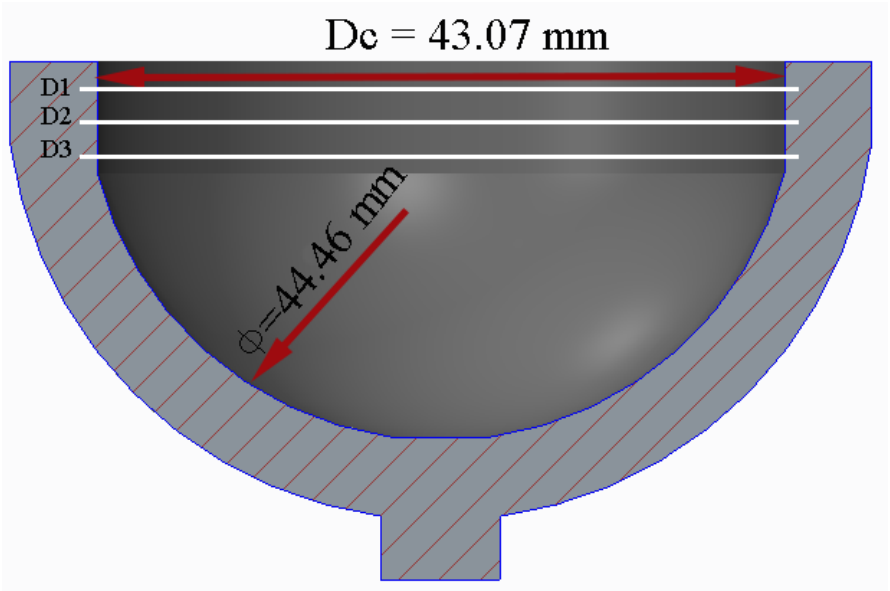

Figure 7.13 Schematic illustration of the simplified geometry of the acetabular cup.

The cylindrical portion of the internal surface, has been stretched to an height of 7 mm allowing the measurement of three diameters namely, D1, D2 and D3 at the fixed distance of 2 mm (see Figure 7.13), to increase the accuracy of the measurement and to allow at the same time the evaluation of the surface cylindricity that can be assessed accurately if more than two circumferences are taken. The diameter of the sphere was acquired touching the surface in continuous with the instrument probe, following five arcs along the circumferential direction according to the sectioned view of the cup showed in Figure 7.13. The nominal diameters were fixed in the CN part program being equal to 43.07 mm and to 44.36 mm for the cylinder and the sphere respectively. These dimensions that could seem quite bizarre were set according to the real nominal dimension added by the manufacturers of this prosthesis for the same geometrical features. The Figure 7.14 presents the temperature trend inside the tool holder when turning 5 consecutive acetabular cups, stopping the LN_2 flow between one cup and the next one. The first cup was turned since the liquid nitrogen flow became stable and in liquid phase. An interesting temperature trend emerges from the measurements. A saw tooth shape trend is observable in Figure 7.14, where the decreasing portions correspond to the machining phase, while the ascending portions correspond to the set up time, hence the tool holder heats up because no LN_2 is supplied to the cutting zone. At observing more in detail the decreasing trends for each of the 5 machined cups, a jagged curve arises due to the positive heat added by the cutting process that breaks the cooling down of the tool holder. In fact as many steps as the number of the cutting passes can be noted on the lowering trend of the tool holder temperature. A second interesting finding regards to the temperatures measured during the machining process of the entire batch. Just for the first turned acetabular cup, a positive temperature was measured at the beginning of the cutting operation, and a steep lowering trend is than noticed up to a minimum temperature of -60°C. This finding confirms the values measured during turning the test specimen, presented in the Figure 7.10. Due to this drop of the temperature, the tool holder suffers a sensible contraction. Proceeding with the cutting process, a repeatable saw tooth tend of temperature is found. Due to the continuous starting and stopping the liquid nitrogen flow, the tool holder temperature fluctuates between a maximum temperature of around -30°C and a minimum temperature of -63°C, manifesting a quite stable and periodic trend. By considering that the cutting tool zero set - up was performed at room temperature, geometrical deviations might occur due to the contraction of the tool older. To verify this hypothesis, the average values of the dimensional measurements conducted on the machined acetabular cup when returned at room temperature must be checked.

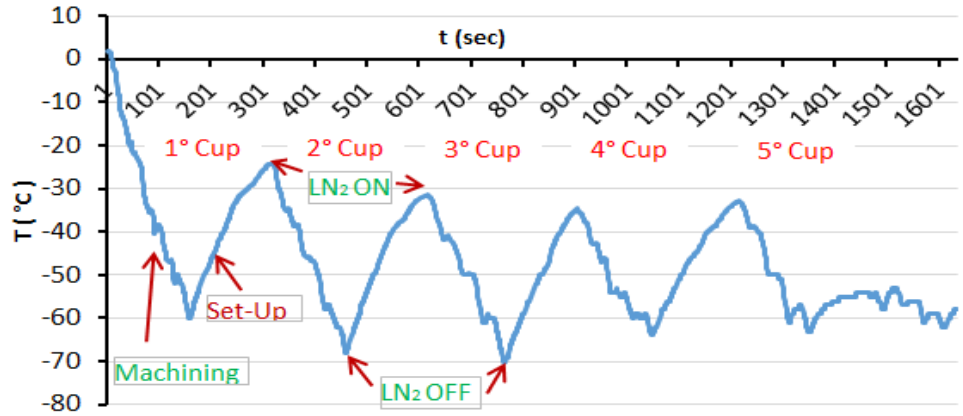

Figure7.14 Saw tooth trend of the tool holder internal temperature during turning 5 acetabular cups in a sequence under cryogenic cooling condition.

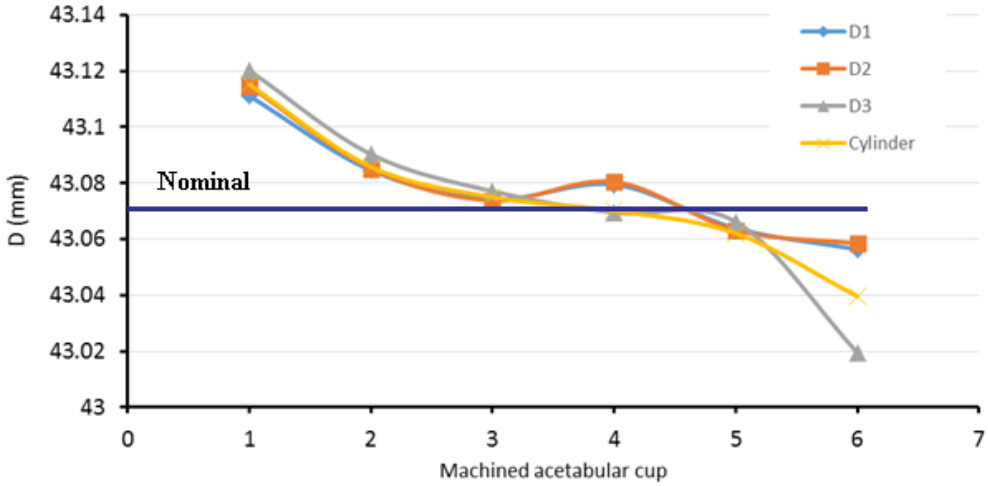

Figure 7.15 Diameters trends D1,D2 and D3 for the entire batch of cryogenically turned acetabular cups in a sequence.

A decreasing trend is noticeable in the Figure 7.15 for the measured diameters and for the cylindricity during the sequential turning process of a 5 acetabular cups batch under cryogenic cooling condition. This trend is provoked by the aforementioned contraction of the tool older due to the cryogenic working condition. Moreover a discrepancy of up to 0.1 mm is reached between the first and the fifth machined cup, regarding the diameter D3. Nevertheless, the nominal diameter equal to 43.07mm was closely achieved by the third machined cup, but the overall trend of measurement is clearly not feasible for an industrial application, because no dimensional repeatability is guaranteed within the entire batch because of the thermal issues. However, this test demonstrates that a different machining strategy should be applied to respect the designed dimensions (and tolerances) of the final workpiece for a batch of several parts turned under cryogenic cooling, rather than machining the batch in a sequence. Even the measured values of the machined sphere are arranged in a decreasing trend starting from the first turned cup towards the last one, but for this case diameters are generally greater than the nominal fixed value equal to 44.46 mm as can be observed in the Figure 7.16.

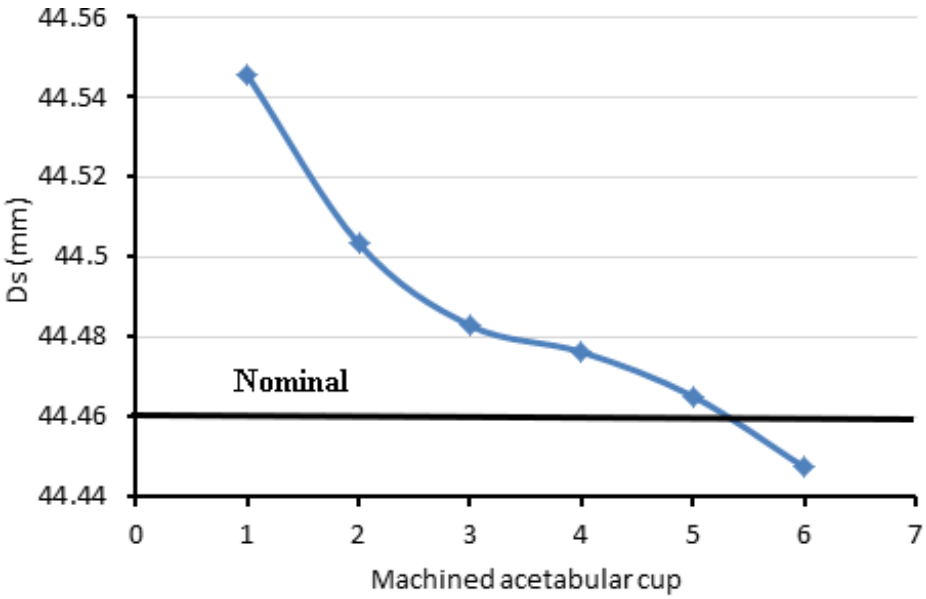

Figure 7.16 Trend of measured diameters of the acetabular cups machined within the entire batch.

By observing the trend plotted in the Figure 7.16, the thermal loads regarding the application of the LN_2 on the tool holder generate a difference between the first and the last diameter value of 0.1 mm with a monotonic decreasing trend that is without doubt not applicable at an industrial scale. The resulting trend is however unexpected because smaller diameters than the nominal one should have been measured due to the contraction of the tool holder, anyhow during turning the sphere, both X and Z axis of the lathe are at in motion contemporarily thus the resulting errors are caused by a combination of both effects, that is more difficult to investigate and to explain rationally. Thermal numerical simulations might help to examine this complex problem by superimposing both the thermal deviations of the tool holder and of the workpiece.

7.4. Chapter concluding remarks

This work was carried out with the main aim to assess the feasibility of cryogenic cooling in turning the internal surface of acetabular cups made by EBM Ti6Al4V alloy. It can be considered as one of the first academic experience regarding the accuracy of the final machined product when liquid nitrogen is used as a cooling mean, instead of more traditional strategies as wet and dry machining. In fact, in literature no works have been published on this topic, focusing the researches on a pure machinability investigation. A specific industrial case is afforded in this work where cryogenic machining could find its ideal industrial application, consisting in the internal turning of acetabular cups made by EBM Ti6AL4V under dry, cryogenic and wet cooling conditions. A preliminary study is carried out on test specimens that discretize the shape of acetabular cups, respecting the mass, the cutting parameters, the cutting lengths, the overall dimension and the shell thickness, presenting an internal step shape cavity with three internal steps of different diameters. This study helps to simplify the individuation of the main influencing factors on the induced thermal distortions, with a simplified geometry than acetabular cup one. Both the test specimen and the acetabular cup are qualified by comparing the final geometry with the nominal one. Two machining strategies are pursued to separate the effects of the cutting length (time) from the geometrical one, hence the three reference internal steps are machined in a sequence (one after the other) and also one at a time, waiting the required time to leave the tool holder and workpiece to return at room temperature. Dry and wet turning generate comparable dimensional deviations, however wet turning guarantees the best stability of the measured dimensions since it maintains the temperature of the workpiece and of the tool holder at an average value of 20 °C. On the other side, the cryogenic conditions reached with the application of LN_2 provoke geometrical deviations, the tool holder contraction is more critical than the workpiece one. If short cutting lengths are employed, corresponding in this case study at machining one diameter at a time (40 sec), cryogenic cooling leads to a comparable accuracy than dry and wet turning, whereas for longer cooling expositions (turning three diameters in a sequence) wider geometrical deviations are found, not comparable with the standard cooling methods. In the following part of this work, the short cutting length strategy is repeated to turn the acetabular cups leading to a good agreement between the geometric dimensions achieved with cryogenic cooling, with those achieved under wet turning. In fact, to limit the tool holder contraction, the LN_2 is interrupted for two minutes between one pass and the following one to avoid a severe cooling of the system. This strategy adds two minutes of dead time at the manufacturing process, but for this particular application where low production volumes are involved, this time is later recovered during the cleaning and sterilizing operations, realised on cleaner products due to the application of LN_2. Nevertheless, aiming to simulate a standard production process, a batch of six acetabular cups are turned one after the other, maintaining the same cutting lengths as those required to turn the test specimens, and maintaining a repeatable production rhythm. This process simulation evidences a great discrepancy of the final dimensions (cylindrical and spherical portions) between the first and the last turned cup, induced by the contraction of the tool holder. In brief, with the goal of speed up the industrialization of such innovating and promising cooling strategy, further steps ahead to achieve desired product accuracy have to be done, acting on both the tool holders and on the production strategies that need to be redesigned to avoid severe thermal distortions.

References

[1] M'Saoubi, R., Axinte, D., Soo, S. L., Nobel, C., Attia, H., et al., 2015, High performance cutting of advanced aerospace alloys and composite materials, CIRP Annals - Manufacturing Technology, 64/2:557–580, DOI:10.1016/j.cirp.2015.05.002.

[2] Pušavec, F., Stoić, A., Kopač, J., 2009, The role of cryogenics in machining processes, Tehnički vjesnik, 16/4:str. 3–9.

Chapter 8

Conclusions and future works

In this Chapter, the findings and results of the current research are summarized with final remarks and conclusions. The concluding remarks are given in order of appearance in the chapters. The directions and recommendations of the future work are discussed briefly based on the results and observations presented in this dissertation.

8.1. Conclusions

Turning experiments with the application of liquid nitrogen as an innovative cooling method were conducted on the additive manufactured biomedical alloy Ti6AL4V produced by Electron Beam Melting. The aim of the research was investigating its machinability through both experimental and numerical approaches under different process conditions (cutting parameters and cooling strategies) and validating the feasibility of cryogenic cooling as the ideal lubricating strategy to machine additive manufactured surgical implants made of EBM Ti6Al4V alloy. Surface integrity modifications on this Ti6AL4V alloy were achieved from cryogenic machining. Sliding wear tests were performed to explore the influence of cryogenic machined induced surface integrity modifications on the wear performance of the studied Ti6Al4V alloy, under process conditions similar to those encountered in real total hip replacements. Finally an industrial case study consisting in turning real acetabular cups with cryogenic cooling and evaluating the geometrical accuracy achievable under such cooling method was presented, aiming to fasten the industrialization of the technology.
The major findings of this research are summarized below:

1) The Ti6AL4V alloy produced by Electron Beam Melting manifested a poor machinability when turned with commercial coated tungsten carbide inserts in semi-finishing turning operations, mainly due to its chemical composition, its low thermal conductivity and its higher mechanical properties than standard wrought Ti6Al4V alloy, imparted by the AM forming process.

2) The tool wear analysis, confirmed the sticky tendency of Ti6Al4V even if produced by the innovative EBM process, hence the adhesion wear mechanism was the principal tool wear degradation mechanism. Regardless of the lubricating strategy and of the adopted cutting parameters, severe adhesion of workpiece material on the tool cutting edge, with the formation of Built Up Layer and Built Up Edge and in the worst cases even with cratering of the rake face were noticed.

3) SEM and EDS analysis revealed the strong dependency of the tool wear adhesion mechanism with the temperature arose in the cutting zone. Thus the lower the temperature the lower was the sticky tendency of the EBM Ti6Al4V alloy. As a consequence, the application of LN_2 induced the smallest values of flank nose wear width (VBc), limited the tool chip contact length and avoided the formation of cratering for all the tested cutting parameters.

4) Dry and Wet turning were both suitable to turn EBM Ti6Al4V alloy when a feed rate of 0.1 mm/rev was set, nonetheless when higher cutting parameters were tested setting a cutting speed equal to 80 m/min and a feed rate equal to 0.2 mm/rev, dry turning should be avoided because severe cratering of the tool rake face was observed since after three minutes of cutting, on the other hand, wet turning retarded the formation of crater wear thanks to the lowest temperature kept in the cutting zone.

5) A novel approach was developed to measure in a repeatable manner the thickness of the adhered layer or the depth of crater wear on the tool rake face, by using optical profilometry technique. Since cryogenic cooling maintained lower cutting temperatures, the thickness of the layer was kept below 10 microns while greater values were measured under dry turning. Regardless of the adopted lubricating strategy, the feed rate was the most influencing cutting parameter.

6) The surface integrity of machined surfaces for three different cutting lengths and cutting conditions was investigated throughout different methodologies. The surface roughness parameters Ra and Rt were weakly influenced by the adopted lubricating strategy because no great differences on the tool wear were noticed. However, cryogenic cooling determined better (lower) surface roughness parameters when a cutting speed equal to 80 m/min and a feed rate equal to 0.2 mm/rev were applied, due to the lowest flank wear. If the feed rate was kept at 0.1 mm/rev, a good surface roughness even lower than 0.5 microns could be obtained on the final workpiece.

7) SEM and profilometry analyses evidenced different kinds of surface defects according to the adopted lubricating strategy. More in detail, dry machining rose the cutting temperature in the cutting zone, improving the plasticity of the material and its tendency to adhere on the fresh machined surface, hence several chip fragments and BUE particles were released by the chip flow and by the tool motion. In this term, cleaner

surfaces were achievable by adopting a cooling mean, in particular under cryogenic cooling effect. The cleanest surfaces were obtained with cryogenic cooling, nevertheless other kinds of surface defects appeared due to a drop in material plasticity. Jagged feed marks, wrinkles and wavy surface topography were consequences of the cryogenic cooling effect, hence further development of the cooling apparatus, by optimizing the mass flow, the nozzles directions should to be done in order to reduce this kind of surface defects to foster a possible industrialization of this cooling strategy.

8) Cryogenic machining manifested its beneficial effects more on the microstructure altered layer, by increasing the surface micro-hardness and by inducing in general higher compressive residual stresses within a 25 microns depth layer beneath the machined surface. Its beneficial effects weakened when a feed rate of 0.2 mm/rev was set. On the other hand, dry machining was less suitable to turn EBM Ti6AL4V because the worst results were achieved among the tested lubricating strategies in terms of residual stresses and surface micro-hardness.

9) Sliding wear tests of turned cylindrical pins on CoCrMo flat plates under physiological process conditions (loads and physiological fluid) highlighted quite interesting findings that could encourage a future application of cryogenic cooling in the biomedical industry. For all the cryogenically turned cylindrical pins, adhesion wear mechanism between workpiece and counterpart material generated an increment in Pin's weight with severe adhesion of CoCrMo chemical elements on the worn pins. On the other hand, dry machined pins exhibited a weight loss due to a more abrasion wear mechanism caused by the harder counterpart material. These opposite wear behaviours were ascribed to the different initial surface states of cryogenically machined pins that demonstrated higher compressive residual stresses and higher surface micro-hardness. In the ambit of machining surgical implants made of EBM Ti6Al4V alloy such as turning the modular neck hip replacement, these findings proved the capability of cryogenic cooling to enhance the wear resistance of turned surfaces present in surgical implants, and they can be translated in a reduced release of metallic particles within surgical implants joint interfaces, such as the taper joint made by the modular neck and the femoral head. Future investigation could be carried out shifting from a pure material testing to a test in vitro, by reproducing these tests on real hip replacements under physiological test conditions to verify the beneficial effects on the final product.

10) In chapter six, a Finite Element model was implemented to simulate the experimental turning tests on EBM Ti6Al4V alloy by setting different cutting parameters and cooling conditions. The model was implemented in the commercial FE code STFC DEFORM 3D®. Due to the lack of material constitutive models in literature, capable to describe the thermo-mechanical behaviour of EBM Ti6Al4V alloy under temperatures, strain and strain rates conditions arose during cutting operations, a modified Johnson-Cook model well calibrated for wrought Ti6Al4V alloy was used. Aiming to take into account the different material properties of the AM alloy, the model was initially calibrated by setting the proper material coefficients in parallel with the hybrid sticking-sliding friction model chosen to simulate the friction forces between the chip and the tool. The model was

calibrated and validated by comparing measured and predicted cutting forces and temperatures. Good agreements between numerical and experimental results for the main cutting forces were achieved, however wider discrepancies were found for the feed cutting force and for the cutting temperatures, nevertheless the developed FE code was able to predict correctly the cryogenic effect. Lately the numerical model was improved, implementing empirical equations by means of User Sub-routines to predict the effects of cutting conditions on the deformation of the alpha phase lamellae and on the nano - hardness trend within the sever plastic deformed layer. The model predicted correctly the physical effects induced by the cryogenic cooling, showing narrow discrepancies with experimental results. Further improvements for the prediction of cutting forces and temperatures might be gained by adopting a more complex friction model that takes in consideration more influencing parameters such as the tool nose radius. A better approach to measure the temperature experimentally by fixing the thermo camera solidly with the CNC revolver to follow the tool motion, might improve the accuracy of the temperature predictions.

11) Finally, cryogenic turning was tested to turn the internal surface of AM acetabular cups made of EBM Ti6Al4V alloy, simulating an industrial case. A preliminary turning tests on discretized test specimens designed to simplify the shape of acetabular cups, evidenced the main causes of the induced thermal distortions on the final geometry. The tool holder contraction was more critical than the workpiece one due to cryogenic environment; hence if short cutting times were set, cryogenic turning outperformed comparable accuracies than wet and dry turning. On the other side, if longer cutting lengths were applied, the inevitable drop in temperatures led to poorer geometrical accuracy in the case of cryogenic machined test specimens. Based on these considerations, short turning lengths allowed the achievement of satisfying final geometrical accuracy in cryogenic machined acetabular cups, consisting in a machining strategy applicable to turn AM surgical replacements. To better certify the critical tool holder contraction, a standard machining approach was applied to turn a batch of 5 acetabular cups in a row, and the progressive cooling of the tool holder determined unacceptable discrepancies between the first and the last machined cups.

8.2. Future research directions

1) The cryogenic cooling apparatus developed in this work could be better optimized to lower the LN_2 mass flow hitting the workpiece, hence avoiding a severe reduction of surface material plasticity that caused jagged feed marks, waviness and wrinkles. A possible technical solution consists in the installation of a phase separator before the nozzles system. A dedicated tool holder with internal cooling channels could also be designed to allow fixed and more precise LN_2 flow directions on the cutting zone.

2) The beneficial effects of cryogenic machining on EBM Ti6Al4V alloy microstructure might be tested under fretting wear conditions, rather than sliding wear, because the former is encountered during the service life of surgical hip replacements rather than the latter.

3) Thermal FE simulations of tool and workpiece contractions due to the cryogenic effects could be carried out to clarify their mutual interaction during cryogenic turning of acetabular cups, to correlate these findings with the geometrical deviations measured in this work.

4) A dedicated tool holder that compensates its contraction due to the cryogenic cooling could be designed, by implementing a temperature controlled heating system or by using high thermal insulation materials.

5) The developed FE code to simulate the turning process of EBM Ti6Al4V alloy can be optimized by characterizing the material constitutive model through experimental tests instead of opting for a set of parameters calibrated for wrought Ti6Al4V alloy. Furthermore a more complex friction model calibrated for 3D machining should be more suitable rather than the selected one that has been calibrated for orthogonal cutting.

6) The experimental approach to measure the cutting temperature in the cutting zone should be revised; a fixing infra-red camera positioned at constant distance from the cutting zone could avoid the loss of the optical focus during the turning pass, hence allowing a better measurement of the cutting temperature.

Acknowledgments

I want to express a sincere gratitude to Professor Paolo Francesco Bariani for having granted me the possibility to pursue the PhD, and to Professor Stefania Bruschi, my supervisor, for her continuous help, inspiration and positive encouragement throughout these years and for the given opportunity to present the main findings at International Conferences.

I would also like to express my sincere gratitude to Professor Domenico Umbrello and to Dr. Stano Imbrongo from the University of Calabria for their valuable contribute at this thesis, in the development of numerical models, and for the time dedicated at the numerical simulations.

I am very grateful to Dr. Ing. Luca Facchini from Eurocoating S.p.a for his profound knowledge on metal Additive Manufacturing technologies, and for having continuously inspired and guided me throughout the research project NEMO.

I would like to thank all the Faculty members and the staff of the Department of Industrial Engineering, in particular to Ing. Riccardo Manzetto, for their continued support and cooperation.

I would also like to thank my colleagues in Padova and Rovigo for their invaluable support during these years and for the strong friendship established.

Last but not the least, I want to express my thanks to my family and my friends for their support. A special thought goes to Piera, without her I would have never reached this goal.